TESIS DE LA UNIVERSIDAD DE ZARAGOZA

2021

377

Erik Arturo Vanegas Vásquez

Contribución al diseño de sensores vestibles y ambientales para medir la respiración y el salto vertical en adultos mayores y frágiles.

Director/es

Dra. Dª. Plaza García, Inmaculada

Dr. D. Igual Catalán, Raúl

ISSN 2254-7606

Prensas de la Universidad Universidad Zaragoza

ISSN 2254-7606

Universidad Zaragoza
1542

Tesis Doctoral

CONTRIBUCIÓN AL DISEÑO DE SENSORES VESTIBLES Y AMBIENTALES PARA MEDIR LA RESPIRACIÓN Y EL SALTO VERTICAL EN ADULTOS MAYORES Y FRÁGILES.

Autor

Erik Arturo Vanegas Vásquez

Director/es

Dra. Dª. Plaza García, Inmaculada
Dr. D. Igual Catalán, Raúl

UNIVERSIDAD DE ZARAGOZA
Escuela de Doctorado

2021

Universidad Zaragoza
1542

Tesis Doctoral

Contribución al diseño de sensores vestibles y ambientales para medir la respiración y el salto vertical en adultos mayores y frágiles

Autor

Erik Arturo Vanegas Vásquez

Directores

Raúl Igual Catalán

Inmaculada Plaza García

ESCUELA DE DOCTORADO
2021

AGRADECIMIENTOS

Primero que nada, quiero agradecer al Consejo Nacional de Ciencia y Tecnología (CONACyT-México) por la beca que me fue otorgada para realizar mis estudios de doctorado. Así mismo, también agradezco al Consejo de Ciencia y Tecnología del Estado de Durango (COCYTED) por el apoyo que me ofrecieron a lo largo de mis estudios.

De igual manera agradezco a mis asesores de tesis, la Dra. Inmaculada Plaza y el Dr. Raúl Igual, por haberme otorgado la oportunidad de realizar mis estudios dentro del grupo de investigación EduQTech. Además, también agradezco a todos los integrantes del grupo de investigación que me brindaron su ayuda siempre que la necesité.

Finalmente quiero agradecer a todos mis familiares y amigos que me brindaron su apoyo a lo largo de mis estudios. A mis padres, a mis hermanos, a mi esposa y a mis hijos, que sin todo su apoyo yo sé que no habría llegado tan lejos.

RESUMEN

Con el avance de la tecnología, se ha popularizado entre la población el uso de dispositivos para medir su estado de salud. Para lograr esto, se suelen utilizar dispositivos vestibles como los *smartwatch* y *smartbands*, dispositivos ambientales embebidos en los alrededores, e incluso dispositivos conectados a aplicaciones móviles. El uso de estas tecnologías también se ha popularizado entre los profesionales de la salud.

Esta tesis se centra en el desarrollo de dispositivos para monitorizar la salud de adultos mayores y adultos frágiles. Se desarrollaron dos líneas de trabajo: en la primera se diseñó e implementó un sistema vestible para monitorizar en tiempo real la respiración de los usuarios; en la segunda se desarrolló un sistema ambiental capaz de medir la altura del salto vertical efectuado por los usuarios sobre él.

Sistema vestible para monitorizar la respiración:

– Dentro de esta línea de trabajo se investigó un nuevo sensor de respiración que venía a cubrir algunas lagunas existentes en el estado de la técnica: la integración de todos los elementos electrónicos del sistema en un encapsulado compacto, la liberación del diseño para su reutilización y mejora por parte de otros investigadores y el bajo coste de los elementos que componen el sistema, entre otros. El sistema vestible consiste en un dispositivo que se coloca alrededor del pecho mediante una cinta ajustable. Este sistema funciona mediante un sensor piezoresistivo que detecta las variaciones en el diámetro del pecho ocasionadas al inhalar y exhalar; las variaciones detectadas son enviadas de forma inalámbrica mediante Bluetooth a una estación de visualización elegida por el usuario (PC, *Tablet* o *Smartphone*). El sistema se encuentra embebido en un armazón impreso en 3D. Para validar el funcionamiento de este sistema, se realizaron pruebas con 21 voluntarios que efectuaron diferentes ritmos de respiración. Para obtener los ritmos respiratorios de cada señal generada, se utilizaron dos algoritmos. Estos algoritmos calculan el ritmo respiratorio al segmentar la señal original en ventanas de tiempo desde 6 hasta 30 segundos. Los resultados obtenidos muestran que, con una ventana de tiempo de 27 segundos, se obtiene el menor error para cada algoritmo (4,02 % y 3,40 %).

Sistema ambiental para medir el salto vertical:

– Dentro de esta segunda línea de trabajo se investigó en un novedoso sistema ambiental para medir la altura del salto, lo que supuso una innovación respecto a los sensores utilizados actualmente para este fin. El sistema ambiental consiste en una plataforma que detecta objetos sobre ella mediante la presión, y mide el tiempo transcurrido desde que un objeto se retira y se coloca de nuevo. El sistema detecta los objetos mediante una matriz de sensores piezoresitivos (*Force Sensitive Resistors - FSR* realizados con velostat). Las dimensiones de la plataforma son 30 cm x 30 cm, área sobre la cual se distribuyen un total de 256 sensores FSR. El salto vertical se calcula mediante la fórmula de tiempo de vuelo, y el resultado es enviado mediante Bluetooth a un PC o *Smartphone*. Se realizaron dos experimentos: en el primero participaron un total de 38 voluntarios, con el objetivo de validar el funcionamiento del sistema con una cámara de alta velocidad como referencia (120 fps); en el segundo experimento se capturaron los datos en crudo de 15 voluntarios, con estos datos se emularon 10 frecuencias de muestreo (desde 20 Hz hasta 200 Hz) y se analizaron los efectos de utilizar frecuencias más bajas. Del primer experimento se obtuvo un error relativo medio de 1.98 % con un coeficiente de determinación $r^2 = 0,996$. Del segundo experimento se determinó que las frecuencias de muestreo de 200 Hz y 100 Hz muestran un desempeño similar al mantener un error relativo por debajo del 5 % en el 95 % de las mediciones.

Finalmente, este trabajo de tesis concluye indicando las principales aportaciones realizadas para cada una de las dos líneas de trabajo, así como el trabajo futuro que podría desarrollarse en cada una de ellas.

Índice

1. Introducción **1**

1.1. Antecedentes 2

1.2. Motivación de la tesis 3

1.3. Objetivos generales 3

1.4. Estructura de la tesis 4

2. Estado del arte **7**

2.1. Sistemas vestibles 7

2.1.1. Definición 7

2.1.2. Sistemas vestibles de respiración 8

2.1.3. Sistemas vestibles para salto vertical 10

2.2. Sistemas ambientales 12

2.2.1. Definición 12

2.2.2. Sistemas ambientales de respiración 12

2.2.3. Sistemas ambientales para salto vertical 14

2.3. Técnicas híbridas vestibles-ambientales 14

2.4. Parámetros medidos 15

3. Metodología **17**

3.1. Sistema vestible para monitorizar la respiración 17

3.1.1. Desarrollo del sistema 17

3.1.2. Procesado de datos 21

3.1.3. Marco experimental 25

3.2. Sistema ambiental para medición del salto vertical 31

3.2.1. Desarrollo del sistema 31

3.2.2. Procesado de datos 34

3.2.3. Marco experimental 36

4. Resultados **39**

4.1. Sistema vestible para respiración 39

4.1.1. Resultados . . . 39
4.1.2. Discusión . . . 40
4.1.3. Efecto de las tendencias en las señales de respiración . . . 40
4.1.4. Versión mejorada del sistema vestible . . . 43
4.2. Sistema ambiental para medición del salto vertical . . . 47
4.2.1. Resultados . . . 47
4.2.2. Discusión . . . 53

5. Conclusiones principales **55**
5.1. Sistema vestible para respiración . . . 55
5.1.1. Trabajo futuro . . . 57
5.2. Sistema ambiental para salto vertical . . . 57
5.2.1. Trabajo futuro . . . 59

6. Bibliografía **61**

Listado de Figuras **89**

Listado de Tablas **93**

Anexos **95**

A. Producción científica **97**
A.1. Publicaciones en revistas indexadas . . . 97
A.2. Publicaciones en congresos internacionales . . . 98

B. Comparación de tecnologías **99**

C. Diseños del sistema vestible de respiración: Versión 1.0 **101**
C.1. Circuito esquemático y PCB . . . 101

D. Diseños del sistema vestible de respiración: Versión 2.0 **105**
D.1. Circuito esquemático y PCB . . . 105

E. Comparación de señales obtenidas: Primera y segunda versión del sistema vestible para la medición de la respiración **109**

F. Valores *p* obtenidos de la prueba t a una muestra **117**

G. Diseños del sistema ambiental para el salto vertical **119**
G.1. Circuito esquemático y PCB . . . 119

H. Piezoresistive Breathing Sensing System with 3D Printed Wearable Casing **123**

I. Sensing Systems for Respiration Monitoring: A Technical Systematic Review **143**

J. Force-Sensitive Mat for Vertical Jump Measurement to Assess Lower Limb Strength: Validity and Reliability Study **227**

K. The effect of measurement trends in belt breathing sensors **243**

L. Repositorio **249**

Capítulo 1

Introducción

En los últimos años, con el avance de la tecnología, se ha popularizado entre la población el uso de dispositivos para medir su estado de salud. Hay diferentes formas en las que las personas pueden hacer esto. Para visualizar sus señales fisiológicas como el ritmo cardiaco, el ritmo respiratorio, la temperatura corporal, entre otros, se utilizan dispositivos vestibles (wearable devices) tales como los *smartwatch* o *smartband* [1]. Existen aplicaciones móviles que también se utilizan para estos fines. Principalmente se usan para registrar diferentes actividades que repercuten en la salud de las personas, tales como llevar un registro de los alimentos ingeridos, el ejercicio realizado, e incluso auxiliarles con la depresión [2]. De igual forma también se utilizan los sensores ambientales, aunque en menor medida. Los sensores ambientales son aquellos que se encuentran embebidos en los lugares en los que las personas pueden interactuar. Por ejemplo, pueden encontrarse en una silla para detectar si una persona está sentada en ella, o incluso para, a su vez, medir la respiración o ritmo cardiaco [3].

El uso de estas tecnologías no solo se ha popularizado en la población en general, sino también entre los profesionales de la salud, que cada vez se apoyan más en dichas tecnologías para el control de pacientes o para evaluar su salud en general [4].

Fundamentalmente, todo dispositivo vestible debe ser capaz de sensar, procesar, almacenar, transmitir o aplicar toda aquella información obtenida de un usuario [1]. En cuanto a sus características físicas, los dispositivos vestibles deben ser ligeros, ergonómicos, cómodos y estéticos. En cuanto a su funcionamiento, deben ser configurables, multi-funcionales (que puedan medir diferentes variables) y deben tener una alta sensibilidad que asegure su velocidad de respuesta.

En cuanto a los sensores ambientales, algunas de sus características principales son el poder obtener datos informativos de la persona siempre que se encuentre en el área de interacción, información como su posición, localización o movimientos [3]. Recientemente se han empezado a utilizar como alternativas para el monitoreo de la salud, aunque debido a la naturaleza de su funcionamiento, es más difícil adecuar su

utilización para dicho fin.

Esta tesis se centra en el desarrollo de dispositivos orientados a la monitorización de la salud de su usuario. Se han desplegado dos líneas de trabajo: la primera es el desarrollo de un sistema vestible para la visualización en tiempo real de la respiración de su usuario, trabajo que va acompañado de una extensa revisión del estado del arte. La segunda línea es el desarrollo de un sistema ambiental, que consiste en una plataforma capaz de medir la altura de los saltos efectuados por los usuarios que se posen sobre ella.

1.1. Antecedentes

La monitorización continua de señales fisiológicas es muy utilizada por los profesionales de la salud, sobre todo con pacientes de hospital. Por ejemplo, el monitoreo del ritmo respiratorio se usa habitualmente para evaluar la salud del paciente [5]. Con esto se pueden diagnosticar enfermedades respiratorias tales como asma, apnea del sueño o enfermedades pulmonares obstructivas crónicas [6].

Otra aplicacion común es en los deportes, y se utiliza para analizar el despempeño de los atletas [7, 8]. Dicha información puede utilizarse para mejorar la metodología de entrenamiento o para prevenir problemas de salud. Entre otras aplicaciones, el control del ritmo respiratorio se ha utilizado para evaluar la salud de trabajadores como constructores o conductores [9–11], y para el reconocimiento de emociones [12–14].

En los adultos mayores, los desórdenes de respiración al dormir están reconocidos como problemas de salud comunes entre esta población. Además, el envejecimiento se ha asociado con un empeoramiento de la calidad del sueño, estando la apnea obstructiva del sueño asociada con un incremento en la mortalidad de los adultos mayores [15].

Por otra parte, la altura del salto vertical se ha utilizado para evaluar el desempeño general del cuerpo humano, más específicamente para evaluar la fuerza de los grupos musculares de los miembros inferiores, que serían los cuadriceps, femorales (o isquiotibiales) y gemelos (o grastrocnemius) [16, 17]. El salto vertical usualmente se mide en atletas, como jugadores de baloncesto [18–20], fútbol [21], nadadores [22], entre otros. No obstante, el salto vertical también puede ofrecer información importante de personas sin antecedentes deportivos relevantes.

La fuerza de las piernas tiene una relación directa con fracturas asociadas a caídas en los adultos mayores [23]. Hay estudios que han investigado en adultos mayores con movilidad limitada la relación que existe entre la fuerza de las piernas y el balance corporal [24].

Para ambos escenarios, monitorizar el ritmo respiratorio y medir la altura del salto

vertical, esta tesis recoge soluciones mediante sistemas vestibles y ambientales, y a su vez, cada tipo de sistema puede utilizar diferentes métodos y sensores para abordar el problema en cuestión. Un análisis más a fondo en cuanto al estado del arte de estos sistemas se realiza en el Capítulo 2.

1.2. Motivación de la tesis

El grupo de investigación EduQTech busca mejorar la calidad de vida de las personas que viven tanto en medios rurales como urbanos. Esto mediante tecnologías móviles, sistemas vestibles, sistemas ambientales, servicios web y análisis de datos. En esta tesis nos enfocamos en el desarrollo de sistemas vestibles y ambientales. Para ambas líneas de trabajo propuestas, la principal motivación es desarrollar sistemas que nos ayuden en futuros estudios con adultos mayores (>50 años [25]) y adultos mayores "frágiles" (adultos con falta de mobilidad, debilidad y baja tolerancia al estrés psicológico [26]), para así poder evaluar ciertos aspectos de su estado de salud, y de esta manera proponer cualquier medida que pueda ser necesaria para mejorar su calidad de vida.

1.3. Objetivos generales

El objetivo principal de esta tesis es el desarrollo de sistemas que ayuden a los profesionales de la salud a monitorizar, día a día, el estado salud de sus pacientes de una forma más práctica. Estos sistemas estarán enfocados a ser utilizados en adultos mayores y adultos frágiles. De igual manera, estos sistemas serán de bajo coste y de fuente abierta (*Open Source*) para que sean fáciles de replicar e incluso mejorar. Siendo así, esta tesis cuenta con dos objetivos específicos, uno para cada línea de trabajo:

- Desarrollar un sistema vestible capaz de medir las señales de respiración en adultos mayores y adultos frágiles de forma precisa, y validar su funcionamiento utilizando dispositivos de referencia. Diseñar el sistema para que sea de bajo coste y ofrecer su diseño como fuente abierta para que sea fácil de replicar por futuros investigadores.

- Desarrollar un sistema ambiental capaz de medir la altura de los saltos de los usuarios para así evaluar la fuerza media de los músculos de las extremidades inferiores de adultos y adultos mayores, y validar el funcionamiento de dicho sistema utilizando un dispositivo de referencia. Diseñar el sistema de tal manera que sea de bajo coste en comparación con los sistemas comerciales.

1.4. Estructura de la tesis

El contenido de esta tesis estará organizado de la siguiente manera:

Capítulo 2 - Estado del arte

- **2.1. Sistemas vestibles -** Se describen las principales características con las que debe contar un sistema para poder ser considerado como "vestible". Así mismo, se describen las técnicas utilizadas por estos sistemas para medir las señales de respiración y los saltos verticales.
- **2.2. Sistemas ambientales -** Se describen las principales características de los sistemas que son considerados como "ambientales". A su vez, se describen las técnicas encontradas en la literatura para medir las señales respiratorias y los saltos verticales.
- **2.3. Técnicas híbridas vestibles-ambientales -** En la literatura se encontraron algunos sistemas que utilizan un tipo de fusión de señales (o *sensor fusion*) al combinar técnicas vestibles y ambientales, las cuales se describen aquí.
- **2.4. Parámetros medidos -** Se describen los tipos de parámetros usualmente registrados por los sistemas vestibles y ambientales, tanto para respiración como para salto vertical.

Capítulo 3 - Metodología

- **3.1. Sistema vestible para monitorizar la respiración -** Se presentan los criterios que se tomaron en cuenta para el diseño del sistema y la forma en que fue desarrollado, así como el marco experimental que se propuso para validar su funcionamiento.
- **3.2. Sistema ambiental para medición del salto vertical -** Se presentan los criterios utilizados para el diseño del sistema y su desarrollo, así como el marco experimental utilizado para validar el funcionamiento del sistema.

Capítulo 4. Resultados

- **4.1. Sistema vestible para respiración -** Se presentan los principales resultados obtenidos tras realizar los experimentos propuestos, así como una nueva versión mejorada del sistema que podrá utilizarse en trabajos futuros.
- **4.2. Sistema ambiental para medición del salto vertical -** Se presentan los principales resultados obtenidos a partir de los experimentos realizados.

Capítulo 5. Conclusiones

- **5.1. Sistema vestible para respiración -** Se presentan las conclusiones derivadas de esta línea de trabajo, así como futuras líneas de trabajo que podrían realizarse.
- **5.1. Sistema ambiental para salto vertical -** De igual manera, se presentan las conclusiones de esta línea de trabajo y el trabajo futuro que podría realizarse.

Capítulo 6. Bibliografía

Anexos

- **Anexo A:** Se muestra la producción científica derivada de la realización de esta tesis, mostrando un listado de artículos publicados en revistas indexadas en JCR y en congresos internacionales.
- **Anexo B:** Se muestra una tabla comparativa de las diferentes tecnologías utilizadas por otros dispositivos vestibles para monitorizar la respiración, los más parecidos al desarrollado en esta tesis.
- **Anexo C:** Se muestran los circuitos esquemáticos y las PCB construidas para el sistema vestible para monitorizar la respiración.
- **Anexo D:** Se muestran los circuitos esquemáticos y las PCB construidas para la versión mejorada del sistema vestible para monitorizar la respiración.
- **Anexo E:** Se muestra una comparativa entre las señales de respiración obtenidas de la primera versión y la versión mejorada del sistema vestible de respiración.
- **Anexo F:** Se muestra una tabla con todos los valores p obtenidos del análisis realizado para el sistema vestible de respiración.
- **Anexo G:** Se muestra el circuito esquemático y las PCB contruidas para el sistema ambiental para medir el salto vertical.
- **Anexo H:** Se muestra el artículo de investigación publicado en la revista internacional indexada *"Journal of Sensors"*. En este artículo se presenta el sistema vestible de respiración que se desarrolló como resultado de esta tesis y que se publicó bajo el nombre de *"Piezoresistive breathing sensing system with 3D printed wearable casing"*.

– **Anexo I:** Se muestra el artículo de investigación publicado en la revista internacional indexada *"Sensors"*. En este artículo se presenta un trabajo de revisión de 198 trabajos relacionados con sistemas vestibles y ambientales para monitorizar la respiración. Este artículo de revisión se publicó bajo el nombre de *"Sensing systems for respiration monitoring: A technical systematic review"*.

– **Anexo J:** Se muestra el artículo de investigación publicado en la revista internacional indexada *"JMIR mHealth and uHealth"*. En este artículo se presenta el sistema ambiental para medir el salto vertical que se desarrolló como resultado de esta tesis y que se publicó bajo el nombre de *"Force-Sensitive Mat for Vertical Jump Measurement to Assess Lower Limb Strength: Validity and Reliability Study"*.

– **Anexo K:** Se muestra el artículo de investigación publicado en el congreso internacional *"8th International Symposium on Sensor Science"* que tuvo lugar en Dresden, Alemania. Este artículo se publicó en formato de *"extended abstract"*. En este artículo se presenta un estudio efectuado sobre la base de datos de señales de respiración obtenidas de un trabajo previo (Anexo H [27]) y que se publicó bajo el nombre de *"The effect of measurement trends in belt breathing sensors"*.

– **Anexo L:** Se muestra un código QR que puede ser escaneado para acceder al repositorio donde se encuentran todos los archivos desarrollados como resultado del trabajo de la presente tesis. Entre los archivos del repositorio se encuentran: Archivos "Gerber" para construcción de las PCB, diseños 3D para impresión de armazones de los sistemas desarrollados, códigos utilizados por los microcontroladores y datos en crudo obtenidos por los sistemas.

Capítulo 2

Estado del arte

2.1. Sistemas vestibles

2.1.1. Definición

Un dispositivo vestible puede definirse como un accesorio que una persona puede portar en diferentes partes de su cuerpo, como en la muñeca (*smartband*), en la cabeza (gafas, casco, auriculares), en el cuerpo (prendas inteligentes), y como se mencionó en el Capítulo I - Introducción, también son capaces de sensar, procesar, almacenar, transmitir y utilizar toda información que pueda adquirirse del sujeto que lo porta [1]. Además, no todos los sensores son vestibles, pero todos los dispositivos vestibles necesitan sensores. Algunos de los atributos principales que necesitan poseer los dispositivos vestibles son:

- Ser ligeros y adaptables a su usuario.
- Ser estéticos, ya que muchos han comenzado a ser incluso tendencias en moda.
- Ser multifuncionales (deben ser capaces de medir múltiples variables).
- Ser fáciles de configurar.
- Ser sensibles en su respuesta, especialmente para adquisición de datos en tiempo real.

Existen diferentes formas de catalogar a los sistemas vestibles [1]. Pueden dividirse en función-simple o multi-funcionales, que se refiere a la cantidad de señales que puede procesar el sistema. También se clasifican como invasivos o no-invasivos. Los sistemas no-invasivos pueden, o no, estar en contacto directo con el usuario. Los sistemas invasivos a su vez pueden catalogarse como “mínimamente invasivos” o implantables. Los mínimamente invasivos son aquellos que penetran la piel y por lo general

son subcutáneos, mientras que los implantables requieren de algún procedimiento quirúrgico para introducirse al cuerpo, como por ejemplo los marca-pasos.

También se pueden identificar los sistemas activos y pasivos. Los activos requieren de una fuente de alimentación para poder funcionar, mientras que los pasivos no la requieren. Dependiendo de la forma en que transmiten su información, pueden ser inalámbricos o cableados. Los sistemas inalámbricos pueden utilizar una variedad de tecnologías que les permita compartir la información con su receptor final, como Bluetooth, Zigbee, radio-frecuencia, o Wifi, por mencionar las más utilizadas. Por otra parte, los sistemas cableados necesitan de una conexión física para transmitir la información a su receptor final. En el caso de sensores que deban ser colocados directamente sobre el cuerpo, estos pueden ser desechables o reutilizables, como es el caso de los sistemas que miden la actividad muscular mediante electrodos.

Finalmente, los sistemas vestibles se pueden catalogar dependiendo de su aplicación. Las aplicaciones más comunes son: salud y bienestar, procesamiento de información, seguridad pública, sensado acústico, entretenimiento, rastreo de posición, y aplicaciones militares, entre otras.

2.1.2. Sistemas vestibles de respiración

En este apartado se mencionan las diferentes técnicas y sensores que se han utilizado en la literatura para lograr monitorizar la respiración. Una revisión más detallada de todas estas técnicas puede consultarse en un trabajo de revisión publicado como resultado de la presente tesis [28], en el que 189 estudios se analizan en profundidad.

Técnicas utilizadas

En la revisión del estado del arte que se efectuó se detectaron diferentes técnicas utilizadas para lograr la medida de la respiración. La utilización de ciertas técnicas sobre otras está muy relacionado con el tipo de sensor del sistema. Las diferentes técnicas son las siguientes:

- **Medición del flujo respiratorio:** Esta técnica se enfoca en medir los cambios del flujo respiratorio al inhalar y exhalar. Los tipos de sensores más utilizados son flujómetros diferenciales, flujómetros de turbina, anemómetros de hilo caliente, sensores fotoeléctricos y sensores de fibra óptica [29–33].

- **Medición de sonidos respiratorios:** Se miden los sonidos de la respiración ocasionados por inhalar y exhalar. Los sensores utilizados con esta técnica son los micrófonos [34–36].

- **Medición de la temperatura del aire:** Se miden los cambios de temperatura al inhalar y exhalar; al exhalar el aire expulsado del cuerpo tiene una mayor temperatura que el aire del ambiente, este cambio es detectado por el sensor, y la acción de inhalar ayuda a bajar la temperatura del aire (al igual que el tiempo sin aire exhalado). Los sensores utilizados suelen ser termistores, termopares, sensores piroeléctricos y sensores de fibra óptica [6, 37–50].

- **Medición de humedad del aire:** Semejante al caso anterior, con esta técnica se miden los cambios en la humedad del aire ocasionados por exhalar e inhalar. Los sensores comúnmente utilizados para este fin son sensores capacitivos, sensores resistivos, sensores de nanocristal y nanopartículas, sensores de impedancia y sensores de fibra óptica [51–60].

- **Modulación de actividad cardiaca:** En principio estas técnicas arrojan algún tipo de señal dentro del cuerpo (eléctrica, óptica, radar, etc.) y se predice el ritmo respiratorio basados en la diferencia entre la señal original y la señal obtenida después de arrojarla "dentro" del cuerpo humano. Los sensores utilizados con esta técnica suelen ser electrodos de electro-cardiograma (ECG) y sensores de fotopletismografía (PPG) [61–66].

- **Medición de movimiento de la caja torácica:** Con esta técnica se miden ya sea los movimientos o los cambios en el diámetro de la caja torácica debidos a la respiración. De esta forma, se pueden distinguir dos técnicas diferentes en esta categoría:

  Medición de tensión/deformación: Con este método se mide la fuerza o deformación ejercida sobre sensores colocados alrededor del pecho. Los sensores usualmente utilizados son sensores resistivos, sensores capacitivos, sensores inductivos, sensores piezoeléctricos, sensores de fibra óptica, y sensores piroeléctricos [7, 47–49, 67–105].

  Medición de movimiento: De esta manera se miden directamente los movimientos efectuados por la caja torácica al respirar. Los sensores comúnmente utilizados para este fin son unidades de medición inercial (IMU) que en su interior incluyen giroscopios, acelerómetros y magnetómetros [61, 64, 106–116].

Localización de los sistemas en el cuerpo

Para lograr obtener satisfactoriamente la señal respiratoria de una persona, la localización del sistema vestible es muy importante. Los lugares más utilizados para colocar un sistema vestible son el pecho y el abdomen a modo de cinta perimetral

[34, 67, 68, 70–73, 106–110] o embebidos en prendas [69]; cercanos a la nariz y/o boca [29–31, 37, 52], o también pueden estar embebidos en una máscarilla facial [51, 53–55]. Hay más lugares para colocarlos como la nuca [32] o las muñecas [112], pero son poco utilizados en la literatura ya que es más difícil obtener la señal de respiración. En la Figura 2.1 se muestran los lugares donde se colocan estos sensores.

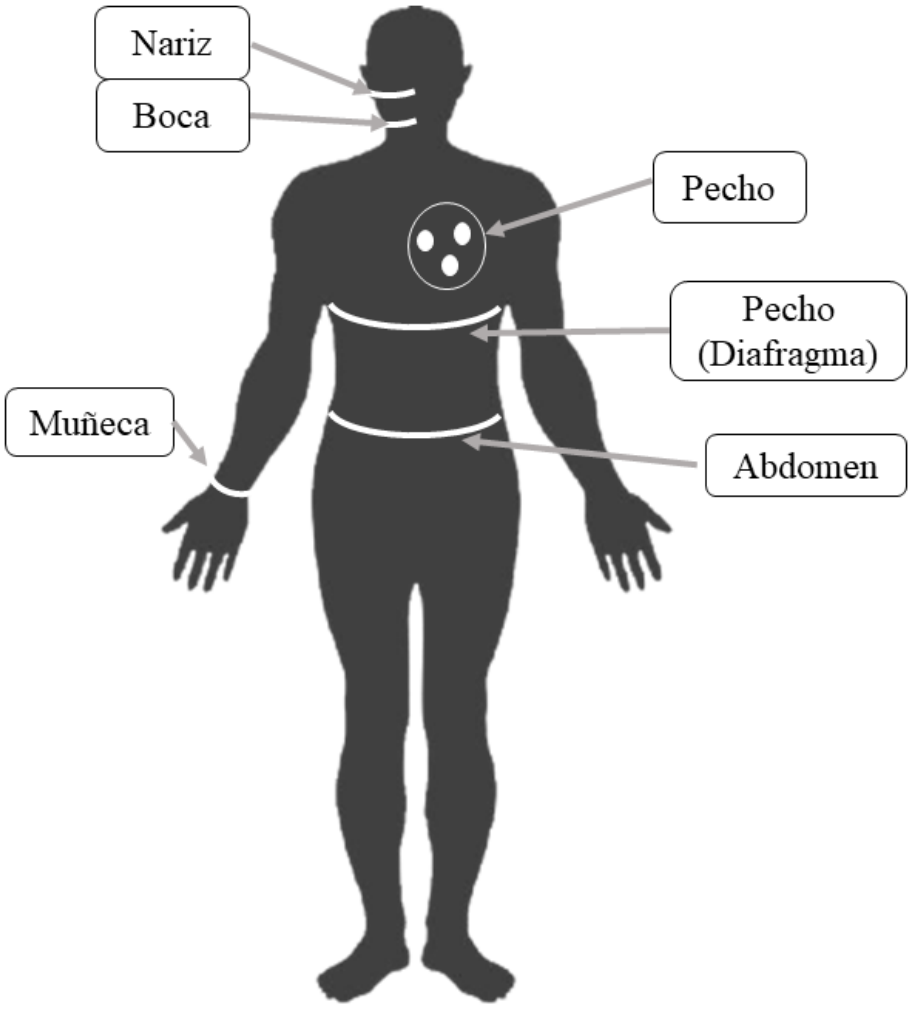

Figura 2.1: Lugares del cuerpo donde usualmente se colocan los sistemas vestibles. Los sistemas mostrados son solo de referencia.

2.1.3. Sistemas vestibles para salto vertical

A diferencia de los sistemas para monitorizar la respiración, para medir el salto vertical no hay muchos sistemas vestibles que se hayan utilizado en la literatura. Esto se debe a la misma naturaleza de la magnitud a medir, ya que resulta difícil adaptar un sistema vestible para lograrlo.

Técnicas utilizadas

Las técnicas utilizadas para medir el salto vertical se muestran a continuación.

- **Medición mediante contacto:** Con este tipo de técnica lo que se busca medir es el tiempo de vuelo del usuario, es decir, el tiempo que pasa desde que el usuario despega del suelo o de una plataforma y el momento en que aterriza de nuevo. Para calcular este tiempo de vuelo en un sistema vestible, se han utilizado sensores resistivos embebidos en zapatillas deportivas [17]. Una vez calculado dicho tiempo, se utiliza la "fórmula de tiempo de vuelo" para predecir la altura alcanzada; dicha fórmula se define como $h = g\Delta t/8$, en donde "h" es la altura alcanzada, "g" es la constante de gravedad igual a $9{,}81 m/s^2$ y Δt es el tiempo de vuelo calculado [18, 117–122].

- **Medición mediante aceleración:** Para estos métodos se utilizan unidades de medición inercial (IMU) que vienen provistas de acelerómetro, giroscopio, y en algunas ocasiones de magnetómetro, dependiendo de los grados de libertad (DOF) que posea la unidad. La altura del salto vertical se calcula mediante las aceleraciones absolutas obtenidas del plano vertical, o plano "Z" de las IMU. En la literatura este método ha sido utilizado por García et al. [17], Howard et al. [117], y Zihajehzadeh et al [123], mientras que Casartelli et al. [19], y Nuzzo et al. [124] utilizan un dispositivo comercial para estos fines. El lugar donde se coloquen estos sistemas no es tan importante, ya que la IMU puede calcular la aceleración del eje vertical independientemente de su posición, sin embargo, usualmente se colocan en la cintura.

- **Medición mediante actividad muscular:** Mediante las señales electromiográficas (EMG) de diferentes músculos de las piernas se ha investigado la viabilidad de predecir de forma acertada la altura durante el salto vertical. En el trabajo de Yahya et al. [20] se midió la actividad de 8 músculos diferentes para este fin. Sin embargo, el principal problema que presenta este método es que se necesita realizar una calibración en base a la máxima contracción voluntaria de cada usuario, por lo que en este estudio se necesitó entrenar un sistema de inteligencia artificial para poder realizar predicciones.

- **Medición por proximidad:** Mediante sensores de proximidad se puede calcular la altura de un salto vertical al medir la diferencia entre la altura inicial del sensor y la altura final. En el estudio de Kassim et al. [125] se utiliza un sensor ultrasónico en un robot trípodo para determinar la altura de sus saltos mediante

un controlador PID. En principio este método puede utilizarse para simplemente medir la altura durante el salto. Sin embargo, el principal inconveniente que presenta este método es que al realizar la medición con referencia al suelo, el sensor debe permanecer siempre perpendicular a este.

2.2. Sistemas ambientales

2.2.1. Definición

Los sistemas ambientales son aquellos que se encuentran embebidos en los alrededores del usuario y con los cuales éste puede interactuar para diferentes fines. Las principales aplicaciones de este tipo de sistemas se encuentran en la domótica. Por ejemplo, suelen utilizarse para saber en qué lugar de un edificio se encuentra alguna persona y de esta forma controlar la iluminación del lugar para maximizar el ahorro energético y ofrecer al usuario la mejor iluminación. Estos sistemas también pueden controlarse por voz. Por lo general existe un "dispositivo madre" al cual el usuario puede darle diferentes órdenes para así controlar otros sistemas que estén bajo su mando. Este tipo de sistemas suelen funcionar mediante el internet de las cosas (IoT), y una característica fundamental es que estos sistemas ambientales funcionan como una red de dispositivos interconectados [126].

De esta forma, hay sistemas ambientales con aplicación en salud y bienestar. Una de las ventajas que ofrecen los sistemas ambientales sobre los vestibles son que suelen ser más cómodos para el usuario (sin necesidad de ajustar el dispositivo a su cuerpo). Cabe resaltar que el utilizar un sistema ambiental o uno vestible depende mucho de la aplicación y del usuario, ya que en la literatura cada sistema muestra sus propias ventajas y desventajas.

2.2.2. Sistemas ambientales de respiración

En este apartado se mencionan las diferentes técnicas y sensores utilizados en la literatura para sistemas ambientales de control de la respiración. Las técnicas y sensores utilizados en la literatura se mencionan más en detalle en la revisión publicada como resultado de la presente tesis [28] (Anexo A). Por lo tanto, solo se mencionarán los aspectos más importantes.

Técnicas utilizadas

Se mencionarán las diferentes técnicas utilizadas en la literatura. Al igual que con los sistemas vestibles, el tipo de técnica a utilizar va muy relacionada con el sensor del

sistema.

- **Movimiento de la caja torácica:** Al igual que con los sensores vestibles, se miden los movimientos o cambios en el diámetro de la caja torácica debidos a la respiración. Se pueden destacar dos métodos derivados:

  Medición de tensión/deformación: El principio es el mismo que con los sistemas vestibles, ya que se utilizan sensores capaces de medir una fuerza ejercida sobre ellos. Estos sensores suelen estar embebidos en colchones, esterillas, almohadas o sillas. Los sensores utilizados suelen ser sensores de fibra óptica, sensores piezoeléctricos, sensores capacitivos y sensores resistivos [10, 127–154].

  Medición mediante el movimiento del pecho: Para estos métodos se utilizan diversos tipos de cámaras que suelen colocarse frente al pecho del usuario. Con cámaras convencionales se detecta la respiración mediante el movimiento del pecho o de los hombros del usuario basados en la imagen obtenida. Por otra parte, con cámaras especializadas como el sistema Kinect lo que se mide es el movimiento del pecho pero basado en la profundidad. Con estos métodos suele ser necesario elegir una región de interés (ROI) para que el algoritmo propuesto funcione adecuadamente [155–167].

- **Modulación de la actividad cardiaca:** El principio es el mismo que con los sistemas vestibles, se envía algún tipo de señal dentro del cuerpo humano, y la respiración se obtiene al analizar la diferencia entre la señal original y la señal obtenida después de pasar por el cuerpo. Para este propósito, los sistemas ambientales utilizan señales inalámbricas, y los sensores más utilizados son radares Doppler y nodos de redes WiFi [155, 168–192].

- **Temperatura del aire:** A pesar de que el principio de medición es el mismo, a diferencia de los sistemas vestibles la temperatura del aire se mide mediante visión computacional y no por su acción directa sobre el sensor. Para lograr esto se utilizan camaras infrarrojas [193–197].

Localización de los sistemas ambientales

Como se ha mencionado anteriormente, los sistemas ambientales se encuentran embebidos en los alrededores del usuario, y éste puede interactuar con los sistemas. La localización del sistema depende de la técnica de medición. Los sistemas que funcionan mediante la medición de tensión o deformación del sensor usualmente se encuentran embebidos en lugares donde el usuario reposa, tales como esterillas, colchones, almohadas o sillas [127, 128, 130–134, 169]. Los sistemas que funcionan

mediante cámaras (medición del movimiento del pecho, temperatura del aire) o por modulación de la actividad cardiaca necesitan colocarse frente al usuario a una distancia adecuada y esta distancia varía dependiendo del sistema [156, 168, 170–172, 193]. Los usuarios pueden encontrarse sentados, o incluso acostados en una cama o esterilla, siempre y cuando haya una visión clara de la ROI.

2.2.3. Sistemas ambientales para salto vertical

Estos sistemas son más comunes para la medición del salto vertical. Calculan la altura alcanzada mediante la fórmula del tiempo de vuelo. El tiempo de vuelo se calcula de dos maneras principalmente: por contacto en plataformas o mediante cámaras de alta velocidad.

- **Medición por plataforma de contacto:** Estos métodos utilizan plataformas con algún tipo de sensor embebido. Se pide al usuario colocarse sobre dicha plataforma y efectuar los saltos en ella. De esta forma, el sistema calculará el tiempo que pasa entre que el usuario ha despegado de la plataforma y aterriza de nuevo en ella. Los sistemas de este tipo encontrados en la literatura suelen utilizar sensores resistivos [18, 121], sensores capacitivos [21], sensores ópticos [19, 198] y micro-interruptores [118].

- **Medición por cámara de alta velocidad:** Con estos métodos se debe utilizar una cámara de alta velocidad (al menos 120fps) colocada a una distancia adecuada del sujeto. La cámara debe ubicarse de tal manera que se logre apreciar con claridad los pies del sujeto y se puedan distinguir las fases de despegue y aterrizaje durante el salto. De esta manera, al grabar los saltos del sujeto, posteriormente se seleccionan los "cuadros" del despegue y aterrizaje del video, y de esta manera se obtiene el tiempo de vuelo. Un problema inherente de este método es la subjetividad al momento de elegir los "cuadros" adecuados. En los estudios de Balsalobre-Fernández et al. [119, 122] se valida la efectividad de este método.

2.3. Técnicas híbridas vestibles-ambientales

Con respecto a los sistemas para monitorizar la respiración, en la revisión del estado del arte efectuada [28] no se encontró ningún tipo de sistema híbrido. Por otra parte, para calcular el salto vertical, los investigadores han utilizado métodos que combinan sistemas vestibles y ambientales. Estos sistemas utilizados en la literatura son sistemas de captura de movimiento (motion capture o MOCAP), muy usados en el ámbito del

cine y los videojuegos. Para medir el salto vertical con estos métodos lo que se hace es colocar uno o varios marcadores reflectivos en los usuarios para, mediante una cámara especializada, poder después ser procesados por ordenador y lograr predecir la altura del salto vertical según el desplazamiento de estos marcadores. Este método ha sido utilizado en la literatura por Mijailovic et al [21], Yahya et al. [20], Zihajehzadeh et al. [123] y Leard et al. [199]. Otros estudios que utilizan métodos similares basados en cámaras y marcadores fueron realizados por Casartelli et al. [19] y Dias et al. [120].

2.4. Parámetros medidos

Respecto a los sistemas para medir el salto vertical, el resultado final suele obtenerse en centímetros. Por otra parte, los sistemas para monitorizar la respiración tienen una mayor gama de posibilidades. Independientemente del tipo de sistema utilizado, vestible o ambiental, ambos obtienen los mismos parámetros como resultado del proceso de medición. Los posibles parámetros a obtener se mencionan a continuación:

Ritmo respiratorio (Respiration Rate, RR): Es el número respiraciones realizadas (ciclos de inhalación y exhalación) por el sujeto en un minuto, y se mide en respiraciones por minuto (breaths per minute, bpm) [29–32, 34, 35, 37, 51, 67–74, 106, 107, 110, 127–132, 156, 168, 169, 193]. De este parámetro se pueden derivar otros: periodo de respiración [200, 201], que es el tiempo que dura cada ciclo; tiempo de inspiración [6, 44, 202] y tiempo de expiración [162, 164, 202], que son los periodos de tiempo que dura cada fase respectivamente.

Parámetros de volúmen: Estas medidas ofrecen información relacionadas con el volumen de aire inhalado o exhalado durante los ciclos de respiración. Entre las métricas que entran en esta categoría están las siguientes:

- Volumen tidal o volumen corriente: Es el volumen de aire inhalado o exhalado durante una respiración normal, y se mide en litros [44, 70, 91, 92, 95, 113].
- Volumen por minuto: Es el volumen de aire inhalado o exhalado durante un minuto en una respiración normal, y se mide en litros por minuto (L/min) [44, 95, 102].
- Tasa de flujo, flujo pico o flujo de inspiración pico: Es el flujo máximo en el cual un determinado volumen tidal puede ser entregado, y se mide en litros por minuto (L/min) [44].
- Tasa de flujo espiratorio: Mide cuán rápido una persona puede exhalar aire, y se mide en litros por segundo (L/s) [162, 164].

Patrones de respiración: Hay estudios cuyo propósito es identificar patrones anormales en las señales de respiración obtenidas. Los patrones que usualmente se busca identificar son respiración anormal [202–204], episodios de apnea durante el sueño [202,203,205,206], respiración de Kussmaul, respiración de Cheyne-Stokes o respiración de Biot, entre otros.

Capítulo 3

Metodología

3.1. Sistema vestible para monitorizar la respiración

A continuación se describe el sistema vestible de respiración que se construyó como resultado de la investigación realizada. Los objetivos de este trabajo son:

Objetivo general

- Desarrollar un sistema vestible capaz de medir la señal de respiración de un usuario en tiempo real, y que sea más económico que los existentes en el mercado y fácilmente construible por no especialistas.

Objetivos específicos

- Validar el sensor propuesto con usuarios reales y proporcionar valores objetivos sobre su nivel de desempeño.

3.1.1. Desarrollo del sistema

En base a la revisión realizada del estado del arte, se optó por desarrollar un sistema vestible cuyo sensor fuera resistivo sensible a la fuerza (FSR), ya que se observó que solo el trabajo de Hesse et al. [207] utilizó este tipo de sensores con un enfoque parecido al planeado para nuestra propuesta, por lo que se encontró un área de oportunidad para mejorar lo existente, por ejemplo en relación a la resolución de las mediciones, las dimensiones del dispositivo o los métodos de comunicación inalámbrica, entre otros. Una tabla comparativa de las diferentes tecnologías utilizadas en estudios semejantes se muestran en el Anexo B. La mayor novedad de nuestro sistema con respecto al de Hesse et al. [207] es que el sistema implementado no solo integra el elemento sensor en el encapsulado, sino que incorpora toda la electrónica necesaria para el procesado y transmisión de las mediciones en un encapsulado compacto. Entre

las otras características del sistema se incorporó un microcontrolador con frecuencia de operación de 20MHz y un convertidor analógico a digital (ADC) de 10 bits, un módulo Bluetooth para comunicación inalámbrica y un módulo de carga para la batería integrada de polímero de litio (LiPo) de 3.7V y 150mAh. Se calculó el consumo energético total del sistema (40.51mA), lo que implica que con la batería utilizada se logra un funcionamiento continuo de aproximadamente 3 horas y 45 minutos. Todos estos componentes fueron integrados en una placa de circuito impreso (PCB), y embebidos en un armazón impreso en 3D. La PCB fue diseñada con unas dimensiones de 36mm x 36mm y un espesor de 1.5mm. Los diseños de la placa PCB y el circuito esquemático se muestran en el Anexo C. En cuanto a las temperaturas de operación de los componentes del sistema, ninguno supone un riesgo para la integridad de los usuarios.

Los sensores de tipo FSR (Force Sensitive Resistor) ofrecen una resistencia muy alta y al ejercer fuerza sobre ellos su resistencia cae de forma exponencial. Los valores de resistencia ofrecidos por los FSR varía dependiendo de sus características, pero su máximo valor puede encontrarse en el orden de los mega-óhmios ($M\Omega$). Para el sistema que se desarrolló, la curva característica del sensor se muestra en la Figura 3.1.

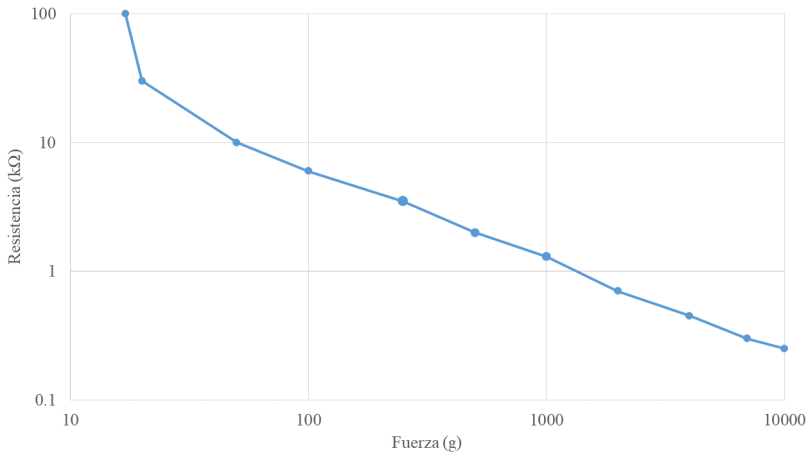

Figura 3.1: Curva característica del FSR utilizado para el sistema vestible.

Por lo general estos sensores necesitan de una linealización para poder utilizarlos correctamente en caso de que su rango dinámico sea amplio. Para esta aplicación no fue necesario realizar una linealización ya que al analizar el rango típico de operación del FSR, se logró apreciar que su respuesta ya era lineal en dicho rango (de $2k\Omega$ a $10k\Omega$). Un histograma con la distribución de la salida del sensor se puede apreciar en la figura 3.2. Ese histograma se ha realizado con los datos del protocolo experimental que se define en el apartado 3.1.3.

El sistema toma muestras a una frecuencia de 50Hz, es decir, una muestra

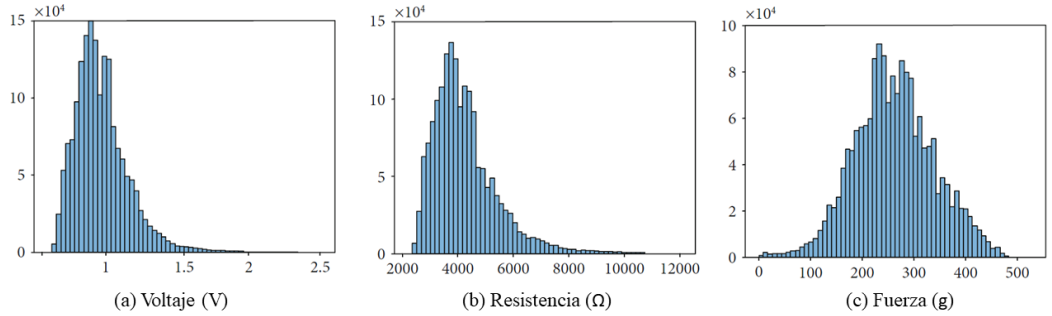

Figura 3.2: Histogramas con la distribución de voltaje (a), resistencia (b), y fuerza (c) de las señales capturadas.

cada 20ms, que es enviada mediante Bluetooth por el módulo correspondiente. El sistema fue diseñado para utilizarse como elemento dentro de un sistema basado en tecnologías móviles como *smartphones* y *tablets*. Sin embargo, también pueden utilizarse ordenadores para este fin. En la figura 3.3 se muestra un diagrama de bloques del funcionamiento del sistema.

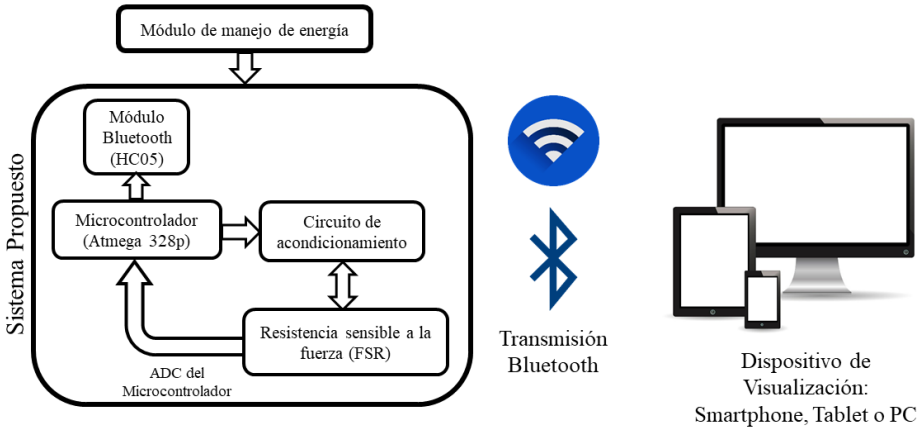

Figura 3.3: Diagrama de bloques del funcionamiento general del sistema desarrollado.

Los datos pueden visualisarse en tiempo real en una aplicación móvil, y a su vez los datos en crudo se van almacenando en un archivo de texto para su posterior análisis. En este trabajo los datos en crudo se analizan "offline" mediante MATLAB, aunque cualquier otro software para procesamiento numérico puede ser utilizado.

La confiabilidad de la transmisión de datos mediante Bluetooth también fue puesta a prueba. Se realizaron cuatro experimentos diferentes para comprobarlo, en los que un voluntario portó el sistema desarrollado y se mantuvo en movimiento, a diferentes distancias, alrededor del dispositivo de control seleccionado, en este caso, un ordenador. Las distancias a las que el usuario se colocó del dispositivo de monitorización fueron

1m, 3m, 5m y 10m. Cada experimento tuvo una duración de 30 minutos. No hubo pérdida significativa de datos transmitidos en ninguno de los experimentos realizados, obteniendo en promedio una pérdida de datos del 0.03 %, con desviación estándar de 0.01 %.

El armazón construido para el sistema fue diseñado con el software SolidWorks, y construido mediante impresión 3D. Se utilizaron dos materiales diferentes para su impresión, ácido poliláctico (PLA) rígido y PLA flexible. La parte que contiene todos los elementos del sistema (microcontrolador, módulo Bluetooth, módulo de carga, batería, y sensor FSR) fue impresa con PLA rígido. Para lograr transmitir hacia el sensor FSR los movimientos de la caja torácica debidos a la respiración, se utilizó PLA flexible. Dicha capa flexible se conectó al sensor FSR mediante un pivote encargado de transmitir los movimientos del pecho al sensor. En la figura 3.4 se muestran los diseños realizados para el armazón, siendo la Figura 3.4 (a) la parte impresa con PLA rígido, mientras que la figura 3.4 (b) muestra la parte impresa con PLA flexible (a excepción de las anillas, impresas con PLA rígido). En la figura 3.5 se muestra el interior de dicho armazón.

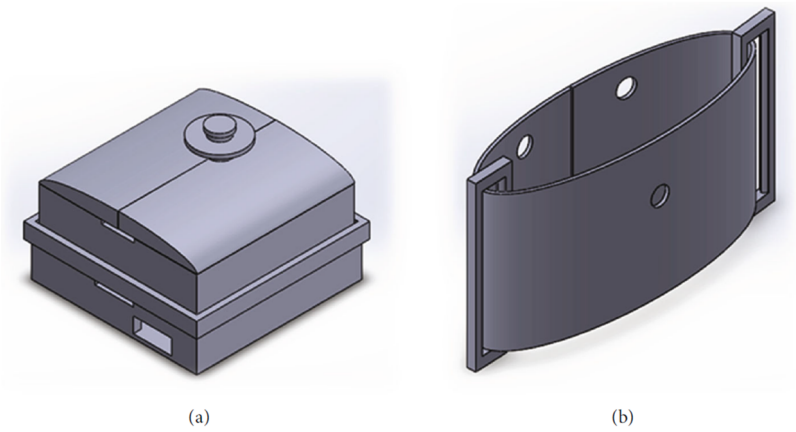

Figura 3.4: Diseño del armazón impreso en 3D, con material rígido (a) y material flexible (b).

El sistema construido se muestra en la figura 3.6. El sistema fue construido para ser utilizado encima de la ropa, aunque también puede usarse directo sobre la piel. Las dimensiones totales del sistema son 73mm de ancho, 45mm de alto, y 37mm de profundidad. El peso total del sistema es de 103g, de los cuales 21g pertenecen a los elementos electrónicos, 23g son del armazón rígido, y 59g son de la cinta utilizada para ajustar el sistema alrededor del pecho. El sistema desarrollado cuenta con diversas ventajas cuando se compara con dispositivos similares encontrados en la literatura [7, 200, 207–218]; las ventajas más destacables son una mayor velocidad de muestreo y la utilización de la tecnología inalámbrica Bluetooth (lo que permite utilizar

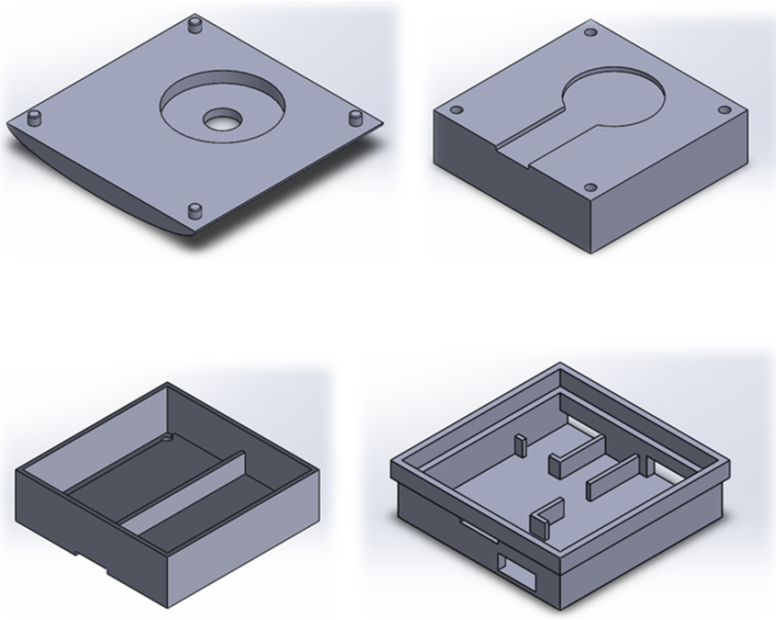

Figura 3.5: Diseño interior del armazón impreso en 3D.

diversas estaciones de monitorización que también cuenten con esta tecnología, como ordenadores, *smartphones* y *tablets*). Una comparativa de estos aspectos se muestra en el Anexo B.

Figura 3.6: Sistema vestible construido.

3.1.2. Procesado de datos

Para poder predecir correctamente el ritmo respiratorio de las señales obtenidas en crudo, en este trabajo los datos son procesados mediante MATLAB. Primero se utiliza un filtro paso-bajo digital con frecuencia de corte $F_c = 0{,}5Hz$ para eliminar

todo el ruido de alta frecuencia. Esta frecuencia de corte fue seleccionada ya que ritmos respiratorios superiores a 30BPM son raros en actividades de la vida cotidiana [219,220]. En concreto se utilizó un filtro de orden mínimo FIR o filtro de respuesta infinita al impulso (IIR) con atenuación de 60dB y compensación al retraso [221].

En las señales obtenidas, al reprresentarlas se observó un incremento o decremento sistemático en la señal (denominado "Bias" de aquí en adelante) ocasionado por el propio sensor o por movimientos de sus usuarios. Para minimizar el efecto que este Bias puede ocasionar sobre el desempeño de la predicción del ritmo respiratorio, se realizó un ajuste lineal a cada señal obtenida, tal y como se muestra en la Figura 3.7.

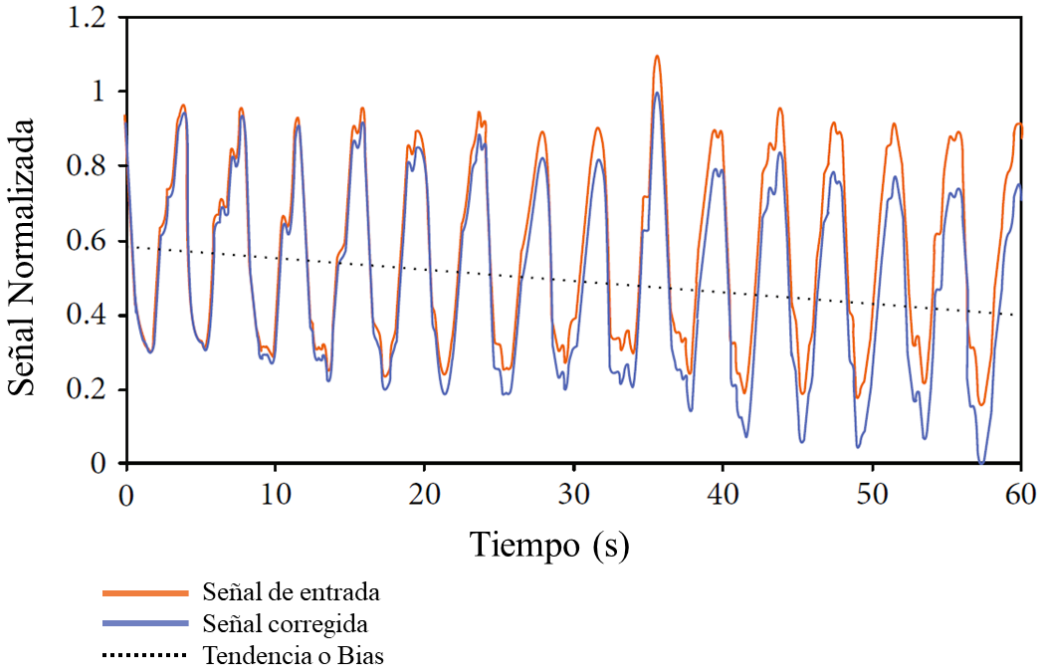

Figura 3.7: Comparación entre la señal original junto al efecto del Bias y la señal ajustada.

Para predecir el ritmo respiratorio de la señal, se propone un algoritmo que funciona basado en el método de cruces por cero o cruces por el origen. Primero se seleccionan los puntos máximos y mínimos de la señal en una ventana de tiempo (w) determinada. De esta forma, utilizando estos puntos se calcula el "eje cero"(ZA) de acuerdo a la siguiente ecuación:

$$ZA = \frac{min(x) + max(x)}{2} \tag{3.1}$$

La señal es segmentada según el valor de la ventana de tiempo w y cada segmento se analiza de forma individual; w se utiliza a lo largo de toda la señal. Para evitar que los valores máximos o mínimos se obtengan debidos a valores atípicos, alterando así el ZA, se detectan los valores pico con prominencia de al menos 0.03V. De esta forma, los valores pico $(max(x), min(x))$ que se utilizan serían la mediana de todos los

picos encontrados. El valor para este umbral de prominencia fue elegido tras mostrar el menor error entre simulaciones efectuadas con valores de 0.013V a 0.13V.

El eje ZA es el que se utiliza como referencia para detectar los cruces por cero. Para esto, del segmento de señal se toman muestras por pares consecutivos (x_k, x_{k+1}). Si una de las desigualdades (3.2) se cumple, entonces un nuevo cruce por cero será detectado y el tiempo $k \cdot (1/f_s)$ será agregado a un vector que contiene los cruces por cero de esa ventana de tiempo **(z)**; f_s es la frecuencia de muestreo del sistema que es de 50Hz.

$$\begin{aligned} x_k \leq ZA < x_{k+1} \\ x_k \geq ZA > x_{k+1} \end{aligned} \tag{3.2}$$

Para evitar detectar dos cruces por cero muy cercanos y provocados por el ruido, se propone un umbral mínimo de separación entre los cruces por cero. Es decir, si se cumple la desigualdad 3.3 (donde TH es el umbral, z_j y z_i son cruces por cero detectados consecutivamente) el cruce por cero en la posición j se eliminará. El valor de TH se ha propuesto de 500ms de forma empírica, bajo la suposición de que ninguna frecuencia respiratoria puede ocurrir en este lapso de tiempo.

$$|z_j - z_i| < TH \qquad \forall i \in [1, N] | i \neq j \tag{3.3}$$

Siendo N el número de cruces por cero detectados en la ventana w. Después de obtener el vector $\boldsymbol{z}$ con los cruces por cero, se proponen dos algoritmos diferentes para calcular el ritmo respiratorio promedio de la señal en cuestión. En la figura 3.8 se muestra un diagrama de bloques del funcionamiento de ambos algoritmos.

Algoritmo 1

El funcionamiento de este algoritmo se basa en la diferencia de tiempos entre cruces por cero consecutivos [212, 222]. La diferencia media de tiempo (MTD) entre pares consecutivos de cruces por cero se obtiene de la siguiente manera:

$$MTD = \frac{\sum_{i=1}^{N-1} |z_i - z_{i+1}|}{N-1} \tag{3.4}$$

Una vez obtenido dicho tiempo, el ritmo respiratorio se calcula en respiraciones por minuto (BPM) según la ecuación (3.5). Esta ecuación fue propuesta al tomar en cuenta que para cada ciclo de respiración deben ocurrir dos cruces por cero (dos MTD equivalen a una respiración) y que se desea obtener el ritmo respiratorio en respiraciones por minuto. Por lo tanto, si una respiración ocurre cada 2 MTD, entonces en 60 segundos debe haber 60/2MTD respiraciones.

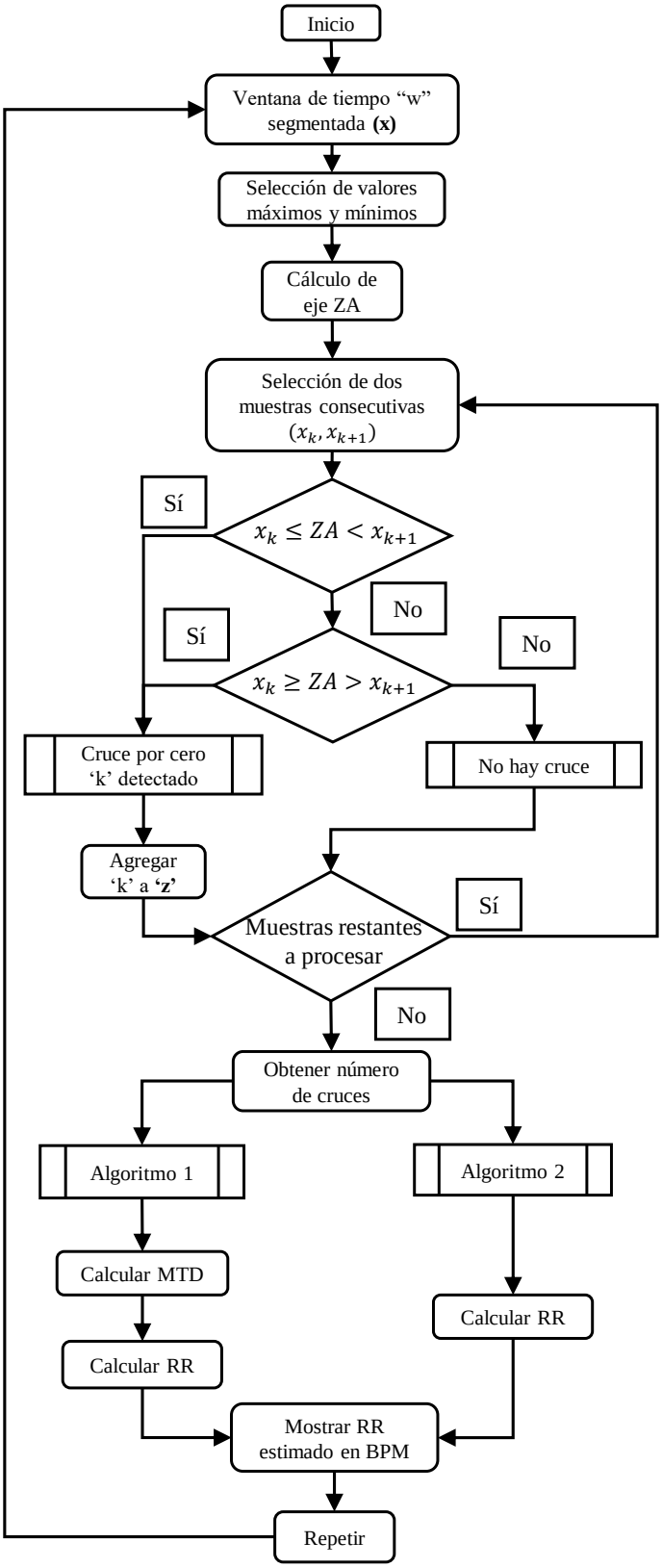

Figura 3.8: Diagrama de bloques de los algoritmos utilizados para predecir el ritmo respiratorio.

$$RR = \frac{30}{MTD} \tag{3.5}$$

Algoritmo 2

Este algoritmo predice el ritmo respiratorio en base al número de cruces por cero [223]. En este caso, se obtiene un vector $\boldsymbol{z}$ que tiene tantos elementos como número de cruces por cero detectados (N). Por lo tanto, el ritmo respiratorio se obtiene según la ecuación (3.6), donde w es la duración de la ventana de tiempo utilizada (en segundos). De nuevo, como hay un ciclo de respiración por cada dos cruces por cero, el resultado se divide entre dos. De esta manera, se realiza una proyección de las respiraciones por minuto basada en las respiraciones obtenidas en la ventana de tiempo utilizada.

$$RR = \frac{30N}{w} \tag{3.6}$$

Como sucede en el algoritmo 1, la ventana de tiempo (w) usada en los algoritmos es un parámetro que puede tomar cualquier valor (en segundos). El ritmo respiratorio se calcula una vez cada w, es decir, cada segmento de ventana de tiempo. Algoritmos similares a los presentados en este estudio han sido utilizados ampliamente en la literatura para el mismo fin [200, 201, 224, 225].

3.1.3. Marco experimental

Protocolo

Para validar el funcionamiento del sistema propuesto y la predicción acertada de los algoritmos, se propuso el marco experimental que se detalla en el siguiente apartado. En este experimento participaron 21 voluntarios, de los que quince fueron hombres y seis fueron mujeres, cuyas edades se encontraban en el rango de 19 a 55 años, con un promedio de 39.95 años y una desviación estándar de $\pm$10.5 años; mientras que el peso promedio variaba de 42 a 95kg, con un promedio de 70.76kg y una desviación estándar de $\pm$14.83kg. En cuanto a sus estaturas, estas se encontraban en el rango de 152 a 183cm, con un promedio de 172cm y una desviación estándar de $\pm$7.51cm.

Otra medida corporal que fue tomada en cuenta es el diámetro del pecho, que se encontraba en el rango de 68 a 103cm, con un promedio de 87.9cm y una desviación estándar de $\pm$12.36cm. En cuanto a su estado de salud, 16 voluntarios declararon no tener dolencia alguna, 5 sufrían de algún tipo de alergia respiratoria y 2 de ellos también padecían asma. No obstante, los voluntarios declararon que estos padecimientos no suponían problema alguno con el protocolo a realizar en este estudio. Todos los voluntarios dieron su consentimiento escrito. En la Tabla 3.1 se realiza una comparativa de estudios encontrados en la literatura que realizan una validación con sistemas vestibles para el monitoreo de la respiración, los cuales funcionan bajo el mismo principio que el sistema desarrollado: la detección de movimientos del pecho.

Tabla 3.1: Comparativa de protocolos de validación realizados por estudios cuyo sistema vestible se basa en la detección de movimientos del pecho.

Trabajo	Número de sujetos	Referencia utilizada	Análisis de datos	Actividades/ Posiciones
Padasdao [217]	20	Espirómetro	Análisis de Bland-Altman	Sentado, parado, caminando
Hoffmann et al. [7]	18	Pneumotacógrafo	Factor de correlación, error relativo	Caminando
Min et al. [212]	16	Biopack MP150 Termistor nasal TSD202A	Análisis de Bland-Altman, coeficiente de correlación	Sentado
Rotariu et al. [208]	10	No especificado	No especificado	Simulación de sueño
De Jonckheere et al. [214]	10	Monitor ECG Philips Intellivue MP50, y monitoreo manual	Análisis de Bland-Altman	Acostado
Hesse et al. [207]	5	Sistema CORTEX Metalyzer para Ergospirometría	No especificado	Caminando
Grlica et al. [210]	4	No especificado	No especificado	No especificado
Teichman et al. [218]	4	Flujómetro TSI 4040	No especificado	Sentado, parado
Witt er al. [213]	1	Espirómetro	Comparación visual	No especificado
Yang et al. [216]	1	Sistema de espirometría, y monitoreo manual	No especificado	Sentado, parado
Ciobotariu et al. [209]	No especificado	No especificado	No especificado	No especificado
Yang et al. [211]	No especificado	No especificado	No especificado	No especificado

Para el protocolo de evaluación del sistema, lo primero que se hizo fue colocar el sistema desarrollado alrededor del pecho a cada voluntario. El sistema se colocó debajo de los pectorales, justo frente al diafragma, como se muestra en la figura 3.9. Una vez hecho esto, el sistema fue conectado via Bluetooth a un ordenador y la captura de datos en crudo se realizó mediante una aplicación desarrollada en el ambiente de desarrollo Processing.

Figura 3.9: Dos voluntarios portando alrededor del pecho el sistema desarrollado.

En cuanto al protocolo realizado por los voluntarios, a cada uno se le pidió respirar durante un minuto a diferentes ritmos determinados mediante un metrónomo. En concreto, el metrónomo se ajustó para ritmos respiratorios de 10, 12.5, 15, 17.5, 20, y 22.5BPM. En la literatura hay varios trabajos previos que utilizan un metrónomo como sistema de referencia [222,224,226–229]. Estos valores de ritmo respiratorio fueron propuestos ya que se encuentran dentro del rango de respiración normal en los seres humanos [230]. Se pidió a los voluntarios repetir estos seis ritmos respiratorios en cinco posiciones diferentes, que fueron: sentados sin movimiento, sentados con movimiento, parados sin movimiento, parados con movimiento y caminando. Se otorgó un periodo de descanso de un minuto entre experimentos.

Para cada experimento, se creó un archivo de texto con los datos en crudo de las señales de respiración obtenidas, dando lugar a un total de 30 archivos diferentes por voluntario (6 ritmos respiratorios por 5 posiciones). En la Figura 3.10 se muestran dos ejemplos de las señales obtenidas de los datos en crudo.

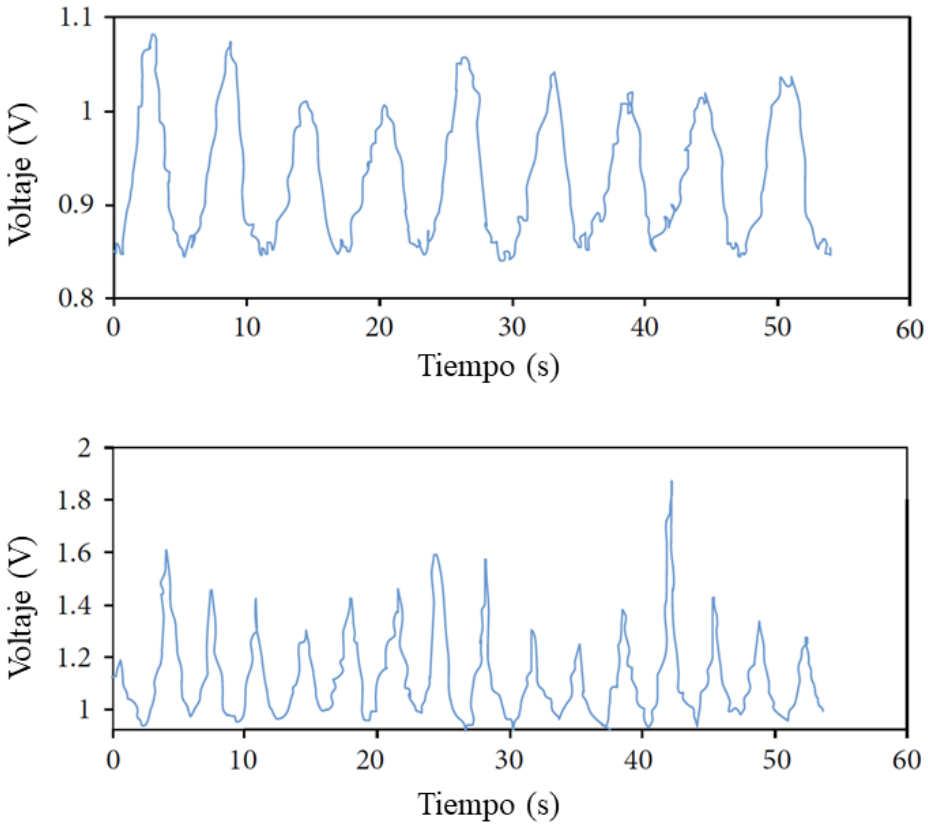

Figura 3.10: Ejemplo de dos señales diferentes obtenidas por medio del sistema vestible, la gráfica superior se obtuvo de un ritmo respiratorio de 10BPM en una posición sentada y sin movimiento, mientras que la gráfica inferior se obtivo a 17.5BPM mientras el sujeto caminaba.

De esta manera, un total de 630 archivos de respiración se obtuvieron de los experimentos realizados. Los datos fueron procesados "offline" mediante MATLAB

y con cada uno de los algoritmos descritos anteriormente.

Como se muestra en la Figura 3.10 las señales de respiración comparten cierta semejanza con las señales sinusoidales. Debido a la naturaleza del propio sistema desarrollado, la señal cuasi-sinusoidal muestra una pendiente negativa cuando el usuario inspira, y una pendiente positiva cuando el usuario expira.

Validación de los experimentos

Una vez obtenidas todas las señales de respiración, estas fueron evaluadas con los dos algoritmos mencionados en la sección 3.1.2. Cada algoritmo calcula el ritmo respiratorio medio de la señal completa. La respuesta obtenida de cada algoritmo se ve influenciada por el tamaño de la ventana de tiempo elegida. Es por esto que el análisis de las señales se hizo con 25 ventanas de tiempo diferentes, variando desde 6 hasta 30 segundos, en pasos de 1 segundo. Ventanas de tiempo menores a 6 segundos no fueron consideradas ya que el ritmo respiratorio con la menor frecuencia obtenida tiene un periodo de 6 segundos. Ventanas de tiempo mayores a 30 segundos no fueron consideradas ya que, como se mencionó anteriormente, como el ritmo respiratorio calculado por los algoritmos se actualiza dependiendo del tamaño de la ventana de tiempo, actualizaciones con tiempo mayor a 30 segundos sería excesivo para muchas aplicaciones [231–233]. Por lo tanto, se realizaron un total de 15.750 predicciones de ritmo respiratorio con cada uno de los algoritmos.

Para obtener la ventana de tiempo óptima, se realizó la prueba-t para una muestra. La hipótesis nula (H_0) sería la siguiente:

$$H_0 : m = \mu \tag{3.7}$$

en donde m es el ritmo respiratorio medio y μ es el valor de referencia de los BPM marcados por el metrónomo. Esta prueba fue realizada para cada valor de la ventana de tiempo, y para todos los valores de referencia del metrónomo, para un total de 150 pruebas diferentes.

De estas pruebas se identificaron aquellas cuyo valor "p" fuera mayor al nivel de significancia (0.05). En pruebas que cumplieran este criterio, la hipótesis nula no podría ser rechazada, es decir, los valores obtenidos de las predicciones de los algoritmos no eran significativamente diferentes a los valores de referencia (del metrónomo). Las ventanas de tiempo cuyo valor p fuera mayor a 0.05 pueden ser consideradas como candidatas a la ventana óptima, para las cuales se puede realizar la "prueba d de Cohen" para cuantificar el tamaño del efecto [234].

También se calculó el error relativo (δ) de acuerdo a la ecuación:

$$\delta = 100 * |1 - \frac{\mu_0}{\mu}| \tag{3.8}$$

en donde μ_0 es la predicción realizada por los algoritmos y μ es el valor de referencia del metrónomo. Para evaluar el desempeño de cada algoritmo, se calculó el error medio para cada ventana de tiempo propuesta (todas las actividades y todos los valores de referencia), es decir, para cada algoritmo se calcularon 25 errores medios.

Para determinar el mejor algoritmo para la ventana de tiempo óptima, se realizó una "prueba t pareada". Esta prueba fue realizada sobre los errores relativos medios (δ) y la hipótesis nula (H_0) en este caso sería:

$$H_0 : m = 0 \tag{3.9}$$

en donde "m" es la media de las diferencias. Si el valor p es menor o igual que el nivel de significancia (0.05) se puede asumir que ambas muestras (el error de los algoritmos) son significativamente diferentes, y en ese caso el algoritmo con menor error se puede considerar como el mejor. En la Figura 3.11 se muestra un esquema de los experimentos de validación realizados.

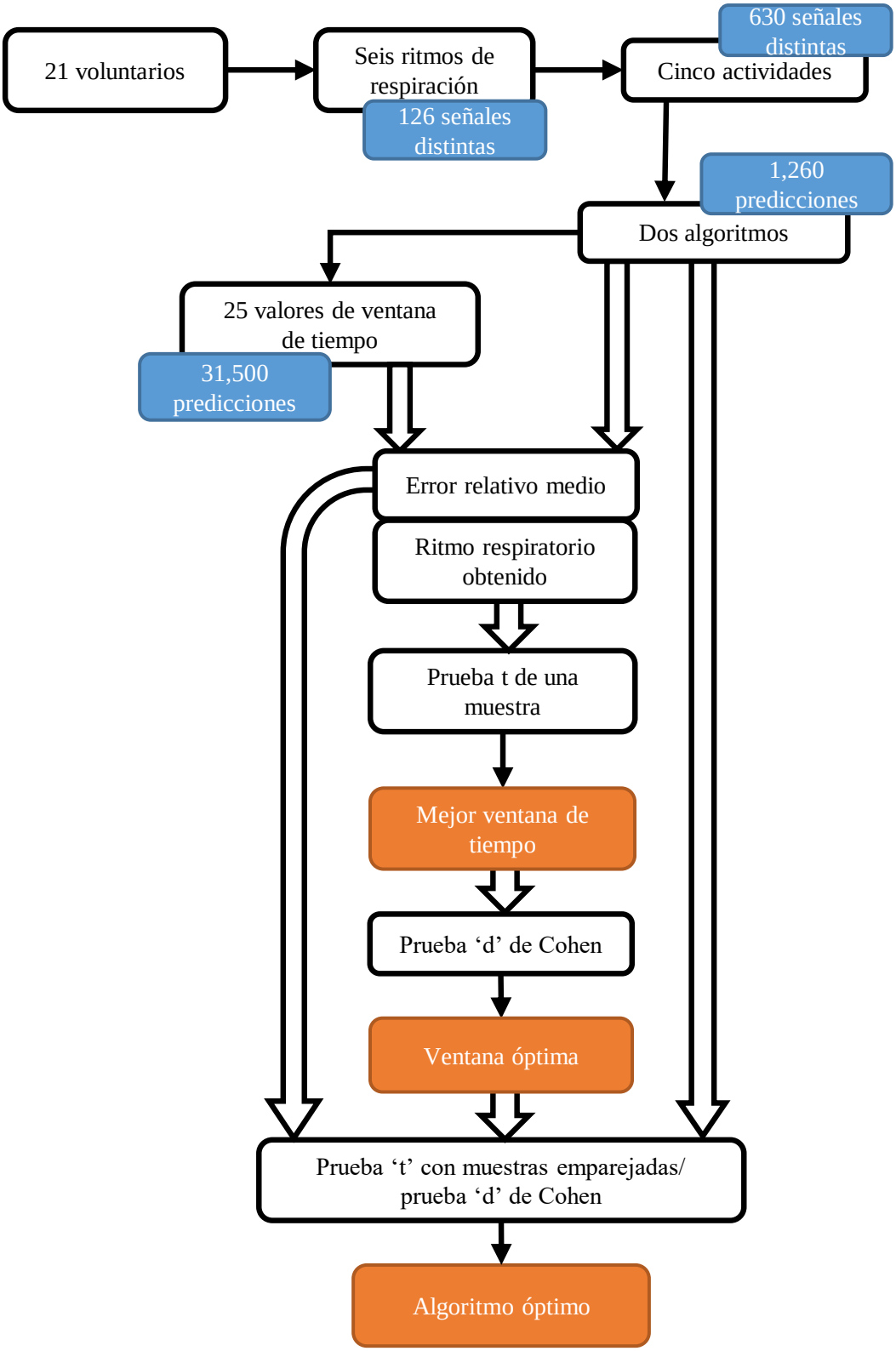

Figura 3.11: Esquema de los experimentos de validación.

3.2. Sistema ambiental para medición del salto vertical

En esta sección se describe cómo se construyó el sistema ambiental para medir el salto vertical [235]. Los objetivos de este trabajo son:

Objetivo general

- Desarrollar un sistema ambiental capaz de medir la altura del salto vertical efectuado por el usuario, que sea más económico que los sistemas comerciales del mercado y sea fácil de construir.

Objetivos específicos

- Validar el funcionamiento del sistema desarrollado frente a un sistema de referencia utilizado comúnmente en la literatura.

- Comprobar los efectos sobre las mediciones calculadas al variar la frecuencia de muestreo del sistema para detectar la frecuencia de operación mínima a la que el sistema sigue midiendo la altura del salto vertical con precisión.

3.2.1. Desarrollo del sistema

La idea de utilizar una malla resistiva para registrar el salto vertical en adultos mayores resultó tanto de un trabajo previo realizado en el grupo de investigación en el que se desarrolló una malla resistiva sensible a la presión [236] como de la propuesta de un médico del deporte para desarrollar un sistema para medir el salto vertical. Considerando esta malla desarrollada y al investigar en la literatura, se observó el potencial de utilizar esta malla para dichos fines, ya que la malla posee una mayor resolución y velocidad de muestreo que otros sistemas en la literatura [17, 18, 121]. Además, esta malla presenta una ventaja competitiva para este fin ya que muchos estudios optan por utilizar alternativas comerciales de alto coste [19, 21, 120, 123, 199].

El sistema desarrollado está compuesto de dos partes: una alfombrilla resistiva sensible a la presión construida con un arreglo de sensores FSR, a través del material piezorresistivo velostat, y el sistema electrónico. La alfombrilla se compone de tres capas. Una capa contiene alambres de cobre planos distribuidos en un arreglo de columnas a lo largo de una superficie cuadriculada flexible impresa en 3D; de la misma manera, otra capa está compuesta de alambres de cobre planos distribuidos en un arreglo de filas también sobre una superficie cuadriculada flexible. Una tercera capa de material Velostat se coloca entre ambas capas. El Velostat es un material sensible a la

presión y se comporta como una resistencia cuyo valor baja cuando se ejerce presión sobre el material. De esta manera, las intersecciones de filas y columnas se comportan como sensores FSR individuales cuando se ejerce presión sobre la alfombrilla. Algunos problemas característicos del Velostat son su falta de repetibilidad, no-linealidad e histéresis [237, 238]. No obstante, estas cualidades del material no afectan al propósito de esta aplicación en específico, ya que en principio solo se necesita detectar cuerpos pesados sobre la alfombrilla (peso humano promedio).

En la figura 3.12 se muestran las diferentes capas de una matriz de sensores FSR desarrollada con menores dimensiones (4 columnas, 4 filas). La figura 3.13 muestra cómo se colocan las diferentes capas de la alfombrilla. El área total de medición de la alfombrilla utilizada para este estudio es de 30x30cm, y se compone de 16 columnas y 16 filas, cada una de 1cm de espesor. De esta manera, el área total de cada sensor FSR individual es de $1cm^2$. En la figura 3.14 se muestra una de las alfombrillas desarrolladas en el grupo de investigación.

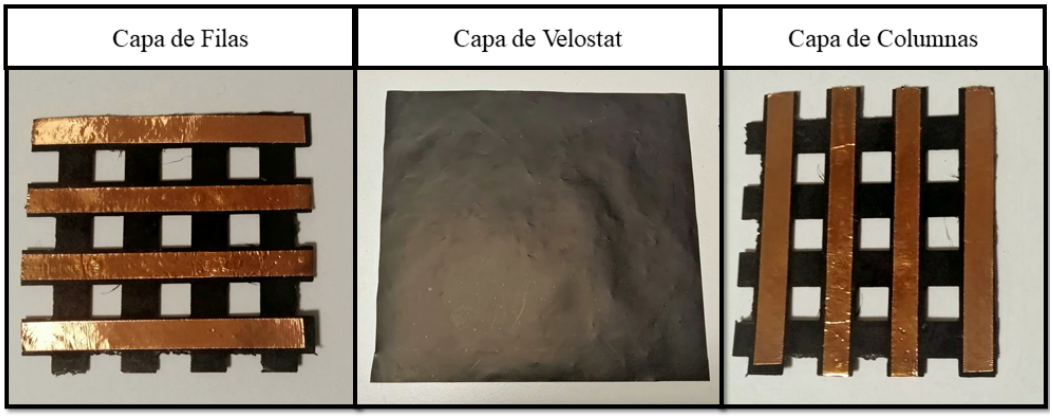

Figura 3.12: Diferentes capas que componen la matriz de sensores FSR (alfombrila) de menores dimensiones.

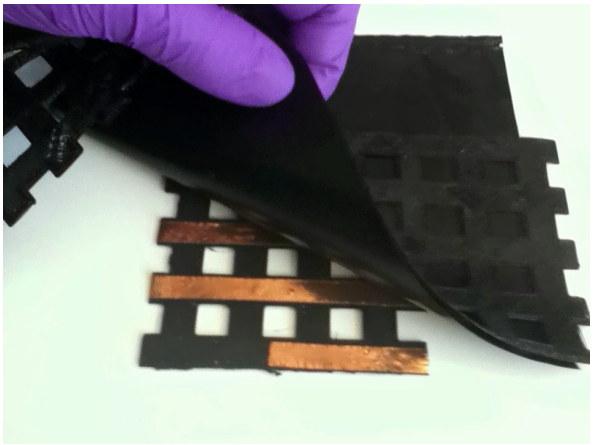

Figura 3.13: Ejemplo de una matriz de sensores FSR de menores dimensiones, y cómo son colocadas sus capas.

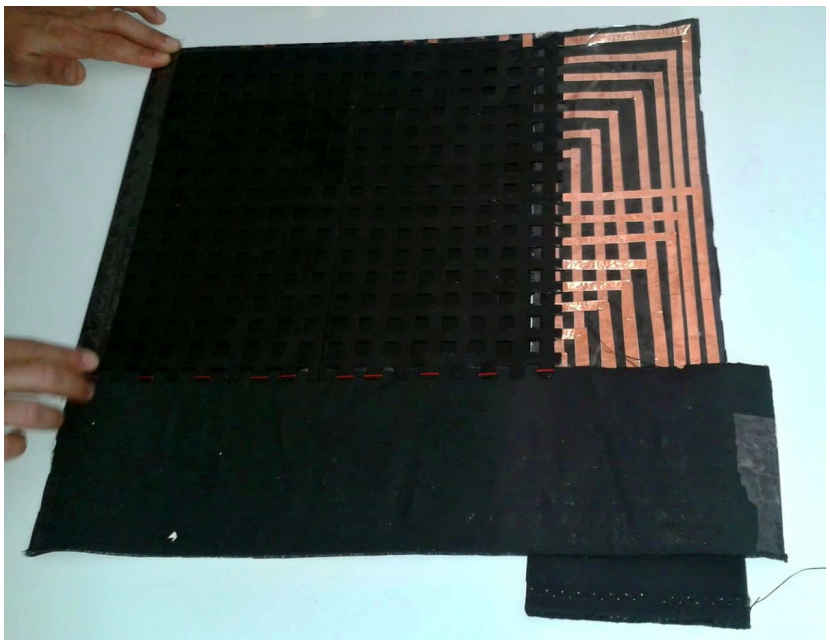

Figura 3.14: Ejemplo de una de las alfombrillas desarrolladas por el grupo de investigación.

Para el procesamiento de datos, debido al número de operaciones necesarias para hacer un barrido completo de la alfombrilla, se necesita utilizar un microcontrolador de alta frecuencia, ya que el tiempo de procesado va asociado a la complejidad de dichas operaciones y crece en orden exponencial [239]. Por lo tanto, el microcontrolador STM32F103C8T6 fue elegido debido a su CPU con frecuencia de operación de 72MHz, con el cual se logró alcanzar una frecuencia de muestreo de 200Hz. Otros microcontroladores con menor frecuencia de muestreo, como el Atmega 328p, no podrían alcanzar una tasa de muestreo tan alta para esta aplicación. De igual forma, se utilizaron dos multiplexores 16-1 (74HC4067) para un barrido eficiente de la alfombrilla. Para la transmisión de datos se eligió hacerlo mediante tecnología Bluetooth, siendo el módulo HC05 el utilizado. Se optó por tecnología Bluetooth dada su facilidad de conexión con diferentes dispositivos, en especial con tecnologías móviles como los *smartphones* y *tablets*, que ofrecen al profesional de la salud la opción de elegir el sistema de visualización a su elección y que además son fáciles de transportar. Otros componentes electrónicos del sistema son: un módulo de carga de batería TP4056, y una batería LiPo con capacidad de 3.7V y 150mAh, permitiendo un uso continuo del sistema por alrededor de dos horas. Como este es un sistema ambiental, la portabilidad no es un elemento crucial, por lo cual la batería puede ser sustituida por una de mayor capacidad para así prolongar el tiempo de funcionamiento continuo. En el Anexo G se muestra el circuito esquemático diseñado y las dos versiones de la PCB desarrolladas. La diferencia entre un diseño y otro radica principalmente en la distribución de los componentes y en utilizar diferentes versiones de los mismos elementos que variaban

principalmente en sus dimensiones. Un diagrama de bloques del funcionamiento de este sistema se muestra en la figura 3.15.

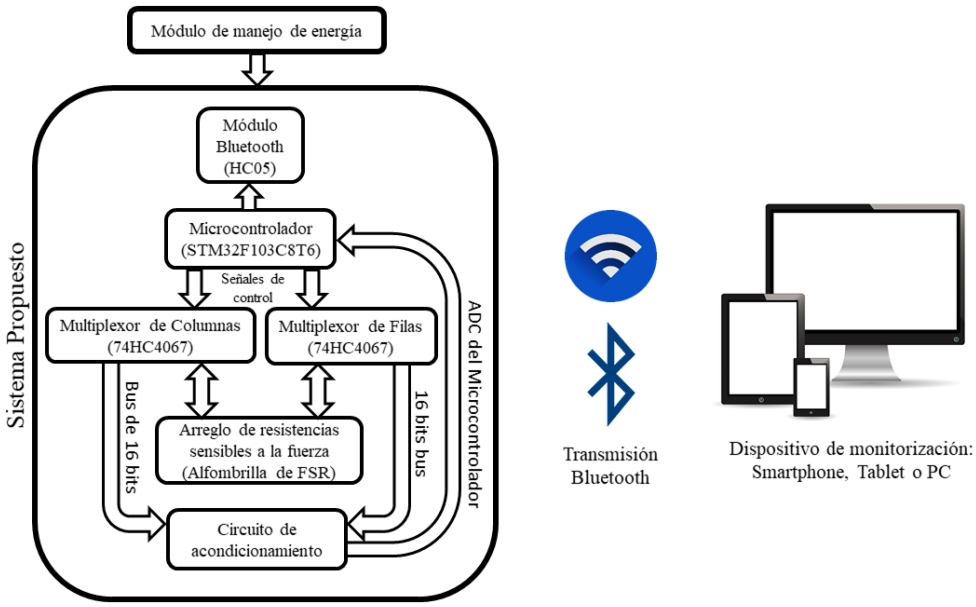

Figura 3.15: Diagrama de bloques del funcionamiento del sistema propuesto.

3.2.2. Procesado de datos

El algoritmo utilizado por el sistema se basa en calcular el sumatorio de cada uno de los valores obtenidos por los sensores FSR individuales de la alfombrilla. De cada sensor FSR se obtiene un valor de voltaje, que es medido por el ADC del microcontrolador en forma de bits (de 0 a 4095 bits), y dicho valor obtenido es utilizado para realizar los cálculos correspondientes. Se utiliza un umbral para determinar si una persona se encuentra parada sobre la alfombrilla. Para proponer un valor apropiado para este umbral, se recolectaron los datos de 16 voluntarios (5 mujeres y 11 hombres), con un peso promedio de $74{,}81 \pm 15{,}25kg$ y un tamaño de pies de $26{,}93 \pm 1{,}94cm$. Se pidió a los voluntarios que se pararan sobre la alfombrilla descalzos y en cuatro posturas diferentes: parados con ambos pies, de puntillas con ambos pies, parados con un solo pie y de puntillas con un solo pie. Los datos obtenidos se normalizaron considerando el porcentaje de sensores FSR activados.

Utilizando este criterio, en promedio, al pararse sobre la alfombrilla con ambos pies, se logró una activación del 71.66 % de los sensores FSR; mientras que al pararse de puntillas con ambos pies se logró una activación del 28.9 % de los sensores. Por otra parte al pararse sobre la alfombrilla únicamente con un pie y de puntillas sobre un pie se logró una activación del 40.37 % y del 18.40 % de los sensores para cada posición, respectivamente. El valor mínimo de activación de los sensores FSR ocurrió con un

voluntario parado sobre un solo pie y de puntillas, alcanzando un valor de 12.09 % de activación de los sensores. Estos resultados pueden verse en la tabla 3.2.

Tabla 3.2: Valores normalizados de activación de los sensores FSR, registrados de los voluntarios al pararse sobre la alfombrilla en diferentes posiciones: de pie y de puntillas con ambos pies, de pie y de puntillas con un solo pie.

Activación de sensores	**Ambos pies**		**Un pie**	
	Parado	**Puntillas**	**Parado**	**Puntillas**
Promedio	71,66 %	28,90 %	40,37 %	18,40 %
Máximo	100,00 %	43,31 %	61,45 %	27,00 %
Mínimo	44,00 %	23,70 %	22,64 %	12,09 %

Si se asume que los voluntarios pueden despegar o aterrizar en la alfombrilla de puntillas con solo un pie al momento de saltar, se debe proponer un umbral apropiado que se encuentre por debajo del valor mínimo de activación de sensores FSR registrado. Para este estudio, se utilizó un umbral del 9 % de activación de sensores FSR. Este umbral se eligió por encontrarse a tres cuartas partes entre el valor mínimo registrado de activación de sensores y el valor de ningún sensor activado, para así evitar cualquier error de lectura debido a oscilaciones mecánicas en el sistema. Cabe destacar que el valor mínimo que se registró de la activación de sensores es un valor atípico. Para trabajos futuros, se plantea la posibilidad de agregar un valor de umbral personalizado para cada usuario del sistema desarrollado.

Para cada porcentaje de activación de sensores obtenido, se realizó un análisis de correlación con el peso y el tamaño de los pies de los voluntarios. Estos análisis sugieren que la activación de sensores FSR de la alfombrilla solo se ve moderadamente afectada por el peso de los voluntarios, mientras que el tamaño de sus pies tiene poco impacto en la activación de los sensores. En la Tabla 3.3 se muestran los valores de correlación obtenidos de las diferentes posiciones analizadas.

Tabla 3.3: Valores de correlación de Pearson (valores R) obtenidos de las diferentes posiciones analizadas, que fueron calculados tanto para peso como para el tamaño del pie de los voluntarios.

Posición		**Peso**	**Tamaño de pie**
Ambos pies	**Parado**	-0,684	-0,522
	Puntillas	-0,411	-0,241
Un pie	**Parado**	-0,447	-0,397
	Puntillas	-0,394	-0,463

Finalmente, el cálculo de la altura alcanzada por los voluntarios durante el salto vertical se realiza del siguiente modo: cuando el voluntario salta y deja de estar en contacto con la alfombrilla, el sistema comienza a contar el tiempo que transcurre hasta que el voluntario aterriza de nuevo (tiempo de vuelo o FT), y una vez calculado

este tiempo, se utiliza la fórmula de FT para predecir la altura alcanzada [18, 117, 118, 120, 121]. Dicha fórmula se define como:

$$Altura = \frac{g\Delta t^2}{8} \tag{3.10}$$

en donde g es la constante de la fuerza de gravedad $g = 9{,}81 m/s^2$ y Δt es el valor del FT medido por el sistema. Una vez que el sistema ha calculado el valor de la altura alcanzada por el usuario, este valor se envía por Bluetooth al dispositivo de seguimiento elegido por el profesional de la salud.

3.2.3. Marco experimental

Protocolo

Se propusieron dos experimentos para validar el funcionamiento del sistema. El primer experimento se propuso para validar la precisión en la medida del salto vertical por parte del sistema, en el cual participaron 38 voluntarios. El segundo experimento se realizó para ver los efectos sobre las alturas calculadas por el sistema al variar la frecuencia de muestreo. En este experimento participaron 15 voluntarios. En ambos experimentos se realizó el mismo protocolo para capturar los datos. La diferencia entre ambos es que, en el primer experimento, el sistema calcula directamente la altura alcanzada por el voluntario, y ese valor se envía a la estación de monitorización seleccionada. En el segundo experimento el sistema envía directamente a la estación de control los datos en crudo obtenidos de la alfombrilla de sensores FSR, y de esta forma se realiza un submuestreo de dichos datos "offline", para así emular diferentes frecuencias de muestreo.

Para la realización de estas pruebas se trabajó en colaboración con un "Centro de Salud y Deportes" en el que se practican diversas actividades como musculación, entrenamiento funcional, ciclismo indoor y Taekwondo (dependiendo de la actividad realizada es el requisito mínimo de edad). Todos los voluntarios dieron su consentimiento escrito para realizar el protocolo propuesto. En cuanto al tipo de salto realizado durante el protocolo se eligieron dos técnicas, el salto con contramovimiento (CMJ) y el salto con contramovimiento y braceo (CMJAS). Estas técnicas de salto se suelen utilizar para evaluar la fuerza en general y la fuerza explosiva en los músculos de las piernas en particular [240], y a su vez éstas se consideran las pruebas más confiables para dicho propósito [241]. Al agregar el braceo al CMJ, con una técnica adecuada se puede incrementar la altura del salto de un 33 % a un 66 % [242–244], lo que incrementa el rango dinámico de las alturas obtenidas de los saltos.

El protocolo propuesto a los voluntarios fue el siguiente. Se les pidió que se

pararan sobre la alfombrilla en una marca colocada en el centro, y una vez parados ahí, efectuaran tres saltos CMJ con sus manos fijas en la cintura y con un esfuerzo medio-máximo. Entre cada salto, se otorgó un descanso de 5 a 10 segundos. En la figura 3.16 se muestra esta técnica.

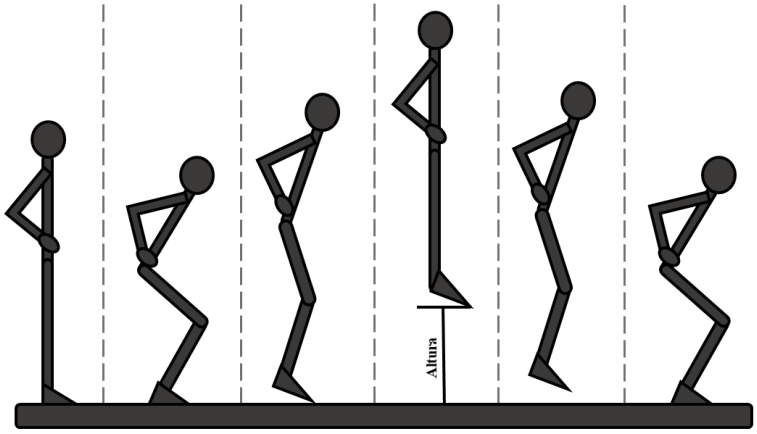

Figura 3.16: Técnica para el salto con contramovimiento (CMJ), ilustrado paso a paso.

Después de esto, a los voluntarios se les pidió realizar saltos CMJAS, siguiendo el mismo esquema. Esta técnica se detalla en la figura 3.17.

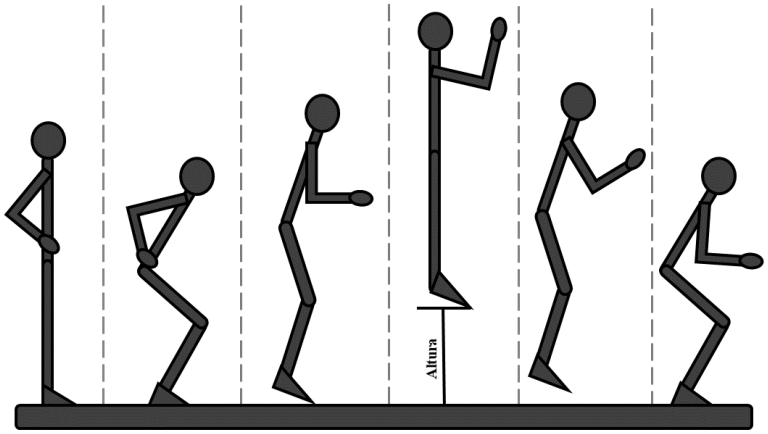

Figura 3.17: Técnica para el salto con contramovimiento y braceo (CMJAS), ilustrado paso a paso.

Como sistema de referencia durante los experimentos, se grabaron todos los saltos mediante una cámara de alta velocidad (120fps). La cámara se colocó a 1.3m de distancia de la alfombrilla, perpendicular al plano sagital del voluntario, y a 20cm del suelo sostenida sobre un trípode. En la Figura 3.18 se aprecia la configuración descrita.

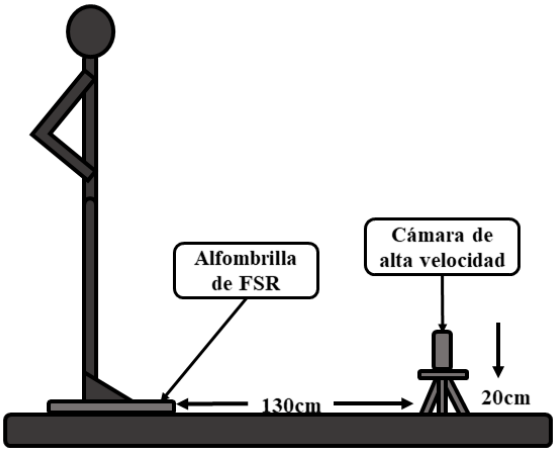

Figura 3.18: Ubicación de todos los elementos durante la ejecución del protocolo propuesto.

Validación de los experimentos

Para medir la altura alcanzada por los sujetos utilizando la cámara de referencia, se utilizó el método validado por Balsalobre-Fernández et al. [119,122], en el que deben seleccionarse de manera manual los cuadros de despegue y aterrizaje de cada salto efectuado. De esta forma, se calcula el tiempo transcurrido entre ambos cuadros y mediante la fórmula de FT se obtiene la altura alcanzada.

El error relativo (δ) se calcula mediante la ecuación 3.8, en donde μ_0 es la altura calculada por el sistema ambiental y μ es la altura calculada mediante la cámara de referencia.

Para el primer experimento se calcula el error relativo medio de todos los saltos y de cada técnica invidualmente (CMJ y CMJAS). Para el segundo experimento se calcula el error relativo medio así como los valores máximo y mínimo de error obtenidos de cada frecuencia de muestreo evaluada.

Capítulo 4

Resultados

En este capítulo se muestran los principales resultados obtenidos de cada uno de los sistemas desarrollados, así como una discusión de otras observaciones que vale la pena destacar para cada sistema.

4.1. Sistema vestible para respiración

4.1.1. Resultados

En la figura 4.1 se muestra el error relativo medio para las veinticinco ventanas de tiempo diferentes analizadas en este estudio para los dos algoritmos utilizados para predecir el ritmo respiratorio.

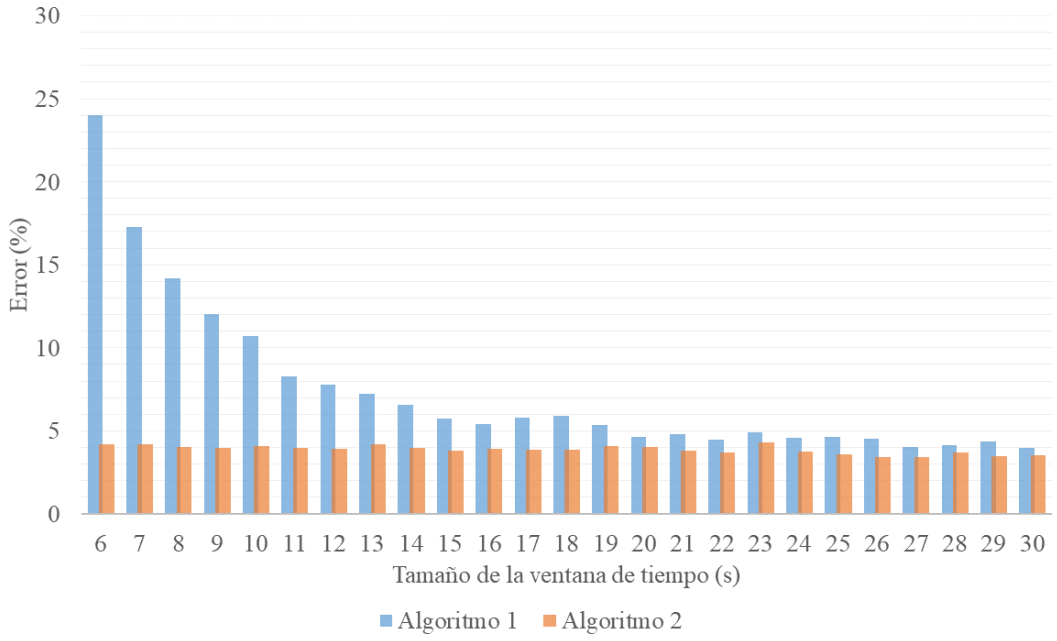

Figura 4.1: Errores relativos δ obtenidos de las predicciones de los dos algoritmos utilizados.

Al obtener los valores p de la prueba t para muestra única se puede concluir que la

ventana de tiempo de 27 segundos es aquella que podemos considerar como la óptima, ya que los valores obtenidos entre las predicciones de los algoritmos y la referencia se pueden considerar iguales. La comparativa de los valores p se puede observar en la tabla F.1 del Anexo F. De la prueba-t emparejada no se pudo concluir cuál de los dos algoritmos resultó mejor, ya que ambos muestran un comportamiento similar (tabla F.2 del Anexo F).

4.1.2. Discusión

A pesar de que la figura 4.1 muestra que el algoritmo 2 tiene un error relativo menor, esto no significa que la diferencia sea estadísticamente significativa. Ambos algoritmos se ven afectados por el tamaño de la ventana de tiempo elegida.

De las pruebas realizadas en las mediciones obtenidas, se pudo concluir que la ventana de tiempo de 27 segundos es la óptima para ambos algoritmos para así obtener una mayor precisión. También cabe destacar que esta ventana de tiempo muestra valores pequeños de desviación estándar, lo que indica bajos niveles de dispersión entre los datos. Sin embargo, a pesar de que una ventana de 27 segundos indica ser la óptima para una predicción más acertada del ritmo respiratorio, existen otras ventanas de tiempo que ofrecen un desempeño similar y un menor tiempo de actualización de las predicciones (i.e. ventanas de 16 a 20 segundos).

Para el algoritmo 1 se puede destacar que las ventanas de tiempo más cortas tienen mayores errores relativos, y esto se debe al propio error estructural que introducen las ventanas que no son múltiplo entero del número de respiraciones por minuto evaluadas, así como al propio error de muestreo. Este error esta cuantificado en este artículo [27]. Por otra parte, las ventanas de tiempo entre 20 y 30 segundos muestran un desempeño similar.

Finalmente, de los resultados obtenidos se puede observar que el sistema vestible desarrollado puede predecir el ritmo respiratorio con un error medio del 3,40 %. Sin embargo, esto se puede concluir en base a los algoritmos utilizados para predecir el ritmo respiratorio. Si se utilizaran otros algoritmos para este fin, el error medio obtenido de todas mediciones bien podría incrementarse o disminuir. Por lo tanto, podemos concluir que las señales respiratorias obtenidas tienen suficiente calidad y resolución como para aplicar algoritmos de procesado sobre ellas.

4.1.3. Efecto de las tendencias en las señales de respiración

Ya que se contaba con la base de datos de las diferentes señales de respiración [245], se dispuso a hacer una comparativa en los ritmos respiratorios calculados por

ambos algoritmos una vez que se retiraron las "tendencias" de las señales [246]. Estas "tendencias" se definen como un aumento o descenso sistemático registrado en la señal debido a movimientos del sistema o de los usuarios. A estas señales se les puede aplicar un ajuste lineal de manera "offline" con el objetivo de reducir cualquier efecto negativo que las tendencias puedan producir [247].

Se utilizaron dos métodos para eliminar las tendencias de la señal original. En el primer método se realizó el ajuste lineal a la señal de respiración completa, mientras que con el segundo método la señal de respiración se segmentó en ventanas desde 6 hasta 30 segundos, y a cada segmento de manera individual se le realizó el ajuste lineal. En la figura 4.2 se muestra de forma gráfica cómo funciona cada método.

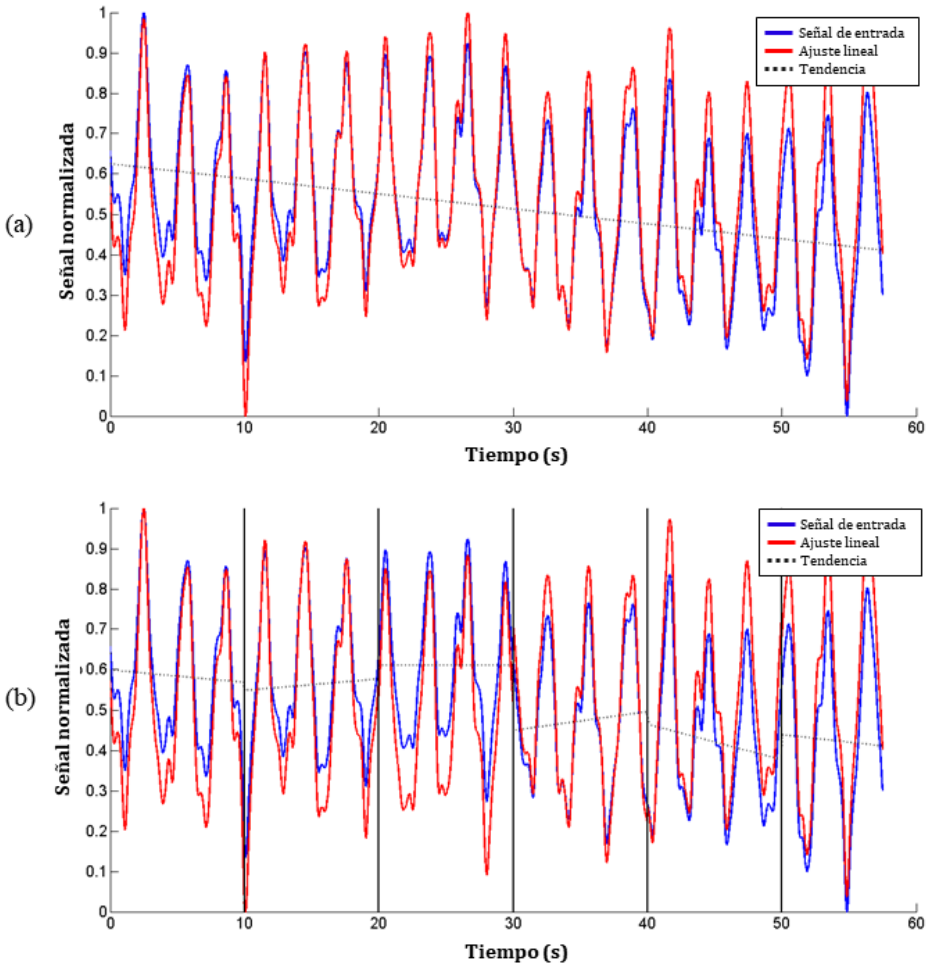

Figura 4.2: Técnicas de ajuste lineal utilizadas: (a) Método 1: Ajuste lineal aplicado a la señal completa; (b) Método 2: Ajuste lineal aplicado de forma individual a cada ventana de tiempo segmentada.

Tras eliminar las tendencias de las señales de respiración se utilizaron los mismos algoritmos descritos en la sección 3.1.2 para calcular el ritmo respiratorio.

Con el primer método de ajuste lineal y el algoritmo 1, la ventana de segmentación de 6 segundos muestra un incremento en el error relativo del 5,46 %, mientras que

para el resto de ventanas el error relativo disminuye. Por lo tanto, al realizar el ajuste lineal de esta manera, con el algoritmo 1 se encontró una mejora (disminución del error relativo) del 1,08 % en el ritmo respiratorio calculado, mostrando una mejora máxima del 2,52 % (ventana de 11 segundos) y un deterioro (incremento en el error relativo) máximo del 5,46 % (ventana de 6 segundos). Con el algoritmo 2 solo las ventanas de 12 a 15 segundos muestran un deterioro en el ritmo respiratorio calculado; también se encontró una mejora promedio del 0,48 %, con una mejora máxima del 1,78 % para la ventana de 30 segundos, y un deterioro máximo del 0,55 % para la ventana de 13 segundos.

Al utilizar el segundo método de ajuste lineal, y aplicando el algoritmo 1, se encontró en promedio una mejora del 1,54 %, con una mejora máxima del 3,19 % con la ventana de 11 segundos, y un máximo deterioro del 3,58 % para la ventana de 6 segundos. Con el algoritmo 2, solo las ventanas de 6 a 8 segundos muestran un deterioro en el ritmo respiratorio calculado con respecto a la señal sin ajuste lineal. También se encontró en promedio una mejora del 1,28 %, encontrando una mejora máxima del 2,88 % en la ventana de 30 segundos, y un deterioro máximo del 2,35 % en la ventana de 6 segundos. Todos estos resultados se muestran en la tabla 4.1. En la figura 4.3 y la figura 4.4 se muestran las mejoras y los deterioros obtenidos en cada ventana de segmentación para el primer y segundo métodos de ajuste lineal, respectivamente.

Tabla 4.1: Mejora en el ritmo respiratorio calculado después del ajuste lineal realizado a la señal respiratoria original, con ambos métodos de ajuste y para ambos algoritmos.

	Algoritmo 1			**Algoritmo 2**		
	Promedio	**MM[1]**	**MD[2]**	**Promedio**	**MM[1]**	**MD[2]**
Método 1	1.08	2.52	5.46	0.48	1.78	0.55
Método 2	1.54	3.19	3.58	1.28	2.88	2.35

[1] Máxima mejora, [2] Máximo deterioro.

De esta forma se puede apreciar que ambos métodos de ajuste lineal, en promedio, mejoran el ritmo respiratorio calculado de las señales de respiración. Sin embargo, el segundo método de ajuste lineal muestra un mejor desempeño al obtener una mejora promedio más alta con los dos algoritmos aplicados. De este segundo método y con el algoritmo 1, solo la ventana de 6 segundos muestra un deterioro en el ritmo respiratorio calculado, mientras que todas las demás ventanas muestran una mejoría, sin embargo, esta mejoría no es uniforme para todas las ventanas de tiempo utilizadas. Por otra parte, al utilizar el algoritmo 2 se puede destacar que, cuando se incrementa la ventana de segmentación, el ritmo respiratorio calculado se mide con un menor error. Por lo tanto, a pesar de que la mejora en el cálculo del ritmo respiratorio es moderada, las señales con ajuste lineal muestran una mejoría al compararse con las señales originales. Para esta aplicación en específico, el segundo método utilizado (segmentación de ventanas

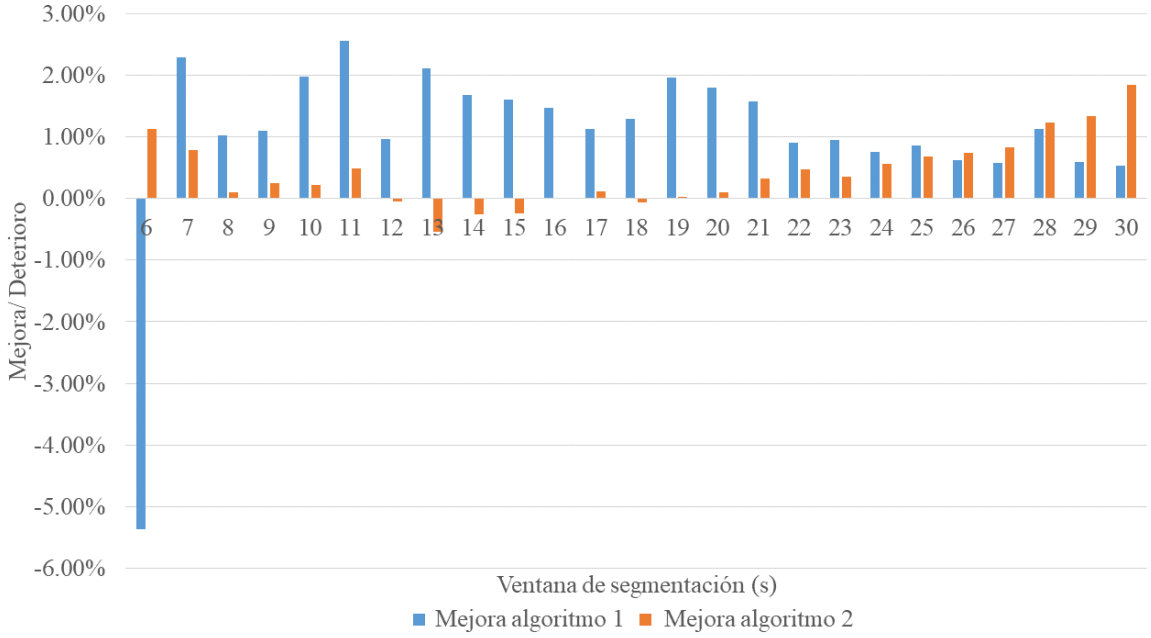

Figura 4.3: Mejora y deterioro obtenidos al calcular el ritmo respiratorio después de realizar el ajuste lineal a las señales respiratorias mediante el primer método descrito.

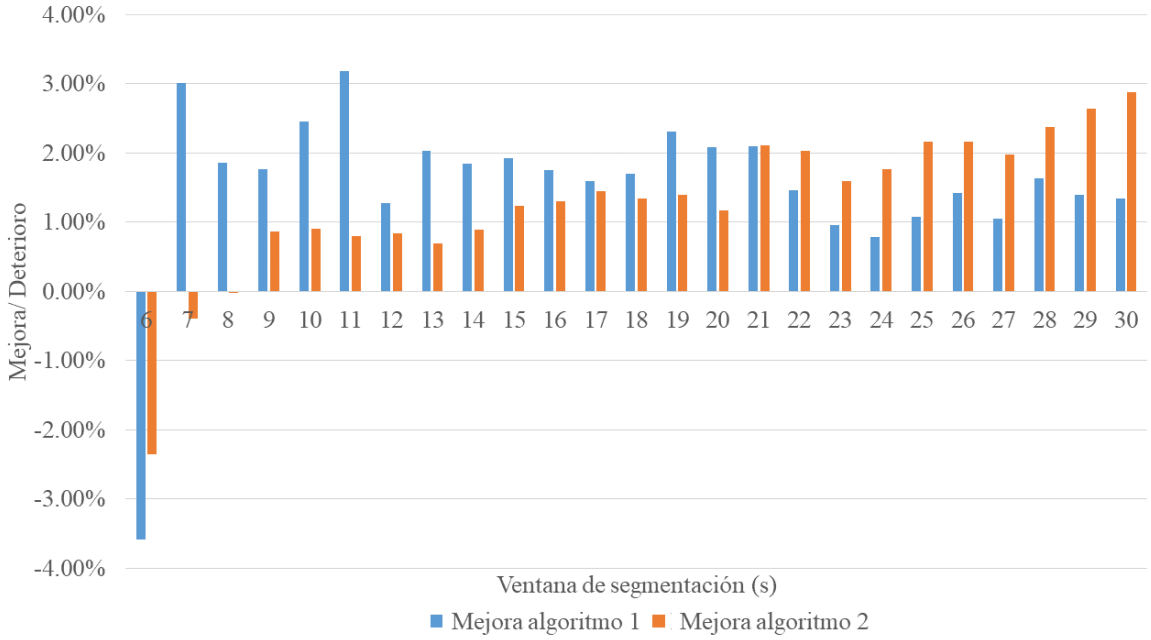

Figura 4.4: Mejora y deterioro obtenidos al calcular el ritmo respiratorio después de realizar el ajuste lineal a las señales respiratorias mediante el segundo método descrito.

de señal) muestra ser mejor.

4.1.4. Versión mejorada del sistema vestible

A raíz de haber verificado el correcto funcionamiento de este sistema vestible, se realizó una versión mejorada del mismo, el cual incluye las siguientes mejoras:

- Una reducción del 30 % de las dimensiones del armazón de PLA rígido.
- Reducción del 15 % de las dimensiones del armazón de PLA flexible.
- Diseño mejorado que facilita su ensamblaje.
- Mayor sensibilidad a las lecturas obtenidas, gracias a su nuevo diseño.
- Implementación de un ADC de 12 bits que incrementa en cuatro veces la resolución de las lecturas obtenidas.
- Implementación de un filtro analógico, el cual nos permite evitar la implementación de filtros digitales.

Diseño de PCB

Para esta nueva versión del sistema vestible se diseñó una nueva placa PCB que contuviera todos los nuevos elementos necesarios, y, a su vez, mantuviera al menos el mismo tamaño que el diseño anterior. Las dimensiones finales de esta PCB fueron 36mm de alto, 37mm de ancho y 1.5mm de espesor. Una placa de menor tamaño podría incluso realizarse gracias a la disponibilidad de "fuente abierta" de las diferentes placas que la componen. Sin embargo, debido a los tamaños del propio sensor FSR y de la batería utilizada, el tamaño del armazón construido no se vería reducido de forma significativa.

Este nuevo diseño utiliza un microcontrolador AVGA328p de WAVGAT, el cual tiene la misma distribución de pines que el microcontrolador Atmega328p de Arduino utilizado en la versión anterior. La principal mejora del microcontrolador AVGA328p es que el ADC que posee es de 12 bits, mientras que el ADC del microcontrolador Atmega328p es de 10 bits. Esto implica que al utilizar el microcontrolador de WAVGAT la resolución de las mediciones aumenta en 4 veces. No obstante, cualquiera de los dos microcontroladores puede utilizarse, ya que ambos circuitos impresos poseen las mismas dimensiones y distribución de pines (puertos digitales, puertos analógicos y pines de alimentación).

En el Anexo D se adjuntan los diagramas esquemáticos del sistema, y el nuevo diseño de la PCB derivado. Cabe resaltar que el diagrama de bloques del funcionamiento de esta nueva versión es el mismo que el mostrado en la figura 3.3, solo que en la parte del acondicionamiento del sensor se agregaría el filtro analógico diseñado.

Diseño del filtro analógico

Se decidió implementar un filtro analógico tipo Butterworth, ya que ofrece una respuesta más plana que otros filtros conforme se acerca a su frecuencia de corte (f_c).

Para comenzar a diseñar el filtro, lo primero que se tuvo que determinar fueron la frecuencia de corte deseada, la tasa de muestreo del sistema y la resolución del ADC utilizado (dada en bits). Partiendo de aquí se planteó el diseño del filtro analógico según la metodología propuesta por Pérez-García [248].

Siguiendo la metodología recomendada, necesitamos una mínima atenuación desde la frecuencia de corte (f_c) hasta la frecuencia de muestreo (f_s) y con estos valores calculamos el número de décadas que hay en este ancho de banda mediante la ecuación:

$$D = log_{10}\frac{f_s - f_c}{f_c} \tag{4.1}$$

El resultado de esta ecuación nos indica que hay al menos dos décadas en este ancho de banda. Por lo tanto, ahora queda calcular la atenuación total del filtro analógico al tomar en cuenta el número de bits de resolución del ADC (n) en la siguiente ecuación:

$$A = 20log_{10}\frac{1}{2^n} \tag{4.2}$$

Se obtiene que el sistema desarrollado necesita una atenuación mínima de $A \approx 73dB$. Entonces queda calcular cuánta es la atenuación que necesita el sistema para cada década de su ancho de banda, por lo que simplemente se realiza una división como sigue:

$$dB/decada = \frac{A}{D} = \frac{-73dB}{2decadas} = -36{,}5dB/decada \tag{4.3}$$

Esto quiere decir que necesitamos un filtro capaz de ofrecer una atenuación mínima de $36{,}5dB/decada$, por lo tanto, se elige utilizar un filtro de dos polos ya que ofrece una atenuación de $-40dB/decada$. Finalmente elegimos implementar este filtro mediante la topología Sallen-key, y se coloca un seguidor de voltaje entre el circuito de acondicionamiento del FSR y el filtro para aislar ambas etapas. Se incluye un diagrama esquemático del sistema completo en el Anexo D.

Diseño del armazón

Una vez terminado el diseño de la PCB y teniendo sus elementos soldados, se procedió a diseñar el nuevo armazón mediante el software de diseño SolidWorks. Al igual que el diseño anterior, este armazón consta de tres partes principales: el armazón que contiene todos los elementos electrónicos, un pivote que transfiere los movimientos del pecho al sensor FSR, y una capa exterior flexible que se encarga de transmitir los movimientos del pecho al pivote. Las dimensiones totales de la parte que contiene la circuitería son de 26m de alto, 39mm de ancho y 41mm de profundidad .El pivote sobresale 7mm del armazón; la capa exterior flexible se podría describir como una

lámina cuasi-cilíndrica cuyas dimensiones son 34mm de alto, 67mm de ancho y 40mm de profundidad, destacando que solo abarca esas dimensiones de forma perimetral a manera de cilindro con solo 1mm de espesor.

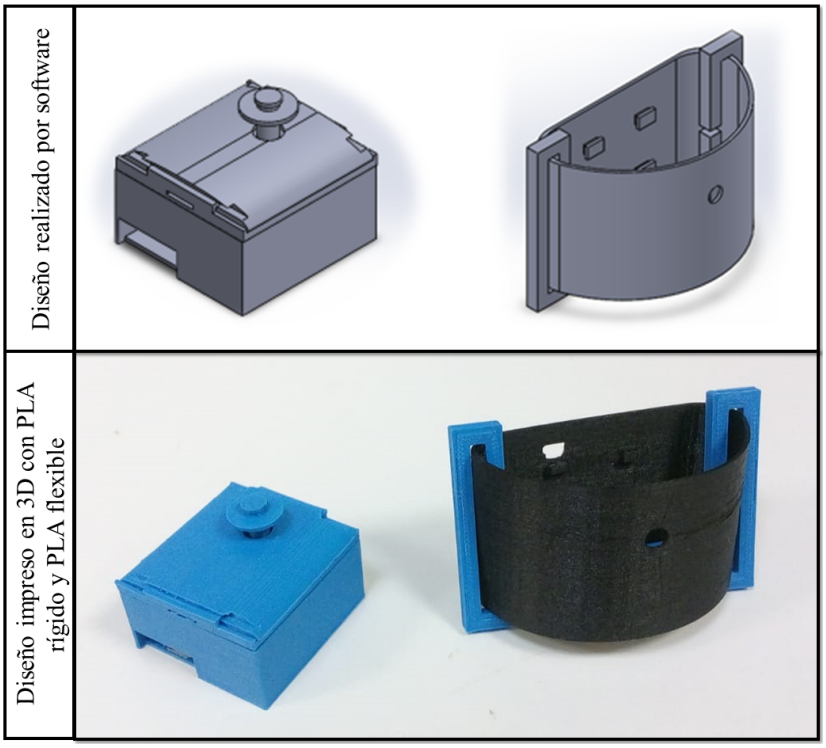

Figura 4.5: Comparación entre el diseño del armazón realizado por software y el diseño construido mediante impresión 3D.

Sensibilidad del sistema

Para medir la sensibilidad de este nuevo diseño se realizaron mediciones con 10 voluntarios. Se les pidió realizar 10 ciclos respiratorios a diferentes ritmos marcados por un metrónomo, para un total de 10 ciclos para 6 ritmos respiratorios diferentes, es decir, 60 ciclos de respiración a cada uno.

Se pudo observar que este rango de sensibilidad variaba entre voluntarios, tanto en tamaño como en "posición" en el rango dinámico. Esto se debe a factores individuales de cada voluntario, tales como tipo somático de cuerpo, el peso, el ajuste de las correas del sistema, o incluso la forma de respiración particular de cada voluntario.

De esta manera se obtuvo una sensibilidad promerio de 367 bits del ADC de 12 bits del microcontrolador (de un total de 4096 bits). Dado que el microcontrolador funciona con un voltaje de referencia igual a 3,3V, si convertimos estos resultados a voltaje entonces la sensibilidad obtenida fue de $296mV$ con una resolución de $0{,}806mV$. La versión anterior del sensor, mediante el mismo método, demostró tener una sensibilidad promedio de 36 bits del ADC de 10 bits, que al utilizar el mismo voltaje de referencia de

3,3V esto sería igual a una sensibilidad de 116mV con una resolución de 3,23mV. Con esto podemos concluir que la sensibilidad de este nuevo diseño del sistema aumentó en un 254 % con respecto al diseño anterior, mientras que la resolución aumentó 4 veces pero esto fue debido a utilizar un ADC de mayor capacidad. Esta comparativa se muestra en la tabla 4.2.

Tabla 4.2: Comparación de la sensibilidad entre ambas versiones del sistema vestible de respiración.

Sensor	**Sensibilidad en bits**	**Sensibilidad en voltaje**	**Resolución en voltaje**
Versión mejorada	367bits	296mV	0,806mV
Versión previa	36bits	116mV	3,223mV

En el Anexo E se muestran comparaciones directas de las señales normalizadas obtenidas mediante cada una de las versiones del sistema desarrollado. Estas señales se muestran en crudo sin aplicarles filtros digitales, con lo cual es evidente la mejoría en la calidad de la señal obtenida mediante la versión nueva. Cabe resaltar que la mejora en la calidad de la señal es más evidente cuando el ritmo respiratorio es mayor. Además, al estar normalizadas las señales obtenidas, se aprecia el aumento de la sensibilidad (rango dinámico de variaciones) de la señal obtenida de la versión nueva del sistema, resultado que es independiente del aumento en la relución lograda gracias al ADC de 12 bits.

4.2. Sistema ambiental para medición del salto vertical

4.2.1. Resultados

Primer experimento: Validación del sistema

En este experimento se realizaron un total de 228 saltos (114 CMJ y 114 CMJAS), comparando el sistema desarrollado con la referencia utilizada. En la figura 4.6 se muestra un ejemplo de las grabaciones obtenidas mediante la referencia.

Para evaluar el desempeño del sistema desarrollado, se calculó el error relativo medio (MRE) y el error absoluto medio (MAE) para todos los saltos efectuados, y para cada una de las técnicas (CMJ y CMJAS). El MRE obtenido de todos los 228 saltos fue de 1,98 %, mientras que para cada técnica de salto, CMJ y CMJAS, el MRE obtenido fue de 2,17 % y 1,78 %, respectivamente. El MAE para todos los saltos fue de 0,38cm, y para el CMJ y el CMJAS fue de 0,34cm y 0,42cm, respectivamente. Estos resultados se muestran en la Tabla 4.3.

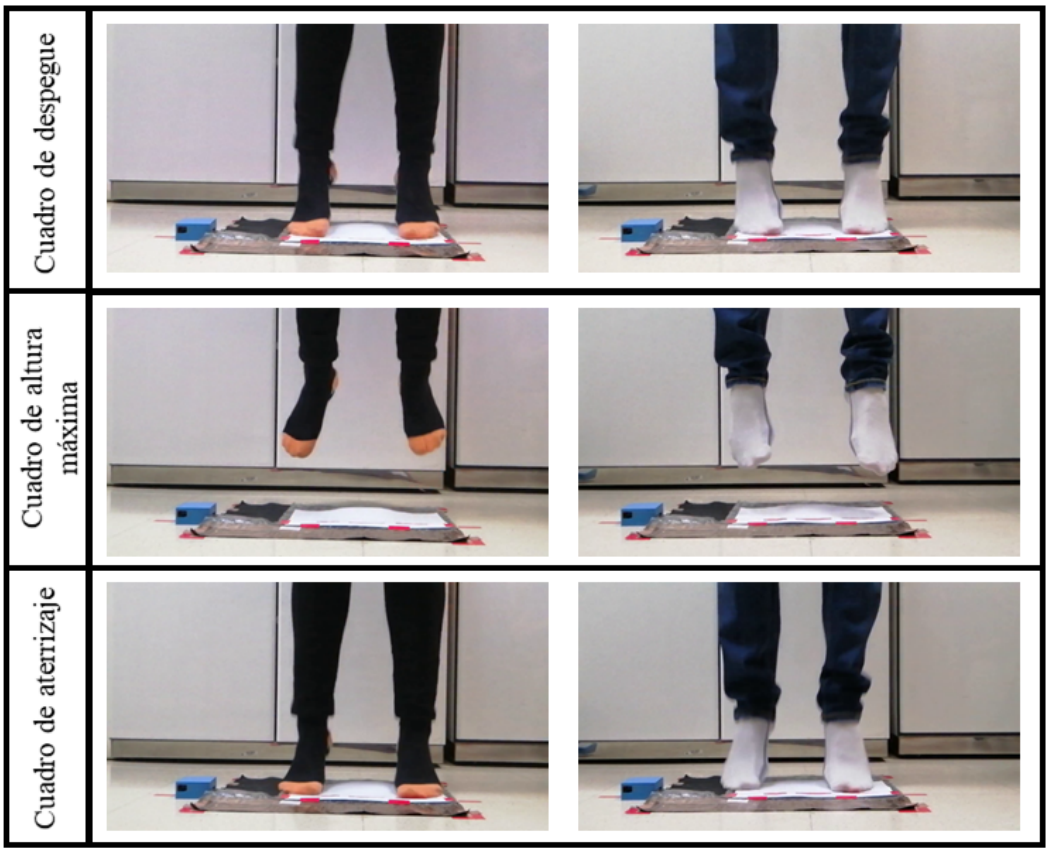

Figura 4.6: Dos voluntarios ejecutando saltos según el protocolo prupuesto. Se muestran diferentes fases del salto: el cuadro de despegue, el cuadro de altura máxima y el cuadro de aterrizaje.

Tabla 4.3: Valores de MAE y MRE para todos los saltos, solo los saltos CMJ y solo los saltos CMJAS.

Saltos	**MAE**	**MRE**
Todos	0,38cm	1,98 %
CMJ	0,34cm	2,17 %
CMJAS	0,42cm	1,78 %

Se realizaron análisis de correlación y de Bland-Altman para comparar ambos métodos, que se muestran en la figura 4.7 y la figura 4.8, respectivamente. El análisis de correlación muestra un coeficiente de determinación igual a $R^2 = 0{,}996$. De estos dos análisis no solo se muestra un alto coeficiente de correlación, si no que también se observa que la diferencia entre cada medición emparejada es baja, y que ambos métodos producen sistemáticamente los mismos resultados.

En la figura 4.9 se muestran los valores de MRE y MAE normalizados y divididos en diferentes alturas alcanzadas por los voluntarios. Los rangos de altura que se muestran son menores a 10cm, de 10 a 20cm, de 20 a 30cm y mayores a 30cm. Para estos rangos de altura, los valores de MRE obtenidos fueron de 2,38 %, 2,07 %, 1,90 % y 1,54 % respectivamente, mientras que los valores del MAE fueron de 0,18cm, 0,31cm, 0,46cm y 0,50cm respectivamente. De estos datos, no se pueden apreciar diferencias relevantes entre los diferentes rangos de altura alcanzada. Sin embargo, se logra apreciar que

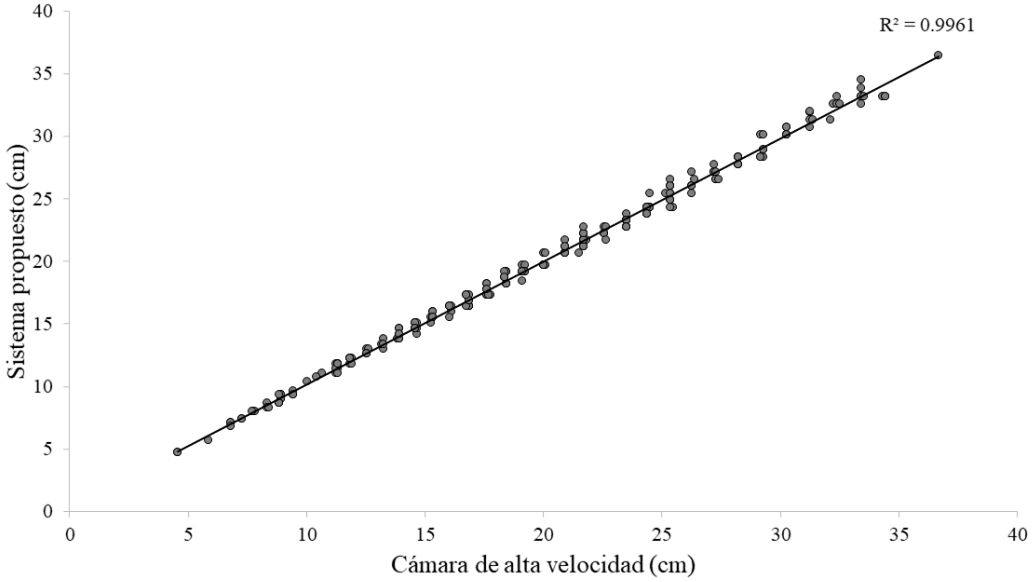

Figura 4.7: Gráfica de correlación que compara ambos métodos de medición para el primer experimento, mostrando un coeficiente de determinación $R^2 = 0{,}996$.

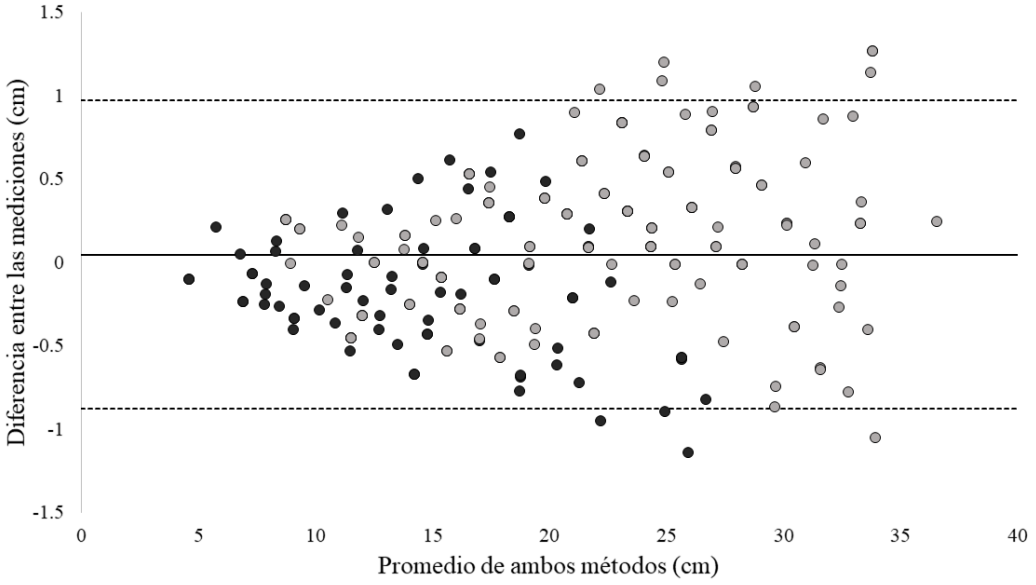

Figura 4.8: Análisis de Bland-Altman de los dos métodos de medición. Los CMJ se muestran con los puntos gris oscuro, mientras que los CMJAS se muestran con los puntos gris claro.

el MAE se incrementa conforme aumenta la altura alcanzada, mientras que el MRE disminuye.

En la figura 4.10 se muestran gráficas con la distribución de las diferentes alturas alcanzadas por los voluntarios en el salto vertical. Se puede apreciar que ningún voluntario logró superar la altura de 30cm con la técnica de salto CMJ. Sin embargo, al agregar el braceo al salto, el 22 % de los voluntarios lograron superar los 30cm. Otro aspecto a destacar es que, con el salto CMJAS, el 69 % de los voluntarios alcanzaron una altura mayor a los 20cm, mientras que con el salto CMJ solo el 31 % de los voluntarios

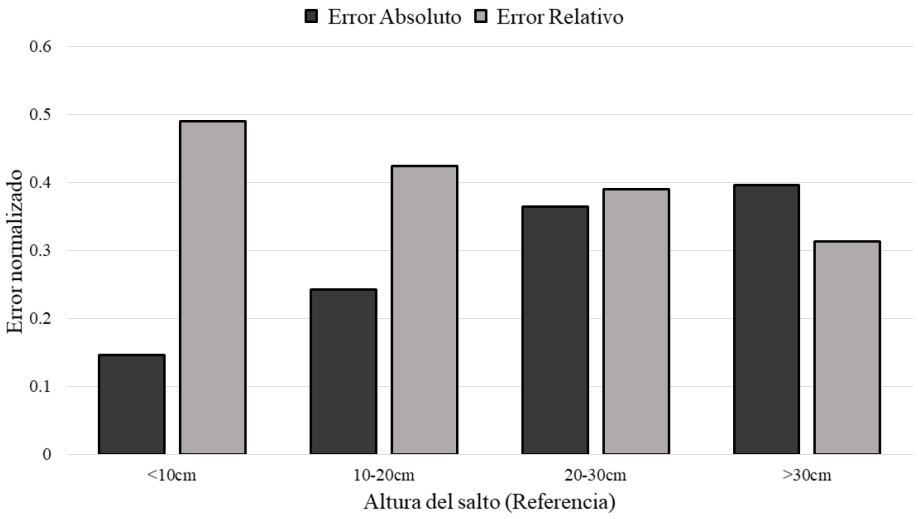

Figura 4.9: MRE y MAE normalizados, divididos en diferentes rangos de altura alcanzados por los voluntarios.

logró hacerlo.

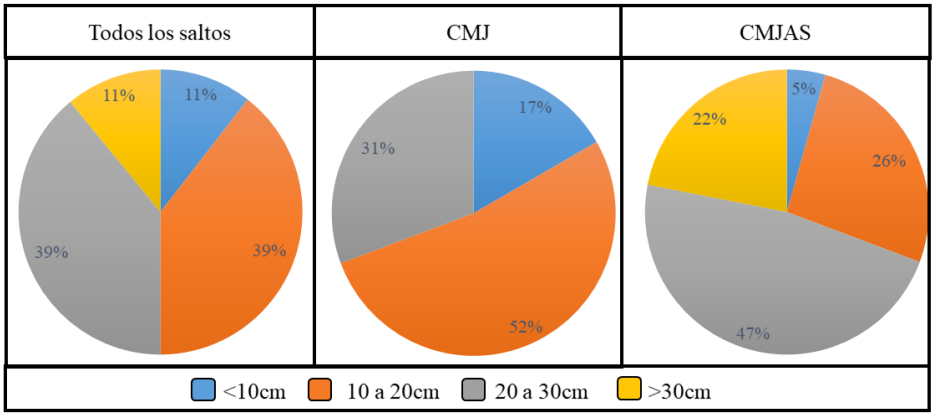

Figura 4.10: MRE y MAE normalizados, divididos en diferentes rangos de altura alcanzados por los voluntarios.

Segundo experimento: Comparación de la frecuencia de muestreo

En este experimento se analizaron los efectos de diferentes frecuencias de muestreo sobre la respuesta del sistema. Se obtuvieron datos en crudo para un total de 90 saltos (45 CMJ y 45 CMJAS). Se realizó de manera "offline" una emulación de diferentes frecuencias de muestreo al realizar un submuestreo de los datos en crudo. Esto quiere decir que se fueron eliminando muestras para estudiar diferentes frecuencias de muestreo. Con el periodo de muestreo base del sistema igual a 5ms, se lograron emular las siguientes frecuencias de muestreo: 200Hz, 100Hz, 66.6Hz, 50Hz, 40Hz, 33.3Hz, 28.5Hz, 25Hz, 22.2Hz y 20Hz.

Al igual que en el primer experimento, se utilizó la misma cámara de alta

velocidad como referencia. Para este análisis, sólo se analizó el MRE de cada frecuencia propuesta, para así evaluar cuáles eran capaces de mantener un error relativo por debajo del 5 %. Los resultados mostraron que las frecuencias de 200Hz, 100Hz y 66,6Hz tienen un desempeño similar, con valores de MRE de 1,88 %, 2,22 % y 2,88 % respectivamente. Sin embargo, para estas mismas frecuencias el valor máximo de error relativo encontrado entre los 90 saltos analizados se incrementa de manera notoria conforme la frecuencia de muestreo disminuye, mostrando valores máximos de 5,27 %, 7,02 % y 8,25 % respectivamente. Las frecuencias de muestreo de 50Hz, 40Hz y 33.3Hz muestran un buen desempeño con valores de MRE menores al 5 %, sin embargo, los errores relativos máximos encontrados aumentan considerablemente en comparación con el conjunto anterior de frecuencias.

En la tabla 4.4 se muestran los valores de MRE, error relativo máximo, y error relativo mínimo para cada una de las frecuencias emuladas. Conforme disminuye la frecuencia de muestreo, se logra apreciar un incremento exponencial en el MRE, tal como se muestra en la figura 4.11, donde se aprecia que frecuencias iguales o menores a 28,5Hz no pueden mantener el MRE debajo de 5 %. De igual manera, frecuencias de muestreo menores a 50Hz y 33,3Hz muestran un error relativo máximo mayor al 10 % y 20 % respectivamente.

Tabla 4.4: MRE y errores relativos máximo y mínimo obtenidos de los 90 saltos analizados para cada una de las frecuencias emuladas.

	Periodos/Frecuencias de Muestreo									
	5ms	**10ms**	**15ms**	**20ms**	**25ms**	**30ms**	**35ms**	**40ms**	**45ms**	**50ms**
	200Hz	**100Hz**	**66,6Hz**	**50Hz**	**40Hz**	**33,3Hz**	**28,5Hz**	**25Hz**	**22,2Hz**	**20Hz**
MRE	1,88 %	2,22 %	2,88 %	3,52 %	4,50 %	4,97 %	6,04 %	6,27 %	8,02 %	8,75 %
MAX	5,27 %	7,02 %	8,25 %	9,73 %	14,25 %	14,25 %	21,30 %	19,73 %	28,39 %	32,11 %
MIN	0,00 %	0,00 %	0,00 %	0,00 %	0,70 %	0,00 %	0,00 %	0,00 %	0,00 %	0,73 %

De este análisis, se puede destacar que las frecuencias de muestreo de 200Hz y 100Hz logran mantener el 95 % de las alturas calculadas con un error relativo menor al 5 %. Frecuencias de muestreo menores a 50Hz incrementan notoriamente el porcentaje de alturas calculadas con un error relativo mayor al 5 %. Estos resultados sugieren que las frecuencias de muestreo de 200Hz y 100Hz son las más confiables para esta aplicación; las frecuencias de 66,6Hz y 50Hz tienen un desempeño aceptable, y el resto de frecuencias emuladas no ofrecen resultados confiables para esta aplicación en concreto.

En la tabla 4.6 se muestra como el MRE se encuentra distribuido en diferentes rangos de altura alcanzados por los voluntarios. Cuando para cada frecuencia emulada obtenemos el MRE de los diferentes rangos de altura alcanzados (menor a 10cm, de 10 a 20cm, de 20 a 30cm y mayor a 30cm), se destaca la importancia de una frecuencia de

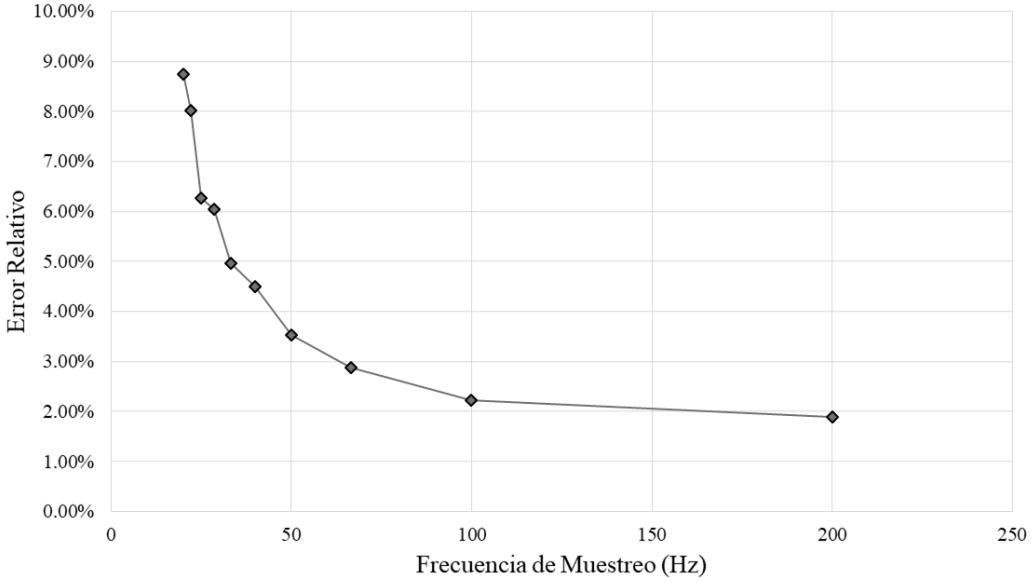

Figura 4.11: MRE obtenido de cada frecuencia de muestro utilizada. Conforme se disminuye la frecuencia de muestreo, el error relativo se incrementa exponencialmente.

Tabla 4.5: Porcentaje del total de saltos cuyo error relativo es del 5 % o menos, está entre el 5 % y el 15 %, y es mayor al 15 %.

	Periodos/Frecuencias de Muestreo									
	5ms	**10ms**	**15ms**	**20ms**	**25ms**	**30ms**	**35ms**	**40ms**	**45ms**	**50ms**
Error Relativo	**200Hz**	**100Hz**	**66.6Hz**	**50Hz**	**40Hz**	**33.3Hz**	**28.5Hz**	**25Hz**	**22.2Hz**	**20Hz**
≤5 %	98,89 %	94,44 %	87,78 %	76,67 %	58,89 %	57,78 %	48,89 %	52,22 %	35,56 %	27,78 %
5 %-15 %	1,11 %	5,56 %	12,22 %	23,33 %	41,11 %	42,22 %	47,78 %	43,33 %	54,44 %	57,78 %
>15 %	0,00 %	0,00 %	0,00 %	0,00 %	0,00 %	0,00 %	3,33 %	4,44 %	10,00 %	14,44 %

muestreo apropiada sobre todo en el momento de calcular la altura de saltos menores a 20cm. Con frecuencias menores a 50Hz, el MRE obtenido de los saltos de menos de 20cm siempre es mayor al 5 %, e incluso la menor frecuencia de muestreo (20Hz) muestra un error relativo del 21,50 % para saltos de menos de 10cm. Para aquellos saltos que superaron los 20cm, frecuencias menores a 40Hz muestran un MRE mayor al 5 %, alcanzando hasta un valor de 9,15 % para un muestreo de 20Hz. Estos resultados se muestran en la Tabla 4.6.

Tabla 4.6: MRE obtenido para diferentes rangos de altura alcanzados por los voluntarios, para todas las frecuencias de muestreo analizadas.

	Periodos/ Frecuencias de Muestreo									
	5ms	**10ms**	**15ms**	**20ms**	**25ms**	**30ms**	**35ms**	**40ms**	**45ms**	**50ms**
Altura del salto	**200Hz**	**100Hz**	**66,6Hz**	**50Hz**	**40Hz**	**33,3Hz**	**28,5Hz**	**25Hz**	**22,2Hz**	**20Hz**
<10cm	1,31 %	2,29 %	4,33 %	2,62 %	5,28 %	5,09 %	5,40 %	6,29 %	10,77 %	21,50 %
10-20cm	2,23 %	2,40 %	2,89 %	4,29 %	5,21 %	5,45 %	7,55 %	8,60 %	9,65 %	8,42 %
20-30cm	1,91 %	2,31 %	3,02 %	3,55 %	4,62 %	5,29 %	5,06 %	6,12 %	6,96 %	9,15 %
>30cm	1,60 %	1,95 %	2,50 %	2,92 %	3,63 %	4,17 %	5,83 %	4,34 %	7,32 %	6,85 %

4.2.2. Discusión

Las pruebas de salto vertical suelen utilizarlas los profesionales de la salud para evaluar la fuerza de los músculos de las piernas de las personas. A pesar de que esta prueba es ampliamente utilizada con atletas, se puede obtener información importante de personas sin antecedentes deportivos.

De la captura de datos realizada en ambos experimentos, se pueden extraer algunas conclusiones. A pesar de las ventajas que ofrece el sistema desarrollado y la referencia utilizada, ambos sistemas tienen un error inherente de la misma frecuencia de muestreo que poseen, o más específicamente del periodo de muestreo. El sistema ambiental desarrollado cuenta con una frecuencia de muestreo de 200Hz, por lo tanto su periodo de muestreo es de 5ms. De igual manera, la cámara de alta velocidad al tener una frecuencia de muestreo de 120Hz(fps) su periodo de muestreo es de 8,3ms. Esto quiere decir que cada sistema actualiza sus lecturas cuando transcurre un tiempo igual a su respectivo periodo de muestreo, lo que conlleva un periodo de incertidumbre entre cada actualización.

En otras palabras, existe una incertidumbre inherente en cada sistema durante las lecturas de la fase de despegue y la fase de aterrizaje del salto vertical, periodo de tiempo utilizado para calcular la altura alcanzada. Entre ambas fases del salto, el sistema ambiental propuesto posee un error de muestreo de 10ms, mientras que la cámara de referencia posee un error de muestreo de 16.6ms. Este error sistemático es inherente en cualquier dispositivo electrónico que sirva para medir el cambio de alguna magnitud frente al tiempo, y se encuentra directamente relacionado con la frecucencia de muestreo. Métodos no-electrónicos para medir el salto vertical tales como el salto Sargent [249] o el dispositivo Vertec [20,118,124], a pesar de no poseer este tipo de error, tienden a sobreestimar las mediciones obtenidas de cada salto, son menos precisos, y además los errores que poseen no son consistentes [124].

En cuanto a la cámara utilizada como referencia, al analizar los videos grabados para seleccionar los cuadros adecuados de despegue y aterrizaje del salto, fue más fácil hacerlo con aquellos voluntarios que ejecutaron una mejor técnica de salto. La técnica de salto deseada fue aquella en que los voluntarios, al saltar, despegaron las puntas de ambos pies al mismo tiempo, y al aterrizar también lo hicieron con ambas puntas de los pies. Por otra parte, hubo voluntarios que al momento de despegar o aterrizar lo hicieron con solo un pie, y en ocasiones no con el mismo pie entre ambas etapas del salto. En estos casos fue un poco más dificil seleccionar los cuadros adecuados. No obstante, hay que resaltar que esto es un reflejo involuntario de cada persona, y para mejorar la técnica de salto deseada, es necesario entrenar o practicar la técnica de salto.

En el protocolo propuesto para este estudio, la inclusión de dos técnicas de salto fue de utilidad para lograr incrementar el rango dinámico de los datos obtenidos de cada voluntario. El incremento en la altura alcanzada por los voluntarios fue notoria al agregar el braceo, ya que en el primer experimento en promedio hubo un incremento del 44,84 % de la altura, mientras que el incremento en el segundo experimento fue de 34,86 %.

Capítulo 5

Conclusiones principales

De acuerdo a los objetivos expuestos al inicio de la presente tesis, se logró hacer aportaciones de valor a la comunidad científica con dispositivos cuyo propósito es la monitorización de variables físicas y fisiológicas en los seres humanos, especialmente en adultos mayores y frágiles. Estos sistemas desarrollados, en las manos de un profesional de la salud, pueden guiar a las personas bajo su cuidado en la mejora de su estilo y calidad de vida. Además, a pesar de que estos sistemas fueron desarrollados para utilizarse con adultos mayores y adultos frágiles, su uso no se limita a esta población.

A continuación se exponen las conclusiones para cada uno de los sistemas desarrollados.

5.1. Sistema vestible para respiración

En el trabajo presente de tesis se han presentado los resultados obtenidos tras desarrollar una revisión del estado del arte comprendiendo 198 artículos relacionados con los sistemas que monitorizan la respiración, tomando en cuenta los aspectos más relevantes de dichos sistemas tales como la técnica de detección de la respiración, el tipo de sensor utilizado, los parámetros respiratorios obtenidos, ubicación del sistema en el cuerpo humano, tamaño del sistema, protocolos de comunicación utilizados (cableados ó inalámbricos), autonomía y consumo energético, lo que ha permitido identificar tendencias y resaltar los desafíos de investigación en el ámbito de los sistemas vestibles y ambientales para monitorizar la respiración.

Se ha desarrollado un sistema basado en un sensor resistivo sensible a la fuerza (FSR), aportando una solución que tan solo se había mencionado en uno de los artículos consultados en la literatura. Frente a ella, el sistema desarrollado integra en un mismo encapsulado el elemento sensor y la electrónica necesaria para el procesado y transmisión de la señal de respiración en tiempo real.

Además, también se han aportado mejoras frente a dispositivos similares

encontrados en la literatura, entre otros, las dimensiones del dispositivo, una mayor velocidad de muestreo y la utilización de tecnología inalámbrica Bluetooth, obteniéndose señales respiratorias de calidad (la mejora en la calidad de las señales es más evidente cuando el ritmo respiratorio es mayor). En el trabajo de tesis se han planteado diferentes alternativas de diseño para así aumentar notablemente la sensibilidad del sistema (sensibilidad promedio de 367 bits usando un ADC de 12 bits - para un total de 4096 bits de resolución - y sensibilidad de $296mV$ con una resolución de $0,806mV$ al utilizar un voltaje de referencia de 3,3V).

El dispositivo finalmente implementado puede utilizarse tanto encima de la ropa como directamente en contacto con la piel, no suponiendo ningún riesgo para la integridad de los usuarios.

Gracias a la utilización de tecnología Bluetooth para la comunicación, puede gestionarse tanto a través de tecnologías móviles, como teléfonos inteligentes o tabletas digitales, como a través de ordenadores, logrando así una visualización de datos en tiempo real.

De las pruebas realizadas, se determinó cuál era la ventana de tiempo óptima a utilizar para predecir el ritmo respiratorio con cada uno de los algoritmos propuestos. Se concluyó que la ventana de tiempo igual a 27 segundos podría considerarse como la óptima. Sin embargo, las ventanas de tiempo entre 20 y 30 segundos ofrecen un desempeño similar, por lo tanto, el elegir una sobre otra puede basarse simplemente en el tiempo deseado para la actualización de las predicciones obtenidas.

También, ya que se contaba con la base de datos de las señales de respiración, se optó por realizar un pequeño estudio sobre los efectos de eliminar las tendencias de estas señales. Al aplicar el ajuste lineal sobre las señales de respiración se pudo observar que, a pesar de que la mejoría en el cálculo del ritmo respiratorio no era tan grande, en promedio siempre hubo una mejora en los resultados logrando una disminución del error relativo del 0,48 % al 1,54 %, e incluso habiendo casos en los que el error relativo logró disminuirse hasta un 3,19 %. Además, se demostró que una de las técnicas propuestas para el ajuste lineal sobre las señales de respiración (la que eliminaba las tendencias en segmentos de la señal) tuvo un mejor desempeño que la otra. A pesar de que, en promedio, la mejora de las señales no fue tan grande, se muestra siempre una mejora en los resultados del ritmo respiratorio calculado, y que este análisis adicional con las señales de respiración resulta relevante ya que logra mejorar los resultados obtenidos al calcular el ritmo respiratorio.

Las posibles aplicaciones de este sistema desarrollado pueden ser la monitorización ambulatoria, el control de pacientes de hospital, el seguimiento en estudios específicos de respiración, la predicción y prevención de estados de salud peligrosos o el análisis

de emociones humanas, entre otros. El sistema desarrollado se encarga de obtener una señal de respiración con buena resolución entre las muestras, por lo que las diversas aplicaciones mencionadas dependen principalmente de la interpretación de dicha señal respiratoria.

Finalmente, el sistema desarrollado es más económico que los existentes en el mercado [27], y se ha ofrecido la opción de que cualquier investigador interesado en este trabajo pueda desarrollar su propio sistema, ya que los diseños del armazón desarrollado, el circuito esquemático, y materiales utilizados para este sistema han sido publicados de forma abierta [27] para que la comunidad científica pueda utilizarlos libremente y, de ser posible, mejorar este sistema realizando versiones nuevas. Sumado a esto, se han dejado accesibles la base de datos de las señales de respiración obtenida de los experimentos realizados, los ficheros con el cálculo de errores, el código fuente del cálculo del ritmo respiratorio con los dos algoritmos propuestos y el código fuente de las pruebas estadísticas.

5.1.1. Trabajo futuro

Con el mismo diseño desarrollado, se pueden implementar nuevas versiones del sistema pero con diferentes tipos de sensores, tales como sensores capacitivos o piezoeléctricos, y ver qué tipo de sensor ofrece una mejor respuesta en la detección de la señal respiratoria.

Así mismo, se puede realizar una "*fusión de datos/fusión de sensores*" (sensor fusion [250]) con la que se combinen los datos obtenidos de diferentes tecnologías y obtener una mejor señal de la que se obtendría con cada sistema de forma individual.

Además, a pesar de que este sistema se desarrolló para ser utilizado con adultos mayores y adultos frágiles, su uso no se limita con esta población, y se podrían analizar las diferencias de su uso entre personas mayores y usuarios más jóvenes al realizar un estudio de aceptación del sistema.

5.2. Sistema ambiental para salto vertical

Se ha diseñado e implementado un sistema ambiental capaz de medir la altura del salto vertical efectuado por el usuario, el cual se logró que fuese más económico que los sistemas comerciales del mercado, siendo de fácil fabricación.

Frente a otros sistemas basados en presión, el área del sistema desarrollado y su resolución son mayores, logrando distribuir 256 sensores en la totalidad de su área mediante una malla de 16 filas y 16 columnas, frente a otros sistemas que utilizan un único sensor.

Si comparamos el sistema desarrollado frente a sistemas vestibles, una de las mayores ventajas que ofrece es que no se necesita de un ajuste en función de las características físicas del usuario (como peso, altura, talla del calzado, etc.).

El sistema diseñado presenta un error sistemático menor al de la cámara utilizada como referencia. Frente a dispositivos no electrónicos que miden el salto vertical y que no presentan este tipo de error, el sistema ambiental propuesto presenta la ventaja de ser más preciso. Además, los dispositivos no electrónicos tienden a sobreestimar las mediciones obtenidas en cada salto y los errores que poseen no son consistentes entre usuarios.

Al evaluar el desempeño del sistema desarrollado, con el primer experimento se demuestra que el sistema es capaz de mantener el error relativo por debajo del 5 % para los 228 saltos analizados, utilizando una frecuencia de muestreo de 200Hz. Por otro lado, en el segundo experimento se logró apreciar que una frecuencia de muestreo de 100Hz muestra un desempeño muy parecido a la frecuencia propuesta de 200Hz. Asímismo, se demuestra que las frecuencias de muestreo de 200Hz y 100Hz logran mantener el error relativo por debajo del 5 % en el 98,89 % y 94,44 % de los saltos analizados, respectivamente.

La fórmula de FT es un método validado para calcular la altura del salto vertical. Del primer experimento, los análisis de correlación y de Bland-Altman sugieren que el sistema desarrollado en el trabajo de esta tesis ofrece sistemáticamente los mismos resultados que la cámara de alta velocidad utilizada como referencia, la cuál ha sido validada como método confiable para medir el salto vertical.

Del segundo experimento realizado se concluye que las frecuencias de muestreo de 200Hz y 100Hz tienen un desempeño parecido, y ambas frecuencias ofrecen resultados confiables. Por lo tanto, se puede concluir que si no se tiene acceso a desarrollar un sistema cuyo hardware pueda ofrecer una frecuencia de muestreo igual o mayor a 200Hz, entonces puede utilizarse un hardware que pueda ofrecer una frecuencia de muestreo de al menos 100Hz. Sin embargo, siempre que puedan utilizarse frecuencias mayores, debería hacerse.

Todos estos resultados demuestran que el sistema ambiental desarrollado es tan confiable como un sistema comercial. El sistema propuesto ofrece una alternativa a los profesionales de la salud de utilizar cualquier estación de visualización de las mediciones de su elección, desde un ordenador hasta un *smartphone*, lo que ofrece una ventaja en cuanto a su portabilidad, sin mencionar que su precio de mercado podría llegar a ser hasta 10 veces menor que el de un dispositivo comercial [235].

5.2.1. Trabajo futuro

Una vez que se ha demostrado que el sistema funciona como se esperaba, se podrían realizar nuevas versiones de la malla. Por lo tanto, se podría:

- Incrementar el área total de la malla, para así permitir que una postura más cómoda a todos los usuarios.
- Incrementar el tamaño de cada sensor FSR individual para lograr un mayor tamaño de la malla y obtener la misma resolución.
- Disminuir el tamaño de la matriz pero incrementando el tamaño de cada sensor FSR individual. Esto disminuiría la resolución del sistema, pero aumentaría la velocidad de procesado.
- Agregar al sistema la selección de un umbral de detección personalizado para cada individuo, para asegurar de una forma más precisa la detección de cada fase del salto vertical.
- Comparar el desempeño de las diferentes versiones de la malla, para concluir bajo qué circunstancias qué versión es mejor.

Al medir la altura alcanzada por un usuario durante el salto vertical, se puede estimar tanto la fuerza explosiva que se tiene en los músculos de las piernas, como el nivel de actividad física (sedentario, normal, activo) que los usuarios tienen cotidianamente [251]. De esta manera, se ha propuesto la posibilidad de realizar estudios en colaboración con médicos del deporte, con el objetivo de evaluar la fuerza de los músculos de las piernas en adultos mayores a través de la altura alcanzada mediante el salto vertical. No obstante, el uso de este sistema no se limita a esta población y también puede utilizarse con adultos y adolescentes en general, siendo especialmente interesante para aquellos que practican algún tipo de deporte.

Capítulo 6

Bibliografía

[1] Sungmee Park, Kyunghee Chung, and Sundaresan Jayaraman. Wearables: Fundamentals, advancements, and a roadmap for the future. In *Wearable sensors*, pages 1–23. Elsevier, 2014.

[2] Kevin Anderson, Oksana Burford, and Lynne Emmerton. Mobile health apps to facilitate self-care: a qualitative study of user experiences. *PloS one*, 11(5):e0156164, 2016.

[3] Norbert Noury, Robert Picard, Marie-Noëlle Billebot, Frédéric Durand-Salmon, Myriam Lewkowicz, and Henri Noat. Challenges and limitations of data capture versus data entry. In *Connected Healthcare for the Citizen*, pages 85–97. Elsevier, 2018.

[4] C Lee Ventola. Mobile devices and apps for health care professionals: uses and benefits. *Pharmacy and Therapeutics*, 39(5):356, 2014.

[5] Aleksandar Milenković, Chris Otto, and Emil Jovanov. Wireless sensor networks for personal health monitoring: Issues and an implementation. *Computer communications*, 29(13-14):2521–2533, 2006.

[6] Zhe Cao, Rong Zhu, and Rui-Yi Que. A wireless portable system with microsensors for monitoring respiratory diseases. *IEEE Transactions on Biomedical engineering*, 59(11):3110–3116, 2012.

[7] T Hoffmann, B Eilebrecht, and S Leonhardt. Respiratory monitoring system on the basis of capacitive textile force sensors. *IEEE sensors journal*, 11(5):1112–1119, 2010.

[8] Billy Sperlich, Kamiar Aminian, Peter Düking, and Hans-Christer Holmberg. Wearable sensor technology for monitoring training load and health in the athletic population. *Frontiers in physiology*, 10:1520, 2020.

[9] Umberto C Gatti, Suzanne Schneider, and Giovanni C Migliaccio. Physiological condition monitoring of construction workers. *Automation in Construction*, 44:227–233, 2014.

[10] Lukasz Dziuda, Franciszek Wojciech Skibniewski, Mariusz Krej, and Jaroslaw Lewandowski. Monitoring respiration and cardiac activity using fiber bragg grating-based sensor. *IEEE Transactions on Biomedical Engineering*, 59(7):1934–1942, 2012.

[11] Zdzisław Kowalczuk, Michał Czubenko, and Tomasz Merta. Emotion monitoring system for drivers. *IFAC-PapersOnLine*, 52(8):200–205, 2019.

[12] Dijana Ćosić. Neuromarketing in market research. *Interdisciplinary Description of Complex Systems: INDECS*, 14(2):139–147, 2016.

[13] Marco Granato. Emotions recognition in video game players using physiological information. 2019.

[14] Agata Kołakowska, Agnieszka Landowska, Mariusz Szwoch, Wioleta Szwoch, and Michal R Wrobel. Emotion recognition and its applications. In *Human-Computer Systems Interaction: Backgrounds and Applications 3*, pages 51–62. Springer, 2014.

[15] JP Janssens, S Pautex, H Hilleret, and JP Michel. Sleep disordered breathing in the elderly. *Aging Clinical and Experimental Research*, 12(6):417–429, 2000.

[16] Carlos Rodrigues, Miguel Correia, João MCS Abrantes, Jurandir Nadal, and Marco A Benedetti Rodrigues. Consistency of surface electromyography assessment at lower limb selected muscles during vertical countermovement. In *2017 39th Annual International Conference of the IEEE Engineering in Medicine and Biology Society (EMBC)*, pages 402–405. IEEE, 2017.

[17] M Rico Garcia, L-J Morantes Guzmán, J-S Botero Valencia, and V Madrid Henao. Portable measurement system of vertical jump using an inertial measurement unit and pressure sensors. In *2016 XXI Symposium on Signal Processing, Images and Artificial Vision (STSIVA)*, pages 1–5. IEEE, 2016.

[18] John F Drazan, Heather Danielsen, Matthew Vercelletto, Amy Loya, James Davis, and Ron Eglash. A case study for integrated stem outreach in an urban setting using a do-it-yourself vertical jump measurement platform. In *2016 38th Annual International Conference of the IEEE Engineering in Medicine and Biology Society (EMBC)*, pages 3027–3030. IEEE, 2016.

[19] Nicola Casartelli, Roland Müller, and Nicola A Maffiuletti. Validity and reliability of the myotest accelerometric system for the assessment of vertical jump height. *The Journal of Strength & Conditioning Research*, 24(11):3186–3193, 2010.

[20] Umar Yahya, SMN Arosha Senanayake, and Abdul Ghani Naim. Intelligent integrated wearable sensing mechanism for vertical jump height prediction in female netball players. In *2017 Eleventh International Conference on Sensing Technology (ICST)*, pages 1–7. IEEE, 2017.

[21] Nikola Mijailovic, Radivoje Radakovic, Aleksandar Peulic, Ivan Milankovic, and Nenad Filipovic. Using force plate, computer simulation and image alignment in jumping analysis. In *2015 IEEE 15th International Conference on Bioinformatics and Bioengineering (BIBE)*, pages 1–4. IEEE, 2015.

[22] Amador García-Ramos, Igor Štirn, Paulino Padial, Javier Argüelles-Cienfuegos, Blanca De la Fuente, Vojko Strojnik, and Belén Feriche. Predicting vertical jump height from bar velocity. *Journal of sports science & medicine*, 14(2):256, 2015.

[23] Benjamin KS Chan, Lynn M Marshall, Kerri M Winters, Kimberly A Faulkner, Ann V Schwartz, and Eric S Orwoll. Incident fall risk and physical activity and physical performance among older men: the osteoporotic fractures in men study. *American journal of epidemiology*, 165(6):696–703, 2007.

[24] Douglas J Mayson, Dan K Kiely, Sharon I LaRose, and Jonathan F Bean. Leg strength or velocity of movement which is more influential on the balance of mobility limited elders? *American journal of physical medicine & rehabilitation/Association of Academic Physiatrists*, 87(12):969, 2008.

[25] Nicole Wagner, Khaled Hassanein, and Milena Head. Computer use by older adults: A multi-disciplinary review. *Computers in human behavior*, 26(5):870–882, 2010.

[26] Fred Chau-Yang Ko. The clinical care of frail, older adults. *Clinics in geriatric medicine*, 27(1):89–100, 2011.

[27] Erik Vanegas, Raul Igual, and Inmaculada Plaza. Piezoresistive breathing sensing system with 3d printed wearable casing. *Journal of Sensors*, 2019, 2019.

[28] Erik Vanegas, Raul Igual, and Inmaculada Plaza. Sensing systems for respiration monitoring: A technical systematic review. *Sensors*, 20(18):5446, 2020.

[29] Marcel Fajkus, Jan Nedoma, Radek Martinek, Jindrich Brablik, Jan Vanus, Martin Novak, Stanislav Zabka, Vladimir Vasinek, Pavla Hanzlikova, and Lubomir Vojtisek. Mr fully compatible and safe fbg breathing sensor: A practical solution for respiratory triggering. *IEEE Access*, 7:123013–123025, 2019.

[30] Carlo Massaroni, Andrea Nicolò, Michele Girardi, Angelica La Camera, Emiliano Schena, Massimo Sacchetti, Sergio Silvestri, and Fabrizio Taffoni. Validation of a wearable device and an algorithm for respiratory monitoring during exercise. *IEEE Sensors Journal*, 19(12):4652–4659, 2019.

[31] Thanh-Vinh Nguyen and Masaaki Ichiki. Mems-based sensor for simultaneous measurement of pulse wave and respiration rate. *Sensors*, 19(22):4942, 2019.

[32] Daniela Lo Presti, Carlo Massaroni, Joshua Di Tocco, Emiliano Schena, Arianna Carnevale, Umile Giuseppe Longo, Jessica D'Abbraccio, Luca Massari, Calogero Maria Oddo, and Michele Arturo Caponero. Single-plane neck movements and respiratory frequency monitoring: A smart system for computer workers. In *2019 II Workshop on Metrology for Industry 4.0 and IoT (MetroInd4. 0&IoT)*, pages 167–170. IEEE, 2019.

[33] Ryotaro Nakazumi, Makito Inoue, Takashi Yoshimi, Shozo Fuchiyama, and Hiroshi Tsuchiya. Development of a respiration monitoring sensor for diving worker. In *2017 56th Annual Conference of the Society of Instrument and Control Engineers of Japan (SICE)*, pages 206–208. IEEE, 2017.

[34] Yusuke Yuasa and Kenji Suzuki. Wearable device for monitoring respiratory phases based on breathing sound and chest movement. *Advanced Biomedical Engineering*, 8:85–91, 2019.

[35] Alexis Martin and Jérémie Voix. In-ear audio wearable: Measurement of heart and breathing rates for health and safety monitoring. *IEEE Transactions on Biomedical Engineering*, 65(6):1256–1263, 2017.

[36] Atefeh Valipour and Reza Abbasi-Kesbi. A heartbeat and respiration rate sensor based on phonocardiogram for healthcare applications. In *2017 Iranian Conference on Electrical Engineering (ICEE)*, pages 45–48. IEEE, 2017.

[37] Daniel E Hurtado, Angel Abusleme, and Javier AP Chávez. Non-invasive continuous respiratory monitoring using temperature-based sensors. *Journal of clinical monitoring and computing*, pages 1–9, 2019.

[38] Anshul Basra, Bodhibrata Mukhopadhayay, and Subrat Kar. Temperature sensor based ultra low cost respiration monitoring system. In *2017 9th International Conference on Communication Systems and Networks (COMSNETS)*, pages 530–535. IEEE, 2017.

[39] Rajarshi Bhattacharya, Niladri Bandyopadhyay, and S Kalaivani. Real time android app based respiration rate monitor. In *2017 International conference of Electronics, Communication and Aerospace Technology (ICECA)*, volume 1, pages 709–712. IEEE, 2017.

[40] Tarak Das, Sayanti Guha, Nisha Banerjee, and Piyali Basak. Development of thermistor based low cost high sensitive respiration rate measurement system using audio software with audio input. In *2017 Third International Conference on Biosignals, Images and Instrumentation (ICBSII)*, pages 1–3. IEEE, 2017.

[41] Stefano Milici, Javier Lorenzo, Antonio Lazaro, Ramon Villarino, and David Girbau. Wireless breathing sensor based on wearable modulated frequency selective surface. *IEEE Sensors Journal*, 17(5):1285–1292, 2016.

[42] Sina Moradian and Reza Abdolvand. Mems-based passive wireless respiration profile sensor. In *2016 IEEE SENSORS*, pages 1–3. IEEE, 2016.

[43] A Raji, P Kanchana Devi, P Golda Jeyaseeli, and N Balaganesh. Respiratory monitoring system for asthma patients based on iot. In *2016 Online International Conference on Green Engineering and Technologies (IC-GET)*, pages 1–6. IEEE, 2016.

[44] Peng Jiang, Shuai Zhao, and Rong Zhu. Smart sensing strip using monolithically integrated flexible flow sensor for noninvasively monitoring respiratory flow. *Sensors*, 15(12):31738–31750, 2015.

[45] Chia-Ling Wei, Yu-Chen Lin, Tse-An Chen, Ren-Yi Lin, and Tin-Hao Liu. Respiration detection chip with integrated temperature-insensitive mems sensors and cmos signal processing circuits. *IEEE transactions on biomedical circuits and systems*, 9(1):105–112, 2014.

[46] P Sanchez, CR Zamarreno, CR Zamarreo, M Hernaez, IR Matias, and FJ Arregui. Exhaled breath optical fiber sensor based on lmrs for respiration monitoring. In *SENSORS, 2014 IEEE*, pages 1142–1145. IEEE, 2014.

[47] Wook Jae Yoo, Kyoung Won Jang, Jeong Ki Seo, Ji Yeon Heo, Jin Soo Moon, Jae Hoon Jun, Jang-Yeon Park, and Bongsoo Lee. Development of optical

fiber-based respiration sensor for noninvasive respiratory monitoring. *Optical review*, 18(1):132–138, 2011.

[48] Wook-Jae Yoo, Kyoung-Won Jang, Jeong-Ki Seo, Ji-Yeon Heo, Jin-Soo Moon, Jang-Yeon Park, and Bong-Soo Lee. Development of respiration sensors using plastic optical fiber for respiratory monitoring inside mri system. *Journal of the Optical Society of Korea*, 14(3):235–239, 2010.

[49] W Yoo, K Jang, J Seo, Ji Yeon Heo, Jin Soo Moon, Bongsoo Lee, and Jang-Yeon Park. Development of nasal-cavity-and abdomen-attached fiber-optic respiration sensors. *J. Korean Phys. Soc*, 57:1550–1554, 2010.

[50] Yu-Pei Huang and Ke-Nung Huang. Monitoring of breathing rate by a piezofilm sensor using pyroelectric effect. In *2013 1st International Conference on Orange Technologies (ICOT)*, pages 99–102. IEEE, 2013.

[51] Shinya Kano, Akio Yamamoto, Akira Ishikawa, and Minoru Fujii. Respiratory rate on exercise measured by nanoparticle-based humidity sensor. In *2019 41st Annual International Conference of the IEEE Engineering in Medicine and Biology Society (EMBC)*, pages 3567–3570. IEEE, 2019.

[52] Afaque Manzoor Soomro, Faiza Jabbar, Muhsin Ali, Jae-Wook Lee, Seong Woo Mun, and Kyung Hyun Choi. All-range flexible and biocompatible humidity sensor based on poly lactic glycolic acid (plga) and its application in human breathing for wearable health monitoring. *Journal of Materials Science: Materials in Electronics*, 30(10):9455–9465, 2019.

[53] Songhua Xiao, Jianxia Nie, Rou Tan, Xiaochuan Duan, Jianmin Ma, Qiuhong Li, and Taihong Wang. Fast-response ionogel humidity sensor for real-time monitoring of breathing rate. *Materials chemistry frontiers*, 3(3):484–491, 2019.

[54] Shahid Malik, Meraj Ahmad, Meera Punjiya, Aydin Sadeqi, Maryam Shojaei Baghini, and Sameer Sonkusale. Respiration monitoring using a flexible paper-based capacitive sensor. In *2018 IEEE SENSORS*, pages 1–4. IEEE, 2018.

[55] Yu Pang, Jinming Jian, Tao Tu, Zhen Yang, Jiang Ling, Yuxing Li, Xuefeng Wang, Yancong Qiao, He Tian, Yi Yang, et al. Wearable humidity sensor based on porous graphene network for respiration monitoring. *Biosensors and Bioelectronics*, 116:123–129, 2018.

[56] Shinya Kano and Minoru Fujii. Battery-powered wearable respiration sensor chip with nanocrystal thin film. In *2017 IEEE SENSORS*, pages 1–3. IEEE, 2017.

[57] Hailong Yan, Li Zhang, Ping Yu, and Lanqun Mao. Sensitive and fast humidity sensor based on a redox conducting supramolecular ionic material for respiration monitoring. *Analytical chemistry*, 89(1):996–1001, 2017.

[58] Firat Güder, Alar Ainla, Julia Redston, Bobak Mosadegh, Ana Glavan, TJ Martin, and George M Whitesides. Paper-based electrical respiration sensor. *Angewandte Chemie International Edition*, 55(19):5727–5732, 2016.

[59] Fernando C Favero, Valerio Pruneri, and Joel Villatoro. Microstructured optical fiber interferometric breathing sensor. *Journal of biomedical optics*, 17(3):037006, 2012.

[60] Jinesh Mathew, Yuliya Semenova, and Gerald Farrell. A miniature optical breathing sensor. *Biomedical optics express*, 3(12):3325–3331, 2012.

[61] Nicholas N Lepine, Takuro Tajima, Takayuki Ogasawara, Ryoichi Kasahara, and Hiroshi Koizumi. Robust respiration rate estimation using adaptive kalman filtering with textile ecg sensor and accelerometer. In *2016 38th Annual International Conference of the IEEE Engineering in Medicine and Biology Society (EMBC)*, pages 3797–3800. IEEE, 2016.

[62] Syed Absar Kazmi, Mansoor Hussain Shah, Sheroz Khan, and Othman O Khalifa. Respiratory rate (rr) based analysis of ppg signal for different physiological conditions. In *2015 International Conference on Smart Sensors and Application (ICSSA)*, pages 166–171. IEEE, 2015.

[63] Margus Metshein. A device for measuring the electrical bioimpedance with variety of electrode placements for monitoring the breathing and heart rate. In *2015 26th Irish Signals and Systems Conference (ISSC)*, pages 1–4. IEEE, 2015.

[64] Alexander M Chan, Nandakumar Selvaraj, Nima Ferdosi, and Ravi Narasimhan. Wireless patch sensor for remote monitoring of heart rate, respiration, activity, and falls. In *2013 35th Annual international conference of the IEEE engineering in medicine and biology society (EMBC)*, pages 6115–6118. IEEE, 2013.

[65] Sardar Ansari, Ashwin Belle, Kayvan Najarian, and Kevin Ward. Impedance plethysmography on the arms: Respiration monitoring. In *2010 IEEE International Conference on Bioinformatics and Biomedicine Workshops (BIBMW)*, pages 471–472. IEEE, 2010.

[66] Roman Trobec, Aleksandra Rashkovska, and Viktor Avbelj. Two proximal skin electrodes–a body sensor for respiration rate. *Sensors*, 12:13813–13828, 2012.

[67] Arman Aitkulov and Daniele Tosi. Optical fiber sensor based on plastic optical fiber and smartphone for measurement of the breathing rate. *IEEE Sensors Journal*, 19(9):3282–3287, 2019.

[68] Arman Aitkulov and Daniele Tosi. Design of an all-pof-fiber smartphone multichannel breathing sensor with camera-division multiplexing. *IEEE Sensors Letters*, 3(5):1–4, 2019.

[69] Harini Balasubramaniyam, MS Vignesh, A Abhirami, Abanah Abanah, et al. Design and development of a iot based flexible and wearable t-shirt for monitoring breathing rate. In *2019 3rd International Conference on Computing Methodologies and Communication (ICCMC)*, pages 376–379. IEEE, 2019.

[70] Michael Chu, Thao Nguyen, Vaibhav Pandey, Yongxiao Zhou, Hoang N Pham, Ronen Bar-Yoseph, Shlomit Radom-Aizik, Ramesh Jain, Dan M Cooper, and Michelle Khine. Respiration rate and volume measurements using wearable strain sensors. *NPJ digital medicine*, 2(1):1–9, 2019.

[71] Titus Jayarathna, Gaetano D Gargiulo, and Paul P Breen. Polymer sensor embedded, iot enabled t-shirt for long-term monitoring of sleep disordered breathing. In *2019 IEEE 5th World Forum on Internet of Things (WF-IoT)*, pages 139–143. IEEE, 2019.

[72] Carlo Massaroni, Joshua Di Tocco, Daniela Lo Presti, Umile Giuseppe Longo, Sandra Miccinilli, Silvia Sterzi, Domenico Formica, Paola Saccomandi, and Emiliano Schena. Smart textile based on piezoresistive sensing elements for respiratory monitoring. *IEEE Sensors Journal*, 19(17):7718–7725, 2019.

[73] Daniela Lo Presti, Carlo Massaroni, Jessica D'Abbraccio, Luca Massari, Michele Caponero, Umile Giuseppe Longo, Domenico Formica, Calogero Maria Oddo, and Emiliano Schena. Wearable system based on flexible fbg for respiratory and cardiac monitoring. *IEEE Sensors Journal*, 19(17):7391–7398, 2019.

[74] Yuya Koyama, Michiko Nishiyama, and Kazuhiro Watanabe. Smart textile using hetero-core optical fiber for heartbeat and respiration monitoring. *IEEE Sensors Journal*, 18(15):6175–6180, 2018.

[75] Talha Agcayazi, Murat A Yokus, Max Gordon, Tushar Ghosh, and Alper Bozkurt. A stitched textile-based capacitive respiration sensor. In *2017 IEEE SENSORS*, pages 1–3. IEEE, 2017.

[76] Raluca Maria Aileni, Sever Pasca, Rodica Strungaru, and Carlos Valderrama. Biomedical signal acquisition for respiration monitoring by flexible analog wearable sensors. In *2017 E-Health and Bioengineering Conference (EHB)*, pages 81–84. IEEE, 2017.

[77] Marcel Fajkus, Jan Nedoma, Radek Martinek, Vladimir Vasinek, Homer Nazeran, and Petr Siska. A non-invasive multichannel hybrid fiber-optic sensor system for vital sign monitoring. *Sensors*, 17(1):111, 2017.

[78] Stepan Gorgutsa, Simon Bellemare-Rousseau, Philippe Guay, Amine Miled, and Younes Messaddeq. Smart t-shirt with wireless respiration sensor. In *2017 IEEE SENSORS*, pages 1–3. IEEE, 2017.

[79] Philippe Guay, Stepan Gorgutsa, Sophie LaRochelle, and Younes Messaddeq. Wearable contactless respiration sensor based on multi-material fibers integrated into textile. *Sensors*, 17(5):1050, 2017.

[80] Wern Kam, Waleed S Mohammed, Gabriel Leen, Kieran O'Sullivan, Mary O'Keeffe, Sinead O'Keeffe, and Elfed Lewis. All plastic optical fiber-based respiration monitoring sensor. In *2017 IEEE SENSORS*, pages 1–3. IEEE, 2017.

[81] Wern Kam, Waleed Soliman Mohammed, Gabriel Leen, Mary O'Keeffe, Kieran O'Sullivan, Sinead O'Keeffe, and Elfed Lewis. Compact and low-cost optical fiber respiratory monitoring sensor based on intensity interrogation. *Journal of Lightwave Technology*, 35(20):4567–4573, 2017.

[82] Wern Kam, Waleed S Mohammed, Sinead O'Keeffe, and Elfed Lewis. Portable 3-d printed plastic optical fibre motion sensor for monitoring of breathing pattern and respiratory rate. In *2019 IEEE 5th World Forum on Internet of Things (WF-IoT)*, pages 144–148. IEEE, 2019.

[83] Eugen Koch and Andreas Dietzel. Stretchable sensor array for respiratory monitoring. In *2017 19th international conference on solid-state sensors, actuators and microsystems (TRANSDUCERS)*, pages 2227–2230. IEEE, 2017.

[84] Seong Won Park, Partha Sarati Das, Ashok Chhetry, and Jae Yeong Park. A flexible capacitive pressure sensor for wearable respiration monitoring system. *IEEE Sensors Journal*, 17(20):6558–6564, 2017.

[85] Neil M White, Jordan Ash, Yang Wei, and Harry Akerman. A planar respiration sensor based on a capaciflector structure. *IEEE sensors letters*, 1(4):1–4, 2017.

[86] Ifana Mahbub, Salvatore Andrea Pullano, Hanfeng Wang, Syed Kamrul Islam, Antonino S Fiorillo, Gary To, and MR Mahfouz. A low-power wireless piezoelectric sensor-based respiration monitoring system realized in cmos process. *IEEE Sensors Journal*, 17(6):1858–1864, 2017.

[87] K Chethana, AS Guru Prasad, SN Omkar, and S Asokan. Fiber bragg grating sensor based device for simultaneous measurement of respiratory and cardiac activities. *Journal of biophotonics*, 10(2):278–285, 2017.

[88] Anindya Nag, Subhas Chandra Mukhopadhyay, and Jürgen Kosel. Flexible carbon nanotube nanocomposite sensor for multiple physiological parameter monitoring. *Sensors and Actuators A: Physical*, 251:148–155, 2016.

[89] Raul I Ramos-Garcia, Fernanda Da Silva, Yashvanth Kondi, Edward Sazonov, and Lucy E Dunne. Analysis of a coverstitched stretch sensor for monitoring of breathing. In *2016 10th international conference on sensing technology (ICST)*, pages 1–6. IEEE, 2016.

[90] Ozgur Atalay, William Richard Kennon, and Erhan Demirok. Weft-knitted strain sensor for monitoring respiratory rate and its electro-mechanical modeling. *IEEE Sensors Journal*, 15(1):110–122, 2014.

[91] Marco Ciocchetti, Carlo Massaroni, Paola Saccomandi, Michele A Caponero, Andrea Polimadei, Domenico Formica, and Emiliano Schena. Smart textile based on fiber bragg grating sensors for respiratory monitoring: Design and preliminary trials. *Biosensors*, 5(3):602–615, 2015.

[92] Gaetano D Gargiulo, Upul Gunawardana, Aiden O'Loughlin, Mohammad Sadozai, Elham Shabani Varaki, and Paul P Breen. A wearable contactless sensor suitable for continuous simultaneous monitoring of respiration and cardiac activity. *Journal of Sensors*, 2015, 2015.

[93] P Bifulco, GD Gargiulo, G d'Angelo, A Liccardo, M Romano, F Clemente, M Cesarelli, G Angelo, A Liccardo, M Romano, et al. Monitoring of respiration, seismocardiogram and heart sounds by a pvdf piezo film sensor. *Measurement*, 11:786–789, 2014.

[94] Marek Krehel, Michel Schmid, René M Rossi, Luciano F Boesel, Gian-Luca Bona, and Lukas J Scherer. An optical fibre-based sensor for respiratory monitoring. *Sensors*, 14(7):13088–13101, 2014.

[95] Marija D Petrović, Jovana Petrovic, Aleksandar Daničić, Miodrag Vukčević, Bosko Bojović, Lj Hadžievski, T Allsop, Glynn Lloyd, and David J Webb. Non-invasive respiratory monitoring using long-period fiber grating sensors. *Biomedical optics express*, 5(4):1136–1144, 2014.

[96] Jianghai Wo, He Wang, Qizhen Sun, Perry Ping Shum, and Deming Liu. Noninvasive respiration movement sensor based on distributed bragg reflector fiber laser with beat frequency interrogation. *Journal of biomedical optics*, 19(1):017003, 2014.

[97] Subrata Kumar Kundu, Shinya Kumagai, and Minoru Sasaki. A wearable capacitive sensor for monitoring human respiratory rate. *Japanese Journal of Applied Physics*, 52(4S):04CL05, 2013.

[98] Yi-Yuan Chiu, Wan-Ying Lin, Hsin-Yao Wang, Song-Bin Huang, and Min-Hsien Wu. Development of a piezoelectric polyvinylidene fluoride (pvdf) polymer-based sensor patch for simultaneous heartbeat and respiration monitoring. *Sensors and Actuators A: Physical*, 189:328–334, 2013.

[99] Janusz Zieba, Michał Frydrysiak, and Jan Błaszczyk. Textronic clothing with resistance textile sensor to monitoring frequency of human breathing. In *2012 IEEE International Symposium on Medical Measurements and Applications Proceedings*, pages 1–6. IEEE, 2012.

[100] Rovira Carlos, Shirley Coyle, Brian Corcoran, Dermot Diamond, Ward Tomas, McCoy Aaron, Florin Stroiescu, and Kieran Daly. Web-based sensor streaming wearable for respiratory monitoring applications. In *SENSORS, 2011 IEEE*, pages 901–903. IEEE, 2011.

[101] Li Guo, Lena Berglin, YJ Li, Heikki Mattila, A Kalantar Mehrjerdi, and M Skrifvars. 'disappearing sensor'-textile based sensor for monitoring breathing. In *2011 International Conference on Control, Automation and Systems Engineering (CASE)*, pages 1–4. IEEE, 2011.

[102] Shaopeng Liu, Robert X Gao, and Patty S Freedson. Non-invasive respiration and ventilation prediction using a single abdominal sensor belt. In *2011 IEEE Signal Processing in Medicine and Biology Symposium (SPMB)*, pages 1–5. IEEE, 2011.

[103] AF Silva, JP Carmo, PM Mendes, and JH Correia. Simultaneous cardiac and respiratory frequency measurement based on a single fiber bragg grating sensor. *Measurement Science and Technology*, 22(7):075801, 2011.

[104] Edmond Mitchell, Shirley Coyle, Noel E O'Connor, Dermot Diamond, and Tomas Ward. Breathing feedback system with wearable textile sensors. In *2010 International Conference on Body Sensor Networks*, pages 56–61. IEEE, 2010.

[105] Zhengbo Zhang, Hao Wu, Weidong Wang, and Buqing Wang. A smartphone based respiratory biofeedback system. In *2010 3rd International Conference on Biomedical Engineering and Informatics*, volume 2, pages 717–720. IEEE, 2010.

[106] Aurélien Bricout, Julie Fontecave-Jallon, Damien Colas, Grégoire Gerard, Jean-Louis Pépin, and Pierre-Yves Guméry. Adaptive accelerometry derived respiration: Comparison with respiratory inductance plethysmography during sleep. In *2019 41st Annual International Conference of the IEEE Engineering in Medicine and Biology Society (EMBC)*, pages 6714–6717. IEEE, 2019.

[107] Tamer Elfaramawy, Cheikh Latyr Fall, Soodeh Arab, Martin Morissette, Francois Lellouche, and Benoit Gosselin. A wireless respiratory monitoring system using a wearable patch sensor network. *IEEE Sensors Journal*, 19(2):650–657, 2018.

[108] Gürkan Karacocuk, Fabian Höflinger, Rui Zhang, Leonhard M Reindl, Bernhard Laufer, Knut Möller, Mareike Röell, and Denise Zdzieblik. Inertial sensor-based respiration analysis. *IEEE Transactions on Instrumentation and Measurement*, 68(11):4268–4275, 2019.

[109] K Anmol Puranik and M Kanthi. Wearable device for yogic breathing. In *2019 Amity International Conference on Artificial Intelligence (AICAI)*, pages 605–610. IEEE, 2019.

[110] He Zhang, Jiwei Zhang, Zhiwei Hu, Liwei Quan, Lin Shi, Jinkai Chen, Weipeng Xuan, Zhicheng Zhang, Shurong Dong, and Jikui Luo. Waist-wearable wireless respiration sensor based on triboelectric effect. *Nano Energy*, 59:75–83, 2019.

[111] Luis Estrada, Abel Torres, Leonardo Sarlabous, and Raimon Jané. Respiratory signal derived from the smartphone built-in accelerometer during a respiratory load protocol. In *2015 37th Annual International Conference of the IEEE Engineering in Medicine and Biology Society (EMBC)*, pages 6768–6771. IEEE, 2015.

[112] Javier Hernandez, Daniel McDuff, and Rosalind W Picard. Biowatch: estimation of heart and breathing rates from wrist motions. In *2015 9th International Conference on Pervasive Computing Technologies for Healthcare (PervasiveHealth)*, pages 169–176. IEEE, 2015.

[113] Atena Roshan Fekr, Katarzyna Radecka, and Zeljko Zilic. Tidal volume variability and respiration rate estimation using a wearable accelerometer sensor. In *2014 4th International Conference on Wireless Mobile Communication and Healthcare-Transforming Healthcare Through Innovations in Mobile and Wireless Technologies (MOBIHEALTH)*, pages 1–6. IEEE, 2014.

[114] Ja-Woong Yoon, Yeon-Sik Noh, Yi-Suk Kwon, Won-Ki Kim, and Hyung-Ro Yoon. Improvement of dynamic respiration monitoring through sensor fusion of accelerometer and gyro-sensor. *Journal of electrical engineering & technology*, 9(1):334–343, 2014.

[115] Guan-Zheng Liu, Yan-Wei Guo, Qing-Song Zhu, Bang-Yu Huang, and Lei Wang. Estimation of respiration rate from three-dimensional acceleration data based on body sensor network. *Telemedicine and e-health*, 17(9):705–711, 2011.

[116] Tomohiro Ono, Hideki Takegawa, Tatsuya Ageishi, Masaaki Takashina, Hodaka Numasaki, Masao Matsumoto, and Teruki Teshima. Respiratory monitoring with an acceleration sensor. *Physics in Medicine & Biology*, 56(19):6279, 2011.

[117] Róisín Howard, Richard Conway, and Andrew J Harrison. Estimation of force during vertical jumps using body fixed accelerometers. 2014.

[118] Tyler D Whitmer, Andrew C Fry, Charles M Forsythe, Matthew J Andre, Michael T Lane, Andrea Hudy, and Darric E Honnold. Accuracy of a vertical jump contact mat for determining jump height and flight time. *The Journal of Strength & Conditioning Research*, 29(4):877–881, 2015.

[119] Carlos Balsalobre-Fernández, Mark Glaister, and Richard Anthony Lockey. The validity and reliability of an iphone app for measuring vertical jump performance. *Journal of sports sciences*, 33(15):1574–1579, 2015.

[120] Jonathan Ache Dias, Juliano Dal Pupo, Diogo C Reis, Lucas Borges, Saray G Santos, Antônio RP Moro, and Noé G Borges Jr. Validity of two methods for estimation of vertical jump height. *The Journal of Strength & Conditioning Research*, 25(7):2034–2039, 2011.

[121] S Boukhenous and M Attari. A vertical jumping performance with and without arms swing by using a dynamometric platform. In *International Workshop on Systems, Signal Processing and their Applications, WOSSPA*, pages 17–20. IEEE, 2011.

[122] Carlos Balsalobre-Fernández, Carlos M Tejero-González, Juan del Campo-Vecino, and Nicolás Bavaresco. The concurrent validity and reliability of a low-cost, high-speed camera-based method for measuring the flight time of vertical jumps. *The Journal of Strength & Conditioning Research*, 28(2):528–533, 2014.

[123] Shaghayegh Zihajehzadeh, Tien Jung Lee, Jung Keun Lee, Reynald Hoskinson, and Edward J Park. Integration of mems inertial and pressure sensors for vertical trajectory determination. *IEEE transactions on Instrumentation and Measurement*, 64(3):804–814, 2014.

[124] James L Nuzzo, Jonathan H Anning, and Jessica M Scharfenberg. The reliability of three devices used for measuring vertical jump height. *The Journal of Strength & Conditioning Research*, 25(9):2580–2590, 2011.

[125] Anuar Mohamed Kassim, Mohammad Fahmi Miskon, NHA Rahim, and Takashi Yasuno. Effectiveness of reference height control system for tripod hopping robot. In *2011 4th International Conference on Mechatronics (ICOM)*, pages 1–4. IEEE, 2011.

[126] Phillip A Laplante, Mohamad Kassab, Nancy L Laplante, and Jeffrey M Voas. Building caring healthcare systems in the internet of things. *IEEE systems journal*, 12(3):3030–3037, 2017.

[127] Praveen Gunaratne, Hiroki Tamura, Chika Yoshida, Keiko Sakurai, Koichi Tanno, Nobuya Takahashi, and Junko Nagata. A study on breathing and heartbeat monitoring system during sleeping using multi-piezoelectric elements. In *2019 Moratuwa Engineering Research Conference (MERCon)*, pages 382–387. IEEE, 2019.

[128] Shijie Guo, Xingli Zhao, Kazuya Matsuo, Jinyue Liu, and Toshiharu Mukai. Unconstrained detection of the respiratory motions of chest and abdomen in different lying positions using a flexible tactile sensor array. *IEEE Sensors Journal*, 19(21):10067–10076, 2019.

[129] Shiroh Isono, Natsuko Nozaki-Taguchi, Makoto Hasegawa, Shinichiro Kato, Shinsuke Todoroki, Shigemi Masuda, Norihito Iida, Toshiaki Nishimura, Masatoshi Noto, and Yasunori Sato. Contact-free unconstraint respiratory measurements with load cells under the bed in awake healthy volunteers: Breath-by-breath comparison with pneumotachography. *Journal of Applied Physiology*, 126(5):1432–1441, 2019.

[130] Rohan Joshi, Bart Bierling, Loe Feijs, Carola Van Pul, and Peter Andriessen. Monitoring the respiratory rate of preterm infants using an ultrathin film sensor embedded in the bedding: a comparative feasibility study. *Physiological measurement*, 40(4):045003, 2019.

[131] Mariusz Krej, Paulina Baran, and Łukasz Dziuda. Detection of respiratory rate using a classifier of waves in the signal from a fbg-based vital signs sensor. *Computer methods and programs in biomedicine*, 177:31–38, 2019.

[132] Sooji Park, Hyong-Ho Choi, Hyung Chae Yang, Jin-Sang Yoon, and Hangsik Shin. Force-sensing-based unobtrusive system for awakening and respiration rate analysis during sleep. *IEEE Sensors Journal*, 19(5):1917–1924, 2018.

[133] Shuwen Chen, Nan Wu, Long Ma, Shizhe Lin, Fang Yuan, Zisheng Xu, Wenbo Li, Bo Wang, and Jun Zhou. Noncontact heartbeat and respiration monitoring based on a hollow microstructured self-powered pressure sensor. *ACS applied materials & interfaces*, 10(4):3660–3667, 2018.

[134] Ibrahim Sadek, Edwin Seet, Jit Biswas, Bessam Abdulrazak, and Mounir Mokhtari. Nonintrusive vital signs monitoring for sleep apnea patients: a preliminary study. *IEEE Access*, 6:2506–2514, 2017.

[135] H Azimi, S Soleimani Gilakjani, Martin Bouchard, S Bennett, Rafik A Goubran, and Frank Knoefel. Breathing signal combining for respiration rate estimation in smart beds. In *2017 IEEE International Symposium on Medical Measurements and Applications (MeMeA)*, pages 303–307. IEEE, 2017.

[136] Lennart Leicht, Pascal Vetter, Steffen Leonhardt, and Daniel Teichmann. The physiobelt: A safety belt integrated sensor system for heart activity and respiration. In *2017 IEEE International Conference on Vehicular Electronics and Safety (ICVES)*, pages 191–195. IEEE, 2017.

[137] Kunpu Li, Wei Xu, Na Zhan, Ketian Wan, Cheungchuen Yu, and Changyuan Yu. Non-wearable respiration monitoring based on mach-zehnder interferometer. In *2017 Conference on Lasers and Electro-Optics Pacific Rim (CLEO-PR)*, pages 1–2. IEEE, 2017.

[138] Fatih Erden, Ali Ziya Alkar, and Ahmet Enis Cetin. Contact-free measurement of respiratory rate using infrared and vibration sensors. *Infrared Physics & Technology*, 73:88–94, 2015.

[139] Jason J Liu, Ming-Chun Huang, Wenyao Xu, Xiaoyi Zhang, Luke Stevens, Nabil Alshurafa, and Majid Sarrafzadeh. Breathsens: A continuous on-bed respiratory monitoring system with torso localization using an unobtrusive pressure sensing array. *IEEE journal of biomedical and health informatics*, 19(5):1682–1688, 2014.

[140] Zhihao Chen, Doreen Lau, Ju Teng Teo, Soon Huat Ng, Xiufeng Yang, and Pin Lin Kei. Simultaneous measurement of breathing rate and heart rate using a microbend multimode fiber optic sensor. *Journal of biomedical optics*, 19(5):057001, 2014.

[141] Juan Aponte Luis, Laura M Roa Romero, Juan Antonio Gómez-Galán, David Naranjo Hernández, Miguel Ángel Estudillo-Valderrama, Gerardo Barbarov-Rostán, and Carlos Rubia-Marcos. Design and implementation of a smart sensor for respiratory rate monitoring. *Sensors*, 14(2):3019–3032, 2014.

[142] Toshiharu Mukai, Kazuya Matsuo, Yo Kato, Atsuki Shimizu, and Shijie Guo. Determination of locations on a tactile sensor suitable for respiration and heartbeat measurement of a person on a bed. In *2014 36th Annual International Conference of the IEEE Engineering in Medicine and Biology Society*, pages 66–69. IEEE, 2014.

[143] Shoko Nukaya, Manabu Sugie, Yosuke Kurihara, Tomoyuki Hiroyasu, Kajiro Watanabe, and Hiroshi Tanaka. A noninvasive heartbeat, respiration, and body movement monitoring system for neonates. *Artificial Life and Robotics*, 19(4):414–419, 2014.

[144] Tal Klap and Zvika Shinar. Using piezoelectric sensor for continuous-contact-free monitoring of heart and respiration rates in real-life hospital settings. In *Computing in Cardiology 2013*, pages 671–674. IEEE, 2013.

[145] Doreen Lau, Zhihao Chen, Ju Teng Teo, Soon Huat Ng, Helmut Rumpel, Yong Lian, Hui Yang, and Pin Lin Kei. Intensity-modulated microbend fiber optic sensor for respiratory monitoring and gating during mri. *IEEE Transactions on Biomedical Engineering*, 60(9):2655–2662, 2013.

[146] Sebastijan Šprager and Damjan Zazula. Detection of heartbeat and respiration from optical interferometric signal by using wavelet transform. *Computer methods and programs in biomedicine*, 111(1):41–51, 2013.

[147] Christoph Brüser, Anna Kerekes, Stefan Winter, and Steffen Leonhardt. Multi-channel optical sensor-array for measuring ballistocardiograms and

respiratory activity in bed. In *2012 annual international conference of the IEEE engineering in medicine and biology society*, pages 5042–5045. IEEE, 2012.

[148] Zhihao Chen, Ju Teng Teo, Soon Huat Ng, and Xiufeng Yang. Plastic optical fiber microbend sensor used as breathing sensor. In *SENSORS, 2012 IEEE*, pages 1–4. IEEE, 2012.

[149] Lukasz Dziuda, Franciszek Skibniewski, Krzysztof Rozanowski, Mariusz Krej, and Jaroslaw Lewandowski. Fiber-optic sensor for monitoring respiration and cardiac activity. In *SENSORS, 2011 IEEE*, pages 413–416. IEEE, 2011.

[150] Shongpun Lokavee, Theeraporn Puntheeranurak, Teerakiat Kerdcharoen, Natthapol Watthanwisuth, and Adisorn Tuantranont. Sensor pillow and bed sheet system: Unconstrained monitoring of respiration rate and posture movements during sleep. In *2012 IEEE International Conference on Systems, Man, and Cybernetics (SMC)*, pages 1564–1568. IEEE, 2012.

[151] David Heise and Marjorie Skubic. Monitoring pulse and respiration with a non-invasive hydraulic bed sensor. In *2010 annual international conference of the IEEE engineering in medicine and biology*, pages 2119–2123. IEEE, 2010.

[152] Michiko Nishiyama, Mitsuo Miyamoto, and Kazuhiro Watanabe. Respiration rhythm monitoring in sleep based on weight movement using hetero-core fiber optic sensors. In *ICCAS 2010*, pages 205–208. IEEE, 2010.

[153] Michiko Nishyama, Mitsuo Miyamoto, and Kazuhiro Watanabe. Respiration and body movement analysis during sleep in bed using hetero-core fiber optic pressure sensors without constraint to human activity. *Journal of biomedical optics*, 16(1):017002, 2011.

[154] Łukasz Dziuda, Mariusz Krej, and Franciszek Wojciech Skibniewski. Fiber bragg grating strain sensor incorporated to monitor patient vital signs during mri. *IEEE Sensors Journal*, 13(12):4986–4991, 2013.

[155] Arturs Ivanovs, Agris Nikitenko, Mario Di Castro, Toms Torims, Alessandro Masi, and Manuel Ferre. Multisensor low-cost system for real time human detection and remote respiration monitoring. In *2019 Third IEEE international conference on robotic computing (IRC)*, pages 254–257. IEEE, 2019.

[156] Carlo Massaroni, Daniela Lo Presti, Domenico Formica, Sergio Silvestri, and Emiliano Schena. Non-contact monitoring of breathing pattern and respiratory rate via rgb signal measurement. *Sensors*, 19(12):2758, 2019.

[157] AP Prathosh, Pragathi Praveena, Lalit K Mestha, and Sanjay Bharadwaj. Estimation of respiratory pattern from video using selective ensemble aggregation. *IEEE Transactions on Signal Processing*, 65(11):2902–2916, 2017.

[158] Aleš Procházka, Martin Schätz, Oldřich Vyšata, and Martin Vališ. Microsoft kinect visual and depth sensors for breathing and heart rate analysis. *Sensors*, 16(7):996, 2016.

[159] Daniel Myklatun Tveit, Kjersti Engan, Ivar Austvoll, and Øyvind Meinich-Bache. Motion based detection of respiration rate in infants using video. In *2016 IEEE International Conference on Image Processing (ICIP)*, pages 1225–1229. IEEE, 2016.

[160] Tsukasa Ushijima and Junji Satake. Development of a breathing detection robot for a monitoring system. In *2016 Joint 8th International Conference on Soft Computing and Intelligent Systems (SCIS) and 17th International Symposium on Advanced Intelligent Systems (ISIS)*, pages 790–795. IEEE, 2016.

[161] Natascia Bernacchia, Lorenzo Scalise, Luigi Casacanditella, Ilaria Ercoli, Paolo Marchionni, and Enrico Primo Tomasini. Non contact measurement of heart and respiration rates based on kinect™. In *2014 IEEE International Symposium on Medical Measurements and Applications (MeMeA)*, pages 1–5. IEEE, 2014.

[162] Dangdang Shao, Yuting Yang, Chenbin Liu, Francis Tsow, Hui Yu, and Nongjian Tao. Noncontact monitoring breathing pattern, exhalation flow rate and pulse transit time. *IEEE Transactions on Biomedical Engineering*, 61(11):2760–2767, 2014.

[163] Marek Bartula, Timo Tigges, and Jens Muehlsteff. Camera-based system for contactless monitoring of respiration. In *2013 35th Annual International Conference of the IEEE Engineering in Medicine and Biology Society (EMBC)*, pages 2672–2675. IEEE, 2013.

[164] Hirooki Aoki, Masaki Miyazaki, Hidetoshi Nakamura, Ryo Furukawa, Ryusuke Sagawa, and Hiroshi Kawasaki. Non-contact respiration measurement using structured light 3-d sensor. In *2012 Proceedings of SICE annual conference (SICE)*, pages 614–618. IEEE, 2012.

[165] Junyi Xia and R Alfredo Siochi. A real-time respiratory motion monitoring system using kinect: proof of concept. *Medical physics*, 39(5):2682–2685, 2012.

[166] Se Dong Min, Jin Kwon Kim, Hang Sik Shin, Yong Hyeon Yun, Chung Keun Lee, and Myoungho Lee. Noncontact respiration rate measurement system using an ultrasonic proximity sensor. *IEEE sensors journal*, 10(11):1732–1739, 2010.

[167] K Song Tan, Reza Saatchi, Heather Elphick, and Derek Burke. Real-time vision based respiration monitoring system. In *2010 7th International Symposium on Communication Systems, Networks & Digital Signal Processing (CSNDSP 2010)*, pages 770–774. IEEE, 2010.

[168] Ali Al-Wahedi, Mojtaba Al-Shams, Mohammed Aieash Albettar, Saleh Alawsh, and Ali Muqaibel. Wireless monitoring of respiration and heart rates using software-defined-radio. In *2019 16th International Multi-Conference on Systems, Signals & Devices (SSD)*, pages 529–532. IEEE, 2019.

[169] Ying Chen, Masahiko Kaneko, Shinichi Hirose, and Wenxi Chen. Real-time respiration measurement during sleep using a microwave sensor. In *2019 41st Annual International Conference of the IEEE Engineering in Medicine and Biology Society (EMBC)*, pages 3791–3794. IEEE, 2019.

[170] Ingo Walterscheid, Oliver Biallawons, and Patrick Berens. Contactless respiration and heartbeat monitoring of multiple people using a 2-d imaging radar. In *2019 41st Annual International Conference of the IEEE Engineering in Medicine and Biology Society (EMBC)*, pages 3720–3725. IEEE, 2019.

[171] Tianben Wang, Daqing Zhang, Leye Wang, Yuanqing Zheng, Tao Gu, Bernadette Dorizzi, and Xingshe Zhou. Contactless respiration monitoring using ultrasound signal with off-the-shelf audio devices. *IEEE Internet of Things Journal*, 6(2):2959–2973, 2018.

[172] Yanni Yang, Jiannong Cao, Xiulong Liu, and Xuefeng Liu. Multi-breath: Separate respiration monitoring for multiple persons with uwb radar. In *2019 IEEE 43rd Annual Computer Software and Applications Conference (COMPSAC)*, volume 1, pages 840–849. IEEE, 2019.

[173] Alexander Tataraidze, Lesya Anishchenko, Lyudmila Korostovtseva, Mikhail Bochkarev, Yurii Sviryaev, and Irina Alborova. Detection of movement activity and breathing cycles on bioradiolocation signals. In *2017 IEEE International Conference on Microwaves, Antennas, Communications and Electronic Systems (COMCAS)*, pages 1–4. IEEE, 2017.

[174] Xuyu Wang, Runze Huang, and Shiwen Mao. Sonarbeat: Sonar phase for breathing beat monitoring with smartphones. In *2017 26th International Conference on Computer Communication and Networks (ICCCN)*, pages 1–8. IEEE, 2017.

[175] Ruthvik Kukkapalli, Nilanjan Banerjee, Ryan Robucci, and Yordan Kostov. Micro-radar wearable respiration monitor. In *2016 IEEE SENSORS*, pages 1–3. IEEE, 2016.

[176] Gregory P Heldt and Raymond J Ward. Evaluation of ultrasound-based sensor to monitor respiratory and nonrespiratory movement and timing in infants. *IEEE transactions on biomedical engineering*, 63(3):619–629, 2015.

[177] Ruth Ravichandran, Elliot Saba, Ke-Yu Chen, Mayank Goel, Sidhant Gupta, and Shwetak N Patel. Wibreathe: Estimating respiration rate using wireless signals in natural settings in the home. In *2015 IEEE International Conference on Pervasive Computing and Communications (PerCom)*, pages 131–139. IEEE, 2015.

[178] Eriko Sasaki and Akihiro Kajiwara. Multiple respiration monitoring by stepped-fm uwb sensor. In *2015 IEEE International Conference on Computational Intelligence & Communication Technology*, pages 406–409. IEEE, 2015.

[179] Mari Zakrzewski, Antti Vehkaoja, Atte S Joutsen, Karri T Palovuori, and Jukka J Vanhala. Noncontact respiration monitoring during sleep with microwave doppler radar. *IEEE Sensors Journal*, 15(10):5683–5693, 2015.

[180] Philippe Arlotto, Michel Grimaldi, Roomila Naeck, and Jean-Marc Ginoux. An ultrasonic contactless sensor for breathing monitoring. *Sensors*, 14(8):15371–15386, 2014.

[181] Tayebeh Taheri and Anita Sant'Anna. Non-invasive breathing rate detection using a very low power ultra-wide-band radar. In *2014 IEEE International Conference on Bioinformatics and Biomedicine (BIBM)*, pages 78–83. IEEE, 2014.

[182] Gabor Vinci, Stefan Lindner, Francesco Barbon, Sebastian Mann, Maximilian Hofmann, Alexander Duda, Robert Weigel, and Alexander Koelpin. Six-port radar sensor for remote respiration rate and heartbeat vital-sign monitoring. *IEEE Transactions on Microwave Theory and Techniques*, 61(5):2093–2100, 2013.

[183] Ehsan Yavari, Hsun Jou, Victor Lubecke, and Olga Boric-Lubecke. Doppler radar sensor for occupancy monitoring. In *2013 IEEE Topical Conference on Power Amplifiers for Wireless and Radio Applications*, pages 145–147. IEEE, 2013.

[184] Changzhan Gu, Ruijiang Li, Hualiang Zhang, Albert YC Fung, Carlos Torres, Steve B Jiang, and Changzhi Li. Accurate respiration measurement using dc-coupled continuous-wave radar sensor for motion-adaptive cancer radiotherapy. *IEEE Transactions on biomedical engineering*, 59(11):3117–3123, 2012.

[185] Nao Shimomura, Mitsugu Otsu, and Akihiro Kajiwara. Empirical study of remote respiration monitoring sensor using wideband system. In *2012 6th International Conference on Signal Processing and Communication Systems*, pages 1–5. IEEE, 2012.

[186] Joshua Chong Yue Lai, Ying Xu, Erry Gunawan, Eric Chern-Pin Chua, Arash Maskooki, Yong Liang Guan, Kay-Soon Low, Cheong Boon Soh, and Chueh-Loo Poh. Wireless sensing of human respiratory parameters by low-power ultrawideband impulse radio radar. *IEEE Transactions on Instrumentation and Measurement*, 60(3):928–938, 2010.

[187] Mitsugu Otsu, Ryohei Nakamura, and Akihiro Kajiwara. Remote respiration monitoring sensor using stepped-fm. In *2011 IEEE Sensors Applications Symposium*, pages 155–158. IEEE, 2011.

[188] Octavian Postolache, Pedro Silva Girão, Gabriela Postolache, and Joaquim Gabriel. Cardio-respiratory and daily activity monitor based on fmcw doppler radar embedded in a wheelchair. In *2011 Annual International Conference of the IEEE Engineering in Medicine and Biology Society*, pages 1917–1920. IEEE, 2011.

[189] Domenico Zito, Domenico Pepe, Martina Mincica, Fabio Zito, Alessandro Tognetti, Antonio Lanatà, and Danilo De Rossi. Soc cmos uwb pulse radar sensor for contactless respiratory rate monitoring. *IEEE transactions on biomedical circuits and systems*, 5(6):503–510, 2011.

[190] K Mostov, E Liptsen, and R Boutchko. Medical applications of shortwave fm radar: Remote monitoring of cardiac and respiratory motion. *Medical physics*, 37(3):1332–1338, 2010.

[191] Lorenzo Scalise, Paolo Marchionni, and Ilaria Ercoli. Optical method for measurement of respiration rate. In *2010 IEEE International Workshop on Medical Measurements and Applications*, pages 19–22. IEEE, 2010.

[192] Jerry Silvious and David Tahmoush. Uhf measurement of breathing and heartbeat at a distance. In *2010 IEEE Radio and Wireless Symposium (RWS)*, pages 567–570. IEEE, 2010.

[193] Ilde Lorato, Tom Bakkes, Sander Stuijk, Mohammed Meftah, and Gerard de Haan. Unobtrusive respiratory flow monitoring using a thermopile array: A feasibility study. *Applied Sciences*, 9(12):2449, 2019.

[194] Youngjun Cho, Nadia Bianchi-Berthouze, Simon J Julier, and Nicolai Marquardt. Thermsense: Smartphone-based breathing sensing platform using noncontact low-cost thermal camera. In *2017 Seventh International Conference on Affective Computing and Intelligent Interaction Workshops and Demos (ACIIW)*, pages 83–84. IEEE, 2017.

[195] Aleš Procházka, Hana Charvátová, Oldřich Vyšata, Jakub Kopal, and Jonathon Chambers. Breathing analysis using thermal and depth imaging camera video records. *Sensors*, 17(6):1408, 2017.

[196] Carina B Pereira, Xinchi Yu, Vladimir Blazek, and Steffen Leonhardt. Robust remote monitoring of breathing function by using infrared thermography. In *2015 37th Annual International Conference of the IEEE Engineering in Medicine and Biology Society (EMBC)*, pages 4250–4253. IEEE, 2015.

[197] Laura Boccanfuso and Jason M O'Kane. Remote measurement of breathing rate in real time using a high precision, single-point infrared temperature sensor. In *2012 4th IEEE RAS & EMBS International Conference on Biomedical Robotics and Biomechatronics (BioRob)*, pages 1704–1709. IEEE, 2012.

[198] Julia F Glatthorn, Sylvain Gouge, Silvio Nussbaumer, Simone Stauffacher, Franco M Impellizzeri, and Nicola A Maffiuletti. Validity and reliability of optojump photoelectric cells for estimating vertical jump height. *The Journal of Strength & Conditioning Research*, 25(2):556–560, 2011.

[199] John S Leard, Melissa A Cirillo, Eugene Katsnelson, Deena A Kimiatek, Tim W Miller, Kenan Trebincevic, and Juan C Garbalosa. Validity of two alternative systems for measuring vertical jump height. *Journal of Strength and Conditioning Research*, 21(4):1296, 2007.

[200] Daniela Lo Presti, Carlo Massaroni, Domenico Formica, Paola Saccomandi, Francesco Giurazza, Michele Arturo Caponero, and Emiliano Schena. Smart textile based on 12 fiber bragg gratings array for vital signs monitoring. *IEEE Sensors Journal*, 17(18):6037–6043, 2017.

[201] Carlo Massaroni, M Ciocchetti, Giulia Di Tomaso, Paola Saccomandi, Michele A Caponero, Andrea Polimadei, Domenico Formica, and Emiliano Schena. Design and preliminary assessment of a smart textile for respiratory monitoring based on an array of fiber bragg gratings. In *2016 38th Annual International Conference of the IEEE Engineering in Medicine and Biology Society (EMBC)*, pages 6054–6057. IEEE, 2016.

[202] Edgar A Bernal, Lalit K Mestha, and Eribaweimon Shilla. Non contact monitoring of respiratory function via depth sensing. In *IEEE-EMBS International Conference on Biomedical and Health Informatics (BHI)*, pages 101–104. IEEE, 2014.

[203] Yogesh Nijsure, Wee Peng Tay, Erry Gunawan, Fuxi Wen, Zhang Yang, Yong Liang Guan, and Ai Ping Chua. An impulse radio ultrawideband system for contactless noninvasive respiratory monitoring. *IEEE Transactions on Biomedical Engineering*, 60(6):1509–1517, 2013.

[204] Yee Siong Lee, Pubudu N Pathirana, Christopher Louis Steinfort, and Terry Caelli. Monitoring and analysis of respiratory patterns using microwave doppler radar. *IEEE journal of translational engineering in health and medicine*, 2:1–12, 2014.

[205] Ching-Wei Wang, Andrew Hunter, Neil Gravill, and Simon Matusiewicz. Unconstrained video monitoring of breathing behavior and application to diagnosis of sleep apnea. *IEEE Transactions on Biomedical Engineering*, 61(2):396–404, 2013.

[206] Xinming Huang, Ling Sun, Tian Tian, Zeyan Huang, and Edward Clancy. Real-time non-contact infant respiratory monitoring using uwb radar. In *2015 IEEE 16th International Conference on Communication Technology (ICCT)*, pages 493–496. IEEE, 2015.

[207] Marc Hesse, Peter Christ, Timm Hörmann, and Ulrich Rückert. A respiration sensor for a chest-strap based wireless body sensor. In *SENSORS, 2014 IEEE*, pages 490–493. IEEE, 2014.

[208] Cristian Rotariu, Ciprian Cristea, Dragos Arotaritei, Radu G Bozomitu, and Alexandru Pasarica. Continuous respiratory monitoring device for detection of sleep apnea episodes. In *2016 IEEE 22nd international symposium for design and technology in electronic packaging (SIITME)*, pages 106–109. IEEE, 2016.

[209] Razvan Ciobotariu, Cristian Rotariu, Felix Adochiei, and Hariton Costin. Wireless breathing system for long term telemonitoring of respiratory activity. In *2011 7th International Symposium on Advanced Topics in Electrical Engineering (ATEE)*, pages 1–4. IEEE, 2011.

[210] Josip Grlica, Toni Martinović, and Hrvoje Džapo. Capacitive sensor for respiration monitoring. In *2015 IEEE Sensors Applications Symposium (SAS)*, pages 1–6. IEEE, 2015.

[211] CM Yang, TL Yang, CC Wu, SH Hung, MH Liao, MJ Su, and HC Hsieh. Textile-based capacitive sensor for a wireless wearable breath monitoring system. In *2014 IEEE International Conference on Consumer Electronics (ICCE)*, pages 232–233. IEEE, 2014.

[212] Se Dong Min, Yonghyeon Yun, and Hangsik Shin. Simplified structural textile respiration sensor based on capacitive pressure sensing method. *IEEE Sensors Journal*, 14(9):3245–3251, 2014.

[213] Jens Witt, François Narbonneau, Marcus Schukar, Katerina Krebber, Julien De Jonckheere, Mathieu Jeanne, Damien Kinet, Bernard Paquet, Annick Depre, Lorenzo T D'Angelo, et al. Medical textiles with embedded fiber optic sensors for monitoring of respiratory movement. *IEEE sensors journal*, 12(1):246–254, 2011.

[214] M Jeanne, F Narbonneau, J Witt, B Paquet, Damien Kinet, K Kreber, R Logier, et al. Ofseth: A breathing motions monitoring system for patients under mri. In *2010 Annual International Conference of the IEEE Engineering in Medicine and Biology*, pages 1016–1019. IEEE, 2010.

[215] Carlo Massaroni, Paola Saccomandi, Domenico Formica, Daniela Lo Presti, Michele Arturo Caponero, Giulia Di Tomaso, Francesco Giurazza, Mario Muto, and Emiliano Schena. Design and feasibility assessment of a magnetic resonance-compatible smart textile based on fiber bragg grating sensors for respiratory monitoring. *IEEE Sensors Journal*, 16(22):8103–8110, 2016.

[216] Xiufeng Yang, Zhihao Chen, Chia Ser Ming Elvin, Lam Hong Ying Janice, Soon Huat Ng, Ju Teng Teo, and Ruifen Wu. Textile fiber optic microbend sensor used for heartbeat and respiration monitoring. *IEEE Sensors Journal*, 15(2):757–761, 2014.

[217] Bryson Padasdao, Ehsaneh Shahhaidar, Christopher Stickley, and Olga Boric-Lubecke. Electromagnetic biosensing of respiratory rate. *IEEE Sensors Journal*, 13(11):4204–4211, 2013.

[218] Daniel Teichmann, Dennis De Matteis, Thorsten Bartelt, Marian Walter, and Steffen Leonhardt. A bendable and wearable cardiorespiratory monitoring device fusing two noncontact sensor principles. *IEEE journal of biomedical and health informatics*, 19(3):784–793, 2015.

[219] David L Schriger. Approach to the patient with abnormal vital signs. In *Goldman's Cecil Medicine*, pages 27–30. Elsevier, 2012.

[220] Wilburta Q Lindh, Marilyn Pooler, Carol D Tamparo, Barbara M Dahl, and Julie Morris. *Delmar's comprehensive medical assisting: administrative and clinical competencies*. Nelson Education, 2013.

[221] Mathworks. Lowpass function. `https://es.mathworks.com/help/signal/ref/lowpass.html`, 2021. [Online; consultado 23-Enero-2021].

[222] Guo Dan, Junhao Zhao, Zihao Chen, Huanyu Yang, and Zhemin Zhu. A novel signal acquisition system for wearable respiratory monitoring. *IEEE Access*, 6:34365–34371, 2018.

[223] Janek Mann, R Rabinovich, Andrew Bates, S Giavedoni, W MacNee, and DK Arvind. Simultaneous activity and respiratory monitoring using an accelerometer. In *2011 International Conference on Body Sensor Networks*, pages 139–143. IEEE, 2011.

[224] Carlo Massaroni, Daniela Lo Presti, Paola Saccomandi, Michele Arturo Caponero, Rosaria D'Amato, and Emiliano Schena. Fiber bragg grating probe for relative humidity and respiratory frequency estimation: assessment during mechanical ventilation. *IEEE Sensors Journal*, 18(5):2125–2130, 2017.

[225] Carlo Massaroni, Emiliano Schena, Sergio Silvestri, Fabrizio Taffoni, and Mario Merone. Measurement system based on rbg camera signal for contactless breathing pattern and respiratory rate monitoring. In *2018 IEEE International*

Symposium on Medical Measurements and Applications (MeMeA), pages 1–6. IEEE, 2018.

[226] Yunyoung Nam, Bersain A Reyes, and Ki H Chon. Estimation of respiratory rates using the built-in microphone of a smartphone or headset. *IEEE journal of biomedical and health informatics*, 20(6):1493–1501, 2015.

[227] Christopher G Scully, Jinseok Lee, Joseph Meyer, Alexander M Gorbach, Domhnull Granquist-Fraser, Yitzhak Mendelson, and Ki H Chon. Physiological parameter monitoring from optical recordings with a mobile phone. *IEEE Transactions on Biomedical Engineering*, 59(2):303–306, 2011.

[228] Chen Chen, Yi Han, Yan Chen, Hung-Quoc Lai, Feng Zhang, Beibei Wang, and KJ Ray Liu. Tr-breath: Time-reversal breathing rate estimation and detection. *IEEE Transactions on Biomedical Engineering*, 65(3):489–501, 2017.

[229] Neal Patwari, Joey Wilson, Sai Ananthanarayanan, Sneha K Kasera, and Dwayne R Westenskow. Monitoring breathing via signal strength in wireless networks. *IEEE Transactions on Mobile Computing*, 13(8):1774–1786, 2013.

[230] Kim E Barrett, Scott Boitano, Susan M Barman, and Heddwen L Brooks. Ganong's review of medical physiology twenty. 2010.

[231] Walter Karlen, Ainara Garde, Dorothy Myers, Cornie Scheffer, J Mark Ansermino, and Guy A Dumont. Estimation of respiratory rate from photoplethysmographic imaging videos compared to pulse oximetry. *IEEE journal of biomedical and health informatics*, 19(4):1331–1338, 2015.

[232] Neal Patwari, Lara Brewer, Quinn Tate, Ossi Kaltiokallio, and Maurizio Bocca. Breathfinding: A wireless network that monitors and locates breathing in a home. *IEEE Journal of Selected Topics in Signal Processing*, 8(1):30–42, 2013.

[233] Michael H Li, Azadeh Yadollahi, and Babak Taati. Noncontact vision-based cardiopulmonary monitoring in different sleeping positions. *IEEE journal of biomedical and health informatics*, 21(5):1367–1375, 2016.

[234] Jacob Cohen. *Statistical power analysis for the behavioral sciences*. Academic press, 2013.

[235] Erik Vanegas, Yolocuauhtli Salazar, Raúl Igual, and Inmaculada Plaza. Force-sensitive mat for vertical jump measurement to assess lower limb strength: Validity and reliability study. *JMIR mHealth and uHealth*, 9(4):e27336, 2021.

[236] Carlos Medrano-Sánchez, Raul Igual-Catalán, Victor H. Rodríguez-Ontiveros, and Inmaculada Plaza-García. Circuit analysis of matrix-like resistor networks for eliminating crosstalk in pressure sensitive mats. *IEEE Sensors Journal*, 19(18):8027–8036, 2019.

[237] Diego Andrés Valle-Lopera, Andrés Felipe Castaño-Franco, Jonathan Gallego-Londoño, and Alher Mauricio Hernández-Valdivieso. Test and fabrication of piezoresistive sensors for contact pressure measurement. *Revista Facultad de Ingeniería Universidad de Antioquia*, (82):47–52, 2017.

[238] Davide Giovanelli and Elisabetta Farella. Force sensing resistor and evaluation of technology for wearable body pressure sensing. *Journal of Sensors*, 2016, 2016.

[239] Michael Sipser. Introduction to the theory of computation. *ACM Sigact News*, 27(1):27–29, 1996.

[240] Warren Young. Laboratory strength assessment of athletes. *New studies in athletics*, 10:89–89, 1995.

[241] Goran Markovic, Drazan Dizdar, Igor Jukic, and Marco Cardinale. Reliability and factorial validity of squat and countermovement jump tests. *The Journal of Strength & Conditioning Research*, 18(3):551–555, 2004.

[242] Kuangyou B Cheng, Chih-Hung Wang, Hui-Chuan Chen, Chin-Dai Wu, and Hung-Ta Chiu. The mechanisms that enable arm motion to enhance vertical jump performance—a simulation study. *Journal of biomechanics*, 41(9):1847–1854, 2008.

[243] Michael E Feltner, Daniel J Fraschetti, and Robert J Crisp. Upper extremity augmentation of lower extremity kinetics during countermovement vertical jumps. *Journal of sports sciences*, 17(6):449–466, 1999.

[244] Everett A Harman, Michael T Rosenstein, Peter N Frykman, Richard M ROSenStein, et al. The effects of arms and countermovement on vertical jumping. *Med Sci Sports Exerc*, 22(6):825–833, 1990.

[245] Erik Vanegas, Raul Igual, and Inmaculada Plaza. Breathing data from a piezoresistive breathing sensor. `https://dx.doi.org/10.21227/zcqc-3h94`, 2019. [Cargado 25-Octubre-2019].

[246] Erik Vanegas, Raúl Igual, and Inmaculada Plaza. The effect of measurement trends in belt breathing sensors. In *Presented at the 8th International Symposium on Sensor Science*, volume 17, page 26, 2021.

[247] Mathworks. Remove Trends from Data. `https://www.mathworks.com/help/signal/ug/remove-trends-from-data.html`, 2021. [Online; consultado 07-Abril-2021].

[248] Miguel Ángel Pérez García. *Instrumentación electrónica*. Ediciones Paraninfo, SA, 2014.

[249] Hung Tien Bui, Marie-Isabelle Farinas, Anne-Marie Fortin, Alain-Steve Comtois, and Mario Leone. Comparison and analysis of three different methods to evaluate vertical jump height. *Clinical physiology and functional imaging*, 35(3):203–209, 2015.

[250] Jurek Z Sasiadek. Sensor fusion. *Annual Reviews in Control*, 26(2):203–228, 2002.

[251] David D Patterson and D Fred Peterson. Vertical jump and leg power norms for young adults. *Measurement in Physical Education and Exercise Science*, 8(1):33–41, 2004.

[252] Ifana Mahbub, Hanfeng Wang, Syed K Islam, Salvatore A Pullano, and Antonino S Fiorillo. A low power wireless breathing monitoring system using piezoelectric transducer. In *2016 IEEE International Symposium on Medical Measurements and Applications (MeMeA)*, pages 1–5. IEEE, 2016.

[253] Chang-Ming Yang, Tsu-lin Yang, Chih-chung Wu, and Narisa NY Chu. A breathing game with capacitive textile sensors. In *2011 IEEE International Games Innovation Conference (IGIC)*, pages 134–136. IEEE, 2011.

Listado de Figuras

2.1. Lugares del cuerpo donde usualmente se colocan los sistemas vestibles. Los sistemas mostrados son solo de referencia. 10

3.1. Curva característica del FSR utilizado para el sistema vestible. 18
3.2. Histogramas con la distribución de voltaje (a), resistencia (b), y fuerza (c) de las señales capturadas. 19
3.3. Diagrama de bloques del funcionamiento general del sistema desarrollado. 19
3.4. Diseño del armazón impreso en 3D, con material rígido (a) y material flexible (b). 20
3.5. Diseño interior del armazón impreso en 3D. 21
3.6. Sistema vestible construido. 21
3.7. Comparación entre la señal original junto al efecto del Bias y la señal ajustada. 22
3.8. Diagrama de bloques de los algoritmos utilizados para predecir el ritmo respiratorio. 24
3.9. Dos voluntarios portando alrededor del pecho el sistema desarrollado. . 26
3.10. Ejemplo de dos señales diferentes obtenidas por medio del sistema vestible, la gráfica superior se obtuvo de un ritmo respiratorio de 10BPM en una posición sentada y sin movimiento, mientras que la gráfica inferior se obtivo a 17.5BPM mientras el sujeto caminaba. 27
3.11. Esquema de los experimentos de validación. 30
3.12. Diferentes capas que componen la matriz de sensores FSR (alfombrila) de menores dimensiones. 32
3.13. Ejemplo de una matriz de sensores FSR de menores dimensiones, y cómo son colocadas sus capas. 32
3.14. Ejemplo de una de las alfombrillas desarrolladas por el grupo de investigación. 33
3.15. Diagrama de bloques del funcionamiento del sistema propuesto. 34
3.16. Técnica para el salto con contramovimiento (CMJ), ilustrado paso a paso. 37

3.17. Técnica para el salto con contramovimiento y braceo (CMJAS), ilustrado paso a paso. 37
3.18. Ubicación de todos los elementos durante la ejecución del protocolo propuesto. 38

4.1. Errores relativos δ obtenidos de las predicciones de los dos algoritmos utilizados. 39
4.2. Técnicas de ajuste lineal utilizadas: (a) Método 1: Ajuste lineal aplicado a la señal completa; (b) Método 2: Ajuste lineal aplicado de forma individual a cada ventana de tiempo segmentada. 41
4.3. Mejora y deterioro obtenidos al calcular el ritmo respiratorio después de realizar el ajuste lineal a las señales respiratorias mediante el primer método descrito. 43
4.4. Mejora y deterioro obtenidos al calcular el ritmo respiratorio después de realizar el ajuste lineal a las señales respiratorias mediante el segundo método descrito. 43
4.5. Comparación entre el diseño del armazón realizado por software y el diseño construido mediante impresión 3D. 46
4.6. Dos voluntarios ejecutando saltos según el protocolo prupuesto. Se muestran diferentes fases del salto: el cuadro de despegue, el cuadro de altura máxima y el cuadro de aterrizaje. 48
4.7. Gráfica de correlación que compara ambos métodos de medición para el primer experimento, mostrando un coeficiente de determinación $R^2 =$ 0,996. 49
4.8. Análisis de Bland-Altman de los dos métodos de medición. Los CMJ se muestran con los puntos gris oscuro, mientras que los CMJAS se muestran con los puntos gris claro. 49
4.9. MRE y MAE normalizados, divididos en diferentes rangos de altura alcanzados por los voluntarios. 50
4.10. MRE y MAE normalizados, divididos en diferentes rangos de altura alcanzados por los voluntarios. 50
4.11. MRE obtenido de cada frecuencia de muestro utilizada. Conforme se disminuye la frecuencia de muestreo, el error relativo se incrementa exponencialmente. 52

C.1. Circuito esquemático diseñado para el sistema de respiración; utilizado para la construcción de la PCB. 102

C.2. Diseño de la placa realizada por software (arriba) y placa final construida (abajo). 103

D.1. Circuito esquemático diseñado para el sistema de respiración; utilizado para la construcción de la PCB. 106
D.2. Diseño de la placa realizada por software (arriba) y placa final construida (abajo). 107

E.1. Comparación entre las señales obtenidas de la primera y segunda versión del sistema vestible para la medición de la respiración. En la Figura se muestra arriba la señal obtenida de la primer versión, mientras que la señal de abajo es la obtenida con la segunda versión. Las señales corresponden a un ritmo respiratorio de 10BPM. 110
E.2. Comparación entre las señales obtenidas de la primera y segunda versión del sistema vestible para la medición de la respiración. En la Figura se muestra arriba la señal obtenida de la primer versión, mientras que la señal de abajo es la obtenida con la segunda versión. Las señales corresponden a un ritmo respiratorio de 12.5BPM. 111
E.3. Comparación entre las señales obtenidas de la primera y segunda versión del sistema vestible para la medición de la respiración. En la Figura se muestra arriba la señal obtenida de la primer versión, mientras que la señal de abajo es la obtenida con la segunda versión. Las señales corresponden a un ritmo respiratorio de 15BPM. 112
E.4. Comparación entre las señales obtenidas de la primera y segunda versión del sistema vestible para la medición de la respiración. En la Figura se muestra arriba la señal obtenida de la primer versión, mientras que la señal de abajo es la obtenida con la segunda versión. Las señales corresponden a un ritmo respiratorio de 17.5BPM. 113
E.5. Comparación entre las señales obtenidas de la primera y segunda versión del sistema vestible para la medición de la respiración. En la Figura se muestra arriba la señal obtenida de la primer versión, mientras que la señal de abajo es la obtenida con la segunda versión. Las señales corresponden a un ritmo respiratorio de 20BPM. 114
E.6. Comparación entre las señales obtenidas de la primera y segunda versión del sistema vestible para la medición de la respiración. En la Figura se muestra arriba la señal obtenida de la primer versión, mientras que la señal de abajo es la obtenida con la segunda versión. Las señales corresponden a un ritmo respiratorio de 22.5BPM. 115

G.1. Circuito esquemático diseñado para el sistema de salto vertical; utilizado para la construcción de la PCB. 120
G.2. Diseño de la primera placa realizada por software (arriba) y placa final construida (abajo). 121
G.3. Diseño de la segunda placa realizada por software (arriba) y placa final construida (abajo). 122

L.1. Al escanear este código QR se puede acceder al repositorio con todos los archivos obtenidos como resultado del trabajo de la presente tesis. Entre los archivos del repositorio se encuentran: Archivos “Gerber” para construcción de PCBs, diseños 3D para impresión de armazones de los sitemas desarrollados, códigos utilizados por los mincrocontroladores de los sistemas y datos en crudo obtenidos por los sistemas. 249

Listado de Tablas

3.1. Comparativa de protocolos de validación realizados por estudios cuyo sistema vestible se basa en la detección de movimientos del pecho. . . . 26

3.2. Valores normalizados de activación de los sensores FSR, registrados de los voluntarios al pararse sobre la alfombrilla en diferentes posiciones: de pie y de puntillas con ambos pies, de pie y de puntillas con un solo pie. 35

3.3. Valores de correlación de Pearson (valores R) obtenidos de las diferentes posiciones analizadas, que fueron calculados tanto para peso como para el tamaño del pie de los voluntarios. 35

4.1. Mejora en el ritmo respiratorio calculado después del ajuste lineal realizado a la señal respiratoria original, con ambos métodos de ajuste y para ambos algoritmos. 42

4.2. Comparación de la sensibilidad entre ambas versiones del sistema vestible de respiración. 47

4.3. Valores de MAE y MRE para todos los saltos, solo los saltos CMJ y solo los saltos CMJAS. 48

4.4. MRE y errores relativos máximo y mínimo obtenidos de los 90 saltos analizados para cada una de las frecuencias emuladas. 51

4.5. Porcentaje del total de saltos cuyo error relativo es del 5 % o menos, está entre el 5 % y el 15 %, y es mayor al 15 %. 52

4.6. MRE obtenido para diferentes rangos de altura alcanzados por los voluntarios, para todas las frecuencias de muestreo analizadas. 52

B.1. Comparación de tecnologías utilizadas en diferentes estudios que emplearon sistemas vestibles con el mismo principio de funcionamiento al desarrollado en esta tesis. 100

F.1. Valores p mayores (>) o menores (<) que el nivel de significancia (0.05) para el ritmo respiratorio calculado para cada ventana y valor de referencia. 117

F.2. Comparación de los dos algoritmos. Valores ‘p’ de la prueba-t para muestras emparejadas y ‘d’ de Cohen para errores calculados con una ventana de 27 segundos. 117

Anexos

Anexo A

Producción científica

En este apartado se presenta la producción científica resultado de esta tesis, en la que se incluyen publicaciones en revistas indexadas JCR (Journal Citation Report) y congresos internacionales.

A.1. Publicaciones en revistas indexadas

Título	Piezoresistive Breathing Sensing System with 3D Printed Wearable Casing
Autores	Erik Vanegas, Raul Igual e Inmaculada Plaza
Revista	Journal of Sensors
Factor de impacto (JCR)	1.595 (2019) Q3 ENGENEERING, ELECTRICAL & ELECTRONIC
Fecha de publicación	4 de diciembre de 2019
Enlace web	https://doi.org/10.1155/2019/2431731

Título	Sensing systems for respiration monitoring: A technical systematic review
Autores	Erik Vanegas, Raul Igual e Inmaculada Plaza
Revista	Sensors
Factor de impacto (JCR)	3.576 (2020) Q1 INSTRUMENTS & INSTRUMENTATION
Fecha de publicación	22 de septiembre de 2020
Enlace web	https://doi.org/10.3390/s20185446

Título	Force-Sensitive Mat for Vertical Jump Measurement to Assess Lower Limb Strength: Validity and Reliability Study
Autores	Erik Vanegas, Yolocuauhtli Salazar, Raul Igual e Inmaculada Plaza
Revista	JMIR mHealth and uHealth
Factor de impacto (JCR)	4.773 (2020) Q1 HEALTH CARE SCIENCES & SERVICES
Fecha de publicación	4 de abril de 2021
Enlace web	https://doi.org/10.2196/27336

A.2. Publicaciones en congresos internacionales

Título	The effect of measurement trends in belt breathing sensors
Autores	Erik Vanegas, Raul Igual e Inmaculada Plaza
Conferencia	8th International Symposium on Sensor Science session Sensor Applications and Smart Systems
Lugar	Dresden, Alemania
Fecha	17-28 de mayo de 2021
Enlace web	https://sciforum.net/paper/view/10118 (DOI:10.3390/I3S2021Dresden-10118)

Anexo B

Comparación de tecnologías

Tabla B.1: Comparación de tecnologías utilizadas en diferentes estudios que emplearon sistemas vestibles con el mismo principio de funcionamiento al desarrollado en esta tesis.

Estudio	Sensor	Unidad de procesamiento	Unidad de monitoreo	Frecuencia de muestreo	Transmisión de datos
Sistema desarrollado	Piezoresistivo	Arduino Pro-Mini (Atmega 328p)	Dispositivos móviles, PC	50Hz	Bluetooth
Hesse et al. [207]	Piezoresistivo	MSP430FG4618	PC	100Hz	Memoria interna Radio Frecuencia
Mahbub et al. [252]	Transductor PVDF	ADC	-	-	Banda Ultra-ancha
Rotariu et al. [208]	Cinturón piezoeléctrico	Arduino Leonardo	Tablet, PC	10Hz	Comunicación Serial
Ciobotariu et al. [209]	Cinturón piezoeléctrico	Asistente digital personal	PC	10Hz	WiFi GSM/GPRS Comunicación Serial
Hoffman et al. [7]	Capacitivo	MSP430F1612	PC	6Hz	Bluetooth
Grlica et al. [210]	Capacitivo	Tarjeta de adquisición de datos comercial	PC	9.1Hz	Comunicación Serial
Yang et al. [211]	Capacitivo	-	Smartphone	-	Bluetooth
Yang et al. [253]	Capacitivo	PIC24FJ256	PC	10Hz	Bluetooth
Min et al. [212]	Capacitivo	Tarjeta de adquisición de datos comercial	PC	100Hz	Comunicación Serial
Witt et al. [213]	Fibra óptica	Tarjeta de adquisición de datos comercial	Tarjeta de adquisición de datos comercial	250Hz	Fibra optica
Jonckheere et al. [214]	Fibra óptica	Tarjeta de adquisición de datos comercial	PC	-	Comunicación Serial
Lo Presti et al. [200]	Fibra óptica	Tarjeta de adquisición de datos comercial	PC	250Hz	Comunicación Serial
Massaroni et al. [215]	Fibra óptica	Tarjeta de adquisición de datos comercial	PC	250Hz	Comunicación Serial
Yang et al. [216]	Fibra óptica	Transceptor óptico	PC	-	Bluetooth
Padasdao et al. [217]	Motor DC	-	-	-	-
Teichmann et al. [218]	Bobina de acoplamiento electromagnético	Microcontrolador	Dispositivos móviles, PC	100Hz	Bluetooth

Anexo C

Diseños del sistema vestible de respiración: Versión 1.0

C.1. Circuito esquemático y PCB

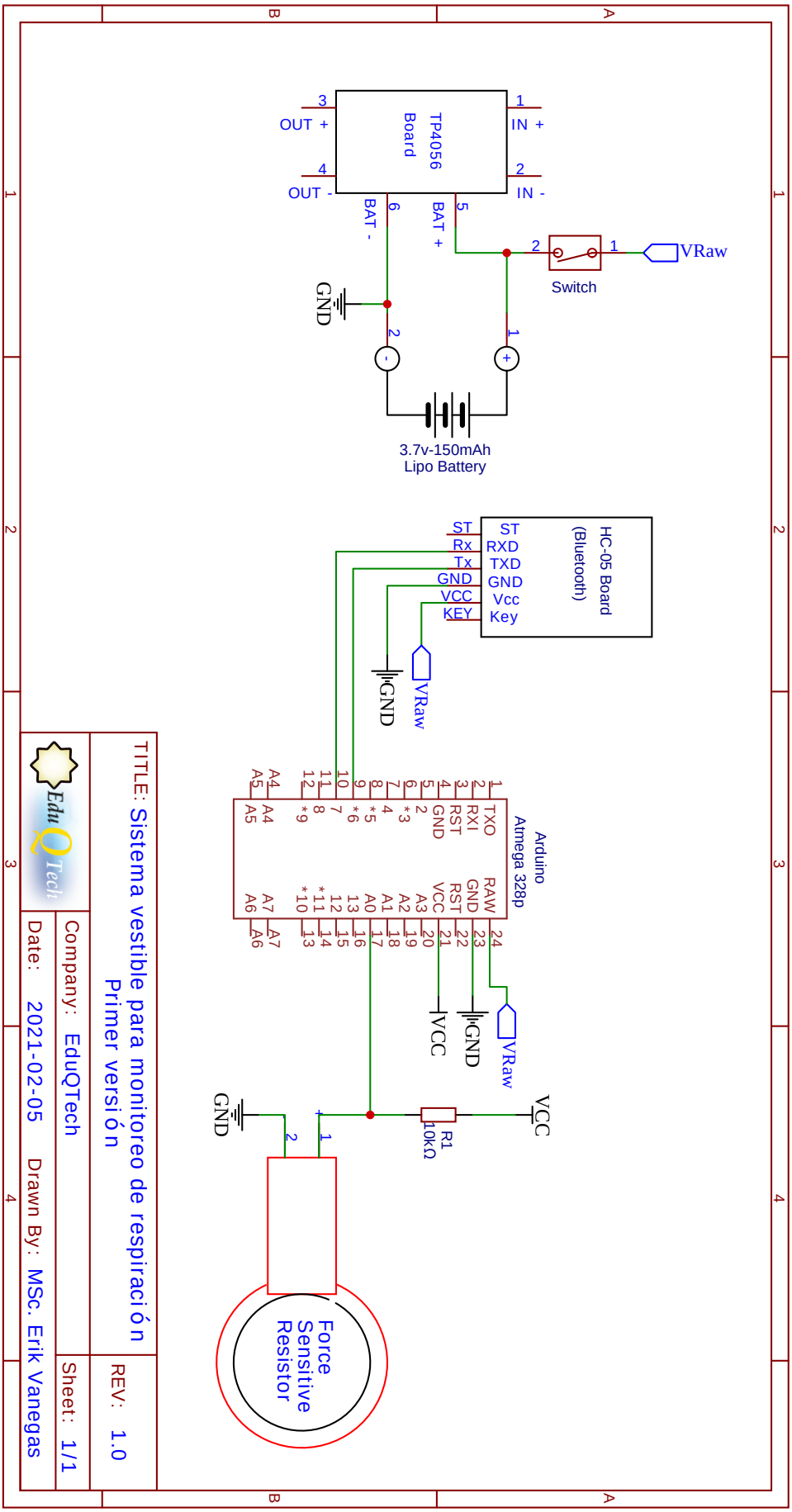

Figura C.1: Circuito esquemático diseñado para el sistema de respiración; utilizado para la construcción de la PCB.

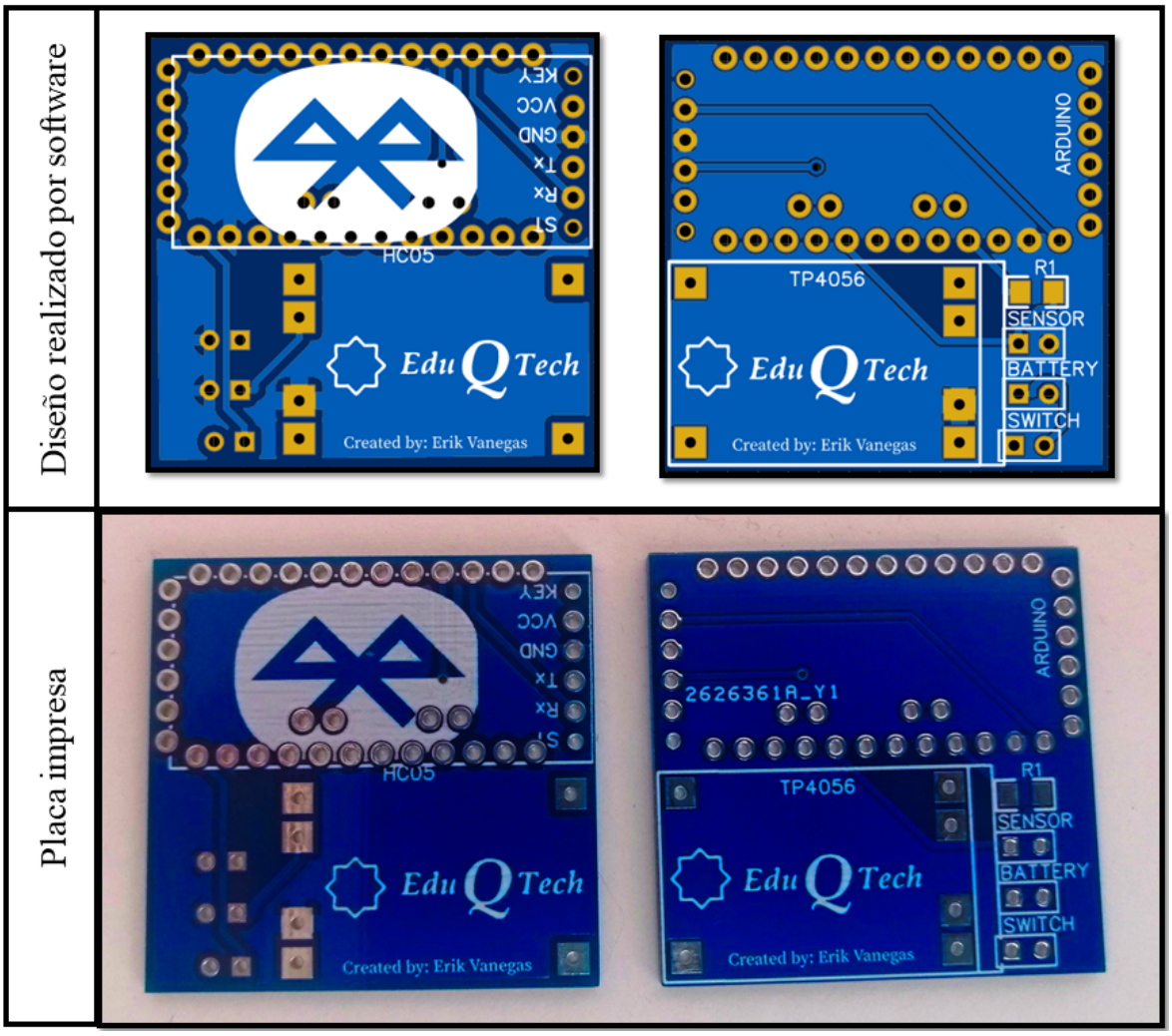

Figura C.2: Diseño de la placa realizada por software (arriba) y placa final construida (abajo).

Anexo D

Diseños del sistema vestible de respiración: Versión 2.0

D.1. Circuito esquemático y PCB

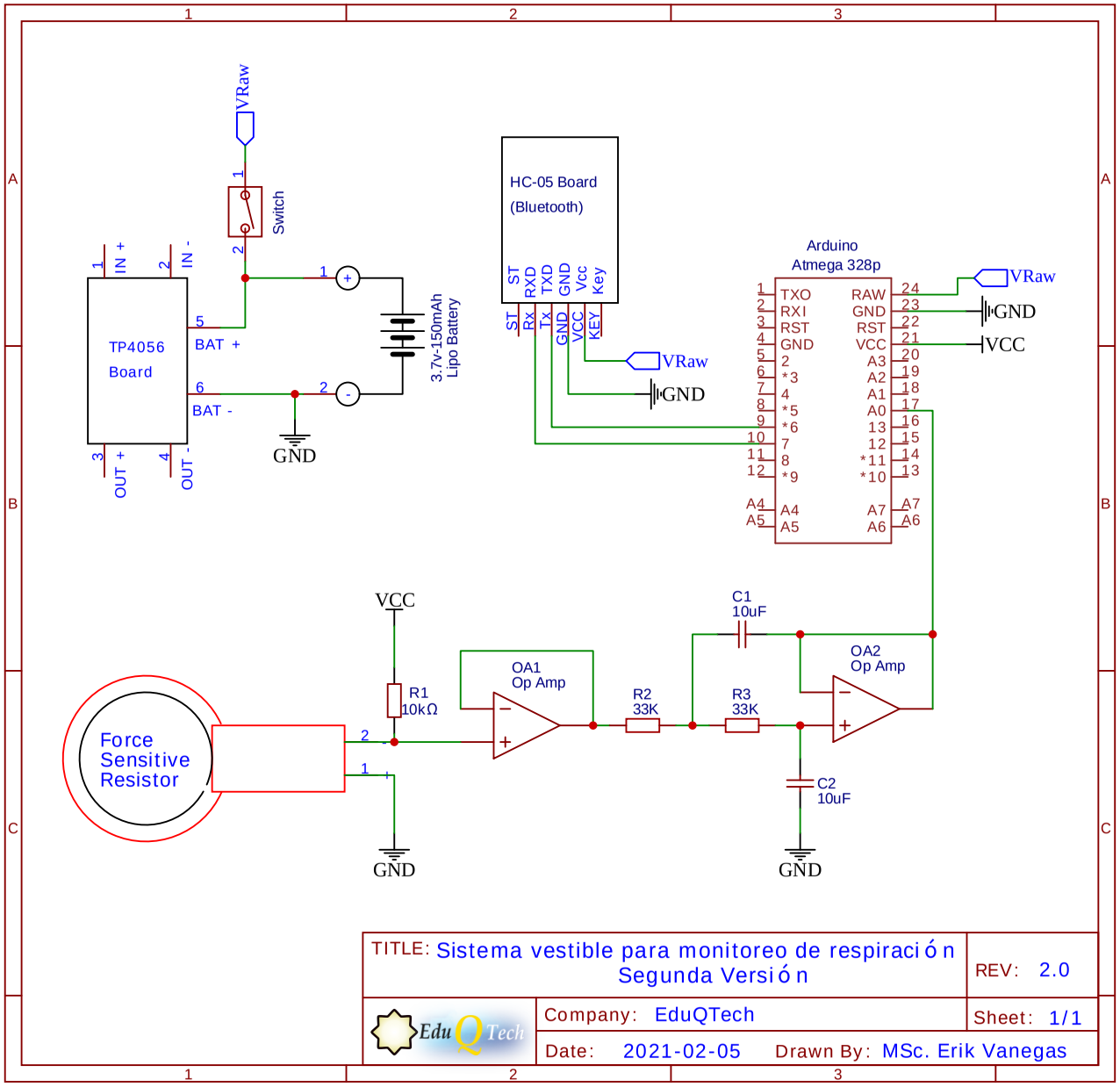

Figura D.1: Circuito esquemático diseñado para el sistema de respiración; utilizado para la construcción de la PCB.

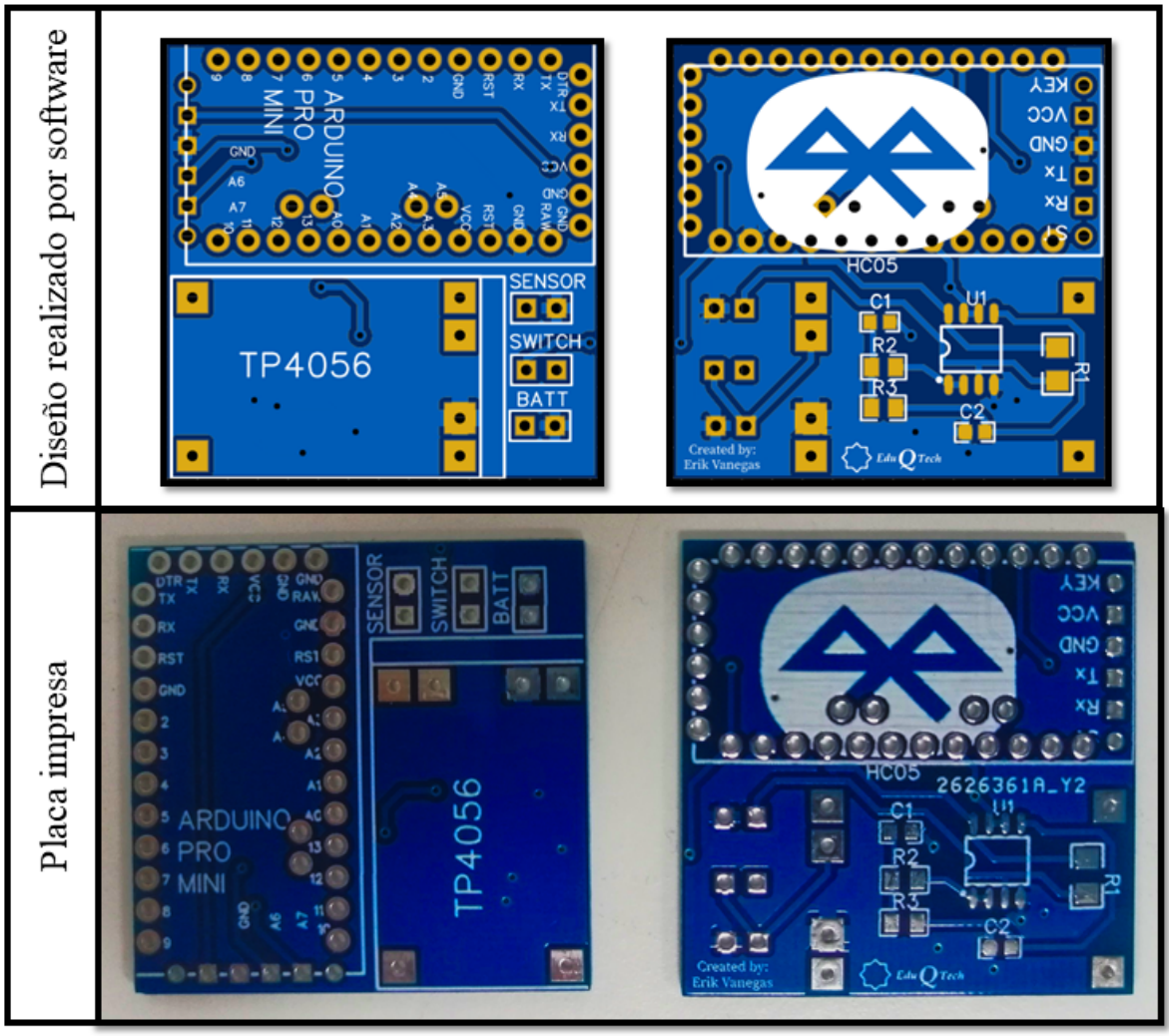

Figura D.2: Diseño de la placa realizada por software (arriba) y placa final construida (abajo).

Anexo E

Comparación de señales obtenidas: Primera y segunda versión del sistema vestible para la medición de la respiración

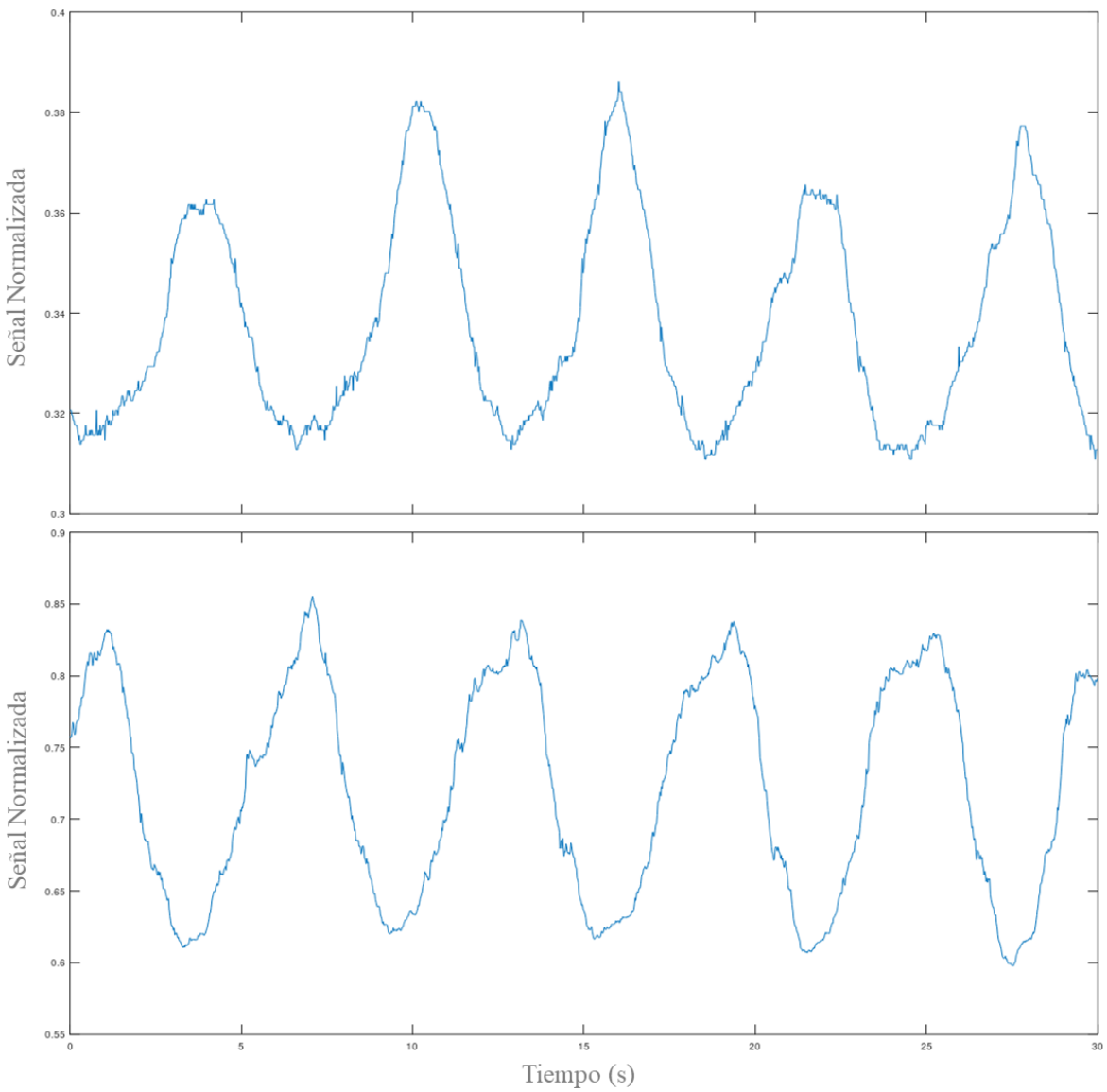

Figura E.1: Comparación entre las señales obtenidas de la primera y segunda versión del sistema vestible para la medición de la respiración. En la Figura se muestra arriba la señal obtenida de la primer versión, mientras que la señal de abajo es la obtenida con la segunda versión. Las señales corresponden a un ritmo respiratorio de 10BPM.

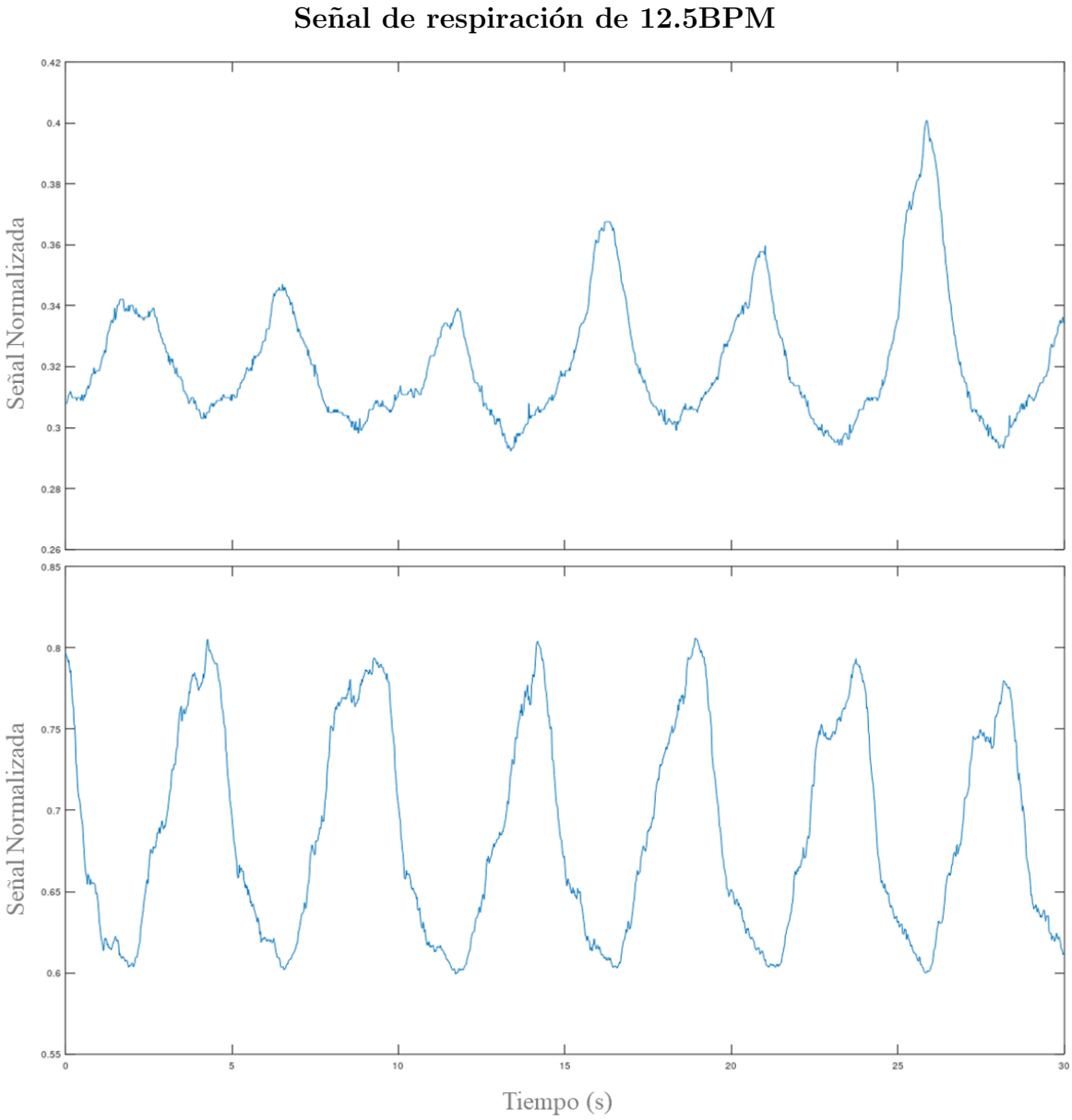

Figura E.2: Comparación entre las señales obtenidas de la primera y segunda versión del sistema vestible para la medición de la respiración. En la Figura se muestra arriba la señal obtenida de la primer versión, mientras que la señal de abajo es la obtenida con la segunda versión. Las señales corresponden a un ritmo respiratorio de 12.5BPM.

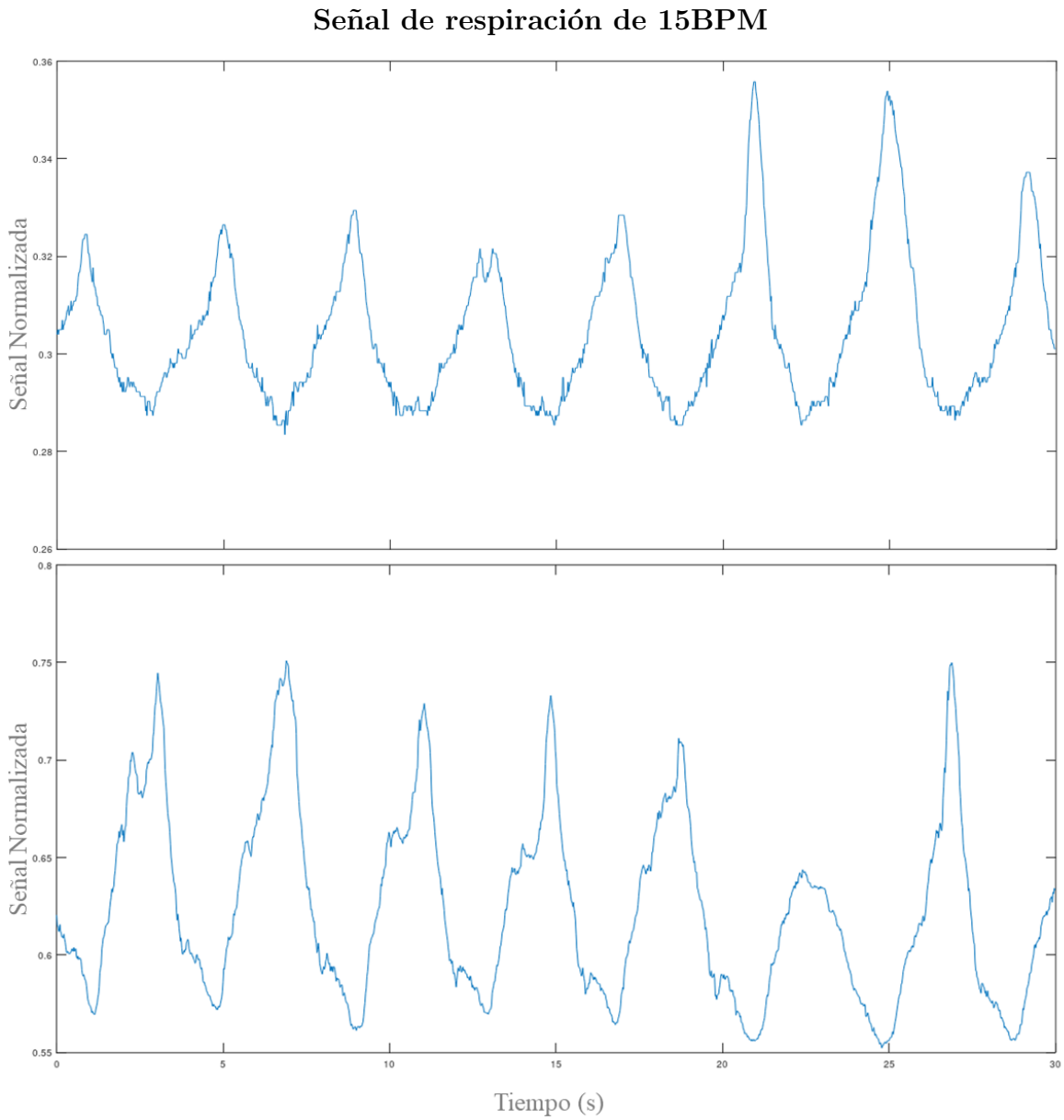

Figura E.3: Comparación entre las señales obtenidas de la primera y segunda versión del sistema vestible para la medición de la respiración. En la Figura se muestra arriba la señal obtenida de la primer versión, mientras que la señal de abajo es la obtenida con la segunda versión. Las señales corresponden a un ritmo respiratorio de 15BPM.

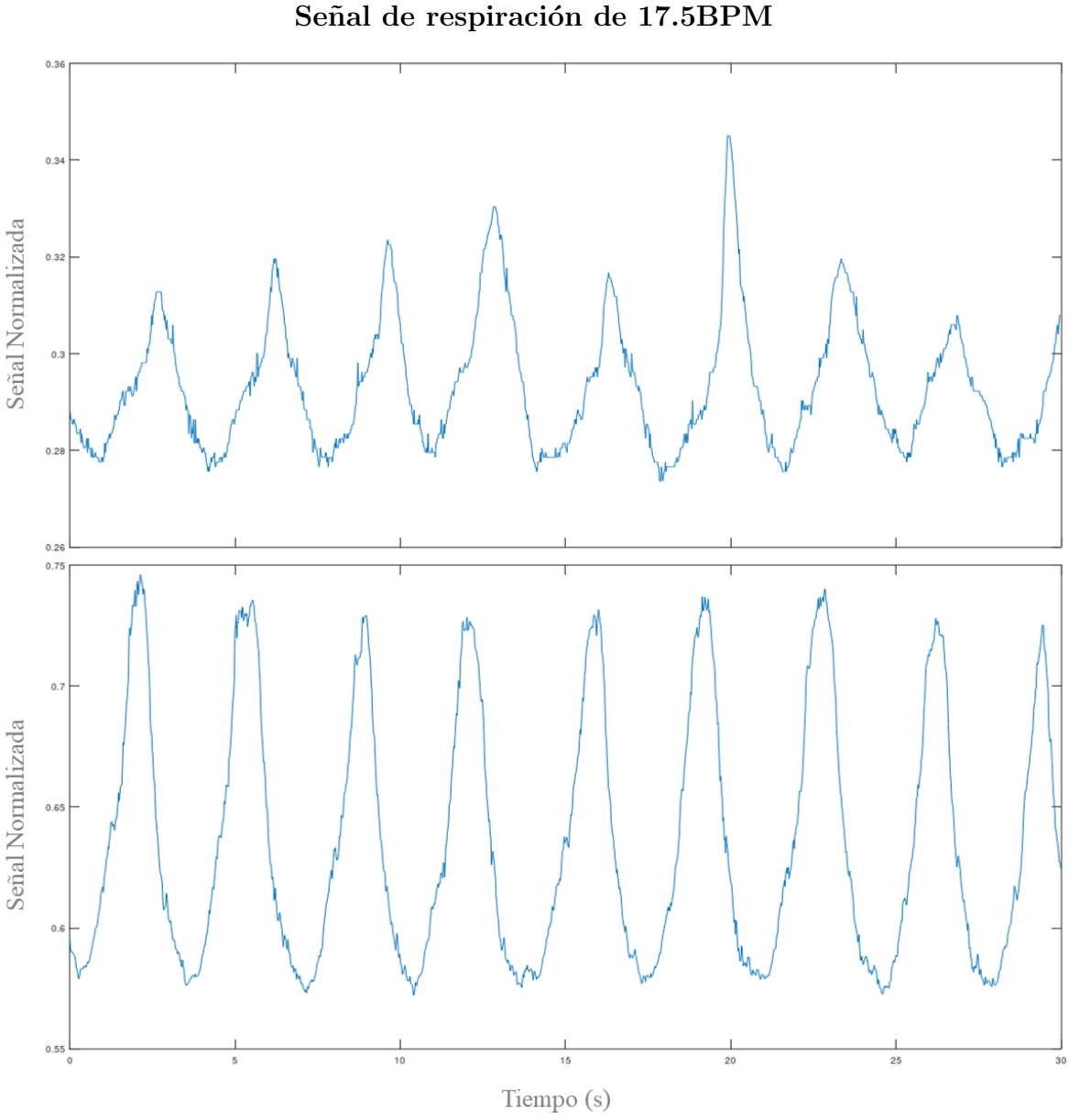

Figura E.4: Comparación entre las señales obtenidas de la primera y segunda versión del sistema vestible para la medición de la respiración. En la Figura se muestra arriba la señal obtenida de la primer versión, mientras que la señal de abajo es la obtenida con la segunda versión. Las señales corresponden a un ritmo respiratorio de 17.5BPM.

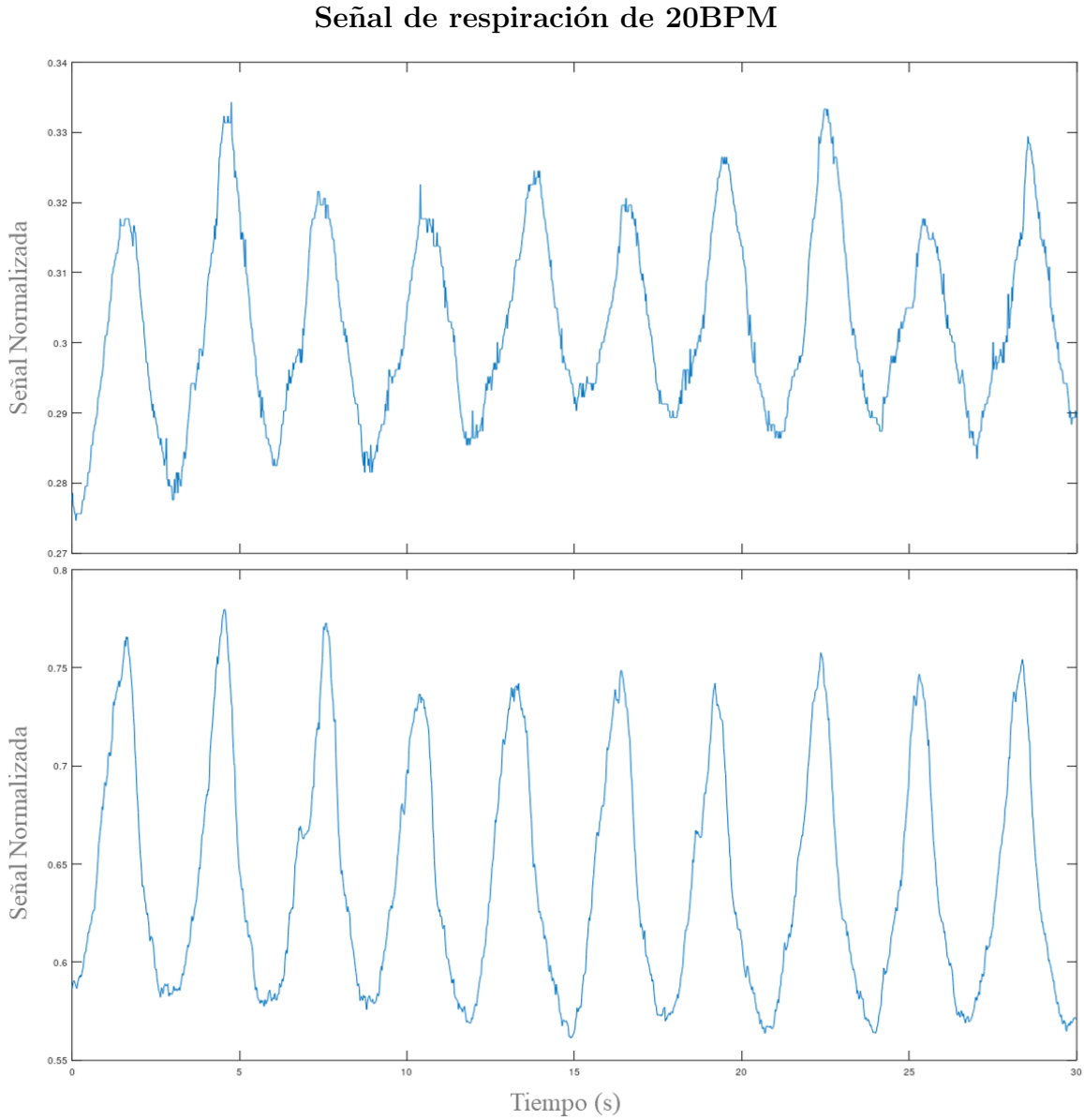

Figura E.5: Comparación entre las señales obtenidas de la primera y segunda versión del sistema vestible para la medición de la respiración. En la Figura se muestra arriba la señal obtenida de la primer versión, mientras que la señal de abajo es la obtenida con la segunda versión. Las señales corresponden a un ritmo respiratorio de 20BPM.

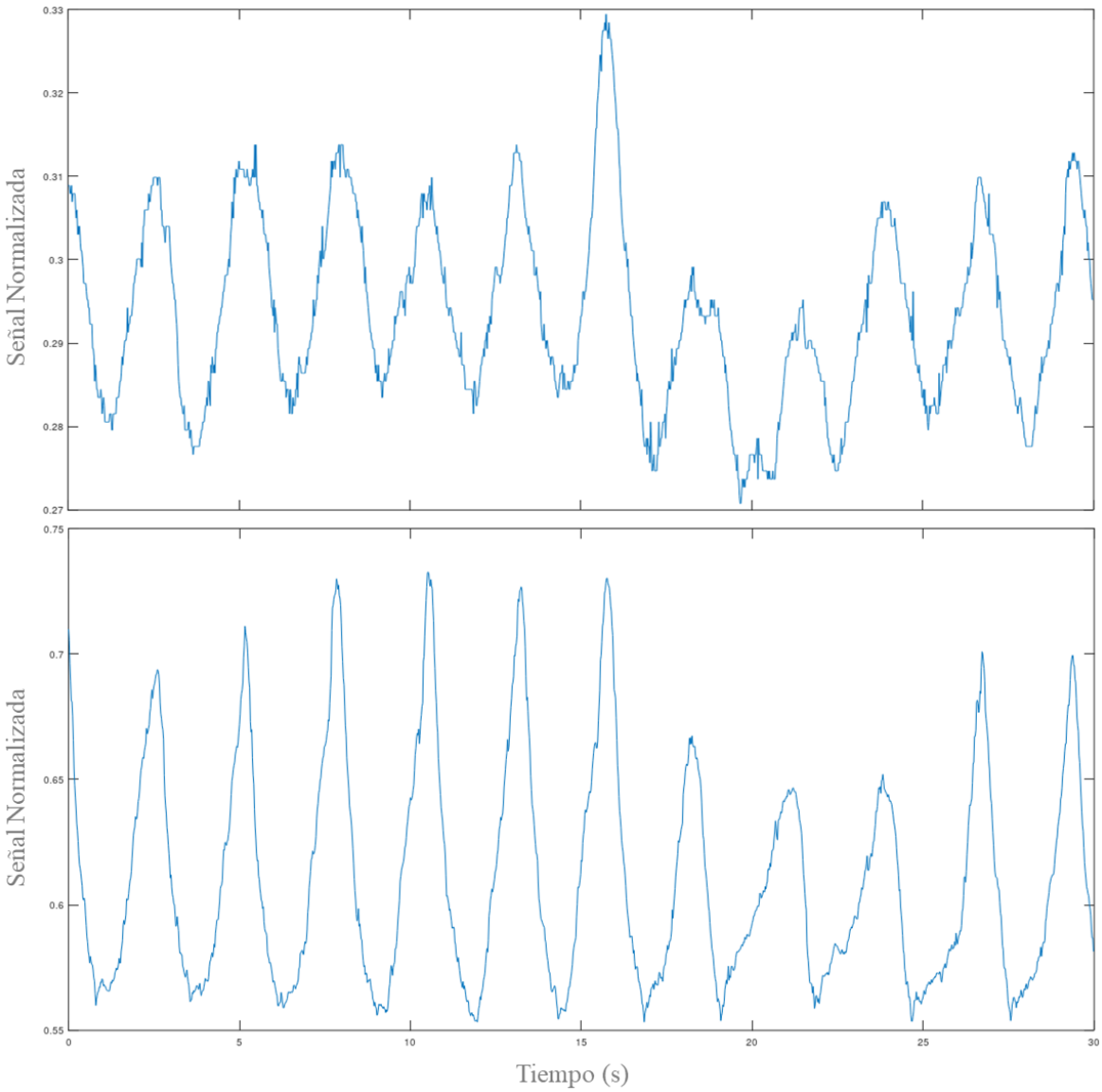

Figura E.6: Comparación entre las señales obtenidas de la primera y segunda versión del sistema vestible para la medición de la respiración. En la Figura se muestra arriba la señal obtenida de la primer versión, mientras que la señal de abajo es la obtenida con la segunda versión. Las señales corresponden a un ritmo respiratorio de 22.5BPM.

Anexo F

Valores p obtenidos de la prueba t a una muestra

Tabla F.1: Valores p mayores (>) o menores (<) que el nivel de significancia (0.05) para el ritmo respiratorio calculado para cada ventana y valor de referencia.

Window (s)	10 BPM	12.5 BPM	15 BPM	17.5 BPM	20 BPM	22.5 BPM
6	<	<	<	<	<	> 0,05
7	<	<	<	<	<	> 0,05
8	<	<	<	<	> 0,05	> 0,05
9	<	<	<	<	> 0,05	<
10	<	<	<	<	> 0,05	<
11	<	<	<	<	> 0,05	> 0,05
12	<	<	<	<	> 0,05	<
13	<	<	<	<	> 0,05	<
14	<	<	<	> 0,05	> 0,05	<
15	<	<	<	> 0,05	> 0,05	<
16	<	<	<	> 0,05	<	<
17	<	<	> 0,05	> 0,05	<	<
18	<	<	> 0,05	> 0,05	> 0,05	<
19	<	<	<	> 0,05	> 0,05	<
20	<	<	<	> 0,05	> 0,05	<
21	<	<	<	> 0,05	> 0,05	<
22	<	<	<	> 0,05	> 0,05	<
23	<	<	<	> 0,05	> 0,05	<
24	<	<	<	> 0,05	<	<
25	<	<	<	> 0,05	<	<
26	<	<	<	> 0,05	> 0,05	<
27	<	<	> 0,05	> 0,05	> 0,05	> 0,05
28	<	<	<	> 0,05	> 0,05	> 0,05
29	<	<	<	> 0,05	> 0,05	<
30	<	<	> 0,05	> 0,05	> 0,05	<

Tabla F.2: Comparación de los dos algoritmos. Valores 'p' de la prueba-t para muestras emparejadas y 'd' de Cohen para errores calculados con una ventana de 27 segundos.

	Prueba-t	**'d' de Cohen**
Valor p	0.0884	0.1320

Anexo G

Diseños del sistema ambiental para el salto vertical

G.1. Circuito esquemático y PCB

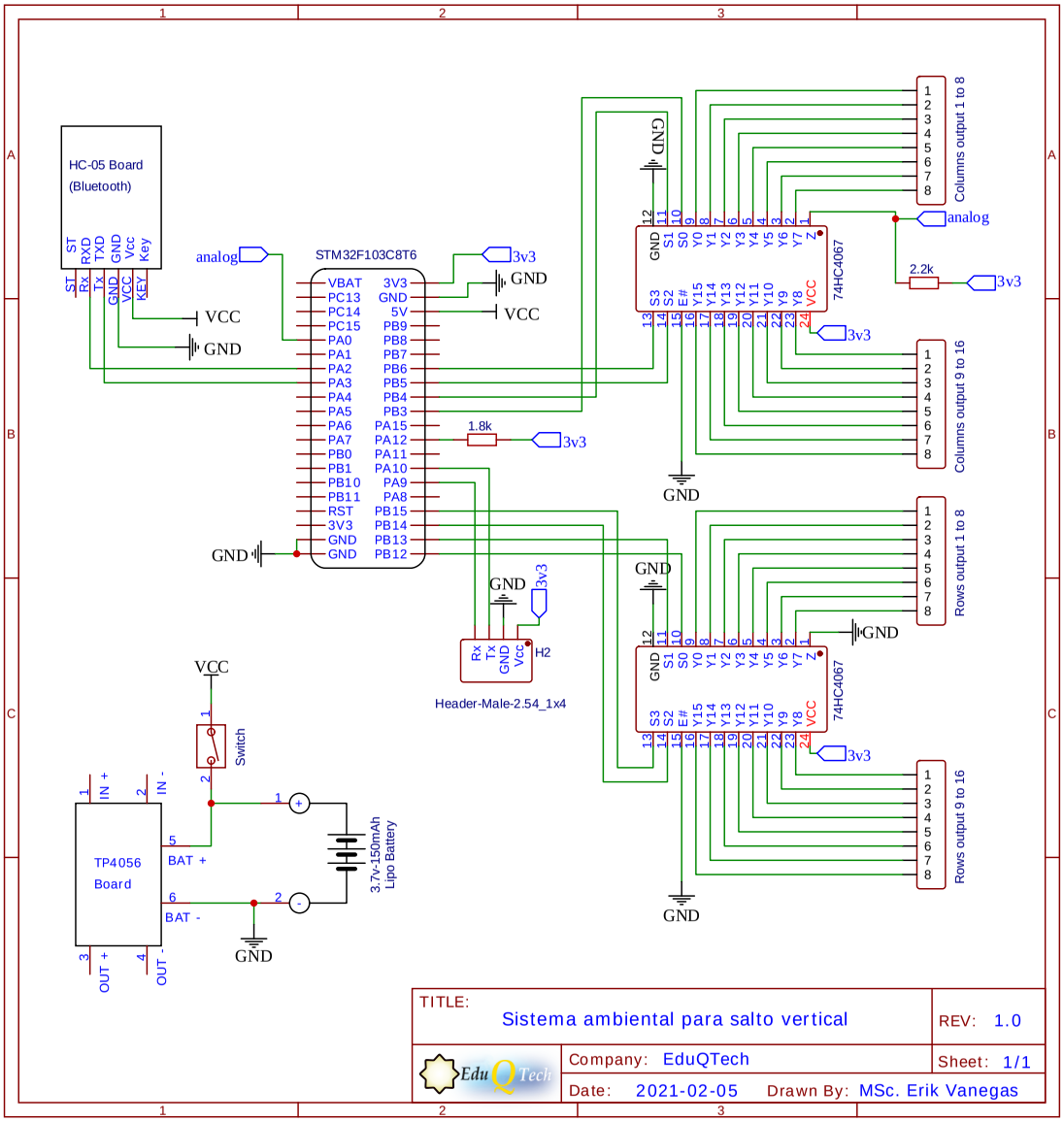

Figura G.1: Circuito esquemático diseñado para el sistema de salto vertical; utilizado para la construcción de la PCB.

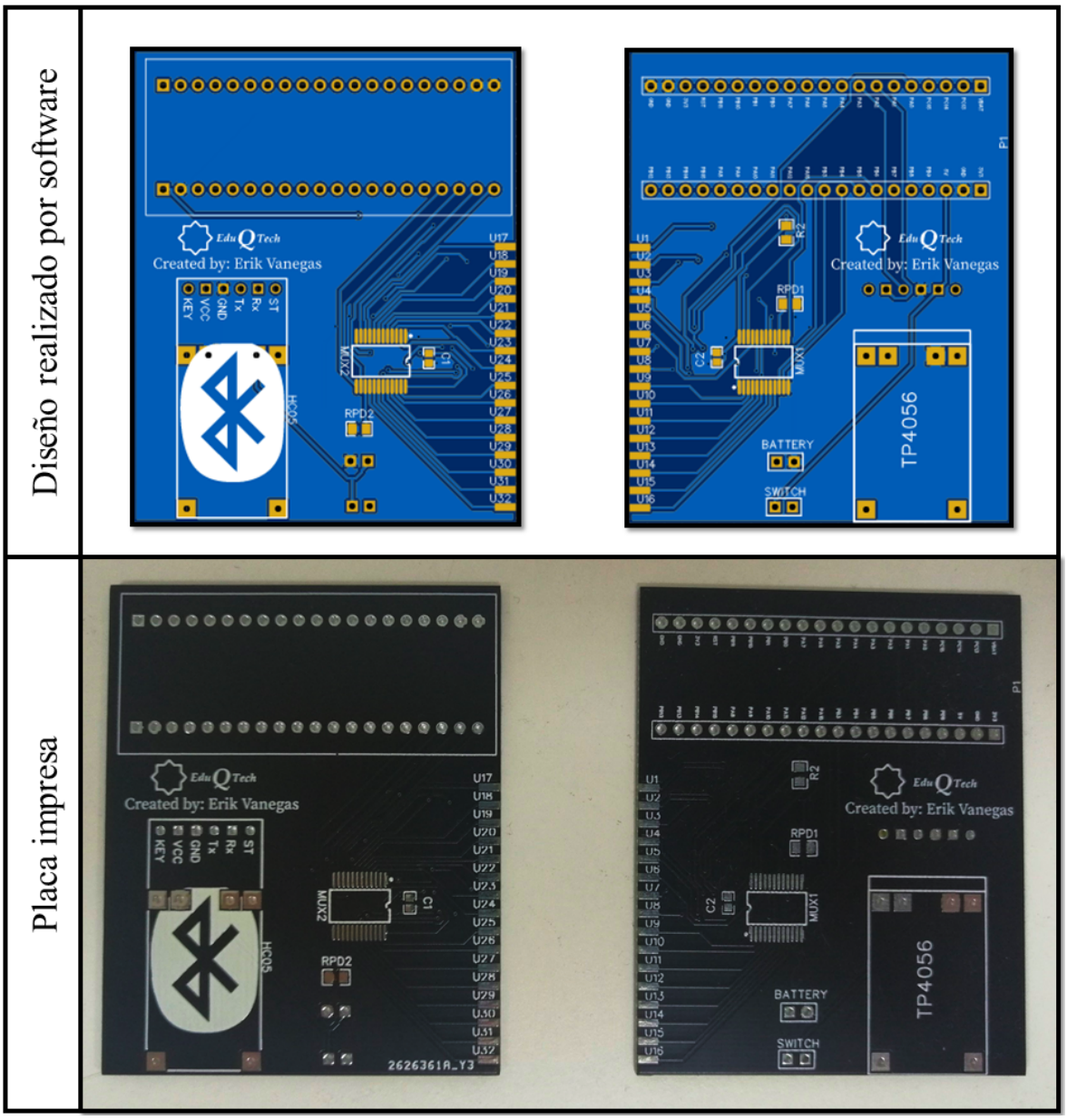

Figura G.2: Diseño de la primera placa realizada por software (arriba) y placa final construida (abajo).

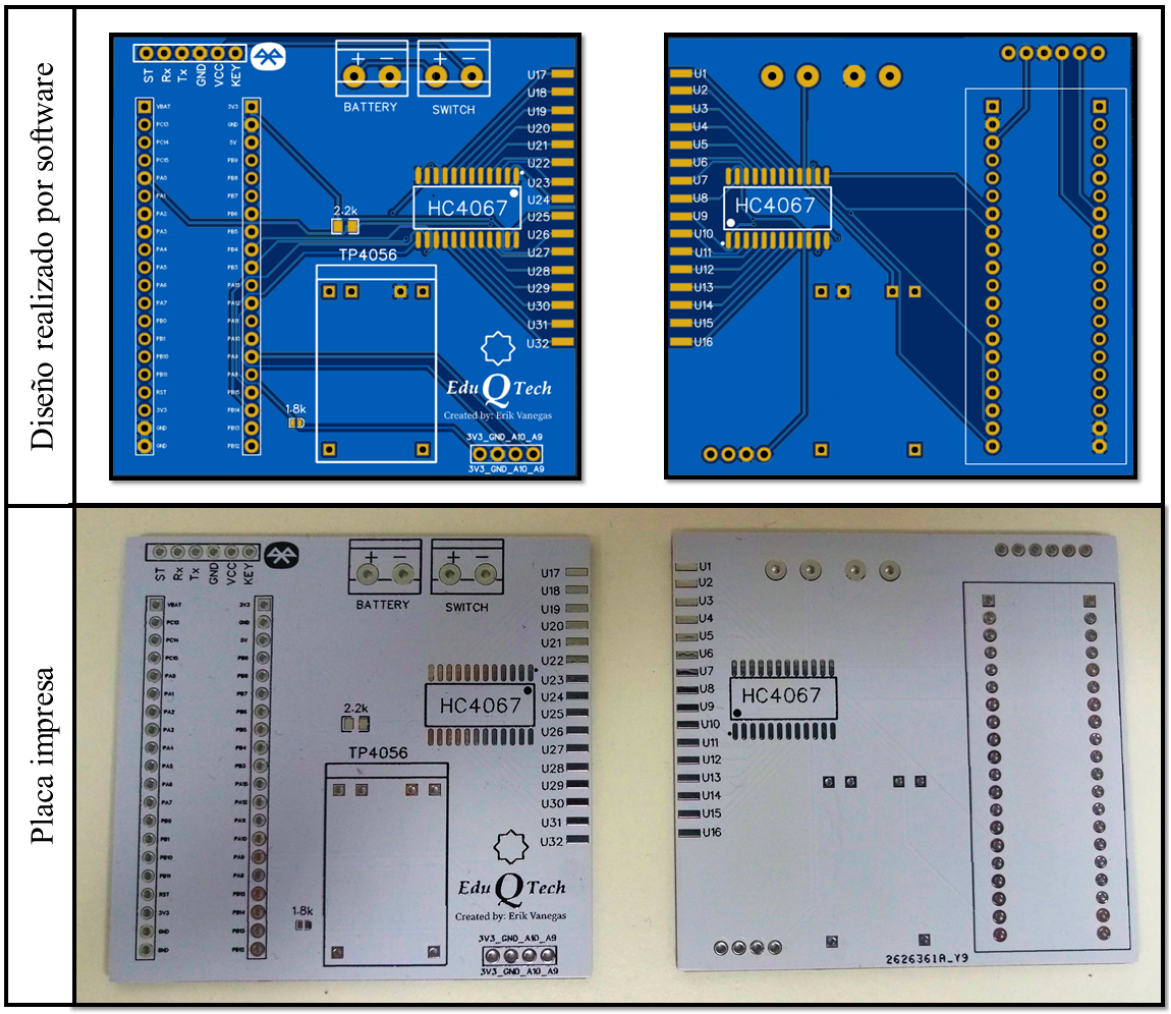

Figura G.3: Diseño de la segunda placa realizada por software (arriba) y placa final construida (abajo).

Anexo H

Piezoresistive Breathing Sensing System with 3D Printed Wearable Casing

Hindawi
Journal of Sensors
Volume 2019, Article ID 2431731, 19 pages
https://doi.org/10.1155/2019/2431731

Research Article

Piezoresistive Breathing Sensing System with 3D Printed Wearable Casing

Erik Vanegas, Raul Igual, and Inmaculada Plaza

EduQTech, Electrical/Electronics Engineering and Communications Department, Escuela Universitaria Politecnica de Teruel, Universidad de Zaragoza, 44003 Teruel, Spain

Correspondence should be addressed to Raul Igual; rigual@unizar.es

Received 4 August 2019; Accepted 5 November 2019; Published 4 December 2019

Guest Editor: Janez Trontelj

Respiratory rate is an important parameter for many health, home care, work, or sport applications. In this paper, a new wearable sensing system based on a piezoresistive FlexiForce sensor has been developed. The sensor can be attached to any common chest strap. A compact 3D casing has been designed and printed with a 3D printer. This casing integrates the sensor and all auxiliary elements of the system: microcontroller, battery, Bluetooth module, connections, battery charger, and acquisition circuit. To the best of our knowledge, this is the first study presenting a FlexiForce respiration sensor that includes all system elements in a single compact casing. The source files with the design of the casing have been published as supplementary material to be reused by any interested researcher. The sensing system was tested with twenty-one subjects for different breathing rates. Two different algorithms were developed to obtain the respiratory rate from the voltage signals recorded by the sensor. Statistical tests were performed to determine the optimal computation time window and algorithm. This approach is also novel in this field. Low error values were obtained for a time window of 27 s with an algorithm based on the calculation of time between zero-crossings (4.02%) and with an algorithm based on counting them (3.40%). To promote research transparency and reusability, the dataset with the recorded data and the source code of the algorithms and statistical tests have also been published. Therefore, an open, replicable, low-error, wearable, wireless, and compact sensing system to measure respiratory rate was developed and tested.

1. Introduction

Monitoring of physiological vital signs in humans, such as heart rate, respiratory rate (RR), blood oxygen concentration, body temperature, or blood pressure, is a field of growing interest with many applications. Specifically, respiratory rate is widely used in health applications such as detection of abnormal breathing patterns [1] or pulmonary disorders [2]; diagnosis of obstructive sleep apnea [3], chronic obstructive pulmonary disease [4], or asthma [5]; monitoring 7 of anaesthetized patients [6]; monitoring during magnetic resonance imaging (MRI) [7]; indication for cardiac arrest [8], imbalance or failure in the nervous, cardiovascular, or excretory 9 systems [8]; prevention of sudden infant death syndrome [9]; or admission to intensive care unit, among others. Respiratory rate monitoring has also be applied to occupational health [10]. Respiratory rate provides information on the psychophysiological condition of workers, which is especially interesting for pilots, drivers, or operators of critical machines. It can be used to detect alarming symptoms of fatigue or fainting. It is also useful in other fields like home care [11] or sports [12].

There are several wearable approaches to properly measure respiratory rate [13]. One possible way is to detect variations in the velocity or volume of the respiratory airflow. For example, Liao et al. [14] presented a capacitive flow sensor. Pressure changes caused by airflow induced capacitance changes in the sensing plates. Other sensors that detect airflow variations to monitor breathing are described in [15, 16].

There are studies that presented sensors based on the recording of the sound associated with the air flowing through the airways of subjects. In this regard, Nam et al. [17] used built-in microphones of smartphones or simple headset microphones placed under the nose. The built-in microphone was manually held in a fixed position by

subjects, assuming no displacement during experiments. The amplitude of the envelope of the respiratory sounds was in the range 0.45-0.9 (amplitude units). For reliable estimates of RR, background noise was kept to a minimum. Respiratory rates could be estimated accurately even if microphones were 30 cm away from the nose.

Another set of studies recorded the temperature of inhaled or exhaled air during breathing. Cao et al. [5] presented a Bluetooth-based hot-film flow sensor. It was based on convective heat transfer. Changes in the fluidic flow condition led to variations in the resistance of the film. The sensor consisted of a micro/nanothin film inserted into a tube. Flow rates covering 0.1-100 L/min were considered in sensor design. Motion was incorporated in the validation tests, and three-axis accelerations were also recorded to assess motion intensity. Similar sensors based on this principle were developed by Huang and Huang [18] and Milici et al. [19].

Several authors registered changes in air humidity to obtain RR. Pang et al. [20] designed a porous graphene network to monitor breathing. It can be used to monitor mouth and nose respiration, including breathing patterns such as normal and deep respiration. The system described is an initial prototype that needs to be improved for commercialization. Other approaches to detect humidity variations were described in the reviews by Farahani et al. [21] and Ascorbe et al. [22].

Chemical sensors have also been used in this field to analyze breathing air components and obtain the RR from the results of analyses. Katagiri et al. [23] presented a sensor to measure carbon dioxide (CO_2) based on optical absorption spectroscopy. Other chemical approaches were discussed in the surveys by Imani et al. [24] and Güntner et al. [25].

Images taken with mobile phone cameras were also used to determine RR. The work of Karlen et al. [26] was based on placing a finger on the lens of a mobile phone's camera and extracting imaging photoplethysmogram from the region of interest to estimate the RR. Motion artifacts were detected and labeled. Then, two algorithms were used to obtain the RR. The system presented a root mean square error of 6 breaths/min, being much higher for respiratory rates greater than 20 breaths/min. Recordings with incorrect counts due to artifacts in the reference device were excluded. The same was done with RR recordings of less than 6 breaths/min or greater than 40 breaths/min. Scully et al. [27] presented a similar approach using intensity changes in the green band of the video signal.

A set of studies measured the changes in electrical bioimpedance that occur during breathing. The work of Metshein [28] presented an electrode shirt to measure electrical bioimpedance using large surface plate electrodes. They were made of aluminium foil and covered with contact gel. Electrical bioimpedance measurements were in the range of 175-300 Ω, approximately. The validation experiments included movements to show the influence of motions of human body on the measured signal. Motions and displacement of the electrodes affected the results. Displacement of the shirt was specially important in long experiments. The best electrode placement configurations were identified, matching the locations of the heart, lungs, and large blood vessels. Similarly, Ansari et al. [29] determined RR from electrical impedance. In this case, it was measured in the arms using only four electrodes.

There are also studies that use radar for the measurement of RR. Kukkapalli et al. [30] presented a micro radar-based system designed as a wearable neck pendant. The system used the relative motion between the radar and the chest wall to estimate the RR. The radar was operated at 24 GHz; a custom active analog amplifier circuit was designed to improve sensitivity. A module with WiFi data transfer was used for data collection. Ten subjects participated in the validation experiments performed in static position. Radar technology has been widely used for RR detection, but mainly in nonwearable systems [31].

Several sensing systems were also proposed to detect chest movements associated with breathing. Dan et al. [4] described an inertial sensor platform to obtain angular velocity waveforms to calculate RR. Sensors were place in the suprasternal notch, which is located on the upper border of the sternum. This position caused noises in signals, which had to be filtered. The sensing system was wired, ensuring stability of signal transmission. Inertial sensors were also used in the works of Hernandez et al. [32] and Estrada et al. [33].

Finally, a set of sensors registered deformations in the chest due to breathing. The sensor developed in this work is based on this principle. Several previous works in this category already exist. Table 1 shows a comparison of the sensing system proposed in this paper with several related works found in the state of the art. Some of the most relevant features of respiratory sensing systems are compared. All studies included in Table 1 detect thoracic movements. They have in common the use a chest strap to attach the sensor to the body, which is the approach adopted in the sensor presented in this study. However, there are large differences in sensing principles, hardware processing units, data processing techniques, or data transfer technologies, among other factors.

Hesse et al. [12] designed a respiration sensor using a force-sensing resistor. Thoracic movements were recorded, and the RR was calculated using a peak detection algorithm. A simple mechanical housing mechanism consisting of two quadratic plates integrated the force-sensing resistor exclusively. The housing mechanism was attached to a chest strap, which included the rest of the elements of the system. Therefore, the mechanical housing mechanism did not contain the microcontroller, memory, battery, or any other auxiliary elements since they were attached to the strap separately. The sensor evaluation was performed with five subjects, obtaining good results for normal and deep breathing. Data were processed locally on the same strap.

A sensor to be worn on the chest was also designed by Mahbub et al. [1]. In this case, the sensing element was a piezoelectric transducer composed of a ferroelectric polymer, polyvinylidene fluoride (PVDF). PVDF had fast response time to vibration due to chest dilation. The sensor was modeled by a first-order equivalent circuit composed of a thermal capacitance shunted by a thermal resistance. The sensor generated charge (peak-to-peak amplitude of 400 pA) in response to vibrations due to breathing. A charge amplifier

Table 1: Comparison of several features of the proposed sensor and other state-of-the-art sensors.

Study	Sensor	Processing unit	Data display	Sampling rate (Hz)	Data transfer	Energy storage
Proposal	Piezoresistive FlexiForce A201	Arduino Pro Mini (Atmega 328p)	PC, Android device	50	Bluetooth (HC-05 module)	3.7 V-150 mAh, Li-battery
Hesse et al. [12]	Piezoresistive FlexiForce A201	MSP430FG4618	PC	100	Flash memory/nRF24L01 module	CR2025 coin cell
Mahbub et al. [1]	PVDF transducer	ADC	—	—	IR-UWB	3 V-600 mAh Li-polymer battery
Rotariu et al. [35]	Piezoelectric belt	Arduino Leonardo	Tablet, PC	10	USB serial port	—
Ciobotariu et al. [34]	Piezoelectric belt	Personal digital assistant	PC	10	WiFi, GSM/GPRS, USB serial port	CR2023 3 V, 225 mAh Lithium coin battery
Hoffman et al. [2]	Capacitive	MSP430F1612	PC	6	Bluetooth (Stollmann BlueMod+B20)	590 mAh Li-polymer battery
Grlica et al. [36]	Capacitive	DAQ commercial unit	PC	9.1	USB serial port	2,000 mAh Li-ion battery
Yang et al. [37]	Capacitive	—	Smartphone	—	Bluetooth	Coin battery
Yang et al. [38]	Capacitive	PIC24FJ256	PC	10	Bluetooth	—
Min et al. [39]	Capacitive	DAQ commercial unit	PC	100	USB serial port	—
Witt et al. [6]	FBG	DAQ unit	DAQ unit	250	Optical fiber RF nanoLOC AVR module for telemonitoring	—
Jonckheere et al. [67]	FBG	DAQ unit	PC	—	USB serial comm.	—
Presti et al. [40]	FBG	DAQ commercial unit (interrogator)	PC	250	USB serial comm.	—
Massaroni et al. [41]	FBG	DAQ commercial unit (interrogator)	PC	250	USB serial comm.	—
Yang et al. [42]	Fiber optic microbend	Optical transceiver	PC	—	Bluetooth	—
Padasdao et al. [9]	DC brushed motor	—	—	—	—	—
Teichmann et al. [43]	Electromagnetic coupling sensing coil	Microcontroller	PC, Android device	100	Bluetooth	LiPo 2.95 Wh battery

produces an output voltage proportional to the integrated charge. This voltage ranges from 0.7 to 1 Vpp. A custom integrated circuit was responsible for processing and sending the data wirelessly. The sensor was validated with only one subject, showing respiration detection. Similarly, the works of Ciobotariu et al. [34] and Rotariu et al. [35] presented piezoelectric thoracic belts to measure respiratory activity. The first work is wireless using GSM/GPRS transmission, while the second prototype communicates with a central computer through a USB cable. None of the studies included a structured evaluation of the sensors.

Hoffman et al. [2] estimated respiration volume using a textile integrated force sensor based on the principle of plate capacitors. The sensors were composed of different layers of textiles. A compressible 3D textile was the core of the sensor. On the top and bottom of the 3D textile, conductive fabrics formed the electrodes of the plate capacitor. Expansion of the thorax during breathing caused a change in fabric thickness, which was measured as a change in the value of capacitance. The tightness of the belt that supported the sensor was set at 10 N. The pressure range to be measured was 0.3 to 0.7 N/cm. Position of the belt and the sensor changed frequently during measurements due to body movement. This led to larger errors. The authors stressed that one possible solution could be frequent recalibration of the system. However, this would affect usability and comfort. Eighteen subjects participated in the validation tests and results showed a high correlation of the measurements with respect to a reference device, although the estimation of the respiratory volume was not accurate enough (37.9% error). Tests included activities with movements. Similarly, Grlica et al. [36] presented a capacitive sensor that detected changes in capacitance in the range from 0.1 to 0.5 pF for normal breathing. The sensor consisted of a fixed triangular electrode and a rectangular moveable electrode. Total electrode displacement was approximately 40 mm for deep breathing. The sensor of Yang et al. [37] included a low-energy Bluetooth wireless communication module to transmit capacitance values to a smartphone. This same transmission technology was used in the work of Yang et al. [38] with the sensor integrated in a shirt. Min et al. [39] also presented a capacitive sensor made of conductive fabric and polyester. The sensor designed was linear with sufficient resolution to measure a wide range of breathing from different subjects. Force was increased from 0 to 3 N, producing a capacitance change of 445-510 pF. The authors stressed that the position during tests may affect performance.

Witt et al. [6] designed a system to measure thoracic motion continuously based on optical fiber sensors. Specifically, the sensor was based on fiber Bragg gratings (FBG), macrobending effect, and optical time-domain reflectometry. The sensor was specifically for patients under MRI. It was tested in simulators and in climate chambers. FBG sensor can be stretched up to 3% elongation with a sensitivity 0.32 nm. Results showed that the sensor retained its stability for different elongations. The same principle (FBG) was also used in the sensor of Presti et al. [40]. In that case, an array of 12 FBG was designed. The placement of the 12 FBG in subject's torso was optimized. Five subjects participated in the validation of the sensor and measurements were analyzed offline, obtaining a minimum error. FBG were also used by Massaroni et al. [41] to monitor compartmental and global volumetric parameters. Six subjects participated in the experiments, obtaining an error in the tidal volume of 14%. Similarly, Yang et al. [42] developed a fiber optic respiratory sensor based, this time, on the microbend effect. That study verified the RR by counting the number of breaths manually. The sensing belt was stretched 20 mm and 40 mm, which corresponded to elongations of 2.14% and 4.28%.

Padasdao et al. [9] presented a respiratory chest sensor based on human energy harvesting. An off-the-shelf dc brushed motor was used to detect thoracic movements as a function of average harvested power. The expansion of the chest due to respiration turned the armature, which transmitted the movement to the gears and the rotor of the machine. The motor was integrated into a plastic casing and mounted on a piece of felt to stabilize the device against the body. Displacements of 1 cm and 3 cm were considered in the experiments. Average output power harvested by the motor was in the range 6-72 μW. To eliminate motion artifacts, voltage outputs were filtered with a low-pass finite impulse response (FIR) filter. The sensor was validated with twenty subjects, obtaining that RR was measured with a low error value.

The proposal of Teichmann et al. [43] is also innovative, since they presented a sensor based on magnetic induction to obtain RR. A coil was the core element of the sensor. The sensor detected variations in the distribution of human impedance due to thoracic movements associated with breathing through electromagnetic coupling. The sensing system was completed with a microcontroller and a Bluetooth module. The sensor was placed on a flexible PCB. All other electronic components (except for the power management) were also mounted on there. The impact of coil deformation was also investigated since the sensor was designed to be carried in the shirt pocket. Four subjects participated in the evaluation. The authors stressed that the spatial fusion of different sensors could allow the cancellation of motion artifacts. However, this was not tested in the study.

This paper presents a compact wireless sensing system based on a piezoresistive sensor (A201 FlexiForce sensor, Tekscan [44]) to monitor respiratory rate. As can be seen in Table 1, the proposal of Hesse et al. [12] is the most related work to the sensing system presented in this paper. A systematic search was conducted in the literature, and no other works were found that use a piezoresistive FlexiForce sensor, to the best of our knowledge. This paper contributes with several novelties to the state of the art:

(i) One key aspect of the piezoresistive FlexiForce sensor is the casing, since it determines the sensor detection capabilities. In the work of Hesse et al. [12], a casing was designed only for the sensor, while the rest of the elements (microcontroller, transmission unit, flash memory, etc.) were considered separately. Therefore, the casing did not include them in a compact way. In this paper, we present a wireless FlexiForce sensor integrated in a single casing to

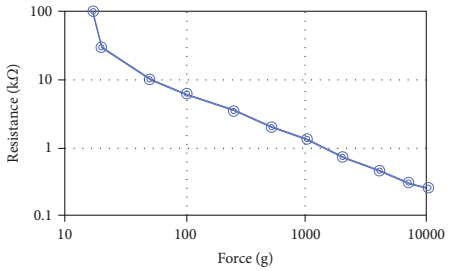

Figure 1: Force-resistance curve of FlexiForce A201 sensor provided by the manufacturer [46].

measure RR. All system components (FlexiForce sensor, microcontroller, Bluetooth module, battery, etc.) are integrated in the wearable casing. A 3D casing was designed and printed on a regular 3D printer. The files with the 3D design of the casing have been published as supplementary material (available here) to be reused by any interested researcher

(ii) The system has been tested with several subjects using a metronome. Two popular algorithms have been used for the calculation of respiratory rate. Additionally, both algorithms have been compared to determine which one measures RR more accurately. Statistical tests have been used for that purpose. The optimal time window of the algorithms has also been determined using statistical tests. This is a novel approach in this field

(iii) Another novelty of this work is that a public dataset has been created with all the data recorded in the tests. It is publicly available for use by any interested researcher [45]. In addition, the files with all data processing (algorithms and statistical tests) have been published as supplementary material to this paper. We have not found any other study on respiratory monitoring that makes public all study data and resources

2. Prototype Design

2.1. Physical Prototype. A sensor has been developed to measure respiratory rate by detecting variations in chest movement. The sensing system was designed to be placed around the chest with a strap. The system uses a force-sensitive resistor (FSR) based on the piezoresistive effect (FlexiForce A201 sensor, Tekscan). The characteristic curve of this sensor is not linear, but logarithmic, as shown in Figure 1 (curve provided by the manufacturer). The resistance provided by the sensor drops as the exerted force increases. This sensor is suitable for applications in which force variations must be detected. This is the case of RR measurement. The conditioning circuit for this sensor is a simple voltage divider as shown in Figure 2. An analysis of the typical operating region of the

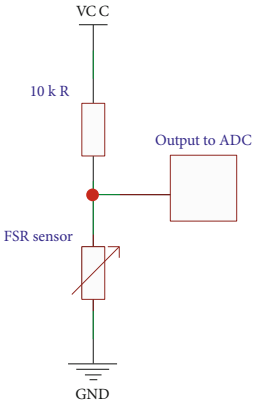

Figure 2: Conditioning circuit of the piezoresistive FlexiForce sensor.

FSR has been performed for the application presented in this paper. For this analysis, the data collected according to the experiments described in Experimental Setup have been used. First, the histogram associated with the voltage recorded by the sensor has been represented in Figure 3(a). For this application, it is important that the voltage varies over a wide range. The typical operating region ranges from 0.2 V to 1.7 V. Second, the histogram of resistance variation is represented in Figure 3(b). Third, Figure 3(c) shows the histogram of the forces related to those resistance values. The typical operating region corresponds to force values in the range of 50-500 g. These force values have been calculated after fitting the equation of the resistance-force curve provided by the manufacturer.

$$\text{Force(g)} = \sqrt[0.827]{\frac{399.88}{R(\text{k}\Omega)}}. \quad (1)$$

In the typical region of operation ($2\text{k}\Omega - 10\text{k}\Omega$), the force can be considered to vary linearly with the conductance, according to the datasheet provided by the manufacturer [46].

The sensing system takes samples from the piezoresistive sensor through an Arduino Pro Mini that operates at a sampling frequency of 50 Hz, and sends the data using an HC-05 Bluetooth module. Data are received by a processing unit with Bluetooth technology (i.e., computer, Android, or iOS device), as shown in Figure 4. Then, they are downloaded to be processed offline in MATLAB or any other numerical computing software. The range of the Bluetooth module is around 10 m with a data transfer rate of up to 3 Mbps [47, 48]. The reliability of the Bluetooth module as part of the sensing system was also measured. For that, four experiments were performed. They consisted of transmitting a known value to the receiving unit at different distances: 1 m,

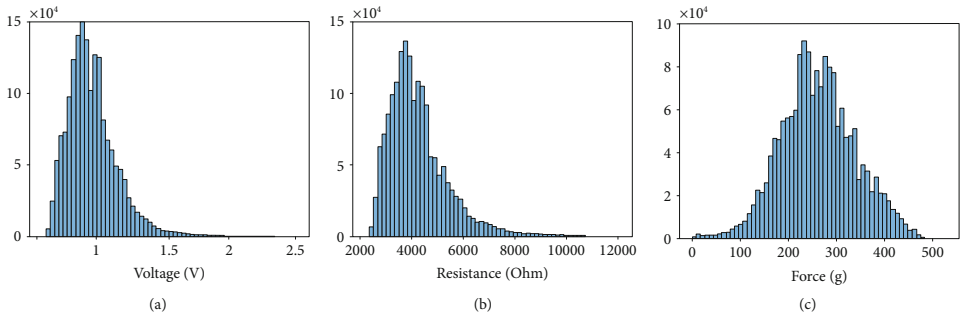

Figure 3: Histograms with the distribution of voltage (a), resistance (b), and force (c) for the signals captured in the experiments performed in this study.

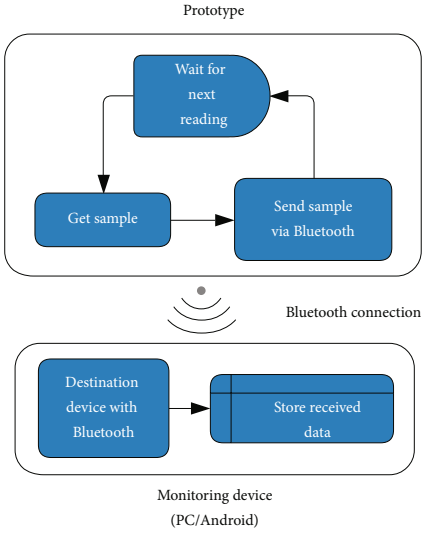

Figure 4: Block diagram of data acquisition and communication of the proposed system.

3 m, 5 m, and 10 m. The transmission frequency was 50 Hz. The sensing system was in motion during the experiments and there were obstacles between the transmitter and the receiver. Each experiment was performed for 30 min. As a result, no corrupted value was received. The average percentage of lost packets was 0.03% (standard deviation of 0.01%).

The sensing unit was powered by a 3.7 V, 150 mAh lithium battery, although the casing was also designed to accommodate batteries of 300 mAh, 400 mAh, and 500 mAh capacity. These batteries were selected since they can be integrated into the casing in a compact way. The current consumption of the different components of the prototype was measured. The average values are shown in Table 2. These values are in line with those provided in the datasheets by the manufacturers [46–49]. The battery life of the prototype was also measured, obtaining average values of 3.83 h, 7.88 h, and 13.01 h for batteries of 150 mAh, 300 mAh, and 500 mAh capacity, respectively. A battery was considered discharged when the voltage was below 3.6 V, following the recommendation of Lee et al. [50]. Regarding their safety, lithium-ion batteries are used massively. Statistically, they are very reliable since failure rates for rechargeable units are on the order of one in 10 million cells [51].

A TP4056 board is used to manage battery recharge. It ensures that both current and voltage remain constant during battery charging. The board consists of a processor and a battery protection circuit. It regulates the charging current

Table 2: Current consumption of the main components of the sensing system.

Component	Current consumption
Arduino Pro Mini	9.65 mA
Bluetooth	30.5 mA
FSR sensor	0.2-360 uA
Total	40.15-40.51 mA

Figure 5: Elements of the sensing system mounted: front of the prototype with the Arduino Pro Mini, battery charger, and FSR (a) and back of the prototype with the Bluetooth module and battery (b).

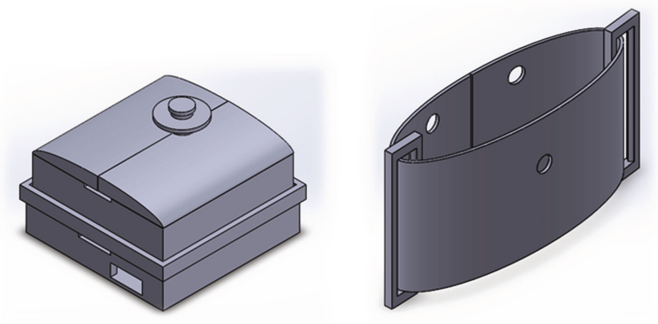

(a) (b)

Figure 6: 3D design of the casing. PLA-printed part (a) and flexible PLA-printed part (b).

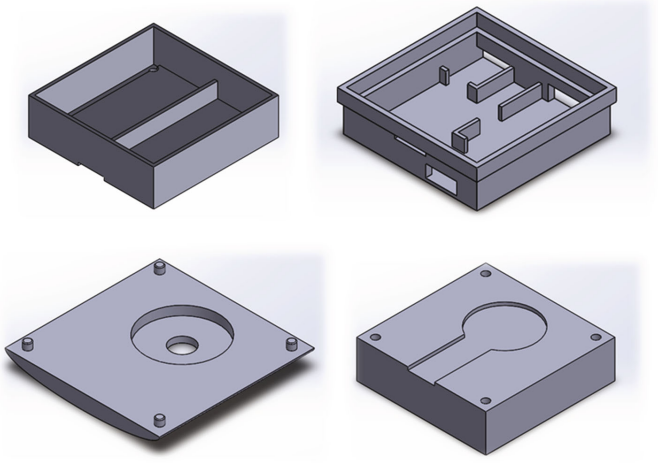

Figure 7: Internal design of the prototype (details in the Supplementary Materials).

under conditions of high power operation or high ambient temperature. The board also ends the charging cycle when the current drops 10% of the programmed value. It also has an internal MOSFET battery disconnect switch to avoid negative charging currents [52].

With respect to the operating temperatures supported by the prototype, the values for the different components were extracted from their datasheets: Bluetooth (-20 to 55°C), Arduino Pro Mini (-40 to 85°C), battery charger (-40 to 85°C), and battery (-20 to 60°C). The sensing system is not designed to be submerged in water. However, it is not different from any other object printed with polylactic acid material, which means that the casing can withstand weak levels of rainwater. Figure 5 shows a photograph of the mounted components of the sensing system outside the casing.

A casing to contain all the elements of the sensing unit was designed in the Autodesk software. This casing has two main parts:

(i) An element printed with standard polylactic acid (PLA) containing the piezoresistive sensor, the conditioning circuit, the microprocessor, the Bluetooth module, the battery, and the battery charger (Figure 6(a), Figure 7, and pink case of Figure 8)

Figure 8: Prototype designed with all the circuitry embedded inside.

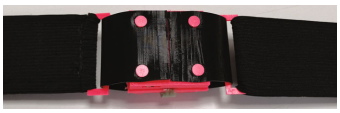

Figure 9: Back of the casing showing the fixation of the flexible part to the solid part. The belt is attached to both sides of the flexible part by two rings.

(ii) An element printed with flexible PLA that allows transmitting chest movements to the sensing element (Figure 6(b) and black cover of Figure 8)

The sensing system is attached to the belt through two rings coupled to the flexible part. Figure 9 shows a photograph of the back of the casing. The sensing unit was designed to be worn on a garment, although direct contact with the skin would also be possible. The total size of this prototype is 73 mm wide × 45 mm high × 37 mm deep (Figure 8). The internal volume of the pink case is 30.42 cm^3, while the weight of the entire prototype is 103 g (21 g for circuitry, 23 g for the 3D printed casing, and 59 g for the belt and the rings). The 3D design of the casing has been published as supplementary material and is available to be reused or reprinted by any interested researcher.

2.2. Data Processing. To measure the respiratory rate of the signals received on the remote unit via Bluetooth, different processing operations are performed. Firstly, data are filtered with a 0.5 Hz-low-pass digital filter, which "smooths" the signals by removing high-frequency noise. A minimum-order FIR or infinite impulse response (IIR) filter with a stop band attenuation of 60 dB and compensation for the delay was used [53]. This frequency has been selected because breathing rates above 30 BPM are rare in daily life activities of humans [54, 55]. An analysis of the system error was also performed considering cut-off frequencies in the range 0.5-4.5 Hz, obtaining the lowest error values for 0.5 Hz. In addition, to prevent that a trend in the signals (systematic increase or decrease) due to sensor or subject movement during the tests affects system performance, a linear fit was made

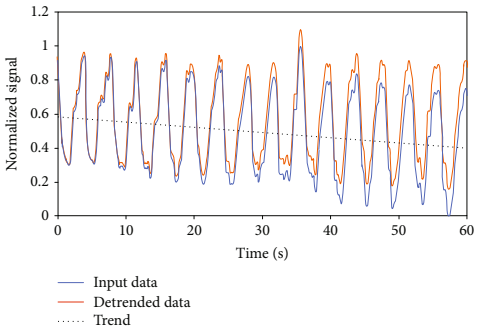

Figure 10: Comparison between original signal, its trend line, and the systematic shift correction.

to each signal and was subtracted from the original signal (Figure 10). In this way, systematic shifts were removed. These shifts are not relevant if signals are analyzed in short time windows. However, they affect system accuracy in large windows. Therefore, this preprocessing helps to prevent the algorithm from malfunctioning in large windows due to sensor movements other than breathing.

Then, the maximum and minimum points are obtained in a given analysis time window (w). For that, a subset of data which includes only the values in the time window is segmented. It has the form of a vector (x). This vector is used to calculate the level corresponding to the "zero 280 axis" (ZA), according to the following equation:

$$\mathrm{ZA} = \frac{\min(x) + \max(x)}{2}, \tag{2}$$

where x is a vector with the filtered data sequence. The length of x depends on the time window, which is a parameter whose optimal value has to be selected (see Validation Experiments). The time window w slides through the entire signal. To avoid that outliers due to isolated deep breaths may raise the ZA value, peaks with prominence of at least 0.03 V 285 are detected and max (x) is set to the amplitude of the median of all the detected peaks. The prominence threshold value was selected after performing simulations in the range of 0.013-0.13 V, since it led to the lowest error values.

ZA will be the reference value used to detect zero-crossings in the data. To detect these crossing points, the segmented data set x will be assessed by taking pairs of two consecutive samples (x_k, x_{k+1}). If inequalities 3 are fulfilled, a new zero-crossing will be detected and the time $k(1/f_s)$ will be added to a vector containing the zero-crossings in the time window (z). f_s is the sampling frequency of the sensing system, in this case, 50 Hz.

$$\begin{aligned} x_k &\leq \mathrm{ZA} < x_{k+1}, \\ x_k &\geq \mathrm{ZA} > x_{k+1}. \end{aligned} \tag{3}$$

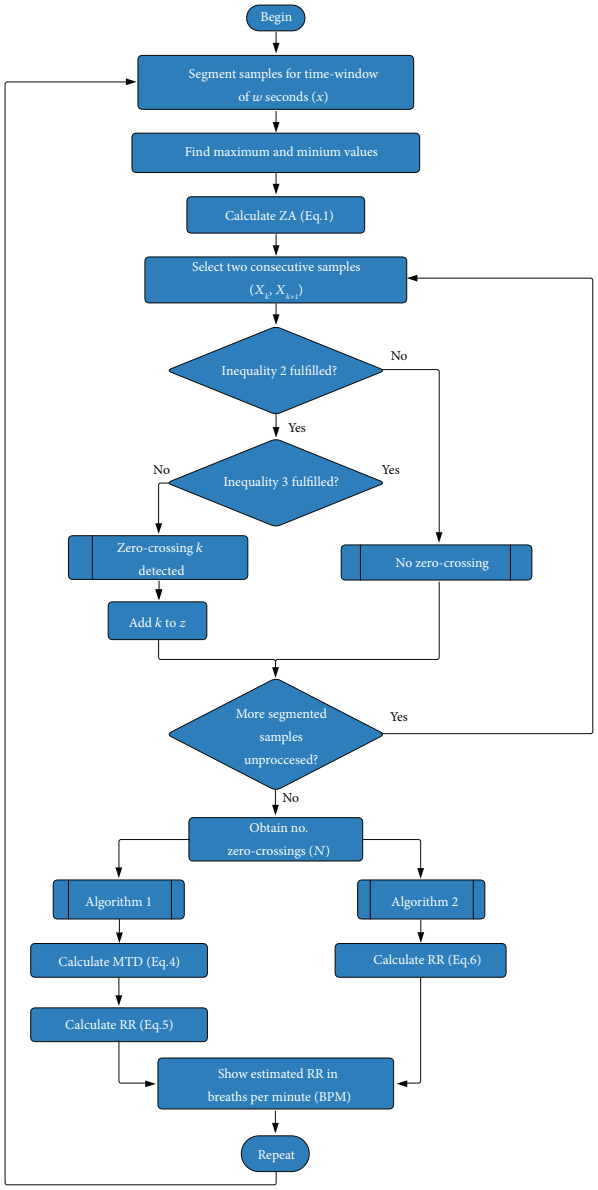

Figure 11: Block diagram of the data processing algorithms used to estimate the RR.

To avoid detecting two close zero-crossings due to noise, the zero-crossing at position $j(z_j)$ will be removed from z if z_j does not differ, at least, a set threshold (TH) from the rest of the elements of z, that is, if inequality 4 is satisfied.

$$|z_j - z_i| < \text{TH}, \quad \forall i \in [1, N] | i \neq j, \tag{4}$$

where N is the length of vector z, j is the index of the zero-crossing under analysis, and i is the index for the rest of zero-crossings in z. The value of TH has been empirically set to 500 ms.

Then, two different algorithms are used to measure the RR. Figure 11 shows a block diagram of both algorithms. The operation of the algorithms is as follows:

Algorithm 1. This algorithm is based on the time difference between consecutive zero-crossings [4, 39]. Firstly, the mean time difference (MTD) between consecutive pairs of zero-crossings is obtained as follows:

$$\text{MTD} = \frac{\sum_{i=1}^{N-1} |z_i - z_{i+1}|}{N-1}. \tag{5}$$

Then, with that average value of all times, the respiratory rate RR (in breaths per minute, 305 BPM) is calculated according to the following equation:

$$\text{RR} = \frac{30}{\text{MTD}}. \tag{6}$$

To obtain that equation, it was taken into consideration that two zero-crossings occur in a breathing cycle (2 MTD s, is a breathing period) and that the RR is given in breaths per minute (if one breath occurs in 2 MTD s, in 60 seconds, there should be 60/2 MTD breaths).

Algorithm 2. This algorithm is based on counting the number of crosses by zero [56]. For that, the length of the vector z is obtained, which is directly the number of zero-crossings (N). Then, the RR is obtained according to the following equation.

$$\text{RR} = \frac{30N}{w}, \tag{7}$$

where w is the duration of the time window (in seconds). Equation (7) is obtained by scaling the number of zero-crossings to 60 seconds ($60N/w$), so that the number of zero-crossings in 1 minute is obtained. As each breath is composed of 2 zero-crossings, by dividing this value by 2, the RR is obtained.

The sliding time window (w) used in the algorithms is a parameter that can take any desired value. Once a time window has been selected, the RR is updated every w seconds. The methods of counting peaks or zero-crossings or measuring distances between them have been widely used in previous studies to obtain RR [10, 40, 57–59].

Figure 12: Two subjects involved in the validation experiments wearing the prototype around the chest.

3. Materials and Methods

3.1. Experimental Setup. An experimental setup was designed to validate the sensor developed. Experiments involved twenty-one subjects. Fifteen were male and six were female. Ages ranged from 19 to 55 years with an average of 35.95 and a standard deviation of 10.5. Subjects' weights were between 42 and 95 kg (average of 70.76 kg and standard deviation of 14.83 kg). As for heights, they were in the range of 1.52-1.83 m with an average of 1.72 m and a standard deviation of 7.51 cm.

The diameter of the thoracic region was also measured, obtaining values from 68 to 103 cm (average of 87.90 cm and standard deviation of 12.36 cm). The health status of the participants was also noted. Sixteen subjects declared no respiratory problems, while five suffered from breathing allergies and two of them also from asthma. Subjects were asked to wear the breathing sensor placed just below the chest, at the level of the diaphragm, as shown in Figure 12. The sensor was connected via Bluetooth to a computer running a program that was developed specifically for this study. The computer program was written in Processing.

Regarding the validation protocol, each subject was asked to breathe during one minute at the rhythm of a metronome. The metronome was set so that subjects followed a rhythm of 10, 12.5, 15, 17.5, 20, and 22.5 BPM. There are studies in the literature that use this method (metronome as a reference) to validate their sensing systems in a controlled breathing scenario [4, 17, 27, 57, 60, 61]. The reference values of BPM considered are in accordance with the typical respiratory rates in humans [62]. Subjects were asked to repeat the experiment in different positions: sitting without moving, sitting with movement, standing without moving, standing with movement, and walking. A one-minute resting time was given between two consecutive experiments. All participants received written and oral information about the study, and informed consent was obtained from them to publish their data anonymously in a public repository.

Each set of breathing data was recorded in a different text file (two example signals are shown in Figure 13). Thirty files were recorded for each subject (six BPM times five activities).

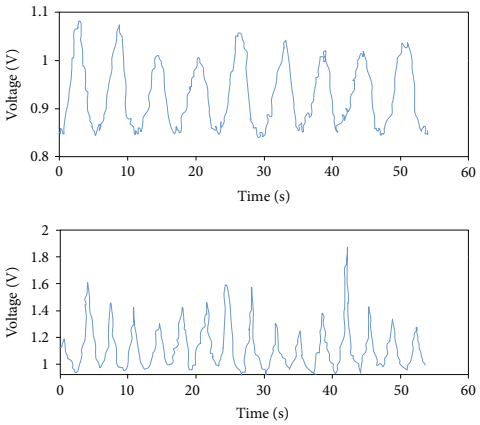

Figure 13: Two raw breathing signals captured by the FlexiForce sensor. The upper graph corresponds to an experiment performed at a rate of 10 BPM in a sitting position without movement. The lower signal was captured at 17.5 BPM during the walking activity.

Therefore, a total of 630 files were collected as a result of the experiments. The files were processed offline to obtain the RR according to the algorithms described in Data Processing. MATLAB was used to perform the processing. The MATLAB code is given as supplementary material to this paper.

Figure 13 shows two example of breathing graphs. The upper signal contains nine breathing cycles. A typical breathing signal has an approximate sinusoidal shape with a negative slope for inspiration and a positive slope for expiration. It also has an upper peak corresponding to the situation in which all the air has been exhaled and a lower peak associated with the moment when all the air is inside the lungs. Typical absolute slope values are 0.1-0.2 V/s for low intensity activities, 0.2-0.28 V/s for moderate intensity activities, and 0.28-0.35 V/s for higher intensity activities. These values were estimated theoretically and from the signals recorded in the experiments. Slope values are low since they were measured in the time-voltage graphs and breathing signals are low frequency.

3.2. Validation Experiments. The validation experiments allow in determining the accuracy of the sensor and the optimal processing algorithm and its parameters.

For that, the collected data were processed with the two algorithms described in Data Processing. For each algorithm, a different RR was obtained for each participant and dataset (in total 1260 values, 630 per algorithm). In addition, the algorithms are influenced by the width of the time window used to perform the RR calculation. Therefore, twenty-five different time windows have been considered: from 6 s to 30 s. Windows below 6 s were not considered since the reference BPM value with the lowest frequency had a period of 6 s. At least one period is required to obtain the RR. Windows above 30 s were not considered, since an update time greater than this value may be excessive for many applications

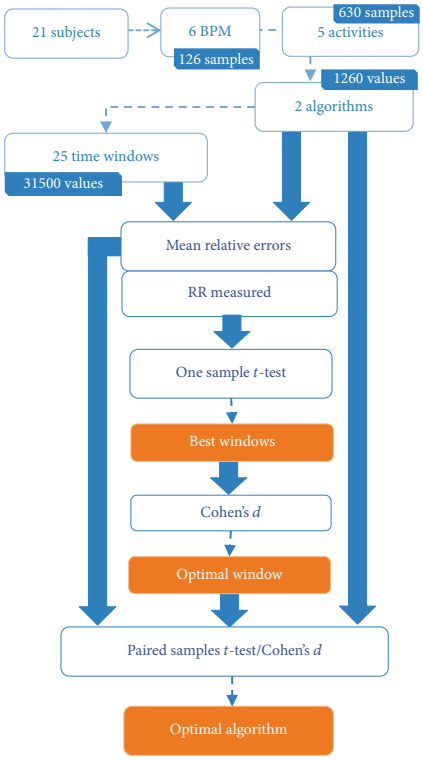

Figure 14: Scheme of the validation experiments performed.

Table 3: Maximum structural relative errors for Algorithm 1 (extreme cases).

	10 BPM	12.5 BPM	15 BPM	17.5 BPM	20 BPM	22.5 BPM
Error (%)	0.67	0.83	1.00	1.17	1.33	1.50

Table 4: Maximum structural relative errors (%) for Algorithm 2 (down and up), considering the time window error and the quantization error for extreme cases. If a single value is provided, it is because the up and down errors are the same.

Window (s)	10 BPM	12.5 BPM	15 BPM	17.5 BPM	20 BPM	22.5 BPM
6	-50, 50	20.0	0.0	-14.3	-25, 25	11.1
7	28.6	2.9	-14.3	22.4	7.1	-4.8
8	12.5	-10.0	-25, 25	7.1	-6.3	-16.7, 16.7
9	0.0	-20.0	11.1	-4.8	-16.7, 16.7	3.7
10	-10.0	20.0	0.0	-14.3	5.0	-6.7
11	-18.2	9.1	-9.1	9.1	-4.5	9.1
12	-25, 25	0.0	-16.7, 16.7	0.0	-12.5, 12.5	0.0
13	15.4	-7.7	7.7	-7.7	3.8	-7.7
14	7.1	-14.3	0.0	10.2	-3.6	4.8
15	0.0	12.0	-6.7	2.9	-10, 10	-2.2
16	-6.3	5.0	-12.5, 12.5	-3.6	3.1	-8.3, 8.3
17	-11.8	-1.2	5.9	-9.2	-2.9	2.0
18	-16.7, 16.7	-6.7	0.0	4.8	-8.3, 8.3	-3.7
19	10.5	-11.6	-5.3	-0.8	2.6	5.3
20	5.0	8.0	-10, 10	-5.7	-2.5	0.0
21	0.0	2.9	4.8	6.1	-7.1, 7.1	-4.8
22	-4.5	-1.8	0.0	1.3	2.3	3.0
23	-8.7	-6.1	-4.3	-3.1	-2.2	-1.4
24	-12.5, 12.5	-10, 10	-8.3, 8.3	-7.1, 7.1	-6.3, 6.3	-5.6, 5.6
25	8.0	5.6	4.0	2.9	2.0	1.3
26	3.8	1.5	0.0	-1.1	-1.9	-2.6
27	0.0	-2.2	-3.7	-4.8	-5.6, 5.6	3.7
28	-3.6	-5.7	-7.1, 7.1	4.1	1.8	0.0
29	-6.9	7.6	3.4	0.5	-1.7	-3.4
30	-10, 10	4.0	0.0	-2.9	-5, 5	2.2

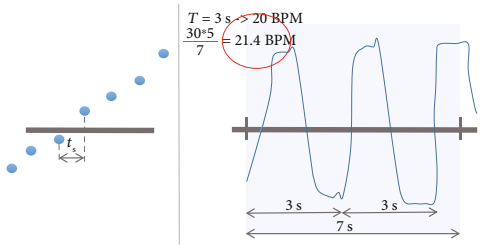

Figure 15: Example of possible structural errors associated with Algorithm 1 (a) and Algorithm 2 (a, b).

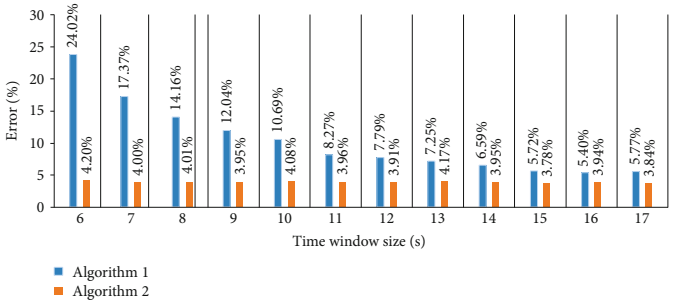

Figure 16: Errors (δ) of the proposed sensor for the two processing algorithms for time windows between 6 and 17 s.

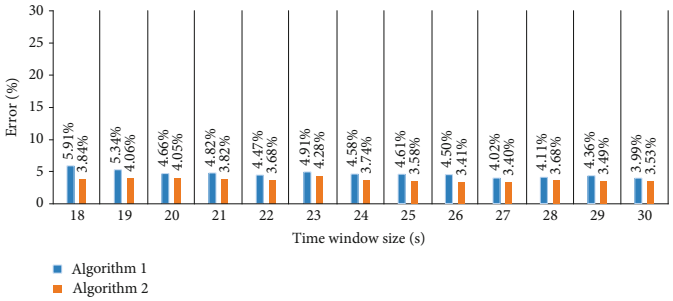

Figure 17: Errors (δ) of the proposed sensor for the two processing algorithms for time windows between 18 and 30 s.

[26, 63, 64]. For each time window, the entire analysis was repeated (in total 31,500 RR values; 15,750 per algorithm). The elimination of trends due to movements in the sensor was only applied to large windows (above 21 s for Algorithm 1 and above 19 s for Algorithm 2) since no decrease in error was perceived in shorter windows. Figure 14 shows the structure of the experiments graphically.

To obtain the optimal time window, the one sample t-test was used. This test is suitable to compare the mean of one sample with a known reference value. The null hypothesis (H_0) is as follows:

$$H_0 : m = \mu, \tag{8}$$

where m is the mean of RR and μ is the reference value of BPM set by the metronome, which was considered the gold standard.

Specifically, this test was performed for each time window and repeated for all reference values of BPM tested. In total, 150 tests were conducted.

As a result of this test, the p values greater than the significance level (0.05) were identified. For the time windows and reference values associated with those p values, the null hypothesis could not be rejected. In other words, sample means cannot be assumed to be significantly different from reference values. Therefore, we can assume that the sensor is measuring RR accurately for those BPM and time windows. The time windows that have the largest number of p values greater than 0.05 could be considered candidates for optimal windows. For those reference values of the candidate windows having p values below 0.05 (the mean is significantly different from the reference value), the Cohen's d test can be performed to quantify the effect size [65]. It can be obtained as the ratio of the difference between two mean values (one of them can be the reference value) divided by their pooled standard deviations. Small effect sizes are desirable. This would indicate that the difference between the means of RR and the reference values is small. A quantification of the effect size magnitude ("rule of thumb") can be made using the thresholds defined in [66]: $d < 0.2$ (negligible effect), $d < 0.5$ (small effect), and $d < 0.8$ 395 (medium effect). Otherwise, the effect can be categorized as large. Therefore, the time window with the smallest effect sizes can be considered optimal.

In parallel, the relative error (δ) was calculated according to the following equation:

$$\delta = 100 \times \left| 1 - \frac{\mu_0}{\mu} \right|, \tag{9}$$

where μ_0 is a measured RR and μ is the reference value of BPM set by the metronome. In total, 1,500 error values were calculated (2 algorithms times 6 reference values times 5 activities times 25 time windows). The means of the errors were made for all activities and reference values, obtaining 50 mean errors (25 per algorithm, 2 per time window).

To determine the optimal algorithm for the optimal time window, the paired sample t-test was performed since it is appropriate to compare the means between two groups of related samples. This test was performed on the means of the relative errors (δ). The null hypothesis (H_0) is as follows:

$$H_0 : m = 0, \tag{10}$$

where m is the mean of differences. If the p value is less than or equal to the significance level (0.05), it can be assumed that the two paired samples (algorithm errors) are significantly different. In that case, the algorithm with the lowest error could be considered the best. Figure 14 presents an overview of the validation experiments. All statistical tests have been performed in the R software. The R code is given as supplementary material to this paper.

In relation to the errors, it is important to highlight that some structural errors are already introduced by the sampling frequency or the time window selected, depending on the algorithm. For Algorithm 1 (based on time measurements), there is a quantization error set by the sampling frequency of up to 1/50 s at each zero-crossing. As one cycle has two zero-crossings, the maximum structural error in one cycle can be expressed in relative terms for each reference BPM value (Table 3). For Algorithm 2 (based on counting zero-crossings), the time window already introduces some error. All time windows that are not divisible by integer multiples of half the breathing period under analysis suffer this error. For this algorithm, the quantization error can also affect in some extreme cases in which the appearance or not of a zero-crossing depends on the sampling frequency (zero-crossings that appear exactly at the beginning or end of a window). Taken into consideration both effects (time window and sampling frequency), their associated maximum relative errors (up and down) are estimated in Table 4. It should be noted that the limits of structural errors calculated in Tables 3 and 4 are maximum values for extreme cases. Figure 15 graphically shows an example of two structural errors.

4. Results

Figures 16 and 17 represent the mean error for the twenty-five time windows under analysis and for the two algorithms used to obtain the RR. The standard deviations of these mean values are shown in Table 5. The values of the RR measured and the source code with the calculation of their mean errors and standard deviations have been attached to this paper as supplementary material.

Table 6 shows the p values of the one-sample t-test for each time window. In view of this table, it is clear that the 27 second window has more p values greater than 0.05: four in this case. This means that RR average values and reference values can be assumed to be equal for this time window and BPM. Therefore, this is the optimal window in the terms defined in this experiment.

Table 5: Standard deviations (%) of the mean relative errors (δ) for each algorithm and time window.

Window (s)	Algorithm 1	Algorithm 2
6	23.87	5.67
7	17.16	4.76
8	15.32	5.10
9	12.71	4.46
10	11.96	4.49
11	8.78	4.32
12	9.41	4.53
13	8.20	4.63
14	8.00	3.78
15	7.04	3.63
16	6.89	4.06
17	7.09	4.12
18	6.70	4.12
19	5.84	5.13
20	5.04	4.51
21	5.54	4.21
22	5.81	4.61
23	6.35	5.04
24	5.84	4.27
25	5.34	4.06
26	4.99	3.95
27	5.09	4.28
28	5.05	3.96
29	5.42	4.09
30	4.94	3.64

Cohen's d was calculated for those BPM of the 27 s window that present statistically significant differences. Table 7 presents the results obtained.

For this window, the error values in the calculation of the RR provided by the two algorithms were compared. Table 8 shows the results. It can be seen that the p value of the t-test for paired samples is above the significance level (0.05). This means that the difference between the two paired means of error values is not significant. Therefore, it is not clear the algorithm that presents the lowest error. Both algorithms seem to behave equally well.

The executable source code associated with all statistical tests has been attached to this paper as supplementary material.

5. Discussion

The accuracy of the sensor designed presents less average error value for Algorithm 2 than for Algorithm 1. However, this difference is not statistically significant. Both algorithms

Table 6: p values greater (>) or less (<) than the significance level (0.05) for the RR calculated for each time window and reference value.

Window (s)	10 BPM	12.5 BPM	15 BPM	17.5 BPM	20 BPM	22.5 BPM
6	<	<	<	<	<	>0.05
7	<	<	<	<	<	>0.05
8	<	<	<	<	>0.05	>0.05
9	<	<	<	<	>0.05	<
10	<	<	<	<	>0.05	<
11	<	<	<	<	>0.05	>0.05
12	<	<	<	<	>0.05	<
13	<	<	<	<	>0.05	<
14	<	<	<	>0.05	>0.05	<
15	<	<	<	>0.05	>0.05	<
16	<	<	<	>0.05	<	<
17	<	<	>0.05	>0.05	<	<
18	<	<	>0.05	>0.05	>0.05	<
19	<	<	<	>0.05	>0.05	<
20	<	<	<	>0.05	>0.05	<
21	<	<	<	>0.05	>0.05	<
22	<	<	<	>0.05	>0.05	<
23	<	<	<	>0.05	>0.05	<
24	<	<	<	>0.05	<	<
25	<	<	<	>0.05	<	<
26	<	<	<	>0.05	>0.05	<
27	<	<	>0.05	>0.05	>0.05	>0.05
28	<	<	<	>0.05	>0.05	>0.05
29	<	<	<	>0.05	>0.05	<
30	<	<	>0.05	>0.05	>0.05	<

Table 7: Effect size quantified with Cohen's d test.

	27 s window
10 BPM	1.06
12.5 BPM	0.53

Table 8: Comparison of the two algorithms. p values of the t-test for paired samples and Cohen's d for errors calculated with a 27 s window.

	t-test	Cohen's d
p value	0.0884	0.1320

are influenced, at the same time, by the time window considered. The validation results presented have allowed determining the optimal time window.

A time window of 27 s seems optimal to obtain the highest sensing accuracy. This has been verified by different means. Firstly, the mean error values (δ) calculated for each time window have the lowest value for 27 s for Algorithm 2 and the second lowest value for Algorithm 1. Their associated standard deviations also show low values for the 27 s window (Table 5). This is an indicator that these low error values also have a low level of dispersion. In other words, the individual errors used in the calculation of the average do not differ much from the average errors obtained. Secondly, the calculated p values of the one sample t-test provide statistical evidence that the 27 s time window is optimal. This time window has the highest number of BPM tested that cannot be considered different from the reference values. The Cohen's d results showed a moderate effect size for the 12.5 BPM reference value and large for the 10 BPM. Slow breathing seems to have higher error values for all time windows. This is an expected result since the number of cycles used to obtain the RR is less than in rapid breathing. If the optimal time window was adopted, it could provide a fairly accurate measurement of RR every twenty-seven seconds. This time step is suitable for many applications. If shorter time windows were desired (e.g., 16-20 s also have acceptable error rates), they can be adopted at the expense of lower accuracy.

Some time windows had large errors for Algorithm 1. This is the case of short time windows (6 s to 10 s). This is a logical result since the number of cycles used to make the calculation of time difference is very limited. These time windows are specially affected by the movements of the subject

Table 9: Performances provided by other studies in this field. If a percentage is given without any other indication, that value corresponds to a relative error. If a value in breaths/min is given without any other indication, that value corresponds to an absolute error.

Study	Performance
System proposed	3.40%
Chen et al. [60]	98.65% (mean accuracy)
Patwari et al. [61]	0.1-0.4 breaths/min
Liu et al. [8]	1.8-5.7%
Massaroni et al. [57]	2%
Dziuda et al. [10]	12% (maximum)
Nam et al. [17]	<1% (median)
Heldt and Ward [68]	1.2 breaths/min
Dan et al. [4]	0.01-0.02 breaths/min (mean differences)
Taheri and Sant'Anna [31]	0.93-1.77 breaths/min
Min et al. [39]	0.0015 breaths/min (mean differences)
Massaroni et al. [41]	1.59% (RR) 14% (tidal volume)
Presti et al. [40]	0.38%
Hoffman et al. [2]	37.9% (volume)
Hesse et al. [12]	0.32 breaths/min
Lau et al. [7]	2 breaths/min
Kukkapalli et al. [30]	>95% (accuracy)
Padasdao et al. [9]	0.23-0.48 breaths/min (mean differences)

or the sensor. It is important to note that the use of time windows greater than 20 s and less than 30 s has quite similar error values. It is also a fact that error values for those windows were not far from the optimal case, so time windows above or around 20 s might also be acceptable.

Regarding the processing algorithm, Algorithm 2 seems more robust to time window variations than Algorithm 1 since its associated error values are small even for short windows. The statistical tests for the optimal window (27 s) did not identify significant differences. According to the typical interpretations of Cohen's d value, the difference between both algorithms was negligible (0.132).

Results show that the designed sensor can determine the RR with an error of 3.40%. If the error value obtained with the proposed sensor is compared with other error values presented in the literature, it is possible to conclude that this value is in line with other studies in this field (Table 9). However, performances among studies cannot be compared fairly, since each study makes personalized tests. There are strong differences among validation experiments, datasets, and performance metrics. The inclusion of movements in the experiments can also compromise system performance. It is also important to highlight that the novelty of this paper with respect to existing studies is that we have presented a compact piezoresistive sensor with a 3D printed casing integrating all required modules into it, which is an advance in terms of wearability.

6. Conclusion

A respiration sensing system based on a piezoresistive FlexiForce sensor to be worn with a chest strap has been developed. This work is novel since it is the first time that this sensor is integrated in a compact casing including all the necessary elements (microcontroller, Bluetooth module, battery, etc.). The casing design has a direct influence on the sensor's detection capabilities. As part of this work, a compact casing has been designed and printed using a 3D printer. The files with the design have been published as supplementary material to be reused by any interested researcher.

A validation experiment was performed with 21 subjects. Two processing algorithms have been developed to determine the RR. Several statistical tests were conducted to identify both the optimal time window of the algorithms and the best algorithm. A time window of 27 s provides optimal results. This has been verified from the p values of the one sample t-test and the relative errors. This time window allows updating the RR every twenty-seven seconds, which is a suitable time for many applications. No statistically significant differences were identified between both algorithms for this time window. If shorter time windows were required, they could be used with a slightly larger error. This is a feasible scenario since error values remain fairly constant for a wide set of time windows (from 10 s for Algorithm 2 and from 20 s for Algorithm 1). This process of statistical verification is novel in this field.

Regarding the possible use of the information provided by this sensing system, it could be applied to several fields such as ambulatory health monitoring, home treatment of respiratory diseases, detection of alarming symptoms of faintness or fatigue in machine operators or drivers, health condition assessment, prediction and prevention of dangerous health states, monitoring of physical activity, and analysis of human emotions like anger and stress, among others. Customized data processing should be performed depending on the specific application.

Several commercial products that measure physiological parameters exist. However, it is not possible to know their working principle, electronic design, or results of validation experiments, since these data are generally not published. Additionally, most commercial products require data to be analyzed on their proprietary platforms. This contrasts with the sensing system presented in this paper. Data can be received online by any device with Bluetooth communication. They can then be processed offline in any numerical computing software. In addition, we have designed a 3D compact casing and uploaded the source files to a public repository to be rebuilt by any interested researcher. Another important aspect is the price of the system. Adding the cost associated with all elements of the system, it is below $50. Different commercial chest breathing sensors can be purchased for several hundreds of dollars. However, system design is not available to be reproduced by researchers. In this paper, the breathing dataset with the measurements from the experiments, the files with the error calculations, the source code of the RR computation with the two algorithms, and the source code of the statistical tests have been

published as supplementary material to be reviewed or reused by researchers in this field. This increases transparency in research and promotes reusability. It is the first time that we see this approach in a study in this field, to the best of our knowledge.

This work also has some limitations. Although sensor validation using a metronome is a well-known and accepted method, it would be desirable to validate this sensor against a reference breathing sensor taken as a gold standard. More subjects could have been included in the study, and other 3D casing designs could have been investigated. In addition, programming a smartphone app that receives sensor data via Bluetooth is a necessary step for the real-world implementation of the sensing system.

Nevertheless, this paper has shown that the compact FlexiForce sensor with the 3D casing designed together with the algorithm based on measuring times between zero-crossings or counting zero-crossings allows determining the RR with a low error and an acceptable refresh rate.

Data Availability

The dataset with the breathing data recorded in the validation experiments is deposited in a public repository [45]. The files corresponding to the 3D design of the casing, the calculation of errors and standard deviations, the algorithms to obtain the RR from raw data, and the statistical tests are provided as supplementary materials.

Conflicts of Interest

The authors declare that there is no conflict of interest regarding the publication of this paper.

Acknowledgments

The authors gratefully acknowledge the efforts of the twenty-one volunteers who participated in the validation experiments. This work was supported by the European Social Fund (grant number: Programa Operativo FEDER 2014-2020 Construyendo Europa desde Aragon), the Gobierno de Aragon (grant number T49-17R), the Consejo Nacional de Ciencia y Tecnología (CONACyT, grant number 709365), and the Universidad de Zaragoza and Centro Universitario de la Defensa de Zaragoza (grant number UZCUD2019-TEC-02).

Supplementary Materials

The supplementary materials are categorized in four different folders: (A) STL files with the 3D design of the compact casing. The casing consists of eight different pieces. They can be printed separately. (B) MATLAB files with the algorithms used to calculate respiratory rate from the recorded data (the dataset of breathing signals is also included in that folder). (C) Excel file with the calculation of sensor error values and standard deviations for different algorithms, time windows, and reference values. (D) R files with the statistical tests applied in the paper (one sample t-test, Cohen's d, and t-test for paired samples). *(Supplementary Materials)*

References

[1] I. Mahbub, H. Wang, S. K. Islam, S. A. Pullano, and A. S. Fiorillo, "A low power wireless breathing monitoring system using piezoelectric transducer," in *2016 IEEE International Symposium on Medical Measurements and Applications (MeMeA)*, pp. 1–5, Benevento, Italy, May 2016.

[2] T. Hoffmann, B. Eilebrecht, and S. Leonhardt, "Respiratory monitoring system on the basis of capacitive textile force sensors," *IEEE Sensors Journal*, vol. 11, no. 5, pp. 1112–1119, 2011.

[3] C. Wang, A. Hunter, N. Gravill, and S. Matusiewicz, "Unconstrained video monitoring of breathing behavior and application to diagnosis of sleep apnea," *IEEE Transactions on Biomedical Engineering*, vol. 61, no. 2, pp. 396–404, 2014.

[4] G. Dan, J. Zhao, Z. Chen, H. Yang, and Z. Zhu, "A novel signal acquisition system for wearable respiratory monitoring," *IEEE Access*, vol. 6, pp. 34365–34371, 2018.

[5] Z. Cao, R. Zhu, and R. Que, "A wireless portable system with microsensors for monitoring respiratory diseases," *IEEE Transactions on Biomedical Engineering*, vol. 59, no. 11, pp. 3110–3116, 2012.

[6] J. Witt, F. Narbonneau, M. Schukar et al., "Medical textiles with embedded fiber optic sensors for monitoring of respiratory movement," *IEEE Sensors Journal*, vol. 12, no. 1, pp. 246–254, 2012.

[7] D. Lau, Z. Chen, J. T. Teo et al., "Intensity-modulated microbend fiber optic sensor for respiratory monitoring and gating during MRI," *IEEE Transactions on Biomedical Engineering*, vol. 60, no. 9, pp. 2655–2662, 2013.

[8] J. J. Liu, M. C. Huang, W. Xu et al., "Breathsens: a continuous on-bed respiratory monitoring system with torso localization using an unobtrusive pressure sensing array," *IEEE Journal of Biomedical and Health Informatics*, vol. 19, no. 5, pp. 1682–1688, 2015.

[9] B. Padasdao, E. Shahhaidar, C. Stickley, and O. Boric-Lubecke, "Electromagnetic biosensing of respiratory rate," *IEEE Sensors Journal*, vol. 13, no. 11, pp. 4204–4211, 2013.

[10] L. Dziuda, F. W. Skibniewski, M. Krej, and J. Lewandowski, "Monitoring respiration and cardiac activity using fiber Bragg grating-based sensor," *IEEE Transactions on Biomedical Engineering*, vol. 59, no. 7, pp. 1934–1942, 2012.

[11] C. Massaroni, D. S. Lopes, D. Lo Presti, E. Schena, and S. Silvestri, "Contactless monitoring of breathing patterns and respiratory rate at the pit of the neck: a single camera approach," *Journal of Sensors*, vol. 2018, Article ID 4567213, 13 pages, 2018.

[12] M. Hesse, P. Christ, T. Hörmann, and U. Rückert, "A respiration sensor for a chest-strap based wireless body sensor," in *SENSORS, 2014 IEEE*, pp. 490–493, Valencia, Spain, November 2014.

[13] C. Massaroni, A. Nicolò, D. Lo Presti, M. Sacchetti, S. Silvestri, and E. Schena, "Contact-based methods for measuring respiratory rate," *Sensors*, vol. 19, no. 4, p. 908, 2019.

[14] S.-H. Liao, W.-J. Chen, and M. S.-C. Lu, "A CMOS MEMS capacitive flow sensor for respiratory monitoring," *IEEE Sensors Journal*, vol. 13, no. 5, pp. 1401-1402, 2013.

[15] G. Tardi, C. Massaroni, P. Saccomandi, and E. Schena, "Experimental assessment of a variable orifice flowmeter for respiratory monitoring," *Journal of Sensors*, vol. 2015, Article ID 752540, 7 pages, 2015.

[16] D. Fan, J. Yang, J. Zhang et al., "Effectively measuring respiratory flow with portable pressure data using back propagation neural network," *IEEE Journal of Translational Engineering in Health and Medicine*, vol. 6, pp. 1–12, 2018.

[17] Y. Nam, B. A. Reyes, and K. H. Chon, "Estimation of respiratory rates using the built-in microphone of a smartphone or headset," vol. 20, no. 6, pp. 1493–1501, 2016.

[18] Y. Huang and K. Huang, "Monitoring of breathing rate by a piezofilm sensor using pyroelectric effect," in *2013 1st International Conference on Orange Technologies (ICOT)*, pp. 99–102, Tainan, Taiwan, March 2013.

[19] S. Milici, J. Lorenzo, A. Lázaro, R. Villarino, and D. Girbau, "Wireless breathing sensor based on wearable modulated frequency selective surface," *IEEE Sensors Journal*, vol. 17, no. 5, pp. 1285–1292, 2017.

[20] Y. Pang, J. Jian, T. Tu et al., "Wearable humidity sensor based on porous graphene network for respiration monitoring," *Biosensors and Bioelectronics*, vol. 116, pp. 123–129, 2018.

[21] H. Farahani, R. Wagiran, and M. N. Hamidon, "Humidity sensors principle, mechanism,and fabrication technologies: a comprehensive review," *Sensors*, vol. 14, no. 5, pp. 7881–7939, 2014.

[22] J. Ascorbe, J. M. Corres, F. J. Arregui, and I. R. Matias, "Recent developments in fiber optics humidity sensors," *Sensors*, vol. 17, no. 4, p. 893, 2017.

[23] T. Katagiri, K. Shibayama, T. Iida, and Y. Matsuura, "Infrared hollow optical fiber probe for localized carbon dioxide measurement in respiratory tracts," *Sensors*, vol. 18, no. 4, p. 995, 2018.

[24] S. Imani, P. P. Mercier, A. J. Bandodkar, J. Kim, and J. Wang, "Wearable chemical sensors: opportunities and challenges," in *2016 IEEE International Symposium on Circuits and Systems (ISCAS)*, pp. 1122–1125, Montreal, QC, Canada, May 2016.

[25] A. T. Güntner, S. Abegg, K. Königstein, P. A. Gerber, A. Schmidt-Trucksäss, and S. E. Pratsinis, "Breath sensors for health monitoring," *ACS Sensors*, vol. 4, no. 2, pp. 268–280, 2019.

[26] W. Karlen, A. Garde, D. Myers, C. Scheffer, J. M. Ansermino, and G. A. Dumont, "Estimation of respiratory rate from photoplethysmographic imaging videos compared to pulse oximetry," *IEEE Journal of Biomedical and Health Informatics*, vol. 19, no. 4, pp. 1331–1338, 2015.

[27] C. G. Scully, J. Lee, J. Meyer et al., "Physiological parameter monitoring from optical recordings with a mobile phone," *IEEE Transactions on Biomedical Engineering*, vol. 59, no. 2, pp. 303–306, 2012.

[28] M. Metshein, "A device for measuring the electrical bioimpedance with variety of electrode placements for monitoring the breathing and heart rate," in *2015 26th Irish Signals and Systems Conference (ISSC)*, pp. 1–4, Carlow, Ireland, June 2015.

[29] S. Ansari, A. Belle, K. Najarian, and K. Ward, "Impedance plethysmography on the arms: respiration monitoring," in *2010 IEEE International Conference on Bioinformatics and Biomedicine Workshops (BIBMW)*, pp. 471-472, Hong Kong, China, December 2010.

[30] R. Kukkapalli, N. Banerjee, R. Robucci, and Y. Kostov, "Micro-radar wearable respiration monitor," in *2016 IEEE Sensors*, pp. 1–3, Orlando, FL, USA, October 2016.

[31] T. Taheri and A. Sant'Anna, "Non-invasive breathing rate detection using a very low power ultra-wide-band radar," in *2014 IEEE International Conference on Bioinformatics and Biomedicine (BIBM)*, pp. 78–83, Belfast, UK, November 2014.

[32] J. Hernandez, D. McDuff, and R. W. Picard, "Biowatch: estimation of heart and breathing rates from wrist motions," in *2015 9th International Conference on Pervasive Computing Technologies for Healthcare (PervasiveHealth)*, pp. 169–176, Istanbul, Turkey, May 2015.

[33] L. Estrada, A. Torres, L. Sarlabous, and R. Jané, "Respiratory signal derived from the smartphone built-in accelerometer during a respiratory load protocol," in *2015 37th Annual International Conference of the IEEE Engineering in Medicine and Biology Society (EMBC)*, pp. 6768–6771, Milan, Italy, August 2015.

[34] R. Ciobotariu, C. Rotariu, F. Adochiei, and H. Costin, "Wireless breathing system for long term telemonitoring of respiratory activity," in *2011 7th International Symposium on Advanced Topics in Electrical Engineering (ATEE)*, pp. 1–4, Bucharest, Romania, May 2011.

[35] C. Rotariu, C. Cristea, D. Arotaritei, R. G. Bozomitu, and A. Pasarica, "Continuous respiratory monitoring device for detection of sleep apnea episodes," in *2016 IEEE 22nd International Symposium for Design and Technology in Electronic Packaging (SIITME)*, pp. 106–109, Oradea, Romania, October 2016.

[36] J. Grlica, T. Martinović, and H. Džapo, "Capacitive sensor for respiration monitoring," in *2015 IEEE Sensors Applications Symposium (SAS)*, pp. 1–6, Zadar, Croatia, April 2015.

[37] C. M. Yang, T. L. Yang, C. C. Wu et al., "Textile-based capacitive sensor for a wireless wearable breath monitoring system," in *2014 IEEE International Conference on Consumer Electronics (ICCE)*, pp. 232-233, Las Vegas, NV, USA, January 2014.

[38] C. M. Yang, T. Yang, C. C. Wu, and N. N. Y. Chu, "A breathing game with capacitive textile sensors," in *2011 IEEE International Games Innovation Conference (IGIC)*, pp. 134–136, Orange, CA, USA, November 2011.

[39] S. D. Min, Y. Yun, and H. Shin, "Simplified structural textile respiration sensor based on capacitive pressure sensing method," *IEEE Sensors Journal*, vol. 14, no. 9, pp. 3245–3251, 2014.

[40] D. L. Presti, C. Massaroni, D. Formica et al., "Smart textile based on 12 fiber Bragg gratings array for vital signs monitoring," *IEEE Sensors Journal*, vol. 17, no. 18, pp. 6037–6043, 2017.

[41] C. Massaroni, P. Saccomandi, D. Formica et al., "Design and feasibility assessment of a magnetic resonance-compatible smart textile based on fiber Bragg grating sensors for respiratory monitoring," *IEEE Sensors Journal*, vol. 16, no. 22, pp. 8103–8110, 2016.

[42] X. Yang, Z. Chen, C. S. M. Elvin et al., "Textile fiber optic microbend sensor used for heartbeat and respiration monitoring," *IEEE Sensors Journal*, vol. 15, no. 2, pp. 757–761, 2015.

[43] D. Teichmann, D. De Matteis, T. Bartelt, M. Walter, and S. Leonhardt, "A bendable and wearable cardiorespiratory monitoring device fusing two noncontact sensor principles," *IEEE Journal of Biomedical and Health Informatics*, vol. 19, no. 3, pp. 784–793, 2015.

[44] *FlexiForce a201 sensor*, 2018, https://www.tekscan.com/productssolutions/force-sensors/a201.

[45] E. Vanegas, R. Igual, and I. Plaza, "Breathing data from a piezoresistive breathing sensor," in *IEEE Dataport*, October 2019.

[46] Adafruit Learning System, "Force sensitive sensor," 2018, August 2018, https://cdn-learn.adafruit.com/downloads/pdf/force-sensitive-resistor-fsr.pdf.

[47] N. Cotta, T. Devidas, and V. K. N. Ekoskar, "Wireless communication using HC-05 Bluetooth module interfaced with Arduino," *International Journal of Science, Engineering and Technology Research*, vol. 5, no. 4, 2016.

[48] S. Numeriques, "BTM-5 Bluetooth," *wireless TTL Master/Slave Transceiver Module*, 2011, http://www.strat-num.fr/IMG/pdf/bluetooth-module-btm5-datasheet.pdf.

[49] ATMEL, "8-bit microcontroller with 4/8/16/32k bytes in-system programmable flash," *Arduino's Pro-mini microcontroller*, 2009, https://www.sparkfun.com/datasheets/Components/SMD/ATMega328.pdf.

[50] S. Lee, J. Kim, J. Lee, and B. H. Cho, "State-of-charge and capacity estimation of lithium-ion battery using a new open-circuit voltage versus state-of-charge," *Journal of Power Sources*, vol. 185, no. 2, pp. 1367–1373, 2008.

[51] M. Jacoby, "Assessing the safety of lithium-ion batteries," *Chemical and Engineering News*, vol. 91, pp. 33–37, 2013.

[52] NanJing Top Power ASIC Corp, "Tp4056," https://dlnmh9ip6v2uc.cloudfront.net/datasheets/Prototyping/TP4056.pdf.

[53] MathWorks, "Lowpass' function," 2019, https://es.mathworks.com/help/signal/ref/lowpass.html.

[54] L. Schriger, "Approach to the patient with abnormal vital signs," in *Goldman's Cecil Medicine*, pp. 27–30, Elsevier, 2012.

[55] W. Q. Lindh, M. Pooler, C. D. Tamparo, B. M. Dahl, and J. Morris, *Delmar's Comprehensive Medical Assisting: Administrative and Clinical Competencies*, Delmar Cengage Learning, 4th edition, 2013.

[56] J. Mann, R. Rabinovich, A. Bates, S. Giavedoni, W. MacNee, and D. K. Arvind, "Simultaneous activity and respiratory monitoring using an accelerometer," in *2011 International Conference on Body Sensor Networks*, pp. 139–143, Dallas, TX, USA, May 2011.

[57] C. Massaroni, D. Lo Presti, P. Saccomandi, M. A. Caponero, R. D'Amato, and E. Schena, "Fiber Bragg grating probe for relative humidity and respiratory frequency estimation: assessment during mechanical ventilation," *IEEE Sensors Journal*, vol. 18, no. 5, pp. 2125–2130, 2018.

[58] C. Massaroni, E. Schena, S. Silvestri, F. Taffoni, and M. Merone, "Measurement system based on RBG camera signal for contactless breathing pattern and respiratory rate monitoring," in *2018 IEEE International Symposium on Medical Measurements and Applications (MeMeA)*, pp. 1–6, Rome, Italy, June 2018.

[59] C. Massaroni, M. Ciocchetti, G. Di Tomaso et al., "Design and preliminary assessment of a smart textile for respiratory monitoring based on an array of fiber Bragg gratings," in *2016 38th Annual International Conference of the IEEE Engineering in Medicine and Biology Society (EMBC)*, pp. 6054–6057, Orlando, FL, USA, August 2016.

[60] C. Chen, Y. Han, Y. Chen et al., "TR-BREATH: time-reversal breathing rate estimation and detection," *IEEE Transactions on Biomedical Engineering*, vol. 65, no. 3, pp. 489–501, 2018.

[61] N. Patwari, J. Wilson, S. Ananthanarayanan, S. K. Kasera, and D. R. Westenskow, "Monitoring breathing via signal strength in wireless networks," *IEEE Transactions on Mobile Computing*, vol. 13, no. 8, pp. 1774–1786, 2014.

[62] K. E. Barrett and W. F. Ganong, *Ganongs Review of Medical Physiology*, McGraw-Hill, 2013.

[63] N. Patwari, L. Brewer, Q. Tate, O. Kaltiokallio, and M. Bocca, "Breathfinding: a wireless network that monitors and locates breathing in a home," *IEEE Journal of Selected Topics in Signal Processing*, vol. 8, no. 1, pp. 30–42, 2014.

[64] M. H. Li, A. Yadollahi, and B. Taati, "Noncontact vision-based cardiopulmonary monitoring in different sleeping positions," *IEEE Journal of Biomedical and Health Informatics*, vol. 21, no. 5, pp. 1367–1375, 2017.

[65] J. Cohen, *Statistical Power Analysis for the Behavioral Sciences*, Lawrence Erlbaum Associates, USA, 2nd edition, 1988.

[66] J. Cohen, "A power primer," *Psychological Bulletin*, vol. 112, no. 1, pp. 155–159, 1992.

[67] J. De Jonckheere, M. Jeanne, F. Narbonneau et al., "Ofseth: a breathing motions monitoring system for patients under MRI," in *2010 Annual International Conference of the IEEE Engineering in Medicine and Biology*, pp. 1016–1019, Buenos Aires, Argentina, August 2010.

[68] G. P. Heldt and R. J. Ward, "Evaluation of ultrasound-based sensor to monitor respiratory and nonrespiratory movement and timing in infants," *IEEE Transactions on Biomedical Engineering*, vol. 63, no. 3, pp. 619–629, 2016.

Anexo I

Sensing Systems for Respiration Monitoring: A Technical Systematic Review

sensors

MDPI

Review

Sensing Systems for Respiration Monitoring: A Technical Systematic Review

Erik Vanegas, Raul Igual * and Inmaculada Plaza

EduQTech, Electrical/Electronics Engineering and Communications Department, EUP Teruel, Universidad de Zaragoza, 44003 Teruel, Spain; 790974@unizar.es (E.V.); inmap@unizar.es (I.P.)
* Correspondence: rigual@unizar.es

Received: 9 August 2020; Accepted: 16 September 2020; Published: 22 September 2020

Abstract: Respiratory monitoring is essential in sleep studies, sport training, patient monitoring, or health at work, among other applications. This paper presents a comprehensive systematic review of respiration sensing systems. After several systematic searches in scientific repositories, the 198 most relevant papers in this field were analyzed in detail. Different items were examined: sensing technique and sensor, respiration parameter, sensor location and size, general system setup, communication protocol, processing station, energy autonomy and power consumption, sensor validation, processing algorithm, performance evaluation, and analysis software. As a result, several trends and the remaining research challenges of respiration sensors were identified. Long-term evaluations and usability tests should be performed. Researchers designed custom experiments to validate the sensing systems, making it difficult to compare results. Therefore, another challenge is to have a common validation framework to fairly compare sensor performance. The implementation of energy-saving strategies, the incorporation of energy harvesting techniques, the calculation of volume parameters of breathing, or the effective integration of respiration sensors into clothing are other remaining research efforts. Addressing these and other challenges outlined in the paper is a required step to obtain a feasible, robust, affordable, and unobtrusive respiration sensing system.

Keywords: respiratory monitoring; respiration sensor; breathing sensor; sensor comparison; systematic review; comprehensive review; technical review

1. Introduction

Continuous monitoring of physiological variables is essential for health and well-being applications. One of the most interesting physiological variables is respiration. Breathing information is useful for health condition assessment [1]. It can help diagnose respiratory diseases, such as asthma, sleep apnea, and chronic obstructive pulmonary diseases (chronic bronchitis, emphysema, and non-reversible asthma) [2]. It is also used to identify heart failure or heart attack [3] and may serve as an indicator of changes in the nervous system, cardiovascular system, or excretory system, among others [4]. Once a disease has been diagnosed, breathing monitoring may be used during the treatment or for the surveillance of patients. It also plays a relevant role in the monitoring of newborn babies. Some of them are born under delicate conditions, and this monitoring may avoid any casualty due to infant sleep apnea [5]. Older people suffering from age-related conditions and diseases, like Parkinson or dementia [6], and sedentary patients could also benefit from unobtrusive health surveillance [7].

Breathing monitoring is also applicable to the field of work health and safety at work [8]. Firstly, having breathing information from workers can be helpful in assessing work-related risks to plan preventive actions to be undertaken before a work disease appears. The analysis of respiratory information may lead to the design of safer work places. Secondly, respiratory monitoring may help

prevent job accidents and is especially useful for jobs, such as plane piloting, industrial machine drivers, car, bus, or train drivers, who can benefit from having breathing information on real time [9].

Respiratory monitoring has also been applied in the analysis of human emotions [10,11]. Respiratory rate (RR) can be associated with emotions, such as fear, stress, anger, happiness, sadness, or surprise [12]. This can be used to prevent mental diseases and in the treatment of patients with mental disorders. Human emotions are also useful in psychological studies, for example, to assess or understand consumer and social trends [13]. They have also been applied in assessing the level of safety of drivers [14] by monitoring their emotional state. They were also used in the computer science field to improve software engineering processes, overcoming the limitations of usability questionnaires and helping to provide more personalized web experiences. For example, they can be used to obtain information about consumer behavior on websites and their interactions. Respiratory monitoring may contribute to real time recognition of emotions, which is an area of active research in the video game industry to generate dynamic gaming experiences [15]. There are also applications in the education field and e-Learning. Some emotional states have positive effects on learning processes, while others hinder them. It is possible to personalize the learning process by providing the most effective resources for each emotional state [16].

Respiratory information is also applied in the sports field to monitor the performance of athletes during their activities [17,18]. This information can be used to optimize their training or to prevent health problems. Similarly, it is used in Magnetic Resonance Imaging (MRI) machines to guarantee the good conditions of patients throughout the process [19] and to reduce their level of stress [20].

Another less common application of respiratory sensing is the evaluation of the health of combat soldiers [21,22]. This has a double utility: it provides information on the integrity of soldiers and allows collecting field information. Breathing monitoring has also been used for emergency situations, such as rescue of or searching for people, in which breathing information is required in a non-contact way for faster and more effective intervention [23].

Figure 1 shows an overview of the applications of respiration monitoring.

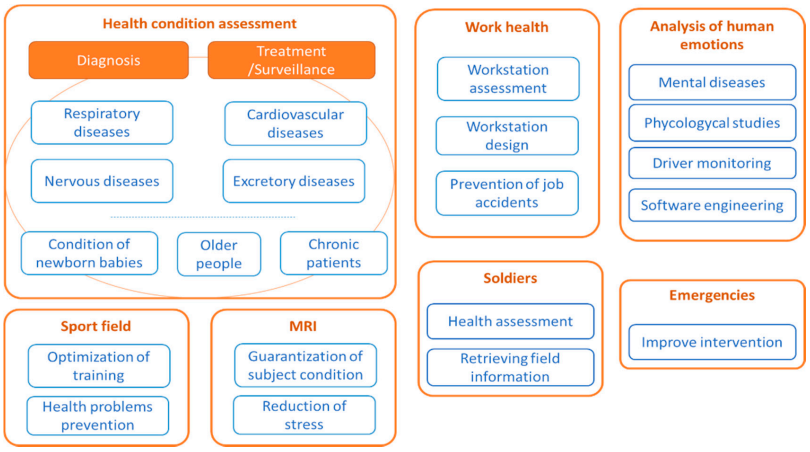

Figure 1. Most common application fields of sensing systems to monitor breathing.

To perform respiratory monitoring, several approaches were proposed in the literature [24]. Monitoring systems use sensors to measure breathing parameters. There are large differences among approaches depending on sensing techniques and sensors, breathing parameters, sensor locations, system setups, communication protocols, processing stations, energy autonomy and power

consumption, field of application, algorithms used to process sensor data, software of analysis, and performance evaluation, among others. Given that the number of studies and approaches has increased dramatically in recent years, it may be useful to review existing systems, discussing trends, challenges and issues in this field.

There are several existing reviews in the field of wearable sensors. For example, the survey of Mukhopadhyay et al. [25] focused on wearable sensors to monitor human activity continuously. They described the typical architecture of a human activity monitoring system based on sensors, microcontrollers, communication modules, and remote processing. The paper outlined transmission technologies and energy harvesting issues and predicted an increase in interest in wearable devices in the near future. Similarly, the work of Nag et al. [26] reviewed flexible wearable sensors to monitor physiological parameters. The study focused on the materials used to manufacture sensors based on different factors, such as application, material availability, cost, or manufacturing techniques. Different operating principles were identified: electromechanical, pressure and strain, chemical, and magnetic field-based, among others. The transmission technologies used in the sensing systems and their possible applications were also reviewed in detail. Finally, the paper identified several challenges and future opportunities. The most relevant was the expected reduction in the cost of manufacturing flexible sensing systems. However, this paper focused exclusively on flexible sensing systems, and no review of other technologies was performed. In addition, it did not specifically address respiration sensing, but instead considered sensors for any type of physiological parameter. Similarly, the reviews of Chung et al. [27] and Bandodkar et al. [28] also focused on wearable flexible sensors, but specifically targeted at sweat analysis. Meanwhile, the review of Lopez-Nava et al. [29] addressed inertial sensors for human motion analysis. Different aspects were studied: sensor type, number of sensing devices and their combination, processing algorithms, measured motion units, systems used for comparison, and number of test subjects and their age range, among others. The review identified a trend toward low-cost wearable systems.

Seshadri et al. [30] presented a work focused on wearable sensors to monitor athletes' internal and external workload. The paper addressed wearable devices for athletes comprehensively, including physical performance, physiological and mental status, and biochemical composition. RR was considered as one more physiological parameter. In fact, sensors to measure position, motion, impact, biomechanical forces, heart rate, muscle oxygen saturation, and sleep quality were also considered. The paper concluded that wearable sensors had the potential to minimize the onset of injuries and evaluate athlete performance in real time.

Aroganam et al. [31] reviewed wearable sensors for sport applications excluding professional sports. Communication technologies, battery life, and applications were widely discussed. The paper concluded that inertial and Global Positioning System (GPS) sensors were predominant in sport wearables. A gap was detected in user experience studies of existing devices. Meanwhile, Al-Eidan et al. [32] presented a systematic review on wrist-worn wearable sensors. They focused on user interface, interaction, and use studies of the sensing systems. Processing techniques were also analyzed showing high variability among them and including machine learning techniques and threshold-based methods. Similarly, validation experiments lasted from 2 s to 14 weeks and most of the experiments were performed under laboratory conditions. Few studies presented real-world setups with target users. Other aspects analyzed were sampling frequencies and features extracted. Challenges of wrist-based systems were identified in relation to weight, battery life, lack of standardization, safety, user acceptance, or design.

Mansoor et al. [33] performed a review on wearable sensors for older adults. The review focused on sensor target population, sensor type, application area, data processing, and usability. Fourteen papers were analyzed. They identified barriers, such as inaccurate sensors, battery issues, restriction of movements, lack of interoperability, and low usability. The paper concluded that these technical challenges should be resolved for successful use of wearable devices.

Heikenfeld et al. [34] conducted a review on wearable sensors that interfaced with the epidermis. Wearable sensors were classified into four broad groups: mechanical, electrical, optical, and chemical. Several subgroups were identified within each category. Body-to-signal transduction, actual devices and demonstrations, and unmet challenges were discussed. The paper concluded that, in general, sensing categories had remained isolated from each other in commercial products, and strategies were still needed to easily attach and detach disposable systems.

Witte and Zarnekow [35] reviewed wearable sensors for medical applications. Ninety-seven papers were analyzed in relation to disease treatments, fields of application, vital parameters measured, and target patients. The paper identified a trend toward heart and mental diseases monitoring. Sensors were used for monitoring or diagnosis, collecting physical activity data, or heart rate data. The work of Pantelopoulos et al. [36] surveyed wearable biosensor systems for health monitoring. The design of multiparameter physiological sensing systems was discussed in detail. Meanwhile, the study of Liang et al. [37] addressed wearable mobile medical monitoring systems. Emphasis was placed on devices based on wireless sensing networks, and special attention was given to textile technologies. Finally, the paper of Charlton et al. [38] reviewed the estimation of the RR using two different signals: the electrocardiogram (ECG) and the pulse oximetry (photoplethysmogram, PPG).

A recent review on contact-based sensors to measure RR was published by Massaroni et al. [24]. This paper identified seven contact-based techniques: measuring of respiratory airflow, respiratory sounds, air temperature, air humidity, air components, chest wall movements, and modulation cardiac activity. Several possible sensors could be used for each technique. Some of the sensors identified in the review were flowmeters, anemometers, fiber optic sensors, microphones, thermistors, thermocouples, pyroelectric sensors, capacitive sensors, resistive sensors, nanocrystal and nanoparticles sensors, infrared, inductive, transthoracic, inertial, ECG sensors, and PPG sensors, among others. The paper presented a detailed description of each sensing technology, focusing on metrological properties and operating principles. Equations were provided for most sensors. In addition, the study compared the optimal techniques for clinical settings (respiratory airflow, air temperature, air components, chest wall movements, and modulation of cardiac activities), occupational settings (respiratory airflow, air components, and chest wall movements) and sport and exercise (respiratory airflow and chest wall movements). These techniques were considered optimal for controlled environments.

A previous work on respiration sensors was published by AL-Khalidi et al. [39]. This paper covered both non-contact and contact-based methods and provided a general description of several sensing techniques. On the one hand, contact-based technologies included five sensing methods: acoustic, airflow detection, chest and abdominal movement measuring, transcutaneous CO_2 monitoring, oximetry prove (SpO_2), and electrocardiogram derived methods. On the other hand, non-contact technologies included radar-based detection, optical methods, thermal sensors, and thermal imaging. The paper concluded that non-contact RR monitoring had advantages over contact methods since they caused the least discomfort to patients.

Three other related surveys were published, to the best of our knowledge. The review by van Loon et al. [40] studied respiratory monitoring from a hospital perspective without analyzing technical items. The review of Rajala and Lekkala [41] focused exclusively in the film-type sensor materials polyvinylidenefluoride (PVDF) and electro-mechanical film (EMFi), while the recent review of Massaroni et al. [42] analyzed fiber Bragg grating sensors for cardiorespiratory monitoring.

In this paper, we present a survey on sensing systems for respiratory monitoring. This paper has several novelties with respect to the existing reviews in the state of the art:

- This review is not exclusively focused on sensor metrological properties or operating principles. Instead, this paper also reviews all the different aspects involved in the design and development of a respiration sensing system: communication protocols, processing stations, energy autonomy and power consumption, general system setups, sensor location and size, breathing parameters, validation methods, details of the test experiments, processing algorithms, software used for

analysis, and performance evaluation. To the best of our knowledge, this is the first review paper that analyzes all these aspects in breathing sensors.
- This paper does not focus exclusively on RR. In addition, sensors that measure other breathing parameters are also surveyed.
- Unlike previous reviews, this survey is systematic. Studies on respiration sensors were obtained using objective selection criteria. They were then subjected to detailed analysis.

Therefore, this paper provides a comprehensive overview of all aspects to consider in the design of respiratory sensing systems. It aims to help engineers and researchers to identify the different options at each design stage.

The structure of this review is as follows: Section 2 presents the study design, selection criteria, and organization of the review results; Section 3 describes the results of the literature search, which are classified into different groups, the items of analysis and the results of the analysis of those items for each study; Section 4 discusses the trends in respiratory monitoring, the issues in the design of respiration sensors, and the current challenges in this field, highlighting the research opportunities; and, finally, Section 5 draws some conclusions.

2. Materials and Methods

2.1. Search and Selection Procedure

A systematic search of the literature was carried out to identify relevant papers in the field of sensors for respiratory monitoring. The IEEE (Institute of Electrical and Electronics Engineers) Explore and Google Scholar were used for this review. IEEE Explore is a reference in engineering studies and Google Scholar provides a broader perspective to complement the results. Four sets of keywords were selected to perform the searches. To identify these keywords, a preliminary study was conducted that examined key studies in this field. As a result, the five search terms selected were the following: (1) "breathing" plus "monitoring", (2) "respiratory" plus "monitoring", (3) "breathing" plus "sensor", (4) "respiratory" plus "sensor", and (5) "respiration" plus "sensor".

To analyze the most recent research, articles from 2010 to 2019 were considered. Searches were conducted in February 2019 and repeated in March 2020. The sort by relevance of IEEE Xplore and Google Scholar was used to obtain the most relevant articles first. According to the official IEEE Xplore website, the search results are "sorted by how well they match the search query as determined by IEEE Xplore" [43]. Regarding the relevance criteria of Google Scholar, its official website points out that the rank is made by "weighting the full text of each document, where it was published, who it was written by, as well as how often and how recently it has been cited in other scholarly literature" [44]. Journals, magazines, and conferences were considered in the searches. As a result of the five searches in the two repositories, more than a million results were obtained. For each search and repository, the 100 most relevant papers were selected, resulting in 1000 studies. This number is high enough to provide a comprehensive review of the topic. The title and abstract of all these studies were examined and those not related to the subject of the review were discarded, resulting in 236 papers. Then, a second selection was made based on the content of the papers, discarding those that did not deal with sensors for respiratory monitoring. Finally, 198 papers were obtained. All of them were subjected to a detailed analysis that is presented in Section 3. Figure 2 (top) shows an overview of the selection procedure. Figure 2 (bottom) presents the PRISMA diagram that details the item selection process [45].

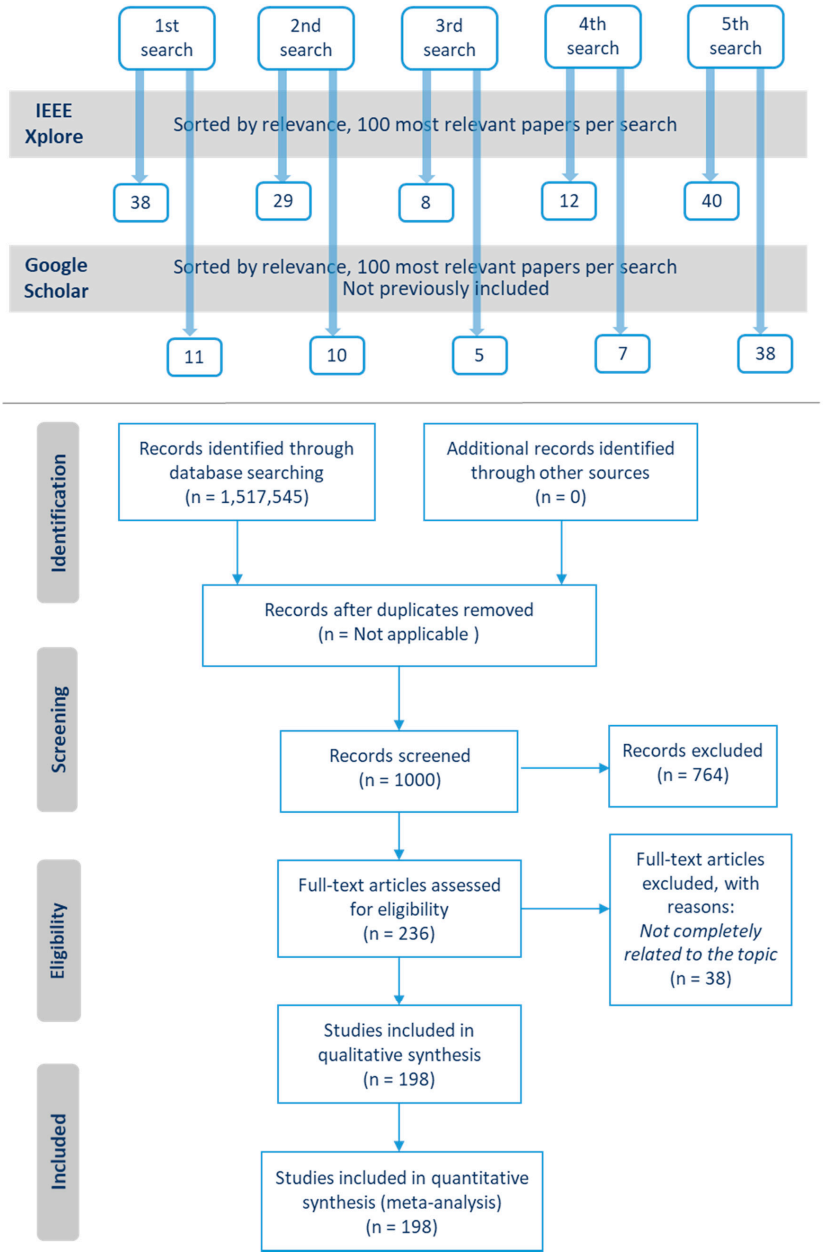

Figure 2. Literature search results and selection procedure (**top**). PRISMA diagram (**bottom**).

2.2. Organization of the Results

The search results were analyzed in detail. For that, papers were divided into two categories: wearable systems and environmental systems. This is a typical classification found in several sensor-related studies [24,46]. Wearable methods require individuals to carry the sensors, while environmental methods place them around subjects. The wearable category includes 113 studies, while the environmental category comprises the remaining 85 studies.

Different aspects of respiratory sensing systems were analyzed for each paper. The items selected can be divided into four categories (Figure 3): (1) sensor and breathing parameter, (2) data transmission and power consumption, (3) experiments performed for sensor validation, and (4) sensor measurement processing.

The category "sensor and breathing parameter" includes the following items of analysis: (1.1) sensing technique and sensor, (1.2) breathing parameter, and (1.3) sensor location and size.

Four items are included in the category "data transmission and power consumption": (2.1) general system setup, (2.2) communication protocol, (2.3) processing station, and (2.4) energy autonomy and power consumption.

The category "sensor validation" comprises several items related to the design of experiments to validate the sensors (they are listed in Section 3.3).

Three items are included in the "sensor measurement processing" category: (4.1) performance evaluation, (4.2) processing algorithm, and (4.3) software used for the analysis.

For each category, we first describe in detail the different items of analysis, except item (1.1) "sensing technique and sensor", which was described extensively in the review of Massaroni et al. [24]. Then, we provide the value of those items for each study selected for both categories (wearable and environmental). Results were subjected to critical analysis and discussion.

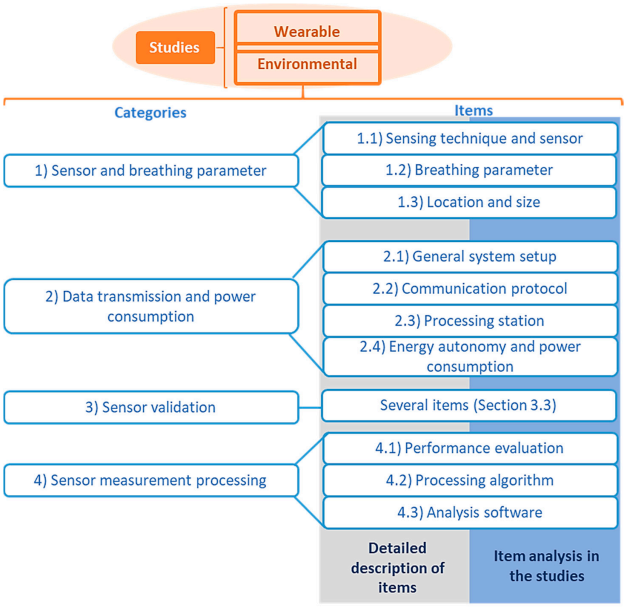

Figure 3. Analysis structure.

3. Results

This section has been structured around the four categories of analysis introduced in Section 2.2. First, the items of analysis and their possible values are described in detail for each category (Sections 3.1.1, 3.2.1, 3.3.1 and 3.4.1). Then, the values of those items provided in the studies selected are analyzed and discussed (Sections 3.1.2, 3.2.2, 3.3.2 and 3.4.2).

3.1. Sensor and Breathing Parameter

3.1.1. Items of Analysis

This category includes the following items of analysis: sensing technique and sensor, breathing parameter, and sensor location and size.

Sensing Technique and Sensor

According to the review of Massaroni et al. [24], two different dimensions can be observed in the operating principle: the technique selected to obtain respiration information and the sensor used to capture that information. For each possible technique, there are several sensors available.

To classify the papers analyzed in this review, the classification established in the work of Massaroni et al. [24] was used. It was expanded to also cover environmental breathing sensors. The techniques and sensors identified were:

- Technique based on measurements of respiratory airflow. Possible sensors are differential flowmeters, turbine flowmeters, hot wire anemometers, photoelectric sensors, and fiber optic sensors.
- Technique based on measurements of respiratory sounds. Possible sensors are microphones.
- Technique based on measurements of air temperature. Possible sensors are thermistors, thermocouples, pyroelectric sensors, fiber optic sensors, infrared sensors, and cameras.
- Technique based on measurements of air humidity. Possible sensors are capacitive sensors, resistive sensors, nanocrystal and nanoparticles sensors, impedance sensors, and fiber optic sensors.
- Technique based on measurements of chest wall movements. Three different types of measurement were identified in this technique:
    - Strain measurements: Possible sensors are resistive sensors, capacitive sensors, inductive sensor, fiber optic sensors, piezoelectric sensors, pyroelectric sensors, and triboelectric nanogenerator.
    - Impedance measurements: Possible sensors are transthoracic impedance sensors.
    - Movement measurements: Possible sensors are accelerometers, gyroscopes and magnetometers, frequency shift sensors, DC (direct current) generators, ultrasonic proximity sensors, cameras, optical sensors, inductive sensors, and Kinect sensors.
- Technique based on measurements of modulation cardiac activity. Possible sensors are ECG sensors (for biopotential measurements), PPG sensors (for light intensity measurements), radar sensors, and Wi-Fi transmitters and receivers.

Equations and details of the different sensors are included in the reference review paper [24].

Breathing Parameters

Breathing parameters are the metrics provided as output of the sensing process. Possible breathing parameters are the following:

- *Respiratory rate (RR)*: Number of breaths (inspiration and expiration cycles) performed by a subject in one minute (Figure 4). It is measured in breaths/min (bpm). Other metrics derived from the RR can also be calculated [10]:

- Breathing period: Time duration of a breathing cycle(s).
- Inspiratory time: Part of the breathing period that corresponds to inspiration (s). According to Figure 4A, it can be obtained as $t_b - t_a$
- Expiratory time: Part of the breathing period that corresponds to expiration (s). According to Figure 4A, it can be obtained as $t_d - t_c$

- *Volume parameters*: Metrics that provide volume information obtained from inhaled or exhaled air during breathing. Volume metrics comprise a set of sub-metrics related to the volume of air available in the lungs [47]. Some of the metrics that could be found in the breathing sensor studies were:
  - *Tidal volume (TV)*: It is the volume of air inhaled or exhaled during normal respiration (without forcing breathing). It is measured in liters (L). From the volume versus time signal represented in Figure 4B, the TV for a given breathing period could be calculated as $TV = |V_{n-1} - V_n| = |V_n - V_{n-1}|$, where V_n is the air volume associated with the n respiration peak or valley.
  - *Minute volume (MV)*: It is the volume of air inhaled or exhaled by a subject in one minute during normal breathing. It is measured in L/min. It can be roughly obtained from the TV and the RR as $MV = TV \cdot RR$. From the representation of Figure 4B, the MV can be calculated as $MV = \sum_{i=2}^{n} |V_{i-1} - V_i|;\ \forall i \in \mathbb{Z} : i \in [2, n] : 2|i$, where n is the number of peaks (or valleys) in the air volume curve that can be found in one minute of breathing.
  - *Peak inspiration flow (PIF)*: According to Warner and Patel [47], it is the maximum flow at which a given tidal volume breath can be delivered. It is measured in L/min. From the representation of Figure 4B, it can be obtained as $PIF = (V_b - V_a)/(t_b - t_a)$, where (V_a, t_a) is the point associated with the valley in the time-volume curve before inspiration, and (V_b, t_b) is the point related to the peak of inspiration at which the given tidal volume is delivered.
  - *Exhalation flow rate (EFR)*: Volume of air exhaled per time unit. It is expressed in L/s and can be calculated as $EFR = (Volume\ of\ exhaled\ air)/(Exhalation\ time)$ [48]. From the representation of Figure 4B, it can be obtained as $EFR = (V_3 - V_4)/(t_4 - t_3)$, where (V_3, t_3) is the point corresponding to a peak of the time-volume curve, and (V_4, t_4) is the next valley of the curve.
  - There are other air volume metrics, such as peak expiratory flow (maximum flow at which a given tidal volume can be exhaled; it can be obtained as $(V_c - V_d)/(t_d - t_c)$ from Figure 4B), vital capacity (volume of air expired after deep inhalation; it can be obtained as $V_e - V_f$ from Figure 4B), or forced vital capacity (same as vital capacity but maximizing the expiratory effort; it can be obtained as $V_g - V_h$ from Figure 4B), among others [49]. They have barely been used in breathing sensor studies.
  - *Compartmental volume*: Instead of considering air volume, this metric measures the change in volume of breathing-related body parts, like chest, thorax, or abdomen [49].

- *Respiration patterns*: There are studies in which the purpose is to identify patterns in the signals obtained from the recording of respiration instead of providing a particular breathing parameter. Common patterns identified are abnormal breathing [50–52], apnea episodes [50,51,53,54], Kussmaul's respiration, Cheyne-Stokes breathing, Biot's respiration, Cheyne-Stokes variant, or dysrhythmic breathing, among others [53]. There are also studies that identified the type of breathing (heavy or shallow breathing, mouth breathing, abdominal breathing, or chest breathing) [53].

Sensor Location and Size

Sensor location and size play a relevant role in system usability and can determine the acceptability of the technology by its potential users [55,56]. Figure 5 shows possible locations for wearable systems. The locations are chest (diaphragm or pectoral muscle), abdomen, waist, arm, forearm, finger, mouth (including mouth mask), nose (nasal bridge, above lip or nostril), wrist, neck (suprasternal notch area), or back. Regarding environmental systems, sensors can be located at a fixed distance from the subject, can be integrated into an object commonly used by the subject (pillow, mat, mattress, etc.), or can be distributed on nodes, among others. The location of a sensor largely depends on its operating principle and the specific application.

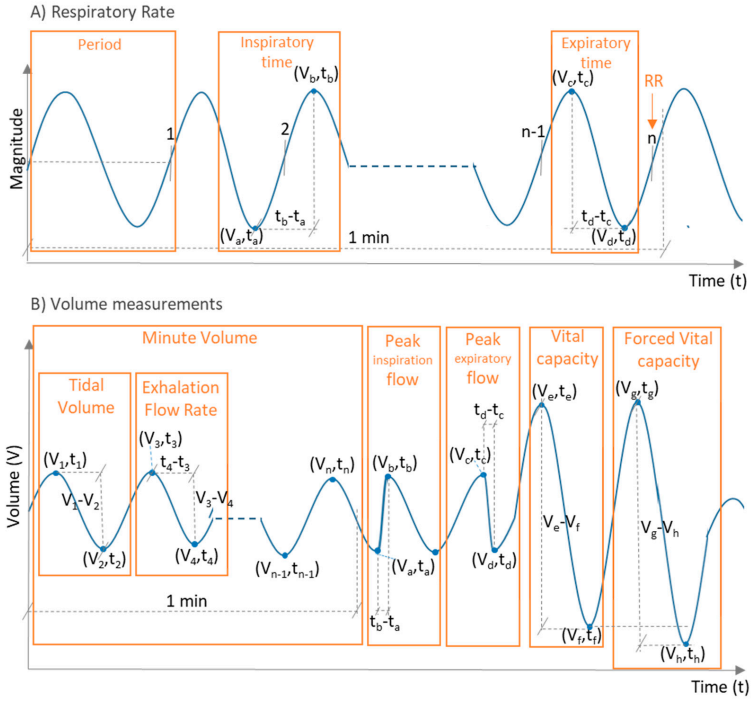

Figure 4. Graphical explanation of the different breathing parameters. Signal (**A**) could come directly from the ADC (analog-to-digital converter) of the sensing system, although it is also possible that it represents physical respiration magnitudes. This figure shows a general representation that is not contextualized to a specific sensing system. The same goes for signal (**B**).

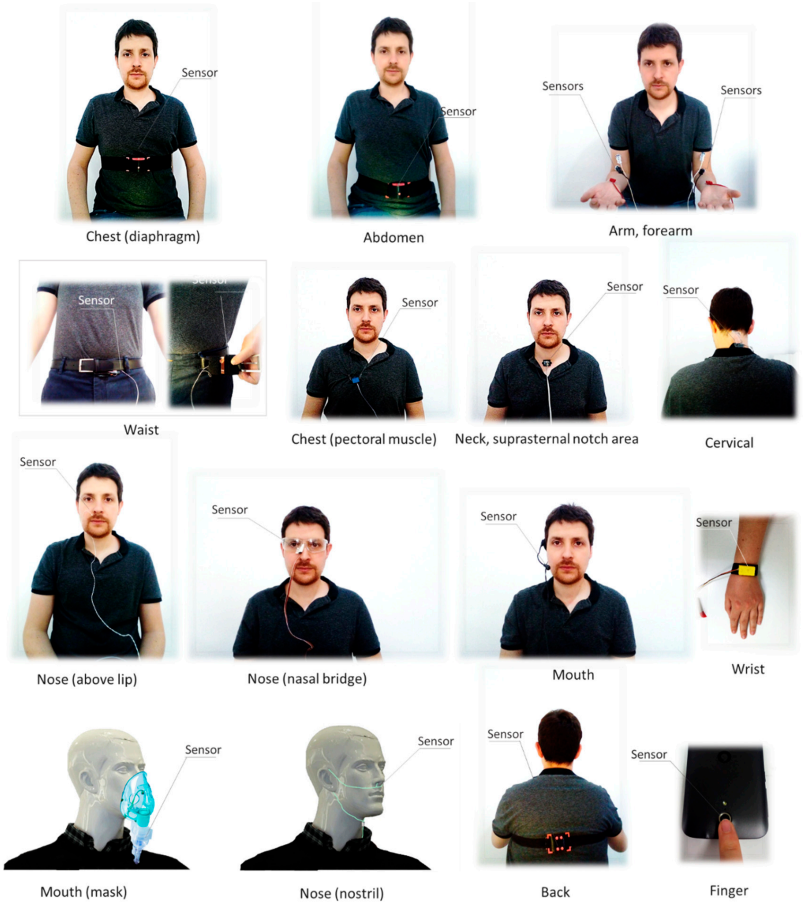

Figure 5. Most common sensor locations for respiration monitoring. The sensors shown are for contextualization purposes.

3.1.2. Results of the Analysis

Table 1 presents the results of the analysis of the items technique, sensor, parameter, and location and size for the studies in the wearable category, while Table 2 shows the results for the environmental papers.

Table 1. Analysis of techniques, sensors, breathing parameters, and sensor locations and sizes for studies of the wearable category.

Study [1]	Technique	Sensor	Measured Parameter	Location	Size
Aitkulov 2019 [57,58]	Chest wall movements	Fiber optic	RR	Chest	-
Balasubramaniyam 2019 [59]	Chest wall movements	Resistive	RR	Abdomen (shirt)	-
Bricout 2019 [60]	Chest wall movements	Accelerometer	RR	Chest Abdomen	-
Chu 2019 [61]	Chest wall movements	Resistive	RR TV	Chest	
Elfaramawy 2019 [62]	Chest wall/abdomen movements	Accelerometer Gyroscope Magnetometer	RR	Chest Abdomen	26.67 × 65.53 mm
Fajkus 2019 [63]	Respiratory air flow	Fiber optic	RR	Nose (nasal oxygen cannula)	
Hurtado 2019 [64]	Air temperature	Pyroelectric	RR	Nose (below)	30 × 16 × 20 mm
Jayarathna 2019 [65]	Chest wall movements	Resistive	RR	Chest (shirt)	-
Kano 2019 [66]	Air humidity	Nanocrystal and nanoparticles	RR	Mouth mask	
Karacocuk 2019 [67]	Chest wall movements	Accelerometer Gyroscope	MV	Chest (front and back)	
Massaroni 2019 [68]	Respiratory air flow (pressure)	Differential pressure	RR	Nose (nostril)	36 mm diameter (PCB)
Massaroni 2019 [69]	Chest wall movements	Resistive	RR	Chest and abdomen (shirt, front and back)	-
Nguyen 2019 [70]	Respiratory air flow (vibration)	Differential pressure sensor	RR	Nose (nasal bridge)	
Presti 2019 [71]	Respiratory air flow	Fiber optic	RR	Cervical spine	90 × 24 × 1 mm
Presti 2019 [72]	Chest/abdomen movements	Fiber optic	RR	Chest	-
Puranik 2019 [73]	Chest wall movements	Gyroscope	Monitoring of breathing	Chest Abdomen	-
Soomro 2019 [74]	Air humidity	Impedance	Monitoring of breathing	Nose (below)	
Xiao 2019 [75]	Air humidity	Resistive	Monitoring of breathing	Mouth mask (2–3 cm from nose)	
Yuasa 2019 [76]	Respiratory sounds Chest wall movements	MicrophoneOptical	RR	Chest (adhesive gel)	
Zhang 2019 [77]	Chest wall movements	Triboelectric nanogenerator	RR	Abdomen	-
Dan 2018 [78]	Chest wall movements	Accelerometer	RR Respiratory phase	Neck (Suprasternal notch area)	-
Koyama 2018 [79]	Chest wall movements	Fiber Optic sensor	RR	Abdomen (Cardigan, garment)	-
Malik 2018 [80]	Air humidity	Capacitive sensor	Monitoring of breathing	Mouth mask	-
Martin 2018 [81]	Respiratory sounds	Microphone	RR	Head (inside ear)	-
Pang 2018 [82]	Air humidity	Nanocrystal and Nanoparticles sensor	Monitoring of breathing	Mouth mask	-

[1] Note: The analysis for studies published before 2018 [2,3,17,21,49,83–162] is included in Appendix A (Table A1).

Table 2. Analysis of sensing techniques, sensors, breathing parameters, and sensor location and size for studies of the environmental category.

Study [1]	Technique	Sensor	Measured Parameter	Location	Size
Al-Wahedi 2019 [163]	Modulation cardiac activity	Radar	RR	Distance from subject (20–75 cm away)	
Chen 2019 [164]	Modulation cardiac activity	Radar	RR	Mat (below bed)	
Gunaratne 2019 [165]	Chest wall movements	Piezoelectric	RR	Mat	7 × 7 cm (each sensor)
Guo 2019 [166]	Chest wall movements	Capacitive	RR	Mat	
Isono 2019 [167]	Chest wall movements	Piezoelectric	RR	Others (under bed legs)	
Ivanovs 2019 [168]	Chest wall movements Modulation cardiac activity	Camera Radar	Respiration detection	-	
Joshi 2019 [169]	Chest wall movements	Capacitive	RR	Mat (below baby mattress)	580 × 300 × 0.4 mm
Krej 2019 [170]	Chest wall movements	Fiber optic	RR	Mat	
Lorato 2019 [171]	Air temperature	Camera	RR	Distance from subject (side and front, 10–50 cm away)	
Massaroni 2019 [172]	Chest wall movements	Camera	RR	Distance from subject (1.2 m away)	
Park 2019 [173]	Chest wall movements	Piezoelectric	RR	User's mat (Chest region)	40 × 750 × 0.25 mm
Walterscheid 2019 [174]	Modulation cardiac activity	Radar	RR	Distance from subject (3.3–4.2 m away)	
Wang 2019 [175]	Modulation cardiac activity	Radar	RR	Distance from subject (50 cm away)	
Xu 2019 [176]	Respiratory sounds	Microphone	RR	Others (instrument panel of vehicle)	
Yang 2019 [177]	Modulation cardiac activity	Radar	RR	Distance from subject (1.5 m height, 0–3 m away)	
Chen 2018 [178]	Modulation cardiac activity	Wi-Fi transmitter and receiver	RR Respiration detection	Nodes	-
Chen 2018 [179]	Chest wall movements	Piezoelectric	RR	Mat	2 × 35 cm
Massaroni 2018 [180]	Chest wall movements	Camera	RR Respiratory pattern	Distance from subject (1.2 m away)	-
Massaroni 2018 [181]	Chest wall movements	Fiber optic	RR	Others (inside ventilator duct)	3 cm
Sadek 2018 [182]	Chest wall movements	Fiber optic	RR Respiratory pattern	Mat	20 × 50 cm

[1] Note: The analysis for studies published before 2018 [5–7,9,10,19,48,50–54,183–234] is included in Appendix A (Table A2).

In relation to the sensing techniques and sensors, Figures 6 and 7 show the main results for the wearable and environmental categories, respectively. Most authors chose to detect chest wall movements (60%). For the environmental category, modulation of cardiac activity was also

very common [5,7,50,52,54,163,164,168,174,175,177,178,189,190,196–199,205–207,213,214,219,221,223–226,229,232,233]. Meanwhile, air temperature and air humidity were the second [2,64,91,104,107,116,120,128,133,145,153–156,162] and third [66,74,75,80,82,89,97,101,137,138] most widely implemented techniques in the wearable category, at great distance. In this category, fiber optic sensors were used in almost 19% of the studies, resistive sensors in 15%, accelerometers in more than 11%, and capacitive sensors in more than 9%. Great variability in sensors can be found in studies of this category, as there is no predominant type. This contrasts with the environmental category since radars are used in more than 33% of the studies, being the leading technology followed by cameras (18%) and fiber optic sensors (14%). There are types of sensors, such as magnetometers, gyroscopes, microphones, optical sensors, inductive sensors, or thermistors, in which its use is very limited in both categories [62,73,76,77,81,91,95,106,107,115,119,120,131,135,156,160,162,185,193,217].

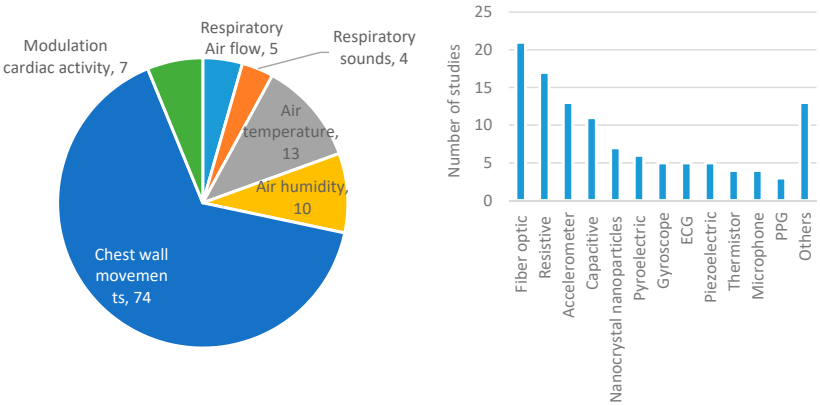

Figure 6. Distribution of sensing techniques (**left**) and sensors (**right**) used in the studies of the wearable category.

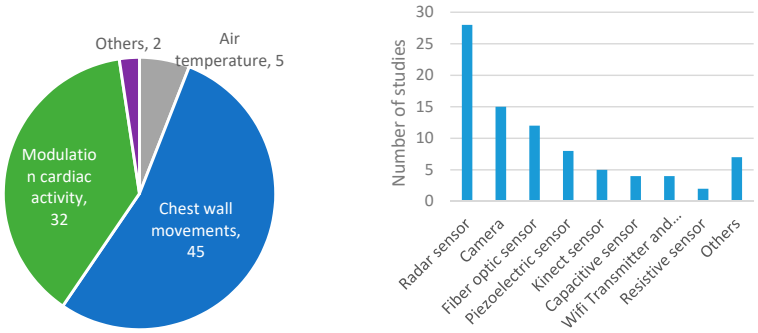

Figure 7. Distribution of sensing techniques (**left**) and sensors (**right**) used in the studies of the environmental category.

Regarding breathing parameters (Figure 8), RR was obtained in 60% of the wearable studies and in 79% of the environmental studies. It was the most widely used parameter by far. Other metrics based on the analysis of the magnitude versus time curve, such as breathing period or expiratory/inspiratory times, were barely used (2% in the wearable category) [94,103]. The representation of the volume

versus time curve or the use of volumetric parameters was not common. They appeared in 10% of the studies of the wearable category [2,17,49,61,67,111,113,116,122,127,147] and in 5% of the studies of the environmental group [48,51,52,215]. Among the possible volume metrics, tidal volume was the most common in the wearable category [2,17,49,61,111,113,116,122,127], while it was found in one study of the environmental category [52]. The rest of the metrics (MV, vital capacity, peak inspiratory flow, peak expiratory flow, and compartmental volume) were used in isolated cases. A considerable number of studies detected respiratory patterns in both wearable [17,143,152,159] and environmental categories [10,19,50–54,180,182,194,218]. The most common approach was to detect abnormal breathing patterns to identify respiratory disorders, such as apnea. This was especially common in environmental systems.

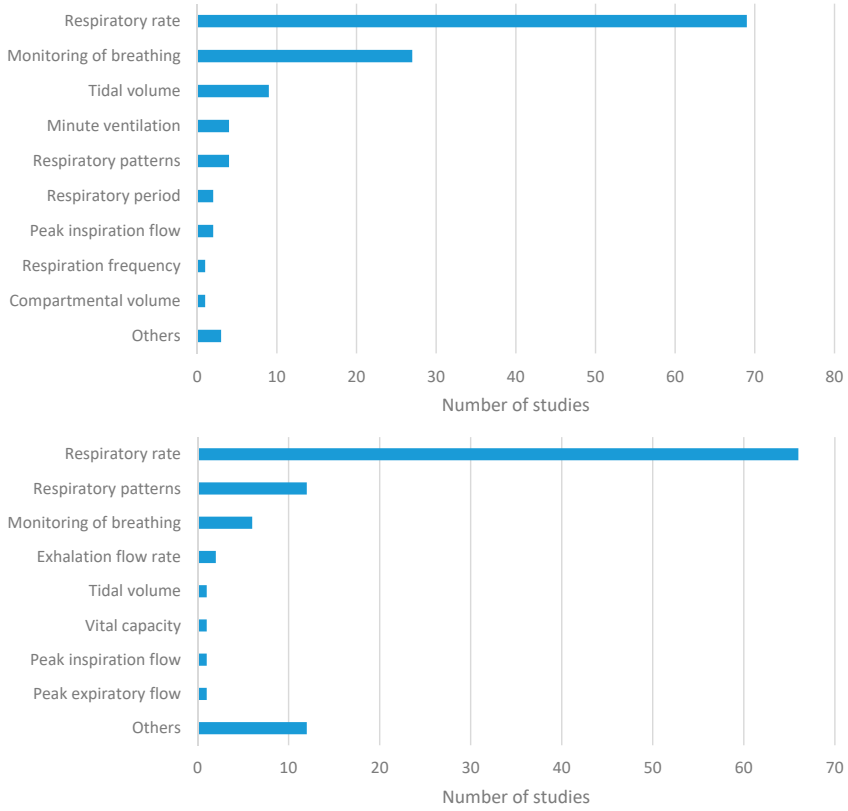

Figure 8. Number of studies obtaining the different respiratory parameters for the wearable (**top**) and environmental (**bottom**) categories.

Regarding sensor location, most wearable studies placed them on the chest or abdomen (Figure 9). This was the most common trend by far. It was also common that sensors were embedded in shirts at chest or abdomen level [21,49,59,65,69,84,85,94,108,113,123,142,143,151,235]. This was the location selected by 15% of the studies. Nose or mouth were also widely used locations to place the sensors. As a particular case of sensors placed in the nose or mouth, several researchers integrated them into a mask [66,75,80,82,92,101,107,137,156]. This contrasts with locations, like fingers, waist, arms, or wrists, in which use was residual [93,115,117,118,126,139,157].

Figure 10 shows the locations adopted in the environmental studies. On the one hand, the most common approach was to place the sensor at a fixed distance from the subject. Fifty-two% of the studies used this setup. On the other hand, Figure 10 shows that placing the sensors as nodes without precise control of the distance between the sensor and the subject was adopted by 6% of the studies. Meanwhile, 29% of the studies integrated the sensors into mats or pillows [9,19,164–166,169,170,173,179,182,183,186,194,201–203,210–212,217,218,220,227,230,231,236] to measure breathing parameters during rest activities mainly. The rest of the environmental locations shown in Table 2 were only used in isolated cases.

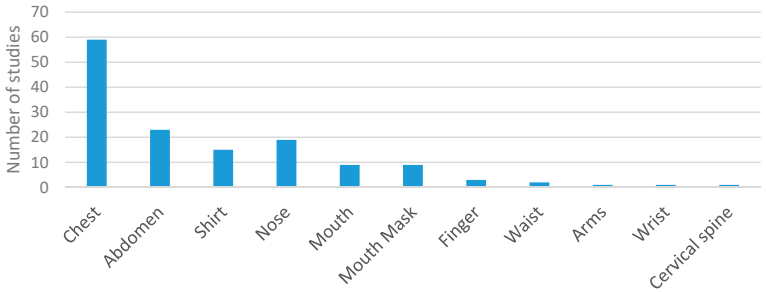

Figure 9. Distribution of sensor location for the wearable studies.

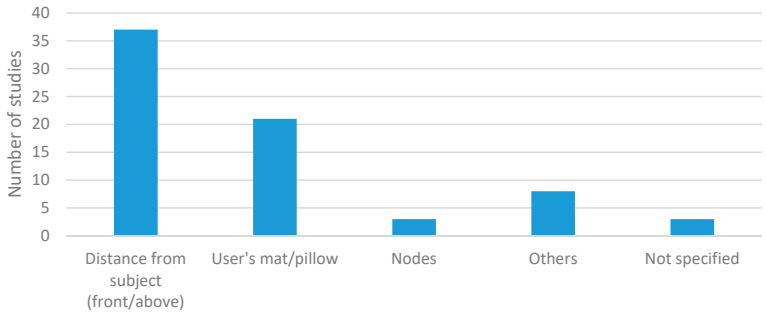

Figure 10. Distribution of sensor location for the environmental studies.

3.2. Data Transmission and Power Consumption

3.2.1. Items of Analysis

This category includes the following items of analysis: general system setup, communication protocol, processing station, and energy autonomy and power consumption.

General System Setup

Different configurations can be found in systems for respiratory monitoring depending on the data transmission architecture. Systems can be roughly divided into two categories (Figure 11): (A) those that perform data processing on a centralized processing platform and (B) those that perform data processing near the remote sensing unit.

- *Systems that perform centralized processing*: Data processing is done in a centralized system that does not need to be close to the subject being monitored. The magnitude values registered by the sensors are acquired and conditioned [24] and then transmitted to a centralized processing unit. Three different approaches can be found depending on the specific point where the acquisition & conditioning module and transmission module are placed:
    - The acquisition & conditioning and transmission modules are in the same package as the sensing unit (cases 1.x of Figure 11A, $\forall x \in [1..2]$).
    - The acquisition & conditioning module is in the same package as the sensing unit, but the transmission module is placed externally (cases 2.x of Figure 11A, $\forall x \in [1..2]$).
    - Both the acquisition & conditioning and transmission modules are not included in the same package as the sensing unit (cases 3.x of Figure 11A, $\forall x \in [1..2]$).

For all three approaches, data visualization can be done in two different ways: next to the processing unit of the registered signals (cases 1.1, 2.1, and 3.1 of Figure 11A) or at a different point (cases 2.1, 2.2, and 3.2 of Figure 11A).

- *Systems that perform remote processing*: Processing of breathing signals to determine the respiratory parameters of interest is performed near the subject whose breathing is being monitored. Three different setups are possible depending on whether the acquisition & conditioning module and the processing module are included in the same package as the sensing unit:
    - The acquisition & conditioning circuits, the microcontroller for the processing and the data transmission module are placed in the same package as the sensing unit (cases 4.x of Figure 11B, $\forall x \in [1..2]$).
    - The acquisition & conditioning circuits are placed in the same package as the sensing unit. However, the microcontroller in charge of the processing and the data transmission module are placed in an external package, which is not compactly integrated with the sensing module (cases 5.x of Figure 11B, $\forall x \in [1..2]$).
    - The acquisition & conditioning circuits, the microprocessor and the data transmission module are placed in a different package than the sensing unit (cases 6.x of Figure 11B, $\forall x \in [1..2]$).

Regarding data visualization, it can be done in two different ways: remotely without the need for data transmission (in this case, the data transmission module is not included) (cases 4.1, 5.1, and 6.1 of Figure 11B) or in a central unit (cases 4.2, 5.2, and 6.2 of Figure 11B).

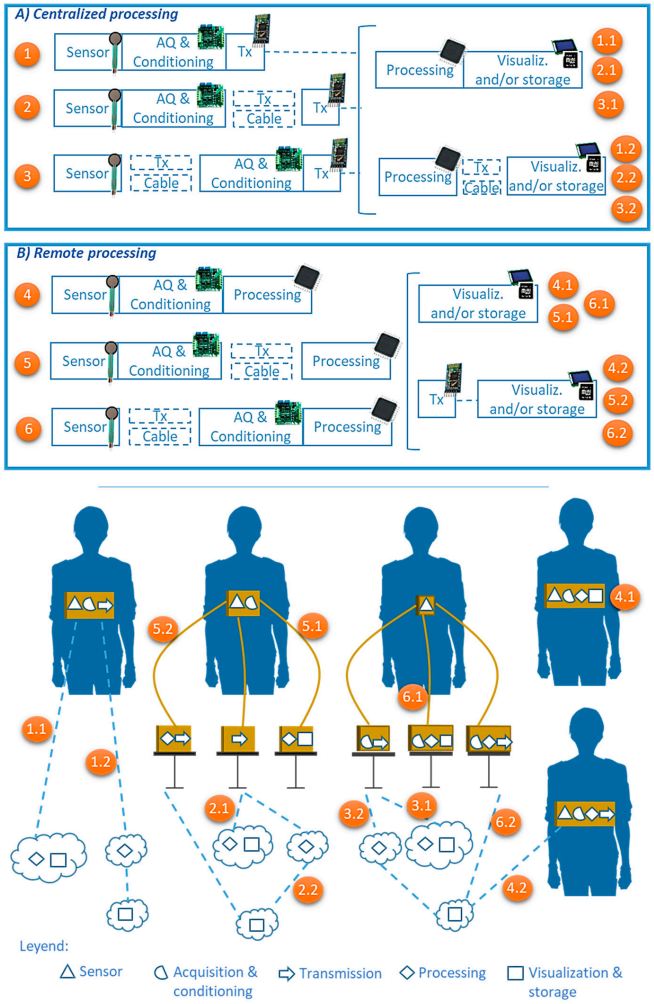

Figure 11. Representation of possible setups of respiratory sensing systems. (**A**) perform data processing on a centralized processing platform and (**B**) perform data processing near the remote sensing unit.

Communication Protocol

Communication between the different modules of the system can be classified according to whether it is wired or wireless:

- *Wired transmission*: All system elements (sensing, acquisition, conditioning, transmission, processing, and visualization) are physically connected. The USB (universal serial bus) protocol is the most common way of transmitting the acquired respiratory signals.
- *Wireless transmission*: Subjects wear the sensing system without cable connections to other elements of the system. The transmission and reception of measurements is carried out through a

wireless transmission technology. Therefore, the usability of the system increases [55]. Different transmission technologies can be found in existing studies [237]:

- *Bluetooth*: It is a standard and communication protocol for personal area networks. It is suitable for applications that require continuous data transmission with a medium data transmission rate (up to 1 Mbps). It uses a radio communication system, which means that the transmitting and receiving devices do not need to be in line of sight. It operates in the 2.4–2.485 GHz band with a low transmission distance (1 to 100 m, typically). There are five Bluetooth classes (1, 1.5, 2, 3, and 4). Most Bluetooth-based respiration monitoring systems use class 2 or higher. This means that the transmission distance is short (less than 10 m, in general), but the power consumption is also moderate [237].
- *Wi-Fi*: This technology is generally used for local area networks instead of personal area networks, like Bluetooth. It has much higher data transmission rates and power consumption is also higher. At a typical 2.4 GHz operating frequency, it can consume a maximum of 100 mW. Wi-Fi operating band is in the 2.4–5 GHz range. In general, the transmission range is between 50 m and 100 m, although it can be greatly extended in some conditions. This technology is suitable for applications where constant high-speed data transmission is required, the transmission distance is relatively large, and power consumption is not an issue [238].
- *GSM/GPRS*: Global System for Mobile Communications (GSM) is a standard for mobile communication that belongs to the second-generation (2G) of digital cellular networks. It requires base stations to which the mobile devices connect. The coverage range of base stations varies from a few meters to dozen of kilometers. Within this 2G technology, it is also possible to find the General Packet Radio Service (GPRS), which is data-oriented. The transmission rate of GPRS is low (around 120 kbps, although this rate is usually lower in real conditions) with a limitation of 2 W of power consumption. The frequency band of this technology is in the range of 850–1900 MHz [239].
- *Zigbee*: It is a specification of several high-level communication protocols. Zigbee is used for the creation of personal area networks that do not need high data transmission rates. ZigBee can operate in the industrial, medical and scientific radio bands, which may vary among countries. This is the reason why it generally works in the 2.4 GHz band that is available worldwide. If the system operates in the 2.4 GHz band, its data transmission rate is 250 kbps. Devices using this technology are generally inexpensive since the required microprocessor is simple due to the low transmission rate of Zigbee. Power consumption is low since nodes can be asleep until some information is received. It is useful for applications that do not require constant transmission. The range of transmission distance is similar to that of Bluetooth technology [237].
- *Radio frequency*: These modules are suitable for applications that do not need a high speed of data transmission. Radio frequency works in the Ultra High Frequency band (433 MHz) and requires a receiver-transmitter pair. It is low power and cheap, with a small module size. Communication range is from 20 to 200 m. This range depends on the input voltage of the module: at higher voltages, greater communication distance is reached. Working voltage for this technology ranges from 3.5 to 12 V. Radio broadcasting is performed through amplitude modulation. Radio frequency requires both receivers and transmitters to incorporate a microcontroller module. Typical power consumption is up to 10 mW.

Table 3 shows a schematic comparison of some key properties of the main wireless transmission technologies used in respiration studies.

Table 3. Comparison of the main transmission technologies used in respiratory monitoring systems [237].

	Operating Bandwidth	Transmission Speed	Power Consumption	Range (m)	Hardware Complexity
Bluetooth	2.4 GHz	1 Mbps	⟷	1–100	↑
Zigbee	2.4 GHz (valid worldwide)	250 kbps at 2.4 GHz band	↓	10–100	↓
Wi-Fi	2.4–5 GHz generally	Up to 1 Gbps	↑	50–100	↑
GSM/GPRS	850–1900 MHz	120 kbps	↑	100 m–several kilometers	↑
Radio frequency	433 MHz	4 kbps	⟷	20–200	↓

Processing Station

Another item of analysis is the platform on which the recorded signals are processed to obtain respiratory information. Several options exist in the state of the art (Figure 12):

- PC (personal computer): The respiration sensing system is connected or linked to a local PC that performs the processing of the registered breathing signals.
- Smartphone/Tablet: The sensing system communicates wirelessly with a smartphone application that runs the processing algorithm ubiquitously.
- Cloud: Breathing signals are sent wirelessly to a remote server, which performs cloud computing.
- Embedded hardware: Processing is performed directly on embedded systems, which are located in or near the sensing unit package.

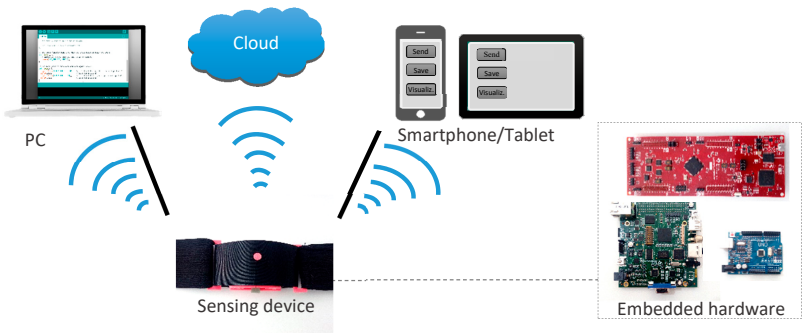

Figure 12. Representation of possible setups of respiratory sensing systems.

Energy Autonomy and Power Consumption

Regarding the power supply, systems can be categorized according to whether (1) they harvest part of the energy required for system operation, (2) they use rechargeable batteries, or (3) they are directly connected to a power source through a cable. This section analyses the first two categories in more detail since systems connected to a power source are of less interest as they have unlimited power availability.

(1) Energy Harvesters

Few were the studies found in the systematic searches conducted in this review that harvested energy [77,84,104]. However, some energy harvesting techniques have been reported experimentally in other wearable systems [240–249]. This section presents a description of these techniques and how they were implemented in the respiratory sensing systems. They were based on magnetic induction, piezo electric effect, triboelectric power generation, pyroelectric effect, thermoelectric effect, electrostatic power generation, and solar cells.

- *Magnetic induction generator*: A small electric generator can be used to transform mechanical energy into electrical energy according to Faraday's law. An electric current is induced in the generator coils by a changing magnetic field produced by the movement of the rotor due to the mechanical energy applied to it during breathing. The amount of generated voltage can be calculated according to Equation (1) [135].

$$V = -\frac{N \times K_1}{K_2} \times \frac{d\Delta C_{Chest}}{dt}, \quad (1)$$

where N is the number of turns of the coil, ΔC_{Chest} is the circumference change of the chest, K_2 is the proportionality constant between ΔC_{Chest} and the angular displacement, and K_1 is the proportionality constant between the magnetic flux and the rate of change of the angular displacement. The prototype presented by Padasdao et al. [135] attached the motor to a plastic housing with an armature fixed to the rotor gears (or shaft) (Figure 13A). A non-elastic wire was wrapped around the chest. One side of the wire was fixed to the plastic housing and the other end was attached to the armature. A piece of hard felt was fixed to the housing to help stabilize the device against the body. A spring was attached between the armature and the plastic housing to provide a restoring force to the armature. During inspiration, the non-elastic wire pulled the armature, leading to rotor rotation. During expiration, the spring pulled the armature back, leading to rotor rotation in the opposite direction. In this way, energy was harvested. In the work of Padasdao et al. [135], the electrical signal generated was used to obtain the RR instead of supplying power to the system. However, this is an example of how respiratory movements can be converted into electrical energy.

Other respiration-based energy harvesting systems can be found in the literature. The works of Delnavaz et al. [240] and Goreke et al. [241] used air flow to produce power with magnetic induction generators. On the one hand, the prototype of Delnavaz et al. [240] was made up of two fixed magnets located at the ends of a tube (opposite poles facing each other) with a free magnet inside the tube (Figure 13B). The free magnet was suspended due to the repulsive forces with the fixed magnets. A coil was wrapped around the outside of the tube. When a subject breathed into the tube, the free magnet moved around its static position. In this way, a voltage was induced in the coil since it was crossed by a variable magnetic field, which caused the magnetic induction. Experimental results showed that more than 3 µW were generated. The induced voltage in a closed circuit (U) was proportional to the magnetic flux gradient (dϕ/dx) and the velocity of the magnet (dx/dt), according to Equation (2).

$$U = -N\frac{d\varnothing}{dt}\frac{dx}{dt}. \quad (2)$$

On the other hand, a microelectromechanical-scale turbine was presented by Goreke et al. [241]. The turbine had 12 blades on its outer contour and ball bearings around the center embedded in grooves (Figure 13C). A permanent magnet was integrated in the area between the ball bearings and the turbine blades. The entire prototype was encapsulated in a package with rectangular openings for the airflow. The prototype presented was under development and not fully implemented. The operating principle of the system could be as follows: by flowing air for the rectangular openings, the blades rotate and move the turbine in such a way that its coils see a variable magnetic field generated by the

fixed magnet. This generates power through magnetic induction. The maximum power generated was 370 mW.

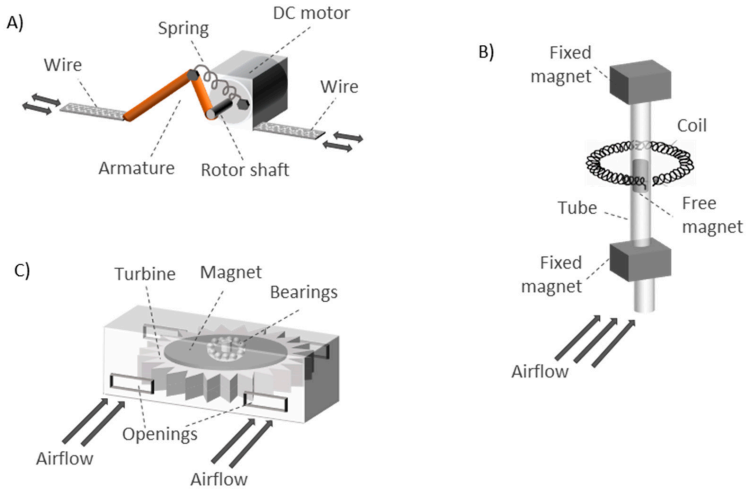

Figure 13. Schemes of energy harvesting using magnetic induction generation: (**A**) DC generator activated by chest movements (figure inspired by Reference [135]), (**B**) tube with fixed and free magnets moved by airflow (figure inspired by Reference [240]), and (**C**) turbine moved by airflow (figure inspired by Reference [241]).

- *Piezoelectric energy harvesting*: These harvesters generate a voltage when compressed or stretched [242]. In the work of Shahhaidar et al. [242], they were embedded in a belt alongside the chest. Due to low capacitance of the piezoresistive materials, the overall harvested energy was low. Therefore, this piezoresistive configuration was unable to provide the necessary energy to power the entire system. The main drawback to adopting this energy harvesting technique for respiration sensors is that the required vibration frequency is much higher than the respiration frequency. In this sense, the paper of Li et al. [243] presented a prototype based on the interaction between a piezoelectric cantilever and a magnet placed on a substrate (Figure 14B). The vertical vibration of the cantilever due to the magnet presence allowed generating a constant amount of energy. The substrate with the magnet was attached to subject body (a limb joint). The movements of the subject led to substrate stretching and contraction, which caused the vibration of the piezoelectric cantilever. The energy generated was stable for different types of movements, since it was tested on different parts of the body. The energy harvester worked correctly for subject movements in the frequency range of 0.5–5.0 Hz. It has potential to be used with breathing movements. Meanwhile, Wang et al. [244] presented a piezoelectric rubber band that could be mounted on an elastic waistband to generate electricity from the circumferential stretch caused by breathing. The paper showed a structure made up of top and bottom electrodes with two solid layers and one void layer in between (Figure 14A). They were made of composite polymeric and metallic microstructures with embedded bipolar charges. Finally, the work of Sun et al. [245] presented an energy harvester from respiration air flow based on the piezoelectric effect. They used piezoelectric polyvinylidene fluoride (PVDF) microbelts that oscillated under low-speed airflow to generate electrical power in the order of magnitude of μW (Figure 14C).

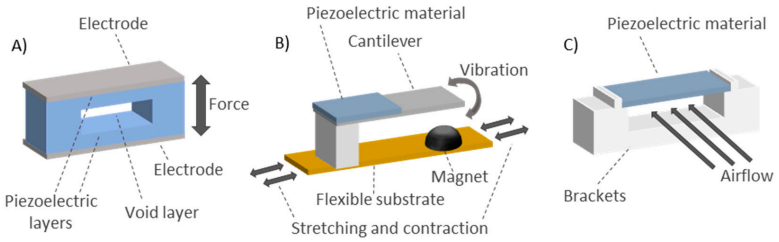

Figure 14. Piezoelectric energy harvesters. Three possible configurations are shown: (**A**) power generation based on compression or stretching movements associated with breathing (figure inspired by Reference [244]), (**B**) energy harvesting based on vibration amplified by a magnet (figure inspired by Reference [243]), and (**C**) technique using low speed airflow (figure inspired by Reference [245]).

- *Triboelectric energy harvesting*: They generate charges by rubbing two different materials (one is an electron donor and the other is an electron acceptor), resulting in the creation of a potential in the contact region [250]. One possible setup is to attach the tribo-pair to a belt to detect variations in abdominal circumference. Triboelectric generators were used in breathing studies as a means of measuring RR, but not as energy harvesters, since the power generated is low for the power requirements of the entire respiration monitoring system that includes also a data transmission module. In the work of Zhang et al. [246] two belts (one extensible and one inextensible) were attached to each side of two materials (Figure 15A). A mechanical experiment was performed to obtain the peak voltage for different sliding amplitudes in the range of 2.5 to 30 mm that represents the typical displacement of a breathing depth. The result of this experiment was Equation (3).

$$V_{peak} = 0.01383 X_{Max} + 0.0092, \quad (3)$$

where $Vpeak$ is the peak value of the voltage, and the X_{max} is the maximum sliding displacement of the tribo-pair. A similar approach was proposed by Zhang et al. [77]. They presented a tribo-pair with both sides of one material fixed to two "Z-shaped" connectors that were attached to a belt with an inextensible part and an extensible part (Figure 15B). The abdominal contraction and expansion associated with respiration caused deformation of the two "Z-shaped" connectors. This deformation led to a process of contact and separation of the tribo-pair, generating an electrical signal.

A self-powered respiratory sensor and energy harvester was also shown in the work of Vasandani et al. [247]. The working principle was very similar to the work of Zhang et al. [77] but, in this case, a prototype was built with movable and fixed supports (Figure 15C). The two materials were fixed to these two supports. The movements associated with respiration caused an angular displacement of the movable support by means of a belt and a lever mechanism, harvesting energy. The voltage obtained between the electrodes was zero in case of full contact and rose to 9.34 V for a 60° separation. The maximum area power density was 7.584 mW/m^2.

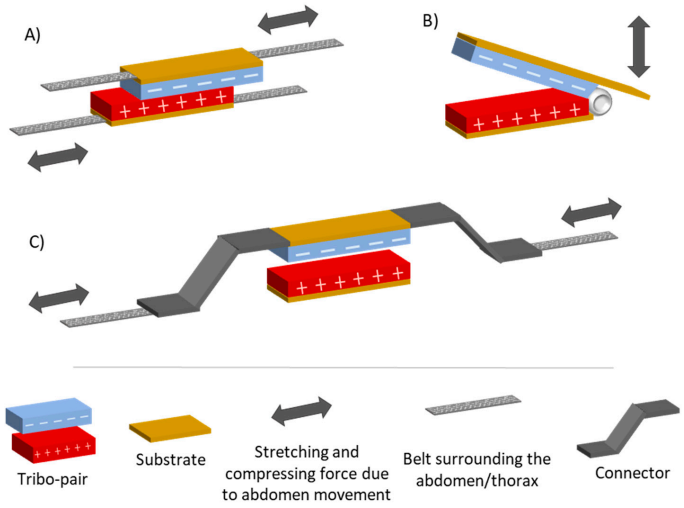

Figure 15. Setups for triboelectric energy harvesting. Three possible configurations are shown: (**A**) flat belt-attached setup (figure inspired by Reference [246]), (**B**) Z-shaped connector (figure inspired by Reference [77]), and (**C**) movable and fixed supports (figure inspired by Reference [247]).

- *Electrostatic energy harvesting*: It is based on the change of parameters of a capacitive device, which is called electrostatic energy harvester. Breathing may cause separation of the capacitor plates or modification of the plate area, among others [251]. This energy harvesting technique is not common in respiratory systems. The prototype of Seo et al. [248] showed a capacitor made of two metal electrodes and an insulating layer in between. The capacitance of the prototype varied with respiration. This was because the area of the top electrode was variable depending on the presence of a wet surface associated with respiration (Figure 16). Humid exhaled breath air was cooled by the ambient air on the top surface of the insulated material. Thus, the water molecules were condensed, acting as part of the upper electrode and changing the capacitance of the prototype. This condensation provided a thick layer that became part of the electrode. Then, the water naturally evaporated due to its vapor pressure and the device returned to its original status. The variable capacitance allowed the charges to circulate, harvesting electrostatic energy. The prototype presented in Reference [248] reported a generated power of 2 $\mu W/cm^2$.
- *Pyroelectric energy harvesting*: These harvesters are based on the reorientation of dipoles owing to temperature fluctuations [252]. Therefore, they need a temperature variation in time. Xue et al. [249] presented a prototype made of a pyroelectric component (metal coated PVDF film) covered with electrodes and mounted on the respirator of a mask at the location where air flows during breathing (Figure 17). The size of the prototype was 3.5 × 3.5 cm. The estimated current generated can be derived from the pyroelectric effect equation:

$$I = Ap\frac{dT}{dt} \tag{4}$$

where I is the generated current, A in the sensing area, p is the pyroelectric coefficient (approximately 27 $\mu C/m^2$ K), and dT/dt is the variation in temperature. Temperature variation is due to the difference between human body temperature and ambient temperature. It is also influenced by the transformation of water vapor into exhaled gas. The pyroelectric generator is heated by expiration and cooled by

inspiration. Therefore, electricity is harvested from a change in temperature over time. Peak power reached up to 8.31 μW with an external load of 50 MΩ.

- *Thermoelectric energy harvesting*: These harvesters are based on the Seebeck effect. They convert a temperature gradient into electric power. Therefore, they need a temperature variation in space [253]. A thermoelectric module is an array of p-type and n-type semiconductors. According to Nozariasbmarz et al. [252], the conversion efficiency of a thermoelectric generator can be calculated as:

$$\eta = \frac{T_H - T_C}{T_H} \frac{\sqrt{(1+ZT)} - 1}{\sqrt{(1+ZT)} + T_C/T_H}, \tag{5}$$

where T_C and T_H are the temperature of the cold and hot sides, respectively. ZT is the dimensionless figure of merit for the thermoelectric module. For the thermoelectric material, ZT can be calculated according to:

$$ZT = \frac{s^2\sigma}{k}T, \tag{6}$$

where s is the Seebeck coefficient, σ is the electrical conductivity, k is the thermal conductivity, and T is the absolute temperature.

Thermoelectric energy harvesters are not usually considered to power respiratory sensors. In the review of Nozariabsbmarz et al. [252], it was reported that several generators used the heat from the wrist for thermoelectric power generation.

- *Solar cells*: This technology has been also used to power respiratory sensing systems. The energy produced by the solar cells is stored in a battery through a charge regulator that also controls the discharge of the battery to power the sensing system. The charge regulator controls that both the battery and the sensing system are supplied with adequate voltage and current levels. Figure 18 shows an example of sensing system powered by solar cells. Solar-powered systems have not been extensively explored in existing studies. As an exception, the work of Gorgutsa et al. [84] presented a Received Signal Strength Indicator through standard Bluetooth protocol using a hybrid-spiral antenna made of multi-material fibers. The system was integrated into a cotton shirt. They used a low-power Bluetooth module that was powered by a rechargeable battery and a solar cell on a custom printed circuit board.

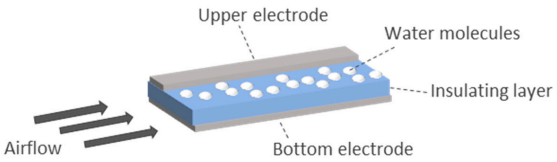

Figure 16. Electrostatic energy harvesting based on the variation of the area of the upper electrode owing to humidity of the exhaled air (figure inspired by Reference [248]).

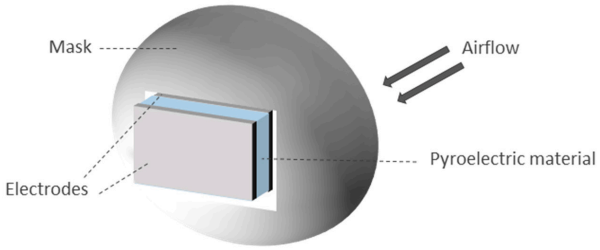

Figure 17. Schematic of a pyroelectric energy harvester using a mask-mounted breathing prototype (figure inspired by Reference [253]).

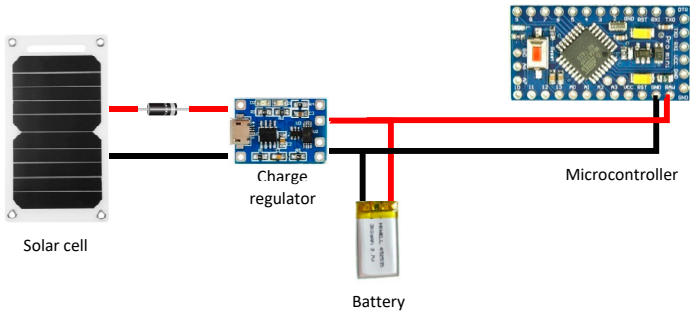

Figure 18. Example of a solar-powered system composed of a solar module, a charge regulator and a microcontroller. The voltage regulator receives an input voltage from the solar cell in the range of 0.3 V to 6 V. The charge regulator manages the charge of the battery (at constant voltage and current). The battery is connected in parallel to the internal voltage regulator of the microcontroller of the system.

(2) Battery-Powered Systems

Battery-powered systems require, at least, a battery and a charger. These two elements should be considered in the sizing of the system. Batteries are usually one of the most limiting components in terms of space (Figure 19).

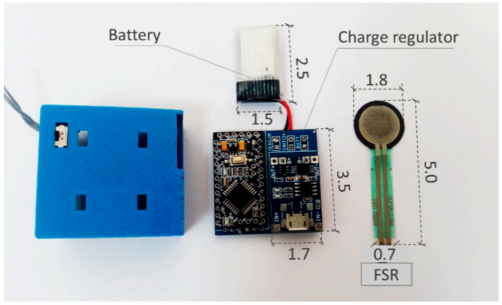

Figure 19. Charge regulator and battery (low capacity, 150 mAh) integrated into the sensing prototype developed by Vanegas et al. [254], slightly modified. The sensor used in that prototype (a force-sensitive resistor) is included separately for size comparison. Units: cm.

Power autonomy determines the viability of a system. The autonomy of a battery-powered respiration sensing system is obtained by calculating or measuring its battery life, which is defined as the time that a system can operate with a fully charged battery. Two different factors must be determined when performing tests to measure battery life: system operating mode and the way of measuring battery life.

Regarding system operating mode, there are essentially two different approaches:

- *Continuous operation*: Battery life is measured with the breathing device operating continuously.
- *Continuous operation + inactivity periods*: A typical daily use of the system is considered, which may include certain inactivity periods in which the device is in "idle" mode or even off (not used).

Regarding the way of measuring battery life, it should be noticed that it depends on the type of battery used and its parameters. The main parameter of a battery is its capacity, which determines the nominal amount of charge that can be stored. It is usually expressed in mAh. As a general rule, the higher the capacity, the longer the battery life. However, capacity depends on several external factors, such as discharge rate, operating temperature, aging, and state of charge (SOC). When a battery is discharged at low rate (low current), the energy is delivered more efficiently. Higher discharge rates (higher currents demanded by the breathing system) lead to a reduction in effective battery capacity [255]. Temperature also affects battery capacity in such a way that low temperatures decrease capacity. Aging may also decrease the capacity [256]. If a battery is not full, the state of charge (SOC) must also be considered. It represents the percentage of capacity that is currently available with respect to the rated capacity.

The most common and sensible approach is that tests are conducted with a new fully-charged battery that operates in the nominal temperature range and discharges within the nominal current range. Under these conditions, the nominal capacity of the battery can be considered its true capacity. Otherwise, different reduction factors (<1) should be applied to rated capacity. Therefore, different ways to measure battery life experimentally can be found in existing studies:

- *Measure of battery life directly*: A battery can be considered discharged when the voltage drops below a certain value (3.6 V [257] for common small batteries). Therefore, by taking a full battery and monitoring the output voltage, it is possible to obtain battery life with expression (7).

$$BatteryLife\ (h) = InitialTime - DischargeTime. \tag{7}$$

- *Measure of current consumption*: Current consumption of the respiratory sensing system can be measured experimentally or estimated from the datasheets of the system components. The formula for calculating battery life is different for each operation mode:
  - *Continuous operation*: The system is assumed to operate continuously consuming an average current value.

$$Batery\ Life\ (h) = \frac{Capacity(mAh) \cdot SOC_{factor} \cdot C_{factor} \cdot Ta_{factor} \cdot Age_{factor}}{OC\ (mA)}, \tag{8}$$

    where SOC_{factor}, C_{factor}, Ta_{factor}, $Age_{factor} \in \mathbb{R}[0,1]$ are reduction factors of the capacity to be applied in case tests are not performed under the optimal conditions mentioned above, and OC is the average value of the operating current.
  - *Continuous operation + inactivity periods (rough estimate)*: Current consumption in the operation and inactivity periods is assumed to be "constant".

$$Batery\ Life\ (h) = \frac{Capacity(mAh) \cdot SOC_{factor} \cdot C_{factor} \cdot Ta_{factor} \cdot Age_{factor}}{OC\ (mAh) \cdot \frac{nmin_{OC}}{nmin_{total}} + IC\ (mAh)\ \frac{nmin_{IC}}{nmin_{total}}}, \tag{9}$$

where *IC(mAh)* is the average value of current consumed by the system in idle or non-active modes, $nmin_{oc}$ is the number of minutes that the breathing system is in operation mode during a certain period of time (for instance, one day), $nmin_{Ic}$ is the number of minutes that the breathing system is in idle or non-active modes for the same time period, and $nmin_{total} = nmin_{OC} + nmin_{IC}$.

- *Continuous operation + inactivity periods (fine estimate)*: The calculation of battery life is performed using a more accurate model. Different values of current consumption are considered in operation and inactivity modes. In this calculation, the system can adopt not only two states, but n states. Let $c = [c_1, c_2, \ldots, c_n]$ be the average current values of each of the n different states of the respiratory system considered, and $nmin = [nmin_1, nmin_2, \ldots, nmin_n]$ the number of minutes in a given period of time (for instance, one day) that the breathing system remains in each state of the n possible states. The calculation can be done with Equation (10).

$$Batery\ Life\ (h) = \frac{Capacity(mAh) \cdot SOC_{factor} \cdot C_{factor} \cdot Ta_{factor} \cdot Age_{factor}}{\sum_{i=1}^{n} c_i \cdot \frac{nmin_i}{\sum_{j=1}^{n} nmin_j}}. \quad (10)$$

3.2.2. Results of the Analysis

The previously described items were analyzed for the studies found as a result of the systematic review. These items were the use of wired or wireless data transmission, the performance of centralized or remote processing, the specific station used to carry out processing and the energy autonomy of the prototypes. They were studied for the wearable category as these elements are limiting in non-contact sensing systems. However, they are less crucial in environmental systems, since most of them use wired communications and are connected to a power source.

Table 4 shows a comparison of the approaches found in the state of the art for the wearable group. The first two columns of Table 4 show the specific studies that used wired and wireless data transmission, and Figure 20 presents the percentage distribution of the type of transmission. The use of wired and wireless technologies was similar.

Table 4. Analysis of transmission technology, processing station, and energy autonomy for studies in the wearable category.

Study [1]	Wireless Transmission	Wired Transmission	Processing Station	Battery Capacity	Battery Life (Type Battery)
Aitkulov 2019 [57,58]	-	Data storage	-	-	-
Balasubramaniyam 2019 [59]	Internet connection	-	Cloud storage, PC, Smartphone	-	-
Bricout 2019 [60]	-	-	-	-	-
Chu 2019 [61]	Bluetooth	-	PC	-	-
Elfaramawy 2019 [62]	Radio-frequency	-	PC	3.7 V, 100 mAh	6 h (Li-ion battery)
Fajkus 2019 [63]	-	Interrogator DAQ (data acquisition)	PC	-	-
Hurtado 2019 [64]	-	-	-	-	-
Jayarathna 2019 [65]	Bluetooth (low energy), SD card	-	PC, smartphone, cloud Storage	600 mAh	5 days (Li-ion battery)
Kano 2019 [66]	Bluetooth	-	Smartphone	3 V	(Cell battery)

Table 4. *Cont.*

Study [1]	Wireless Transmission	Wired Transmission	Processing Station	Battery Capacity	Battery Life (Type Battery)
Karacocuk 2019 [67]	Bluetooth	-	PC, smartphone	-	-
Massaroni 2019 [68]	Bluetooth	-	PC	3.6 V, 650 mAh	8 h (Li-polymer battery)
Massaroni 2019 [69]	Bluetooth	-	-	-	-
Nguyen 2019 [70]	-	-	-	-	-
Presti 2019 [71]	-	Interrogator	PC	-	-
Presti 2019 [72]	-	Interrogator	PC	-	-
Puranik 2019 [73]	Wi-Fi	-	-	3.7 V, 1020 mAh	(Li-ion battery)
Soomro 2019 [74]	-	USB	PC, smartphone	-	-
Xiao 2019 [75]	-	-	PC	-	-
Yuasa 2019 [76]	-	USB	Smartphone	-	-
Zhang 2019 [77]	-	-	Smartphone, PC	-	-
Dan 2018 [78]	-	-	-	-	-
Koyama 2018 [79]	-	Interrogator DAQ	PC	-	-
Malik 2018 [80]	-	DAQ	-	-	-
Martin 2018 [81]	-	-	PC	-	-
Pang 2018 [82]	-	-	-	-	-

[1] Note: The analysis for studies published before 2018 [2,3,17,21,49,83–162] is included in Appendix A (Table A3).

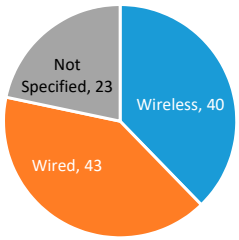

Figure 20. Number of studies adopting wired or wireless data transmission in respiration sensing systems.

Figure 21 shows the distribution of wireless technologies used for data transmission. Bluetooth was the preferred technology, as it is suitable for applications that send point-to-point information over relatively short distances and require high-speed data transmission. Its main drawback is power consumption, which could be a limitation for continuous monitoring, as existing studies state that the battery life is not more than a few hours. However, in view of Table 4, this method seems suitable for many applications. Wi-Fi, radio frequency, or Zigbee were used in a limited number of studies [73,96,144,156,159]. Regarding wired transmission, third column of Table 4 shows that USB communication was the preferred option [74,76,86–88,109,114,118,133,141,158].

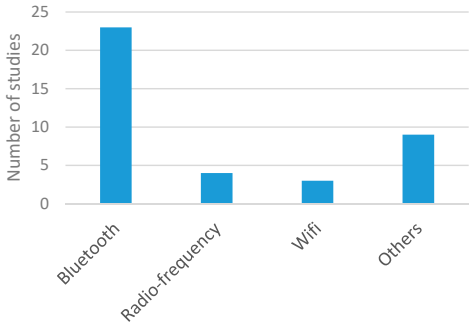

Figure 21. Number of respiratory monitoring studies that considered different types of communication technologies.

Once measurements are transmitted, a main station processes them. Figure 22 shows the percentage distribution of the processing stations used in the studies selected in the systematic searches. PCs were the preferred processing stations, showing that most authors performed centralized processing, while the use of smartphones, tablets or cloud computing was not so common [2,59,65–67,74,76,77,84,91,98,99,101,102,107,109,116,119,122,130,132,134,143,144,156], although they were found in 30% of studies.

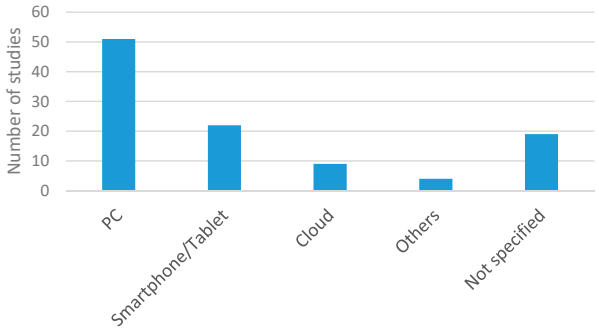

Figure 22. Number of studies adopting the different processing units.

Regarding energy autonomy of systems, the use of energy harvesters was residual [84,104], which can be due to the fact that studies presented complete systems that included data transmission and processing modules. These modules are energy demanding, and therefore the use of energy harvesters can only be used as a complement, but not as the primary power source. In this regard, many studies [2,3,17,62,65,73,84,86,87,89,91,98,99,101,114–116,119,131,144,145,147,162] used rechargeable batteries to power the systems. The most common declared battery lives were in the order of hours (Figure 23) [2,17,62,69,101,115,119], although some studies did not even provide data on this point.

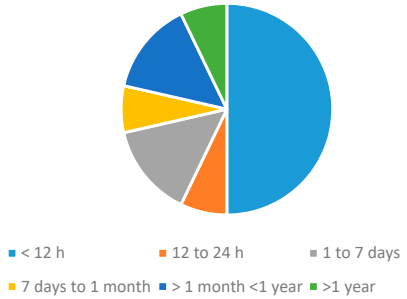

Figure 23. Distribution of battery lives reported in the respiratory monitoring studies.

There were a set of studies focused on minimizing power consumption. They included low power data transmission technologies. In this regard, Milici et al. used wireless transponders [91] to obtain autonomy of more than one year, while Mahbub et al. [98] adopted Impulse Radio Ultra-Wideband (IR UWB), which led to an autonomy of about 40 days. In general, battery live is highly dependent on transmission technology. The works of Bhattacharya et al. [156], Puranik et al. [73], White et al. [96], Ciobotariu et al. [144], and Mitchell et al. [159] used wearable devices with Wi-Fi [73,96,144,156], Zigbee [159], or GSM/GPRS [144], with high variability in power consumption.

3.3. Validation Experiments

3.3.1. Items of Analysis

Different items were considered to analyze the validation experiments carried out in the studies:

- Subjects: Almost all studies used volunteers to assess the respiration sensing systems. In this case, it is required to provide data, such as the number of subjects who participated in the tests and their main characteristics (age, weight, height, sex, and health status). As breathing studies generally involve humans, it is mandatory to have the approval of the competent ethical committee (following the Declaration of Helsinki [258]) to recruit the subjects to participate in the study, to inform them about the study, and to obtain their consent.
- Activities/positions: This item refers to the specific activities or positions that volunteers who participate in the tests are asked to perform as part of the validation experiments. The most common positions adopted in existing studies are represented in Figure 24 with an example sensor.
- Whether or not motion artifacts are included in the different activities.
- Number and values of RRs or volume rates to be tested in the experiments.
- Number of repetitions of the different test scenarios.
- Duration: The designed tests (activities and positions, number of RRs or volume rates, and number of repetitions) determine the duration of the experiments.
- Experiment design: This item refers to the strategies adopted to validate the breathing sensors. Three main methods have been found in the state of the art (Figure 25):

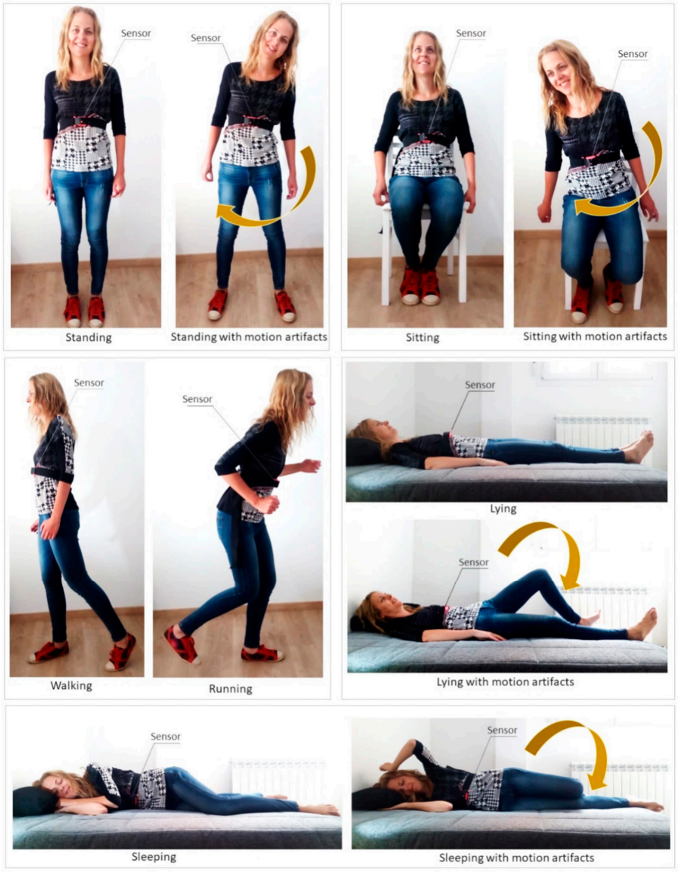

Figure 24. Common positions/activities to validate the breathing sensors (sitting, standing, lying down, walking, running, and sleeping). Chest sensor used as an example.

Artificial validation prototypes: Some studies used artificial prototypes that emulated human conditions rather than real volunteers. On the one hand, if the sensor were worn on the chest, diaphragm, or thorax, a mechanical structure that emulated human respiration could serve for validation. That was the approach adopted by Padasdao et al. [135]: a motor moved a mechanical chest to the rhythm and depth of human breathing (Figure 25A). Similarly, the work of Witt et al. [141] also used a mechanical chest driven by a stepper motor, setting the amplitude and frequency of the movements to simulate breathing activity. Another set of works [77,94,110,114,146] used machines or custom prototypes that applied traction and compression movements to simulate human respiration on strain sensors. On the other hand, if the system is to be worn in the nose or mouth, an artificial prototype can be built that emulates the airflow associated with respiration. For that, Agcayazi et al. [123] used a mannequin equipped with an inflatable cuff bladder that emulated breathing cycles, which is similar to the prototype of Koch et al. [90]. For humidity sensors, authors designed controlled humidity chambers using humidifiers and dry air compressors [74] or switches for controlling nitrogen flow and a motor to control the dispersion of water vapor [97]. Finally, other studies presented artificial

validation prototypes adapted to the specific sensors used for respiration monitoring. Zito et al. [226] validated a radar sensor with a moving target that emulated the movements associated with breathing.

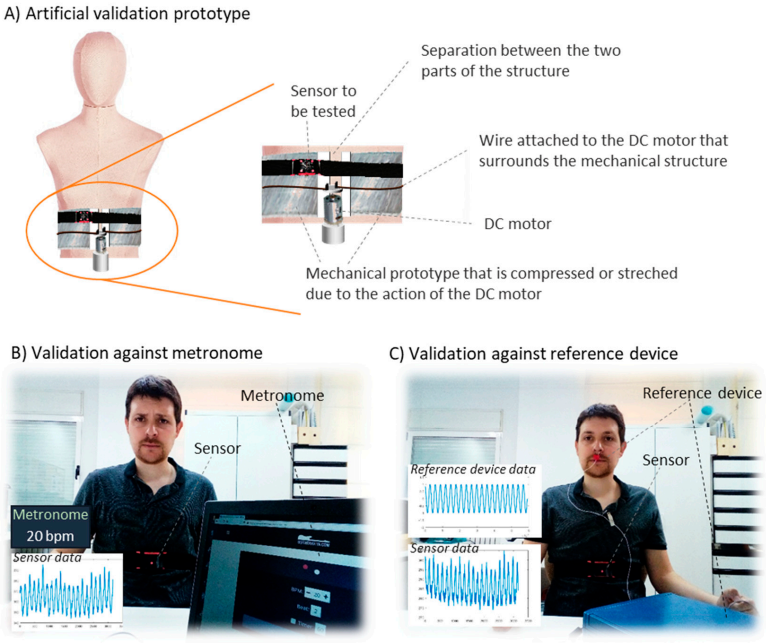

Figure 25. Representation of different validation approaches: (**A**) use of artificial validation prototypes, (**B**) validation using a metronome, and (**C**) validation using a reference device.

Validation using artificial prototypes has the advantage that different respiration or volume rates can be programmed precisely. These theoretical values can be compared with the measurements obtained with the sensor. Thus, no error can be attributed to the validation method. A typical validation workflow using this method is outlined in Figure 26. In this method, sensor measurements may be contained in matrix $\mathbf{A} = \left(a_{ij}\right)\epsilon\mathbb{R}^{k\times m}$, where k is the number of repetitions per parameter, and m is the number of different parameter values to evaluate. This measurement matrix **A** can be compared with the reference matrix $\mathbf{B} = \left(b_{ij}\right)\epsilon\mathbb{R}^{k\times m}$. Matrix **B** contains the reference values used to program the artificial validation prototype. Therefore, all the elements in a given row have the same value as the jth reference parameter (column) remains the same for all repetitions ($\forall i\epsilon[1..k]$, row).

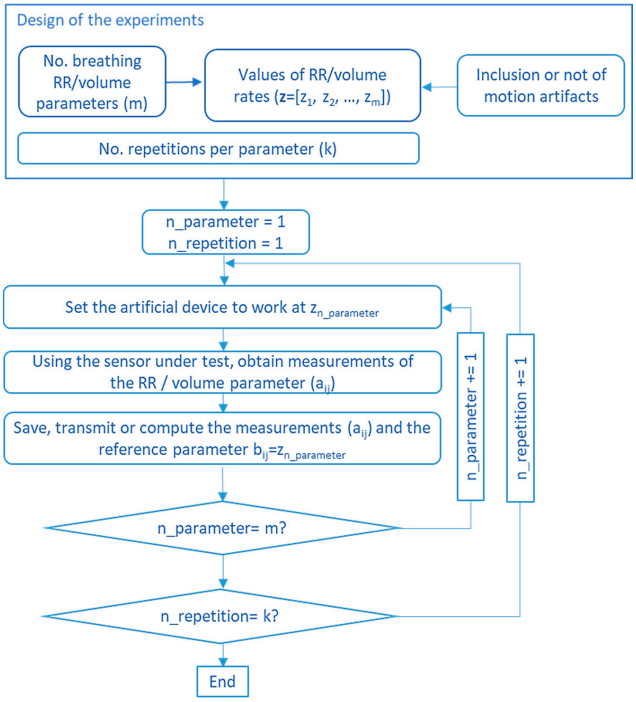

Figure 26. Flow diagram of a typical validation procedure using artificial prototypes.

Metronome as reference: When humans are involved in the validation experiments, one option is to use a metronome to set the rate of respiration that subjects must follow during the tests (Figure 25B). The advantage of this method over artificial prototypes is that the sensing system is tested with the target subjects and not with an emulation of a human chest or throat. However, its weak point is that subjects may not accurately follow the rate of the metronome. Therefore, part of the measurement error can be attributed to the test design itself rather than to the sensing system. A typical validation workflow using a metronome as a reference is summarized in Figure 27. The measurements recorded by the sensor under validation may be contained in matrix $\mathbf{A} = \left(a_{defgh}\right) \epsilon \mathbb{R}^{n \times k \times p \times l \times m}$, which is a five-dimensional matrix with the measured values for each subject d, repetition e, activity f, position g and parameter value h. The reference to compare $\mathbf{A}$ is matrix $\mathbf{B} = \left(b_{defgh}\right) \epsilon \mathbb{R}^{n \times k \times p \times l \times m}$, which contains the reference breathing parameters set in the metronome for each subject d, repetition e, activity f, position g and parameter value h. Therefore, $\mathbf{B}$ exclusively contains the values of vector $z = [z_1, z_2, \ldots z_m]$, which are the possible settings for the metronome (Figure 27).

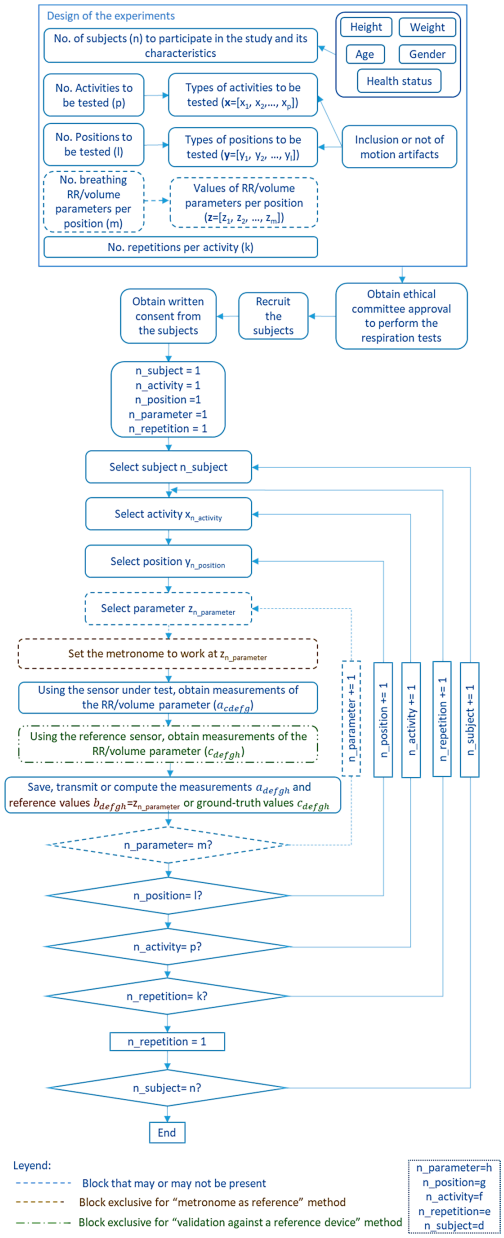

Figure 27. Flow chart for the validation of a respiration sensor using the methods "metronome as reference" and "validation against a reference device".

Validation against a reference device: The most complete way to validate a new sensor is to compare its performance with the performance of a reference sensor considered as a gold standard (Figure 25C). The reference sensor and the sensor under validation must be worn at the same time to obtain synchronized measurements. Having synchronized measurements allows the sensing capabilities of both sensors to be compared fairly. The sensor under test should provide measurements as close as possible to those of the reference sensor. It is important to note that the reference sensor also has a measurement error. Therefore, this error should be considered in the comparison, as it may influence the results. Respiratory values provided by the reference device may differ slightly from real values. This validation method faces several challenges. First, it is essential to synchronize both measuring instrument and this synchronization can be difficult. Second, most commercial products do not provide information on how the final breathing parameter (RR or volume parameter) is obtained, so the comparison of measurements may not be obvious. In addition, most products do not allow selecting the refresh time window or do not even provide information about the length of this window, so it is not possible to know the set of measurements used to calculate the output respiration values. Figure 27 shows a typical block diagram of the validation method when using a reference device. The results of this validation are matrices $\mathbf{A} = \left(a_{defgh}\right)\epsilon\mathbb{R}^{n\times k\times p\times l\times m}$ and $\mathbf{C} = \left(a_{defgh}\right)\epsilon\mathbb{R}^{n\times k\times p\times l\times m}$, which contain the measured values for each subject d, repetition e, activity f, position g, and parameter h for the sensor under evaluation and for the reference sensor, respectively.

3.3.2. Results of the Analysis

Table 5 presents the results of the analysis of different items of the validation experiments for both wearable and environmental systems. Large differences among studies were observed in all aspects of the experiments: protocol, number of subjects, positions, types of breathing, duration, and inclusion of motion artifacts.

In relation to the number of subjects involved in the tests, 71% of the studies that provided this data included 10 subjects or less. Only 13% of the studies included more than 20 subjects [7,10,19,64,81,132,135,147,173,175,211,232]. There were also a considerable number of studies (53) that did not even provide this information. A part of them did not use subjects for sensor validation.

Regarding the duration of the experiments, most of the studies carried out short experiments of a few minutes. In fact, 58% of the studies performed tests of less than 5 minutes [69,70,81,86–88,96,100,102,104,111,125,136,161,163,165,171–174,193,195,196,200,212,215,221,228,229,232]. Most of the works that conducted longer tests included sleep studies [7,17,53,60,115,146,148,164,165,169,173,192,198,205,211,220,223]. Twenty-six studies reported that motion artifacts were considered during testing. They showed that the inclusion of motion artifacts in experiments greatly influenced sensor performance [2,9,17,53,61,62,66–68,81,108,109,117,119,131,132,135,147,157,178,187,190,196,205,210,221,225]. In relation to the activities or positions considered in the experiments, lying down and sitting were the most tested positions. Other positions or activities, like standing, walking, moving, or running, were used in a minority of studies [2,17,21,61,62,66–68,77,79,81,91,94,101–103,108,110,111,115,118,119,124,129,131,132,135,146–149,177,178,188,205,214,233,235]. Most of the studies that provided information on activities considered more than one position [2,6,9,17,21,52,53,61,62,66–68,77,79,85–88,94,102,108,110,115,118,119,124,129,131–133,135,146–148,157,164,165,169,171,177,178,187,196,198,205,210,211,213,214,220,221,223,225,233,235]. It was also common to test different values of the respiration parameter (for example, RRs from 10 to 22.5 bpm in the study of Vanegas et al. [254]).

In relation to the validation protocol, Figure 28 shows the distribution of the analyzed studies in the three categories introduced in Section 3.3.2: validation with an artificial prototype, metronome as reference and validation against a reference device. A new category was created to cover studies that performed informal validation. It was called "human observation", since an expert provided a value of the breathing parameter from direct observation of the signals recorded by the sensors. Figure 28 shows that validation using a reference device was the predominant approach (adopted by 67% of the studies that performed validation), followed by the use of an artificial validation prototype

(10%) [69,74,77,90,93,97,110,114,116,119,123,135,141,146,150,226]. It is also worth noting that 53 studies presented the sensing systems without providing evidence of their validation.

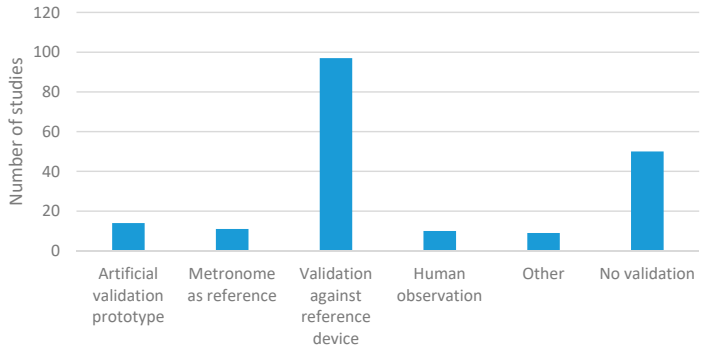

Figure 28. Number of studies that adopted the different validation approaches.

Table 5. Analysis of validation experiments for the studies in the wearable and environmental categories.

Validation Parameters	Number of Subjects						Duration		Activities Considered					
	1	2 to 5	6 to 10	11 to 20	>20	Not specified	<5 min	>5 min	Sitting	Standing	Lying down	Sleeping	Walking, running, moving	Motion artifacts
Number of studies	34	40	30	22	19	63	47	34	59	25	66	16	28	27

3.4. Sensor Measurement Processing

3.4.1. Items of Analysis

This category includes the following items: performance evaluation, software used for the analysis, and processing algorithm. This section describes them in detail.

Performance Evaluation

The evaluation of sensor performance can be done using several figures of merit, such as absolute error, relative/percentage error, root mean square error, correlation factor, Bland-Altman plot, calculation of accuracies, or linear regression.

Absolute error (Δ): Difference between the value measured by the sensor under test (x) and the reference value (y). It is calculated according to Equation (11).

$$\Delta = x - y. \tag{11}$$

It is more common to provide the mean absolute error (MAE) as the mean of the absolute value of all absolute errors:

$$\text{MAE} = \frac{1}{n}\sum_{i=1}^{n}\left|x_i - y_i\right|, \tag{12}$$

where n is the number of measurements obtained from the sensor under test, x_i the values of those measurements, and y_i the reference values associated with those measurements for the "artificial validation prototype" method and the "metronome as reference" method or the measurements of the reference device for the "validation against a reference device" method.

Relative error (RE): Absolute error of the breathing sensor under test (Δ) divided by its reference (true) value (y). Thus, it provides an error value relative to the size of the breathing parameter being measured. It can be obtained according to Equation (13). The mean of the relative errors (MRE) can be obtained using Equation (14).

$$\mathrm{RE} = \frac{\Delta}{y}, \tag{13}$$

$$\mathrm{MRE} = \frac{1}{n}\sum_{i=1}^{n}\frac{\left|x_i - y_i\right|}{yi}, \tag{14}$$

where n, x_i, and y_i are the same parameters as for the MAE.

If the relative error is expressed as a percentage, it is called the percentage error, although many authors also provide the relative error in percentage.

Root mean square error (RMSE): In respiration sensing studies, it is also used to compare the difference between the values measured by the sensor under analysis and the reference results. It is the root mean of these differences and can be obtained according to Equation (15).

$$\mathrm{RMSE} = \sqrt{\frac{\sum_{i=1}^{n}\left(x_i - y_i\right)^2}{n}}, \tag{15}$$

where n, x_i, and y_i are the same parameters as for the MAE.

Correlation factor: It provides a measure of the relationships between the measurements taken by the respiration sensor under test and the reference data. There are different ways to calculate this correlation factor. Pearson correlation factor is one of most extended (Equation (16)).

$$\gamma_{xy} = \frac{n\sum x_i y_i - \sum x_i \sum y_i}{\sqrt{n\sum x_i^2 - \left(\sum x_i\right)^2}\sqrt{n\sum y_i^2 - \left(\sum y_i\right)^2}}, \tag{16}$$

where n, x_i, and y_i are the same parameters as for the MAE. A correlation factor of 1 means maximum agreement between measured and reference data (optimal case), while a factor of 0 means that there is no relationship between the datasets.

Bland-Altman analysis: It is a graphical method to compare the measurements from the breathing sensor under test with the reference breathing values. A scatter diagram is drawn with the horizontal axis representing the mean between measured values and reference values ($\frac{(x_i + y_i)}{2}$) and the vertical axis representing the difference between those values ($x_i - y_i$). In addition, a horizontal line is included in the plot with the mean value of all differences. Two more horizontal lines (one upper and one lower) are plotted representing the limits of agreement (±1.96 times the standard deviation of the differences). The Bland-Altman plot is useful to show relationships between the magnitude of the breathing parameter and the differences between measured values. It may also help to identify systematic errors in measurements or to detect outliers, among others. This method is especially suitable for the validation method in which the sensor under evaluation is compared to a reference device.

Accuracy: It is the proportion of true results with respect to the total number of samples [259]. It can be used in studies of respiration sensors that identify breathing patterns within a given set of k possible patterns. It can also be applied to studies that determine the value of a breathing parameter within a discrete set of k possible values. Let $x = [x_1, x_2, \ldots, x_n]$ be the values of the n measurements taken by a respiration sensing system or the n labels of the breathing patterns recognized by the system. Suppose that, from the n different samples, m samples are correctly identified or measured, since they

belong to the correct class of the k possible classes. Therefore, *(n-m)* samples are not classified correctly. The accuracy of the breathing system can be obtained as:

$$Accuracy\ (\%) = \frac{m}{n} \cdot 100. \tag{17}$$

Linear regression: It models the relationship between the values measured by the respiration sensing system under test (dependent variable) and the reference measurements (independent variable) by fitting a linear equation. The equation to fit has the form of $y = a + bx$, where y is the dependent variable, x is the independent variable, b is the slope of the line, and a is the intercept (value of y_i when $x_i = 0$). This linear fitting is performed using $x = [x_1, x_2, \ldots, x_n]$, which is the set of n reference values of the breathing parameter, and $y = [y_1, y_2, \ldots, y_n]$, which is the set of n values of the parameter measured by the sensing system under evaluation. In these conditions, the values of each x_i and y_i should be as close as possible $\forall i \in [1..n]$. This means that, if the match between the reference values and the measured values was perfect, the linear model should be a line with and intercept of 0 and a slope of 1.

In addition, the coefficient of determination r^2 could also be calculated to obtain what percentage of the variation in the values measured by the sensing system are predictable from the variation of the reference values according to Equation (18).

$$r^2 = 1 - \frac{SE_{res}}{SE_{\overline{y}}}, \tag{18}$$

where $SE_{\overline{y}} = \sum_{i=1}^{n} (y_i - \overline{y})^2$ is the sum of the squares of the difference of each measured value y_i with respect to the mean value of all measurements $\overline{y}$, and $SE_{res} = \sum_{i=1}^{n} (y_i - (a + bx_i))$ is the sum of the squares of the difference of each measured value y_i with respect to the value predicted by the model. If SE_{res} is small, it means that the line is a good fit, and r^2 will be close to 1. Otherwise, if SE_{res} is large, it means that the difference between the measured values y_i and the line is large, and r^2 will be close to 0 (bad linear fit). If the breathing system measured exactly the same values as the reference system, SE_{res} would be zero and r^2 would be 1, which would be the ideal case.

Analysis Software

The most common tools used to analyze the measurements recorded by the sensors are:

- MATLAB: Popular numerical computing environment and programming language that is suitable for the implementation of algorithms, matrix operations, or data plotting, among others.
- Labview: System engineering software for applications that require testing, measurements, control, fast hardware access, and data information.
- Others: An extensive set of tools has been used in existing studies, such as Python (high-level, programming language specially focused on facilitating code readability), R (free software environment and programming language for statistical computing [260]), C# (general-purpose programming language developed by Microsoft [261]), C (general-purpose programming language that supports structured programming), OpenCV (open source software library for computer vision and machine learning [262]), Blynk (Internet of Things platform), Kubios HRV (heart rate variability analysis software for professionals and scientists), Audacity (free open-source audio software), Kinect SDK (suitable for developing gesture or voice recognition applications, using Kinect sensor technology [263]), LabChart (physiological data analysis and acquisition software [264]), Acqknowledge (software to measure, transform, replay and analyze data [265]), mobile/Android (mobile operating system), LabWindows/CVI (software development environment specially focused on measurement applications [266]), microcontroller/microprocessor (suitable if the processing is not done in any external software, but directly in the same microprocessor or

microcontroller that controls the sensor), or custom applications (PC applications in which the native source could not be accurately determined).

Processing Algorithm

A broad set of algorithms has been used to process measurements from respiration sensors such as peak detection, maximum-minimum detection, detection of zero-crossings, threshold detection, frequency analysis, wavelet transform, or Kalman filter, among others. They are briefly described in this subsection.

Peak detection: It is based on the detection of peaks in the signals registered by the sensing system (Figure 29). If no restriction is imposed regarding peak prominence, a peak can be calculated on a signal $x = [x_1, x_2, \ldots, x_n]$ according to Equation (19), where n is the number of samples in the signal. However, this method is extremely sensitive to noise and fluctuations (Figure 29A). To improve detection, it is possible to set a minimum surrounding number of samples (p) in which the values must be below the peak value (Equation (20)) to accept the detected peak (Figure 29B). Another option is to impose a strictly increasing slope on the p samples preceding the peak and/or a strictly descending slope on the p samples after the peak (Figure 29C), according to Equation (21).

$$x_{i-1} < x_i > x_{i+1} \quad \forall i \in \mathbb{Z} : i \in [1, n], \tag{19}$$

$$x_j < x_i > x_h \quad \forall j \in \mathbb{Z} : j \in [i-p, i-1] \;\; ; \;\; \forall h \in \mathbb{Z} : h \in [i+1, i+p], \tag{20}$$

$$x_{j-1} < x_j \quad \forall j \in \mathbb{Z} : j \in [i-p, i] \;\; and \;\; x_{h+1} < x_h \;\; \forall h \in \mathbb{Z} : h \in [i, i+p]. \tag{21}$$

The peak detection method to process respiration signals has several important parameters that determine the number of detected peaks. Peaks selected according to Equations (19), (20), or (21) can be classified according to the prominence of the peak, discarding those peaks that are below a threshold value to avoid the effect of noise and fluctuations. Peak prominence can be defined as the vertical distance between the closest local minima (in horizontal direction) and the peak, although there are other possible definitions [267]. Let $y = [y_1, y_2, \ldots, y_n]$ be a vector containing the magnitude of all local minima of signal x, and $b = [b_1, b_2, \ldots, b_n]$ the position (horizontal value) of the local minima y. If a_i is the position of peak i, and b_k is an element of b that satisfies that $b_k = \min|b - a_i|$ (the position of the local minima closest to i), then, a peak i will only be accepted if its prominence is above a set threshold (PP), $\left|x_i - y_k\right| < PP$ (Figure 29D).

Another parameter that may be used to determine the number of peaks is the distance among them. Breathing signals are low frequency (usually less than 25 bpm [254]); therefore, a threshold (TD) is generally established to discard those peaks that do not differ by, at least, TD from another previously detected peak (Figure 29E). Let $c = \left[c_1, c_2, \ldots, c_q\right]$ be the position of the q peaks detected in a signal. A new peak candidate i, with position on the horizontal axis d_i, will only be accepted if $\left|d_i - c_j\right| < TD$, $\forall j \in \mathbb{Z} : j \in [1, q]$.

It is also common to discard peaks that do not reach a certain level TL ($x_i < TL$) (Figure 29F) or, alternatively, that a new peak i is discarded if its value does not differ a given threshold TV from the q peaks already detected; that is, if $\left|x_i - x_j\right| < TD$, $\forall j \in \mathbb{Z} : j \in [1, q]$ (Figure 29G).

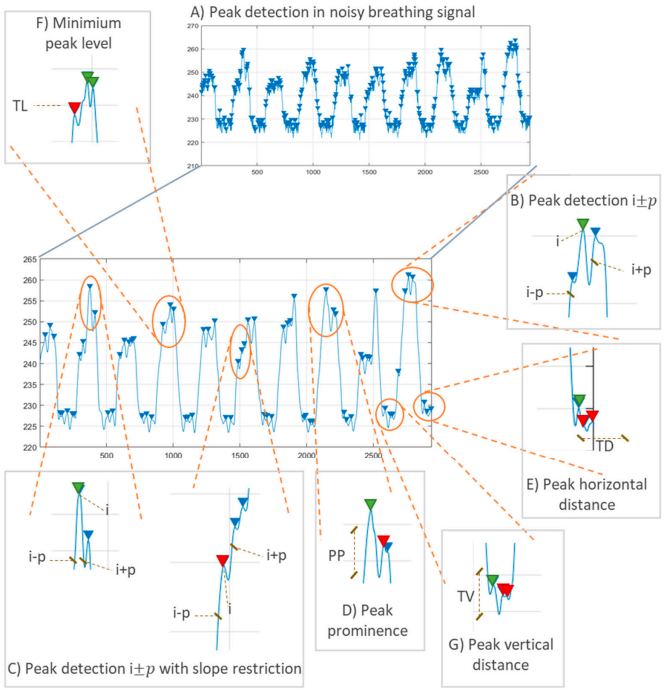

Figure 29. Peak detection of a sample respiration signal obtained from the public breathing dataset published in Reference [254]. (**A**) Peak detection of a noisy signal without filtering. (**B**) Peak detection imposing a restriction of p surrounding number of samples (in green the peak accepted). (**C**) Example of a peak accepted (left, green peak) and a peak discarded (right, red peak) when applying the slope restriction. (**D**) Example of a peak reaching (green) and not reaching (red) the minimum prominence level PP to be considered a valid peak. (**E**) Example of two peaks (red) not fulfilling the minimum horizontal distance restriction TD. (**F**) Example of a peak (red) not fulfilling the vertical minimum level restriction and two peaks that surpass level TL (green peaks). (**G**) Example of two peaks discarded (red) for not differing the imposed tidal volume (TV) level from a detected peak (green).

Maximum-minimum detection: A popular processing technique is to identify maximum and/or minimum points in the breathing signals (x). Massaroni et al. [103] used the maximum and minimum values to obtain the respiratory period (T_r), as well as inspiratory (T_i) and expiratory (T_e) time. The process for detecting maximum and minimum points is similar to peak detection.

Zero-crossings: Technique based on the detection of the crossings of a breathing signal by a "zero" level taken as a reference. Given a respiration signal composed of n values $x = [x_1, x_2, \ldots, x_n]$, a new zero crossing at the i value is detected when inequality (22) is satisfied.

$$x_{i-1} < x_i < x_{i+1} \quad i \in [1..n]. \tag{22}$$

One of the challenges of this method is to find the "zero" level taken as a reference to detect the crossing. One possible option is to detect the maximum and minimum values in a specific window and obtain the "zero" level as the mean of those values $(\max(x) + \min(x))/2$. However, this method is sensitive to outliers (Figure 30A). A possible solution is to take the median of x as the "zero" level

(Figure 30A). Another option is to remove 10–20% of the largest and smallest values of x, obtaining a subset of values $y \subseteq x$. Then, the "zero" level can be calculated as the mean of the maximum and minimum values of y.

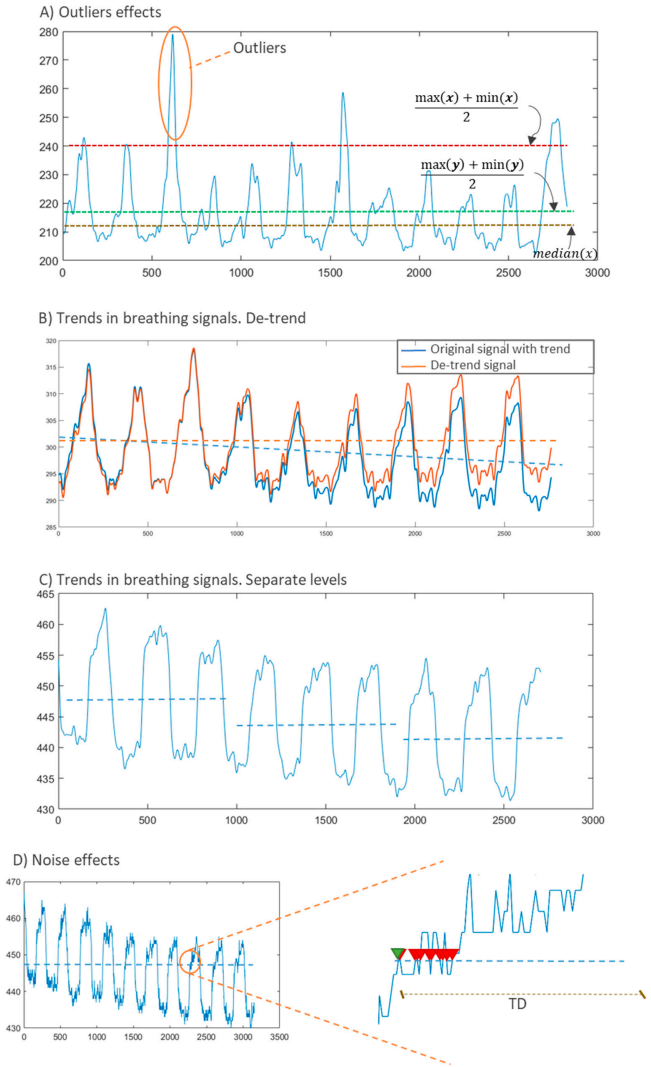

Figure 30. Zero-crossings method exemplified in a real signal obtain from the public breathing dataset of Vanegas et al. [254]. (**A**) Effect of the presence of outliers in the signals in the calculation of the "zero level". (**B**) Example of a signal with trends and results of applying a de-trend processing. (**C**) Example of using different "zero levels" in a signal with trends. (**D**) Example of a noisy signal with several zero-crossings detected when only one of them (green) should have been considered.

The "zero-crossings" technique is also affected by trends or biases in the measurements. Trends may be due to movement of the sensing element or movement of the subject. It is a common phenomenon, especially in belt-attached breathing sensors. Figure 30B shows a real breathing signal with trends (blue curve) from a public dataset [254]. If the "zero" level is calculated on a signal with trends, many crossings may go undetected since the same "zero" level is not a valid reference for the entire signal. To solve this problem, it is possible to eliminate trends in the signal by subtracting the bias (Figure 30B, orange signal). Another option could be to split the signal into shorter windows and calculate a different "zero" level for each window (Figure 30C).

This technique is also sensitive to noise since the number of zero-crossings may increase in noisy signals. Figure 30D shows how noise is confused with multiple crossings at the "zero" level in a breathing signal. This can be avoided by defining a minimum distance in the horizontal direction (TD). Let $z = \left[z_1, z_2, \ldots, z_q\right]$ be the positions in the horizontal axis of q detected "zero-crossings"; then, a new "zero-crossing" i with position d_i will only be considered if $\left|d_i - z_j\right| < TD$, $\forall j \in \mathbb{Z} : j \in [1, q]$.

Threshold detection: This technique is similar to "peak detection", "maximum-minimum detection" or "zero-crossing detection". In this case, the level to detect is not a characteristic point of the curve but a certain threshold value. The same analysis performed for the previous categories could be applied to this method.

Frequency analysis: This category includes different techniques that make use of frequency information to obtain respiration parameters. The most common approach is to use the well-known Fourier Transform (FT). Several studies detected peaks in the spectrum of respiration signals or in their power spectral density (PSD) to obtain the breathing parameters. This method depends on the time window (Figure 31A). To provide meaningful data, long time windows are desirable. However, this limits refresh time of the system. A compromise between accuracy and refresh time is required. Figure 31A shows a breathing signal and its spectra obtained with the FT for different refresh time windows. The example respiration signal has a frequency of 0.33 Hz (20 bpm) and a sampling frequency of 50 Hz. For a 4-s time window, the maximum available resolution is F_s/N, that is, 0.25 Hz. Figure 31A shows that the detected frequency is in the range of 0.25–0.5 Hz. This resolution is 0.125 Hz for the 8-s time window (frequency detected in the 0.25–0.375 Hz range) and 0.0625 Hz for the 16-s time window (frequency detected in the 0.3125–0.344 Hz range). It can be seen that the wider the time window, the more accurate results are obtained using this method. However, wide time windows make it difficult to apply respiration monitoring systems to critical scenarios where instantaneous values must be provided.

This transform is also sensitive to noise fluctuations. Noise fluctuations are generally of a much higher frequency than breathing signals. Therefore, it is common to pre-filter the signals to remove frequencies that exceed those of breathing activities. Figure 31B shows the frequency spectrum of a real respiration signal without filtering and with digital low-pass filtering. It can be seen that the peak of the respiration frequency (0.33 Hz) is more separated from the rest of the spectrum values in the filtered signal (7 units for the filtered signal and 5 for the unfiltered signal). If noise levels increased, it would even be difficult to distinguish the peak associated with the respiration frequency.

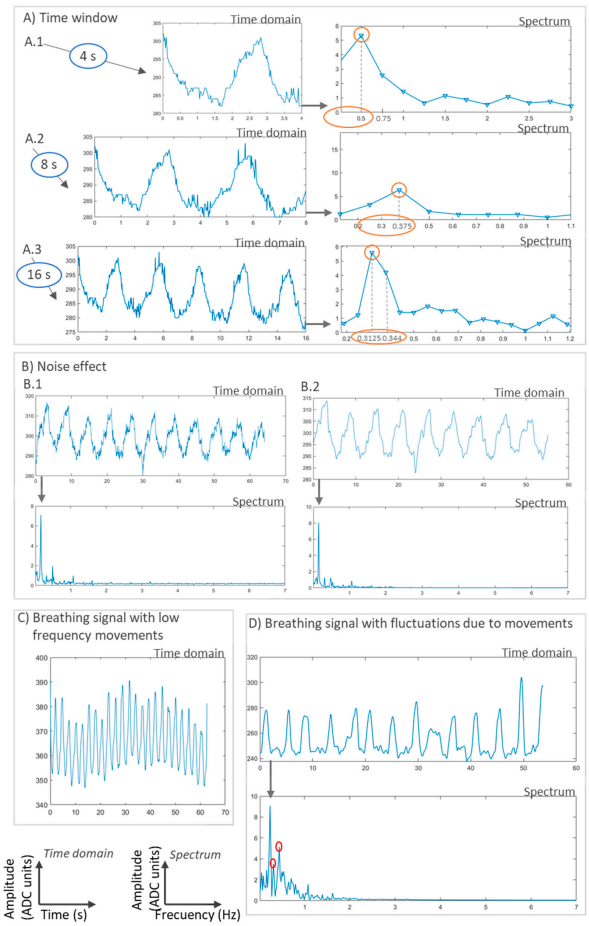

Figure 31. Frequency analysis of sample real respiratory signals obtained from a public dataset [254]. (**A**) Effect of the time window (4 s, 8 s, and 16 s) on the frequency calculation. The true frequency is 0.33 Hz (3 s period) and the sampling frequency is 50 Hz. Results for the 16-s time window (Table A3, 0.3125–0.344 Hz) are closer to the true value. (**B**) Effect of noise on frequency detection (noisy signal and its spectrum -B.1-, filtered signal and its spectrum -B.2-). (**C**) Example of a breathing signal with low frequency fluctuations. (**D**) Example of a breathing signal with fluctuations due to movements of the subject and its spectrum.

On the other hand, low frequency signal fluctuations may appear due to movements in the sensing device or movements of subjects if breathing is measured during dynamic activities, such as walking. These fluctuations must be treated to provide accurate results. They can be mathematically modeled according to Equation (23).

$$v(t) = A\left[1 + \lambda \sin\left(w_f t\right)\right] \sin(wt - \varphi), \tag{23}$$

where w is the angular frequency of the normal breathing signal, w_f represents the angular frequency of the interference-causing activity, and λ is the magnitude of that activity. Figure 31C shows an example

of a real breathing signal with low frequency fluctuations. Those frequency fluctuations can lead to peaks at very low frequency values of the spectrum. As low-pass filters are generally applied, those frequencies would not be removed and could therefore be confused with the respiration parameter, which is also low frequency.

Sudden movements of subjects may also cause fluctuations in signals, which can affect the measurements. Figure 31D shows an example of a real respiration signal with fluctuations due to movements during acquisition tests. The bottom of Figure 31D shows its spectrum with a peak in the respiration frequency and other lower peaks (in red) at close frequencies due to signal fluctuations.

Other studies have also obtained breathing parameters from frequency using frequency modulation (FM) or amplitude modulation (AM).

Wavelet transform: It is used to decompose the breathing signal in such a way that a new representation can be obtained that allows a better detection of respiration peaks or crossings. It has been used in the continuous or in the discrete form [268]. In the continuous wavelet transform (CWT) a comparison is made between the respiration signal and an analyzing wavelet ψ. The wavelet is shifted by applying a dilation factor (b) and is compressed or stretched by applying a scale factor (a). Therefore, the CWT can be calculated according to Equation (24).

$$CWT(a,b) = \int_{-\infty}^{\infty} x(t)\psi^*_{ab}(t)dt, \tag{24}$$

where $x(t)$ is the breathing signal under analysis, and $*$ denotes the complex conjugate [269]. The scale factor (a) has an inverse relationship with the frequency (the higher the value of a, the lower the frequency, and vice versa). The dilation factor (b) allows delaying (or advancing) the wavelet onset. Therefore, it contains time information. In this way, the CWT can provide a kind of time-frequency representation where high frequency resolution is obtained for low frequencies and high time resolution is obtained for high frequencies. This is shown in Figure 32A where a real respiration signal is processed with the CWT. The time-frequency representation of the processed signal is shown in Figure 32A (right). It can be seen that a low frequency value around 0.33 Hz is identified with high resolution in frequency but low resolution in time. In the example respiration signal, the frequency remains fairly constant around the value of 0.33 Hz.

A variant of the WT is the multiresolution analysis (MRA) [269]. The MRA represents the voltage signal at different resolution levels by progressively analyzing the breathing signals into finer octave bands (Figure 32B). For that, the original signal is convolved with high and low pass filters that represent the prototype wavelet. The outputs of the low pass filter are called "approximation coefficients", while the outputs of the high pass filter are called "detail coefficients". Approximation coefficients are down-sampled by a factor of 2 and are again subjected to high-pass and low-pass filtering, obtaining a new set of "detail" and "approximation" coefficients. This process is repeated iteratively, resulting in different resolution levels. For a given decomposition level n, the detail coefficients contain information on a particular set of frequencies (from $f_s/2^n$ to $f_s/2^{n+1}$), with f_s being the sampling frequency. Regarding the "approximation coefficients" of the same decomposition level, they contain low-frequency information in the range $f_s/2^{n+1} - 0$ Hz. The number of decomposition levels of the MRA depends on the specific breathing signal, so the band of the respiration frequencies can be correctly identified. It is affected by the sampling frequency of the system. This decomposition process is explained graphically in Figure 32B. The original respiration signal (x) can be reconstructed from its detail and approximation coefficients as follows:

$$x = \sum_{j=1}^{l} D_j + A_l, \tag{25}$$

where l is the number of decomposition levels. Figure 32B also shows an example of this technique applied to a breathing signal with a sampling frequency of 50 Hz. Six decomposition levels were

selected to obtain five sets of detail coefficients in the ranges 25–12.5 Hz, 12.5–6.25 Hz, 6.25–3.125 Hz, 3.125–1.563 Hz, 1.563–0.781 Hz and one set of approximation coefficients in the range 0.781–0 Hz. The first and third levels of detail coefficients and the sixth level of approximation coefficients were represented in Figure 32B as an example. In this case, the level of interest was the sixth (approximation coefficients) since breathing signals are of low frequency. The Fourier Transform was performed on the coefficients of the sixth level, obtaining a clear peak at the frequency of 0.33 Hz, which matches the breathing frequency of the sample respiration signal (20 bpm).

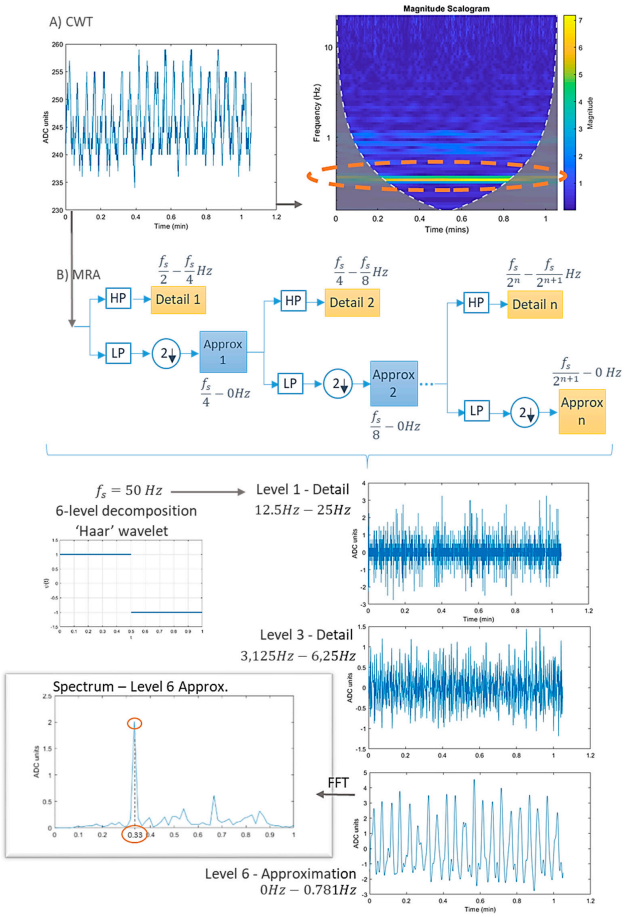

Figure 32. Wavelet transform. (**A**) 2D representation of the continuous wavelet transform (CWT) (**right**) of an example signal (**left**) taken from a dataset of real respiration signals [254] (RR of 20 bpm −0.33 Hz-, and sampling frequency of 50 Hz). (**B**) Multiresolution analysis (MRA) decomposition process (**top**). The lower part shows an example of the MRA analysis applied to the signal above ((**A**), **left**). Six-level decomposition was applied using the 'Haar' wavelet. Two detail levels and the sixth approximation level are represented. The spectrum of the approximation coefficients (level 6) was obtained.

In the work of Scalise et al. [232], the signal was decomposed into 12 levels and level 11 was considered to obtain the RR. Guo et al. [166] performed a 4-level decomposition, selecting level 3 to calculate the RR. Therefore, the wavelet transform is used to obtain the respiration signals in the desired frequency band.

Kalman filter: This technique has been used by several studies as a sensor fusion method. Thus, it is not a method to extract breathing parameters but to fuse measurements from different sensors. When multiple respiration sensors are available, the measurements they provide are not exactly the same. Furthermore, measurements always contain noise. The Kalman filter is used to provide a final value based on the measurements of the different sensors, the model of variation of the breathing parameter, the noise model of the sensors, and the variation model [270]. Figure 33 shows an overview of the Kalman filter algorithm adapted to the fusion of breathing sensors.

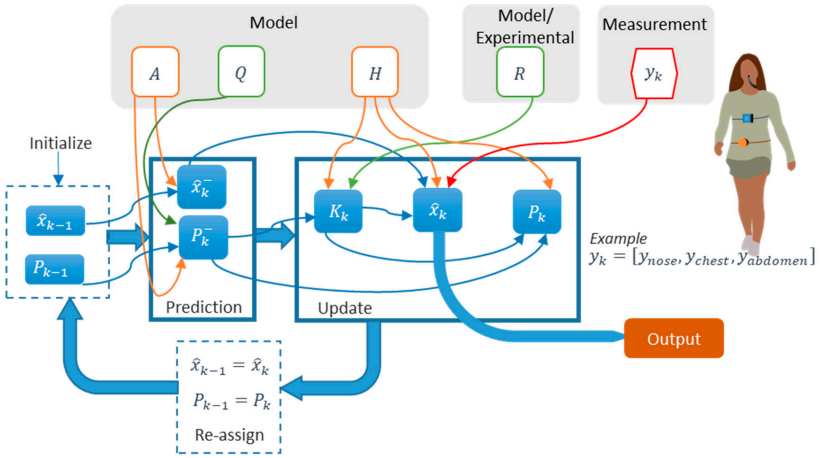

Figure 33. Kalman filter algorithm for the fusion of different respiration sensors.

The Kalman filter has two distinct phases: prediction and update. The prediction phase estimates the state (breathing parameter) in the current time step using the state estimate from the previous time step (previous breathing parameter). The breathing parameter predicted in this phase is called the "a priori" state estimate $\hat{x}_k^-$ and is obtained according to Equation (26).

$$\hat{x}_k^- = A\hat{x}_{k-1}, \tag{26}$$

where $\hat{x}_{k-1}$ is the state estimate in the previous state, in this case the previous breathing parameter estimated, and A is the state transition model. Matrix A represents the expected evolution of $\hat{x}_{k-1}$ for the next transition. As breathing does not vary much in the short term [102], a common approach is to define A as an identity matrix, so the "a priori" state estimate $\hat{x}_k^-$ is equal to the previous state $\hat{x}_{k-1}$. If respiration is not expected to be constant in the short term, A should contain the linear variation model. The "a priori" estimate covariance P_k^- (Equation (27)), which is a measure of the accuracy of the "a priori" state estimate $\hat{x}_k^-$, must also be predicted. It depends on the transition model A, the value of the covariance in the previous transition P_{k-1}, and Q. Q is the covariance of the process noise (the noise of $\hat{x}_k^-$ prediction model). In order to apply the Kalman filter, the process noise must follow a Gaussian distribution with zero mean and covariance $\mathrm{Q_k}(\sim N(0, Q))$. Although A and Q can vary at each time step k, it is common for them to take a constant value. Many methods exist to determine Q. In the

breathing system presented by Yoon et al. [131] Q was a diagonal matrix (which is a common approach) of the order of 10^{-4}.

$$P_k^- = AP_{k-1}A^T + Q. \tag{27}$$

Once the "a priori" state estimate $\hat{x}_k^-$ has been predicted, the update phase comes into play. In the update phase, the "a priori" state estimate $\hat{x}_k^-$ is refined using the measurements y_k recorded by the sensors. The result is the final value of the breathing parameter $\hat{x}_k$, which is called the "a posteriori" state estimate (Equation (28)).

$$\hat{x}_k = \hat{x}_k^- + K_k\left(y_k - H\hat{x}_k^-\right). \tag{28}$$

The estimation of $\hat{x}_k$ depends on the predicted "a priori" state estimate $\hat{x}_k^-$, the measurements registered by the different breathing sensors y_k and the matrices K_k and H. K_k is known in the Kalman filter as the optimal Kalman gain. It minimizes the "a posterior" error covariance. A common way to calculate it is according to Equation (29).

$$K_k = \frac{P_k^- H^T}{HP_k^- H^T + R}. \tag{29}$$

This gain depends on the "a priori" estimate covariance P_k^- and two model parameters (H and R). H is the observation model that relates the measurements taken by the sensors y_k to the state space x_k (breathing parameter), as follows $y_k = H\hat{x}_k$. It is common that previous techniques introduced in this section (peak detection, maximum-minimum detection, zero-crossings, threshold detection, frequency analysis, or wavelet transform) are used to directly estimate the respiration parameter from the measurements. In that case, the measurement space and the state space are the same. Thus, H could simply be the identity matrix. If the respiration parameter (RR, for example) were not provided directly as a result of the measurements, and other parameters were given instead (such as the number of peaks, zero-crossings, etc.), matrix H would contain the equations to calculate the breathing parameter from those values. Those equations were previously introduced in this section.

R is the covariance of the observation noise (the noise associated with the measurements y_k). The observation noise should also follow a Gaussian distribution with zero mean and covariance R (~N(0,R)). Although H and R can vary at each time step k, it is common that they adopt a constant value.

In the update phase, the covariance is also updated to obtain the "a posteriori" estimate covariance P_k according to Equation (30).

$$P_k = P_k^- - K_k H P_k^-. \tag{30}$$

As a result of the update phase, the final breathing parameter $\hat{x}_k$ is estimated, which is the output of this algorithm. However, the Kalman filter is an iterative method that recalculates $\hat{x}_k$ at each time step. Therefore, the "a posteriori" state estimate $\hat{x}_k$ at the current time step will be the previous state estimate $\hat{x}_{k-1}$ at the next time step. The same happens with the covariance since the "a posteriori" estimate covariance P_k at the current time step will be the previous estimate covariance P_{k-1} at the next time step. In this way, the algorithm can start a new prediction process again (Figure 33). The whole process is repeated indefinitely. The output of the system at each transition is the "a posteriori" estimate of the respiration parameters $\hat{x}_k$.

3.4.2. Results of the Analysis

Table 6 presents the results of the analysis for the wearable studies and Table 7 shows the results of the environmental studies. The second column of each table includes the specific data processing techniques used in each study. Figure 34 represents the number of works that use the different processing methods for wearable and environmental studies. The category "custom algorithm" was added to refer to processing algorithms that cannot be classified in any other group, as they are specific to the sensor used for respiration monitoring. It can be seen that "peak detection" in respiration signals and "frequency analysis" using the Fourier Transform were some of the most widely used

methods by both wearable and environmental studies. The sum of the percentages of use of techniques based on the detection of levels in their different forms (peaks, maximum and minimum values, zero crossings, or thresholds) was 42% for the wearable category and 33% for the environmental systems. In the environmental category, the variability in data processing methods was much greater than in the wearable category, as a large number of studies applied "custom algorithms". The use of wavelet decomposition or the Kalman filter was residual [102,131,165,166,193,212,232].

Table 6. Analysis of the processing algorithm, performance evaluation, and software for the studies of the wearable category.

Study [1]	Algorithm	Performance Evaluation	Performance Value	Analysis Software
Aitkulov 2019 [57,58]	Frequency analysis	Graphical comparison	-	-
Balasubramaniyam 2019 [59]	-	-	-	MATLAB
Bricout 2019 [60]	Adaptive reconstruction	Correlation factor	0.64–0.74	-
Chu 2019 [61]	Peak detection	Bland-Altman analysis Correlation factor	0.99 (correlation)	MATLAB
Elfaramawy 2019 [62]	Peak detection	-	-	MATLAB
Fajkus 2019 [63]	Peak detection	Relative error Bland-Altman analysis	3.9% (RE)	Labview
Hurtado 2019 [64]	Zero-crossing detection	Relative error Bland-Altman analysis	0.4 bpm (BA, mean of difference –MOD–)	-
Jayarathna 2019 [65]	Peak detection	-	-	-
Kano 2019 [66]	Peak detection	Correlation coefficient Bland-Altman analysis	0.88 (correlation) 0.026 bpm (BA, MOD)	-
Karacocuk 2019 [67]	Frequency analysis	Correlation	-	MATLAB Microprocessor
Massaroni 2019 [68]	Custom algorithm	Relative error Linear regression Bland-Altman analysis	4.03% (RE) 0.91–0.97 (r^2) −0.06 (BA, MOD)	MATLAB
Massaroni 2019 [69]	Peak detection	Bland-Altman analysis	0.05 bpm (BA, MOD)	-
Nguyen 2019 [70]	Frequency analysis	-	-	-
Presti 2019 [71]	Peak detection	Percentage error	<4.71% (PE)	MATLAB Labview
Presti 2019 [72]	Peak detection	-	-	-
Puranik 2019 [73]	-	-	-	-
Soomro 2019 [74]	-	-	-	-
Xiao 2019 [75]	-	Graphical comparison	-	-
Yuasa 2019 [76]	Peak detection	Accuracy	61.3–65.6%	MATLAB
Zhang 2019 [77]	Frequency analysis	-	-	-
Dan 2018 [78]	Zero-crossing detection	Bland-Altman analysis	0.01–0.02 bpm (BA, MOD)	-
Koyama 2018 [79]	Frequency analysis	Absolute error	4 bpm	Python
Malik 2018 [80]	-	Graphical monitoring	-	Python
Martin 2018 [81]	Custom algorithm	Mean absolute error Mean relative error Bland-Altman analysis	2.7 bpm (MAE) 30.9% (MRE) 2.4 bpm (BA, MOD)	MATLAB
Pang 2018 [82]	-	Graphical monitoring	-	-

[1] Note: The analysis for studies published before 2018 [2,3,17,21,49,83–162] is included in Appendix A (Table A4).

Table 7. Analysis of the processing algorithm, performance evaluation, and software for the studies of the environmental category.

Study [1]	Algorithm	Performance Evaluation	Performance Value	Analysis Software
Al-Wahedi 2019 [163]	Frequency analysis	Manual verification Relative error	4–14% (RE)	Labview
Chen 2019 [164]	Zero-crossing detection	Mean squared error	1.23 bpm	-
Gunaratne 2019 [165]	Wavelet transform Fuzzy logic	Relative error	6.2%	-
Guo 2019 [166]	Wavelet transform	Cross-correlation	0.76–0.85	-
Isono 2019 [167]	Custom algorithm	Linear regression Bland-Altman analysis	0.969 (r^2) 0.07–0.17 bpm (BA, MOD)	LabChart MATLAB
Ivanovs 2019 [168]	Neural networks	Others	-	-
Joshi 2019 [169]	-	Correlation factor Root mean square error Bland-Altman analysis	0.74 (correlation) 4.7 bpm (RMSE) −0.36 (BA, MOD)	-
Krej 2019 [170]	Machine learning methods	Root mean square error Bland-Altman analysis	1.48 bpm (RMSE) 0.16 bpm (BA, MOD)	C# R
Lorato 2019 [171]	Frequency analysis	Root mean square error Bland-Altman analysis	1.59 bpm (RMSE)	MATLAB
Massaroni 2019 [172]	Custom algorithm	Absolute error Standard error Percentage error Bland-Altman analysis	0.39 bpm (AE) 0.02 bpm (SE) 0.07% (PE) −0.01 bpm (BA, MOD)	MATLAB
Park 2019 [173]	Frequency analysis	Accuracy Bland-Altman analysis	99.4% (Acc)	MATLAB
Walterscheid 2019 [174]	Peak detection	Graphical comparison	-	-
Wang 2019 [175]	Custom algorithm	Absolute error Relative error	0.3 bpm (AE) 2% (RE)	MATLAB
Xu 2019 [176]	Custom algorithm	Absolute error Correlation factor	0.11 bpm (AE) 0.95 (correlation)	-
Yang 2019 [177]	Custom algorithm	Absolute error	0.3–0.6 bpm	-
Chen 2018 [178]	Custom algorithm	Accuracy	98.65%	-
Chen 2018 [179]	Frequency analysis	Graphical comparison	-	Mobile app
Massaroni 2018 [180]	Threshold detection Zero-crossing detection Custom algorithm	Correlation factor Bland-Altman analysis Percentage error Others	0.97 (correlation) 0.01 bpm (BA, MOD) 5.5% (PE)	MATLAB
Massaroni 2018 [181]	Peak detection	Relative error	2%	MATLAB
Sadek 2018 [182]	Peak detection Custom algorithm	Correlation factor Bland-Altman analysis Mean absolute error	0.78 (correlation) 0.38 bpm (MAE)	-

[1] Note: The analysis for studies published before 2018 [5–7,9,10,19,48,50–54,183–234] is included in Appendix A (Table A5).

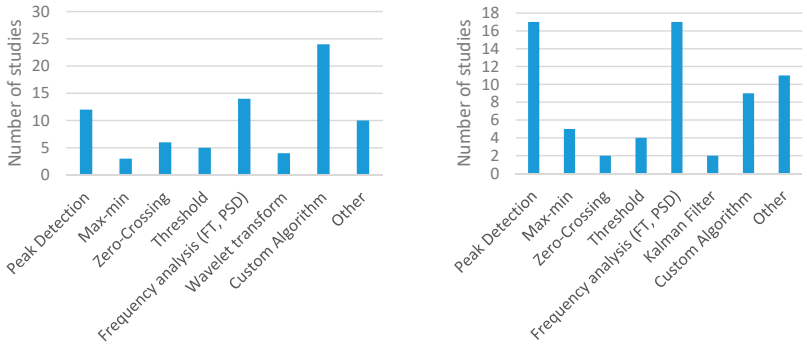

Figure 34. Number of studies using different processing algorithms for the wearable (**left**) and environmental (**right**) categories.

Figure 35 shows the figures of merit used to provide a value of sensor performance for the wearable and environmental studies. The categories "graphical comparison" and "graphical monitoring", which could be considered as informal metrics, were added to the list of evaluation metrics of Section 3.4.1. The category "graphical comparison" refers to studies that visually compared the performance of the sensing system under evaluation with a reference system, but did not use an objective metric. The category "graphical monitoring" indicates that measurements from sensors were plotted, but no formal metric was calculated and no quantitative comparison was made. Figure 35 shows that "absolute error", "relative/percentage error", "Bland-Altman plot", and "correlation coefficient" were the preferred formal metrics for wearable and environmental systems. The use of "root mean square error" [48,52,95,107,115,117,147,164,170,171,187,198], "linear regression" [68,161,167,183,209], and "accuracy" [7,76,133,161,179,190,193,207,216] was limited. Furthermore, the percentage of studies that provided an "informal" figure of merit was much higher for the wearable category (45%) than for the environmental group (17%). Therefore, a stronger assessment can be seen in environmental studies. In general, validation results show low error values and a high correlation with reference devices. The details for the different studies are included in the fourth column of Tables 5 and 6. Fifty-two% of the studies that used relative or percentage errors provided a value less than 5%, while only 12% reported a value greater than 10%. Correlation coefficients greater than 0.95 were provided by 46% of the studies [19,52,61,112,126,149,176,180,208,215,222,228,232]. Regarding absolute error, 78% of the studies that calculated the RR as the breathing parameter provided a value less than 2 bpm [5,19,64,115,124,132,135,172,175–177,182,189,195,201,207,218,224]. No study reported an absolute error value greater than 4 bpm. In relation to the Bland-Altman analysis, the mean of the differences was less than 0.2 bpm in 49% of the studies that provided data on this metric [48,66,68,69,78,94,95,112,115,126,167,170,172,180,195,200,210,228].

Regarding the tools for measurement processing, Figure 36 shows the distribution of use of the different tools for the wearable and environmental respiration monitoring systems. MATLAB was the preferred software for both types of systems, since it was adopted by half of the studies, while NI Labview was the second most used tool as it appeared in 20–30% of the works [2,3,19,63,71,85–88,127,129,131,138,142,146,153,163,201,218–220,223,225]. The rest of the tools relied heavily on the specific sensor used to capture the data. For instance, Audacity, as a sound processing tool, could only be used in microphone-based respiration monitoring [162]; OpenCV, as a computer vision library, was suitable for respiration monitoring through images [187,216]. Therefore, the use of the rest of the tools was residual.

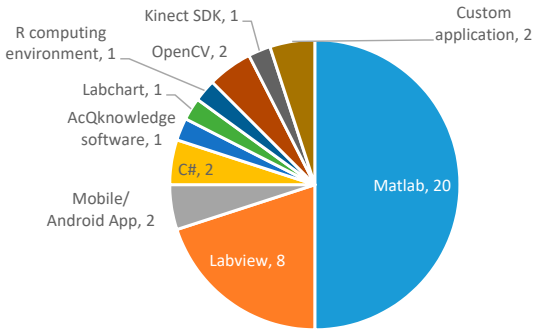

Figure 36. Number of studies using the different processing tools for the wearable (**top**) and environmental (**bottom**) categories.

4. Discussion

Respiratory monitoring has been actively investigated in recent years, as can be deduced from the high number of studies included in this systematic review of the literature. While monitoring breathing in hospital or controlled environments poses fewer problems, the main research challenge is to monitor breathing for a long period in the user's daily environment.

Following the approaches of previous works [24], two different sets of systems for respiratory monitoring were identified. On the one hand, wearable systems have the advantages that they can be used in any environment, either indoors or outdoors, are generally easy to install and, in most cases, inexpensive. However, the level of obtrusiveness can determine the acceptability of this type of systems. Some sensors, such as those designed to be worn on the face or neck, are more obtrusive. A set of wearable sensing technologies are less invasive. This may be the case of those that are worn in the chest, abdomen, arms, or wrist. This might be one of the reasons why the detection of chest movements is the predominant approach. Another reason could be that chest seems to be the part of the body that presents the greatest variations in its state as a result of the respiratory activity. However, most of these technologies require users to wear a belt on the chest or abdomen, electrodes that make contact with the skin, or tight clothing to detect the movement of the thorax [254]. These restrictions might cause discomfort in the long term or, in extreme cases, even skin problems. The proposal of Teichmann et al. [56] is original since the sensor is carried in a pocket of a shirt that does not need to be tight. This represents an advantage over other approaches, although some users may find the lack of integration into clothing uncomfortable. Future research can go in that direction. A common drawback of wearable systems is that they are heavily affected by artifacts caused by non-breathing movements. This leads to larger measurement errors, which can even compromise the viability of the sensing systems in extreme cases. On the other hand, environmental sensors have the advantages that they are non-invasive, data transmission can be done with cable communication and battery life does not limit their operation. However, their scope is restricted to a particular area. Any change in the environment (for example, the relocation of furniture) can modify the detection capabilities. Additionally, some technologies, such as computer vision, present privacy concerns, which may affect user acceptance [271]. Environmental sensors seem suitable for home or hospital applications, but not for continuous monitoring of moving subjects. In fact, usability is a big challenge in respiratory monitoring. Several authors have highlighted this fact [10,19,51,52,115,159,187,254]. However, despite this, we identified a clear gap in the literature since it was not possible to find any usability analysis of the sensors implemented in the existing studies. Future research should also focus on usability. For that, well-known usability tests can be applied to evaluate the level of acceptance of technology by its potential users. For example, the User Acceptance of Information Technology (UTAUT) model [272,273]

may serve. This model was applied previously to evaluate smart wearable devices [274], including health care [275,276], and m-health devices [277]. Other parameters, such as size or weight, can also affect the adoption of the technology. These parameters have only been provided in a limited number of studies [2,3,17,21,49,62,64,68,72,85,93,94,97–99,103,105,108,110,113,114,116,119,120,124,126,135,136,138,141,143,144,146,148,161]. Future works should also consider size and weight as important factors in the design of sensing systems, subjecting them to evaluation.

Regarding the type of sensors used for respiratory monitoring, fiber optic sensors prevailed in the wearable category. This may be due to their insensitivity to electromagnetic fields, their high resistance to water and corrosion, and their compact size and low weight [125]. This technology also allows monitoring different types of physiological parameters simultaneously [278]. In addition, resistive sensors and accelerometers were the second and third most widely used technologies. This might be explained as they are suitable for detecting movement variations, and their design is simpler than other technologies, such as capacitive, pyroelectric, or piezoelectric sensors, among others. In relation to the environmental category, most researchers designed radar-based sensors. Cameras were also widely used. The great development of computer vision technology in recent years [279] makes the detection of chest movements through video image technically feasible. However, cameras present privacy concerns, which may be why radar sensors are the preferred non-contact technology. Radar systems are also small in size, low cost, and simple in structure, which provides advantages in installation and operation [280]. The researches that decided to integrate the sensors into everyday objects again opted for fiber optic technology and sensors based on the measurement of resistance changes. This could be due to the advantages of these technologies, which have been mentioned before. However, the use of non-object-embedded environmental systems was the predominant approach, as they do not require users to be in permanent contact with an object, increasing system applications.

Comparing the performance of sensors is a challenge. It is difficult to compare the performance of different studies, since there is no standardized test to validate the sensors. Authors designed customized experiments with great differences among them. Many aspects were defined differently: the type and values of the respiratory parameters considered, the positions of the subjects during the tests, the number of human participants involved in the experiments, their characteristics, or the duration of the experiments. Differences were also found in the inclusion of motion artifacts and in the mechanical devices that simulated respiration, among others. A consequence of this is that performances provided by existing studies are not comparable, since they were obtained under different test conditions. Therefore, a future research effort is to design a common evaluation framework. This framework should include quiet and rapid breathing and different postures, such as standing, lying, or sitting. Experiments should include motion artifacts since they affect sensor performance, as shown by several studies [53,108,157,158]. Additionally, they should involve a number of users high enough to obtain significant results. In general, the number of subjects participating in existing studies remains low.

In view of the results shown in Section 3.3.2, it is a fact that existing studies carry out short experiments to validate the sensors. However, little attention is paid to their long-term behavior. The effect of temperature, sensor aging, or the characteristics of the carrier subjects (such as height or weight) on the sensing systems have not been actively explored. A sensor that works well in a laboratory environment might not work as well in a real setting when used for a long time. If there were errors in the measurements, this would cause frequent recalibrations of the sensors. Therefore, a research challenge is to test the behavior of respiratory monitoring systems in more realistic environments. The declared performances in laboratory or controlled settings are high. The challenge is to prove that they are equally high in real-world usage. Sensor aging might be a problem in terms of system performance. However, it is less critical in terms of cost as replacement of sensing parts is generally affordable due to its typically low price.

Regarding the declared performances, the validation of the sensors should be done considering reference devices. This is the approach adopted by most of the studies. Other validation methods,

such as the use of metronomes or artificial prototypes, are less common since, unlike reference devices, they are not well-established systems that can be acquired by the scientific community to replicate experiments or compare results. There is less consensus with respect to the figure of merit used to determine the accuracy of the sensing systems. The relative, absolute and RMS errors, the slope of the linear regression line, and the correlation factor have been considered. It is also common to apply the Bland-Altman analysis [281]. It not only provides information on the differences between the measurements of both sensors but also shows the variation of the differences with respect to the magnitude of the measurements. In addition, the standard deviation of the difference is also used to obtain the upper and lower limits of agreement. The high variability of the figures of merit makes it difficult to compare the studies. One issue of respiratory monitoring is that the acceptable margin of error is not clearly defined and, therefore, it is difficult to determine whether a new sensing system is in agreement with reference devices. This may be a consequence of the lack of a common experimental framework, since the margin of error depends on the specific experiments carried out. For example, the acceptable error may be different for slow or rapid breathing. Ideally, both the mean of differences and the limits of agreement in the Bland-Altman analysis should be provided. As complementary information, it would also be interesting to have the mean absolute or relative errors, or the correlation factor. This would facilitate comparison of system performance among studies. However, this is not the most common approach and only a limited number of studies have incorporated it [10,44,57,60,61,65,78,92,100,109,112,114,122–124,132,163,165–169,176,178,191,196,205,206,211,224,228].

Additionally, the parameter to be sensed varies among studies. The most common breathing parameter obtained by existing studies is the RR. However, several studies calculate volume parameters, which are useful for many applications. There are studies that provide both [2,49,52,61,116,122,147], although the calculation of the volume parameters is a challenge since it depends on the specific technology. An approximation for a capacitive textile force sensor can be found in the work of Hoffmann et al. [17]. However, this is still and open research topic. Obtaining an accurate estimate of volume parameters using the sensing techniques presented in this review is not easy, especially for wearable systems.

Regarding processing algorithms, it can be concluded that detection of peaks, maximum and minimum values, thresholds, or zero crossings were effective in determining respiration parameters. Frequency analysis also provided good results. This aspect seems to have been successfully resolved in existing studies. The use of other processing techniques is residual, as they generally require more computing resources, are more complex, and are highly dependent on the specific design of the sensing system.

Wired and wireless transmission are used equally, as the type of transmission is usually determined by the type of sensor. Within wireless systems, Bluetooth was the preferred option. This may be explained because most sensing systems communicate with a smartphone/tablet or PC that is close to the sensing unit. In fact, PC processing is the main trend. This can be a consequence of the majority of studies presenting laboratory prototypes that are far from usable portable systems. In general, authors do not give much thought to the amount of resources that the processing algorithms use as they perform centralized offline processing on a PC using numerical computing software, such as MATLAB. This could compromise the real time operation of the systems when they are running continuously. Future research efforts should focus on designing suitable processing techniques to run ubiquitously in real time on the same microprocessor of the sensing unit or on smartphones.

Power consumption is crucial in wearable respiratory monitoring. Most studies did not provide information on power consumption or battery life. In addition, there was no consensus on the measurement procedure and the energy parameters that should be provided. In this context, it is very difficult to compare the power consumption provided by the different studies fairly. For example, battery life varies greatly depending on factors, such as data transmission procedure (continuous, intermittent, or without transmission), sensor operating time (non-stop, several hours a day, etc.), monitoring visualization (real-time display, without visualization, etc.), or the inclusion of the processing of the

measurements in the power study, among others. When a study provides the battery life of a respiratory sensor, not only must the capacity of the particular battery used in the study be provided, but also other characteristics that affect its performance: depth of discharge, cycle lifetime, or c-rate [282]. It would also be interesting that researchers indicate the power consumption of each component of the system and not just the total autonomy of the device [98]. This would allow the identification of the critical components and facilitate the comparison of different systems. Given that autonomy is a limiting factor, strategies to reduce power consumption are required [135]. However, only a few works have implemented them. Several respiratory monitoring studies focused on transmission technology, since it is usually the most demanding module [91,98]. For example, technologies, such as Wi-Fi or Bluetooth, consume more energy than Impulse Radio Ultra-wideband. Other strategies adopted were the down-sampling of data to reduce computational load [119]. The limited number of works that adopted energy saving strategies may be a symptom that researchers are more focused on validating their sensors than in real-world applications. This can also be inferred from the short battery life indicated by most studies that include this data (less than 12 h typically). Furthermore, the use of energy harvesting techniques in respiratory monitoring is another open research question, since the number of studies that implemented them is still residual [77,84,104,135,240–248,250–253]. Most studies presented laboratory experiments instead of functional prototypes.

An ideal breathing sensor should be mobile, easy to use, imperceptible and immune to body motion [48,119,135]. Several authors agree that a system that covers all these aspect should be successfully integrated into clothing [21,59,65,69,84,85,94,103,108,113,119,123,142,143,151]. This is a consequence of the fact that long-term home monitoring entails direct connection between patient and system. However, this poses several problems, such as the adaptation of the sensing system to different sizes of clothing, the integration of the energy supply, or the washing of sensors, among others. In fact, this is an open research question.

5. Conclusions

This paper presents a systematic review on sensors for respiratory monitoring, filling a gap in the state of the art since no published reviews analyzing respiratory sensors from a comprehensive point of view could be found to the best of our knowledge. As a result of several searches, an overwhelming number of studies was found. They were sorted by relevance and, finally, 198 studies were obtained to be examined in detail. They were classified into two groups: wearable and environmental sensors. Several aspects were analyzed: sensing techniques, sensors, breathing parameters, sensor location and size, general system setups, communication protocols, processing stations, energy autonomy, sensor validation experiments, processing algorithms, performance evaluation, and software used for the analysis. As a result, detection of chest movements was identified as the most common technique using fiber optic sensors for the wearable systems and radar sensors for the environmental systems. The RR was the most common breathing parameter obtained in 68% of the studies. Most of the studies performed centralized measurement processing on a PC using MATLAB software. Bluetooth was by far the prevalent communication technology (60% of the wearable studies adopted it), and almost all wireless respiration sensing systems were battery powered. The most common validation approach was to use a reference device to perform real tests on real subjects. Furthermore, a high percentage of studies obtained the breathing parameter after performing frequency analysis or peak detection on the measurements. Meanwhile, the most common figures of merit selected to provide evidence on sensor performance were absolute and relative errors, Bland-Altman analysis, and correlation coefficients.

This review also identified future research challenges. One of them is the need to define a common framework to validate the sensors, since each author carried out his or her own experiments. This makes it difficult to compare sensor performances. Similarly, measurements of power consumption were made under different conditions. A common measurement procedure is required to compare sensor autonomies fairly. There are no long-term evaluations that study the effect of aging, environmental conditions, or characteristics of the subjects on sensor performance.

Usability tests are also lacking in existing studies. Similarly, the figure of merit to provide sensor performance varies from one study to another. The Bland-Altman analysis was identified as the most appropriate method to validate the sensors against reference devices. Other research challenges are the implementation of energy-saving or energy-harvesting strategies, the application of respiratory sensors to real-world scenarios, or the calculation of volume parameters in the different sensing technologies. All these are remaining research efforts.

Finally, several authors highlighted the integration of respiratory monitoring sensors in clothing as a promising technology. This is a future research effort, which presents several challenges for a feasible, long-term, and unobtrusive solution.

Author Contributions: Conceptualization, R.I. and I.P.; methodology, E.V. and R.I.; formal analysis, E.V. and R.I.; investigation, E.V., R.I. and I.P.; resources, E.V.; data curation, E.V. and R.I.; writing—original draft preparation, R.I.; writing—review and editing, R.I and E.V.; supervision, R.I.; project administration, I.P.; funding acquisition, I.P. All authors have read and agreed to the published version of the manuscript.

Funding: This research was funded by the European Union and the Gobierno de Aragón, grant number "Programa Operativo FEDER Construyendo Europa desde Aragon T49_20R", the Universidad de Zaragoza and the Centro Universitario de la Defensa de Zaragoza, grant number UZCUD2019-TEC-02, and the Consejo Nacional de Ciencia y Tecnología CONACyT, grant number 709365.

Conflicts of Interest: The authors declare no conflict of interest.

Appendix A

Table A1. Analysis of techniques, sensors, breathing parameters, and sensor locations and sizes for studies of the wearable category published before 2018.

Study	Technique	Sensor	Measured Parameter	Location	Size
Agcayazi 2017 [123]	Chest wall movements	Capacitive	-	Chest (shirt)	-
Aileni 2017 [134]	Chest wall movements	Resistive	RR	Chest	-
Basra 2017 [145]	Air temperature	Pyroelectric	RR	Nose (nostril)	-
Bhattacharya 2017 [156]	Air temperature	Thermistor	RR	Mouth mask	-
Das 2017 [162]	Air temperature	Thermistor	-	Nose (near) Mouth (near)	-
Fajkus 2017 [83]	Chest wall movements	Fiber optic	RR	Chest	-
Gorgutsa 2017 [84]	Chest wall movements	Frequency shift	Monitoring of breathing	Chest (shirt)	-
Guay 2017 [85]	Chest wall movements	Frequency shift	Monitoring of breathing	Chest (shirt)	20 × 10 cm
Kam 2017 [86–88]	Chest wall movements	Fiber optic	Monitoring of breathing	Chest	-
Kano 2017 [89]	Air humidity	Nanocrystal and nanoparticles	-	Nose (near) Mouth (near)	-
Koch 2017 [90]	Chest wall movements	Resistive	Monitoring of breathing	Abdomen	-
Milici 2017 [91]	Air temperature	Thermistor	RR Monitoring of respiratory diseases	Nose (near) Mouth (near)	-
Nakazumi 2017 [92]	Respiratory air flow	Photoelectric	Monitoring of breathing	Mouth mask (diving)	-
Park 2017 [93]	Abdomen movements	Capacitive	Monitoring of breathing	Waist	20 × 10 × 1 mm (electrode)

Table A1. *Cont.*

Study	Technique	Sensor	Measured Parameter	Location	Size
Presti 2017 [94]	Chest wall movements	Fiber optic	RR Respiratory period	Chest and abdomen (shirt, front and back)	1.5 cm
Valipour 2017 [95]	Respiratory sounds	Microphone	RR	Nose (near) Mouth (near)	-
White 2017 [96]	Chest wall movements	Capacitive	RR	Chest (below left pectoral muscle)	-
Yan 2017 [97]	Air humidity	Nanocrystal and nanoparticles	Monitoring of breathing	Mouth (4 cm away)	5 × 2 × 1 mm
Mahbub 2016–2017 [98,99]	Chest wall movements	Piezoelectric	RR	Chest	1.6 × 1.6 cm
Chethana 2016 [100]	Chest wall movements	Fiber optic	RR	Chest (interspace of pulmonic area)	
Güder 2016 [101]	Air humidity	Nanocrystal and nanoparticles	Monitoring of breathing	Mouth mask	-
Lepine 2016 [102]	Chest wall movements	Accelerometer ECG	RR	Chest	-
Massaroni 2016 [103]	Chest wall movements	Fiber optic	Respiratory period	Chest and abdomen (textile)	1 cm
Massaroni 2016 [49]	Chest wall movements	Fiber optic	RR TV Compartmental volume	Chest and abdomen (shirt)	10 × 10 cm
Moradian 2016 [104]	Air temperature	Pyroelectric	Monitoring of breathing	Nose (below)	-
Nag 2016 [105]	Chest wall movements	Capacitive	Monitoring of breathing	Chest (diaphragm)	50 mm^2
Nam 2016 [106]	Respiratory sounds	Microphone	RR	Nose (near) Mouth (near)	-
Raji 2016 [107]	Air temperature	Thermistor	RR Monitoring of respiratory diseases	Mouth mask	-
Ramos-García 2016 [108]	Chest wall movements	Resistive	RR	Chest (shirt)	23 × 4 cm
Rotariu 2016 [109]	Chest wall movements	Piezoelectric	RR Monitoring of respiratory diseases	Chest	-
Atalay 2015 [110]	Chest wall movements	Resistive	RR	Chest Abdomen	2.7 × 9.3 cm
Ciocchetti 2015 [111]	Chest wall movements	Fiber optic	TV	Chest	-
Estrada 2015 [112]	Chest wall movements	Accelerometer	RR	Chest	-
Gargiulo 2015 [113]	Chest wall/ abdomen movements	Resistive	TV	Chest and abdomen (shirt)	5 × 7cm (4 units)
Grlica 2015 [114]	Chest wall movements	Capacitive	-	Chest	4.5 × 1.7 cm
Hernandez 2015 [115]	Chest wall movements	Accelerometer Gyroscope	RR	Wrist	-
Jiang 2015 [116]	Air temperature	Pyroelectric	MV, peak inspiratory flow, RR, TV	Nose (below)	5 × 25 × 100 mm
Karlen 2015 [117]	Modulation cardiac activity	PPG	RR	Finger (on sensor)	-

Table A1. *Cont.*

Study	Technique	Sensor	Measured Parameter	Location	Size
Kazmi 2015 [118]	Modulation cardiac activity	PPG	RR	Finger (on sensor)	-
Metshein 2015 [21]	Modulation cardiac activity	ECG	RR	Chest (electrode shirt)	8 × 17cm (electrode surface)
Teichmann 2015 [119]	Chest wall movements	Transthoracic impedance	RR	Chest (pocket of shirt)	10 × 8 cm
Wei 2015 [120]	Air temperature	Other (micro electro-mechanical sensor)	Respiration detection	Nose (5 cm away)	1.8 × 2.4 mm
Yang 2015 [3]	Chest wall movements	Fiber optic	RR	Chest	70 cm (belt)
Bifulco 2014 [121]	Chest wall movements	Piezoelectric	Monitoring of breathing	Chest	-
Fekr 2014 [122]	Chest wall movements	Accelerometer	RR TV	Chest (middle sternum region)	-
Hesse 2014 [124]	Chest wall movements	Resistive	RR	Chest	3 × 1.96 × 2.8 cm
Krehel 2014 [125]	Chest wall movements	Fiber optic	RR	Chest (different regions)	-
Min 2014 [126]	Chest wall movements	Capacitive	RR	Waist	83 × 3.86 × 0.135 cm
Petrovic 2014 [127]	Chest wall movements	Fiber optic	MV TV	Chest (lower third of the thorax)	-
Sanchez 2014 [128]	Air temperature	Fiber optic	Monitoring of breathing	Nose (near) Mouth (near)	-
Wo 2014 [129]	Abdomen movements	Fiber optic	RR	Abdomen	-
Yang 2014 [130]	Chest wall movements	Capacitive	RR	Chest Abdomen	10 × 1 cm
Yoon 2014 [131]	Chest wall movements	Accelerometer Gyroscope	RR	Chest	-
Chan 2013 [132]	Chest wall movements Modulation cardiac activity	Accelerometer ECG	RR	Chest	-
Huang 2013 [133]	Air temperature	Pyroelectric	RR	Nose (near) Mouth (near)	-
Kundu 2013 [161]	Chest wall/ abdomen movements	Capacitive	RR	Chest and abdomen (anterior and posterior region)	9 × 13 cm 16 × 16 cm 5 × 5 cm
Padasdao 2013 [135]	Chest wall movements	DC generator	RR	Chest	Coin size
Cao 2012 [2]	Air temperature	Pyroelectric	RR, MV, peak inspiration flow, TV	Nose (near) Mouth (near)	7 × 4.5 × 1.8 cm
Chiu 2012 [136]	Chest wall movements	Piezoelectric	RR	Chest	48 × 19 × 4 mm
Favero 2012 [137]	Air humidity	Nanocrystal and nanoparticles	Monitoring of breathing	Mouth mask (3 cm from nose)	
Mathew 2012 [138]	Air humidity	Nanocrystal and nanoparticles	Monitoring of breathing	Nose (5 cm away)	1 mm length
Scully 2012 [139]	Modulation cardiac activity	PPG	RR	Finger (on sensor)	-
Trobec 2012 [140]	Modulation cardiac activity	ECG	RR	Chest (different regions)	-

Table A1. *Cont.*

Study	Technique	Sensor	Measured Parameter	Location	Size
Witt 2012 [141]	Chest wall movements	Fiber optic	Monitoring of breathing	Chest	1 cm (elastic part)
Zieba 2012 [142]	Chest wall movements	Resistive	RR	Chest (shirt)	-
Carlos 2011 [143]	Chest wall movements	Resistive	RR Coughing events	Chest and abdomen (shirt)	5.3 × 3.2 cm
Ciobotariu 2011 [144]	Chest wall movements	Piezoelectric	RR Monitoring of respiratory diseases	Chest	28 cm
Guo 2011 [146]	Chest wall movements	Resistive	RR	Chest	10 × 0.25 cm
Hoffmann 2011 [17]	Chest wall movements	Capacitive	Respiration pattern TV (among others)	Chest	3 × 3 cm
Liu 2011 [147]	Chest wall movements	Resistive	RR, MV	Abdomen	-
Liu 2011 [148]	Abdomen movements	Accelerometer	RR	Abdomen	23 mm diameter
Mann 2011 [149]	Chest wall movements	Accelerometer	RR Respiratory disease monitoring	Neck (Midclavicular line and lower costal margin intersection)	-
Ono 2011 [150]	Chest wall movements	Accelerometer	RR	Chest	-
Silva 2011 [151]	Chest wall movements	Fiber optic	RR	Chest (shirt)	-
Yang 2011 [152]	Chest wall movements	Capacitive	Respiration pattern	Chest Abdomen	-
Yoo 2010–2011 [153–155]	Air temperature Abdomen movements	Fiber optic	Monitoring of breathing	Nose (below) Abdomen	-
Ansari 2010 [157]	Modulation cardiac activity	ECG	RR	Arm Forearm	-
De Jonckheere 2010 [158]	Chest wall movements	Fiber optic	Monitoring of breathing	Chest Abdomen	-
Mitchell 2010 [159]	Chest wall movements	Resistive	Respiration pattern	Chest Abdomen	-
Zhang 2010 [160]	Chest wall movements	Frequency shift	Respiration signal	Chest	-

Table A2. Analysis of sensing techniques, sensors, breathing parameters, and sensor location and size for studies of the environmental category published before 2018.

Study	Technique	Sensor	Measured Parameter	Location	Size
Azimi 2017 [183]	Chest wall movements	Pressure (piezoelectric)	RR	Mat	80 × 90 cm
Cho 2017 [184]	Air temperature	Camera	RR Respiratory pattern	-	7.2 × 2.6 × 1.8 cm
Leicht 2017 [185]	Chest wall movements	Inductive	RR	Others (vehicle seatbelt)	-

Table A2. *Cont.*

Study	Technique	Sensor	Measured Parameter	Location	Size
Li 2017 [186]	Chest wall movements	Fiber optic	RR	Mat	-
Li 2017 [187]	Chest wall movements	Camera	RR	Distance from subject (1.4 m above)	-
Prathosh 2017 [10]	Chest wall movements	Camera	RR Respiratory pattern	Distance from subject (0.91 m away)	-
Prochazka 2017 [188]	Air temperature	Camera	RR	Distance from subject (in front of face)	-
Tataraidze 2017 [7]	Modulation cardiac activity	Radar	RR Movement activity periods	Distance from subject	-
Wang 2017 [189]	Modulation cardiac activity	Radar	RR	Distance from subject (5–55 cm away)	-
Heldt 2016 [5]	Modulation cardiac activity	Radar	RR	Distance from subject (15–50 cm away)	-
Kukkapalli 2016 [190]	Modulation cardiac activity	Radar	RR	Others (neck pendant)	-
Prochazka 2016 [191]	Chest wall movements	Kinect	RR	Distance from subject (in front of face)	-
Tveit 2016 [192]	Chest wall movements	Camera	RR	Distance from subject (above)	-
Ushijima 2016 [6]	Chest wall movements	Kinect	Respiration detection	Distance from subject (0.8–4 m away)	-
Erden 2015 [193]	Chest wall movements	Pyroelectric Vibration	RR	Distance from subject (20–100 cm above, pyroelectric) Mat (vibration)	-
Huang 2015 [54]	Modulation cardiac activity	Radar	Respiratory patterns	Distance from subject (1 m away)	-
Liu 2015 [194]	Chest wall movements	Piezoelectric	RR Respiratory pattern	Mat	250 × 125 cm
Pereira 2015 [195]	Air temperature	Camera	RR	Distance from subject (1.5–2 m away)	-
Ravichandran 2015 [196]	Modulation cardiac activity	Wi-Fi transmitter and receiver	RR Falls	Distance from subject (0.9–4.3 m away)	
Sasaki 2015 [197]	Modulation cardiac activity	Radar	RR	Distance from subject (1–2 m above, diagonally)	-
Zakrzewski 2015 [198]	Modulation cardiac activity	Radar	RR	Distance from subject (1.5 m above)	-
Arlotto 2014 [199]	Modulation cardiac activity	Radar	Breathing monitoring	Distance from subject (30 cm away)	
Bernacchia 2014 [200]	Chest wall movements	Kinect	RR	Distance from subject (120 cm above)	-
Bernal 2014 [51]	Chest wall movements	Camera	Respiratory pattern, peak inspiratory and expiratory flow, vital capacity	Distance from subject (above)	-
Chen 2014 [201]	Chest wall movements	Fiber optic	RR	Mat	25 × 20 cm
Lee 2014 [52]	Modulation cardiac activity	Radar	RR TV Respiratory pattern	Distance from subject (80 cm away)	-

Table A2. *Cont.*

Study	Technique	Sensor	Measured Parameter	Location	Size
Luis 2014 [202]	Chest wall movements	Capacitive	Respiration signal	Mat (chest region)	Different electrode sizes: 9 × 24 cm; 14 × 25 cm; 22 × 4 cm; 10 × 10 cm
Mukai 2014 [203]	Chest wall movements	Capacitive	RR	Mat (chest region)	478 × 478 × 3.5 mm
Nukaya 2014 [204]	Chest wall movements	Piezoelectric	Breathing monitoring	Others (below a neonatal bed)	
Patwari 2014 [205]	Modulation cardiac activity	Wi-Fi transmitter and receiver	RR	Nodes	-
Patwari 2014 [206]	Modulation cardiac activity	Wi-Fi transmitter and receiver	RR Amplitude and phase	Nodes	-
Shao 2014 [48]	Chest wall movements	Camera	RR Exhalation flow rate	Distance from subject (0.5 m away)	-
Taheri 2014 [207]	Modulation cardiac activity	Radar	RR	Distance from subject (beside bed)	-
Wang 2014 [53]	Chest wall movements	Camera	Respiratory pattern	-	-
Bartula 2013 [208]	Chest wall movements	Camera	RR	Distance from subject (beside bed)	-
Chen 2013 [209]	Respiratory airflow	Fiber optic	Oxygen concentration	Others (inside measurement instrument)	-
Dziuda 2013 [210]	Chest wall movements	Fiber optic	RR	Mat	220 × 95 × 1.5 mm
Klap 2013 [211]	Chest wall movements	Piezoelectric	RR	Mat (chest region)	-
Lau 2013 [19]	Chest wall movements	Fiber optic	RR Respiratory pattern	Mat	-
Nijsure 2013 [50]	Modulation cardiac activity	Radar	Respiratory monitoring Respiratory pattern	Distance from subject (1–3 m away)	-
Sprager 2013 [212]	Chest wall movements	Fiber optic	RR	Mat	
Vinci 2013 [213]	Modulation cardiac activity	Radar	RR	Distance from subject (1 m above)	
Yavari 2013 [214]	Modulation cardiac activity	Radar	Respiration detection	Distance from subject (1–1.5 m away)	-
Aoki 2012 [215]	Chest wall movements	Kinect	Exhalation flow rate	Distance from subject (1.2 m away, 1.1 m height)	-
Boccanfuso 2012 [216]	Air temperature	Infrared	RR	Distance from subject	-
Bruser 2012 [217]	Chest wall movements	Optical	Respiratory activity	Mat	200 × 90 cm
Chen 2012 [218]	Chest wall movements	Fiber optic	RR Respiratory pattern	Mat	-
Dziuda 2012 [9,236]	Chest wall movements	Fiber optic	RR	Mat (pneumatic cushion)	36 cm diameter, 7 cm height
Gu 2012 [219]	Modulation cardiac activity	Radar	Breathing monitoring	Distance from subject (50 cm above)	5 × 5 cm
Lokavee 2012 [220]	Chest wall movements	Resistive	RR	Mat, pillow	-

Table A2. *Cont.*

Study	Technique	Sensor	Measured Parameter	Location	Size
Shimomura 2012 [221]	Modulation cardiac activity	Radar	RR	Distance from subject (2 m above)	-
Xia 2012 [222]	Chest wall movements	Kinect	Respiration signal	Distance from subject (above)	-
Lai 2011 [223]	Modulation cardiac activity	Radar	RR Respiration amplitude	Distance from subject (1 m away)	3 × 4 cm (antenna)
Otsu 2011 [224]	Modulation cardiac activity	Radar	RR	Distance from subject (0.8 m above)	
Postolache 2011 [225]	Modulation cardiac activity	Radar	RR	Others (embedded in wheelchair)	-
Zito 2011 [226]	Modulation cardiac activity	Radar	Breathing monitoring	Distance from subject (25–40 cm from chest)	
Heise 2010 [227]	Chest wall movements	Resistive	RR	Mat	130 × 7.6 cm
Min 2010 [228]	Chest wall movements	Ultrasonic (proximity)	RR	Distance from subject (1 m away)	-
Mostov 2010 [229]	Modulation cardiac activity	Radar	RR	Distance from subject (2 m away)	10 × 10 × 5 cm
Nishiyama 2010 [230,231]	Chest wall movements	Fiber optic	Respiration monitoring	Mat (bed, chest region)	-
Scalise 2010 [232]	Modulation cardiac activity	Radar	RR	Distance from subject (1.5 m away, perpendicular)	-
Silvious 2010 [233]	Modulation cardiac activity	Radar	RR	Nodes (transmitter: 11.3 m from subject; receiver: 4.3 m from subject)	-
Tan 2010 [234]	Chest wall movements	Camera	RR	Distance from subject (0.5–1 m away)	-

Table A3. Analysis of transmission technology, processing station, and energy autonomy for studies in the wearable category published before 2018.

Study	Wireless Transmission	Wired Transmission	Processing Station	Battery Capacity	Battery Life (Type Battery)
Agcayazi 2017 [123]	Bluetooth (low energy)	-	-	-	-
Aileni 2017 [134]	Bluetooth	-	PC, smartphone, tablet device	-	-
Basra 2017 [145]	-	Serial communication LCD integrated	Microcontroller, PC, mixed signal oscilloscope	9 V, 500 mAh	-
Bhattacharya 2017 [156]	Wi-Fi	-	Smartphone, cloud storage	-	-
Das 2017 [162]	-	Mono audio jack	PC	9 V, 500 mAh	-
Fajkus 2017 [83]	-	Interrogator	PC	-	-
Gorgutsa 2017 [84]	Bluetooth (low energy)	-	PC, tablet device	-	(Rechargeable battery and 630 mV solar cell)
Guay 2017 [85]	-	GPIB interface	PC	-	-
Kam 2017 [86–88]	-	USB	PC	-	(5 V DC power bank)

Table A3. *Cont.*

Study	Wireless Transmission	Wired Transmission	Processing Station	Battery Capacity	Battery Life (Type Battery)
Kano 2017 [89]	Bluetooth	-	-	9 V, 500 mAh	-
Koch 2017 [90]	-	-	-	-	-
Milici 2017 [91]	Backscattered field	-	Cloud storage	330 h	>1 year
Nakazumi 2017 [92]	-	DAQ (Arduino)	PC	-	-
Park 2017 [93]	-	DAQ	PC	-	-
Presti 2017 [94]	-	Interrogator	PC	-	-
Valipour 2017 [95]	Radio-frequency transceiver	-	PC	-	-
White 2017 [96]	Wi-Fi	-	PC	-	-
Yan 2017 [97]	-	-	-	-	-
Mahbub 2016–2017 [98,99]	Impulse radio ultra-wide band	-	Cloud storage	600 mAh	40 days
Chethana 2016 [100]	-	Interrogator	-	-	-
Güder 2016 [101]	Bluetooth	-	Tablet device, smartphone, cloud storage	2600 mAh	9 h
Lepine 2016 [102]	Bluetooth (low energy)	-	Smartphone	-	-
Massaroni 2016 [103]	-	Interrogator	PC	-	-
Massaroni 2016 [49]	-	Interrogator	PC	-	-
Moradian 2016 [104]	Passive ultra-high-frequency RFID	-	Oscilloscope	-	(Self-powered passive sensor)
Nag 2016 [105]	-	-	-	-	-
Nam 2016 [106]	-	Data storage	PC	-	-
Raji 2016 [107]	Radio-frequency	-	Cloud storage	-	-
Ramos-García 2016 [108]	-	Serial communication	PC	-	-
Rotariu 2016 [109]	-	USB	Tablet device	-	-
Atalay 2015 [110]	-	-	-	-	-
Ciocchetti 2015 [111]	-	Interrogator	PC	-	-
Estrada 2015 [112]	-	Data storage	PC	-	-
Gargiulo 2015 [113]	-	-	-	-	-
Grlica 2015 [114]	-	USB	PC	2000 mAh	>25 days
Hernandez 2015 [115]	-	Data storage	PC	-	6–9 h
Jiang 2015 [116]	Bluetooth (low energy)	-	PC, smartphone	-	(Rechargeable battery, wireless charger)
Karlen 2015 [117]	-	Data storage	PC	-	-
Kazmi 2015 [118]	-	USB	PC	-	-
Metshein 2015 [21]	-	-	-	-	-
Teichmann 2015 [119]	Bluetooth	-	Smartphone	2.95 Wh	2.23 h
Wei 2015 [120]	-	-	-	-	-
Yang 2015 [3]	Bluetooth	-	PC	-	-
Bifulco 2014 [121]	-	-	-	-	-
Fekr 2014 [122]	Bluetooth (low energy)	-	PC, smartphone, tablet device, cloud storage	-	-
Hesse 2014 [124]	-	Data storage	PC	-	-
Krehel 2014 [125]	-	Interrogator	PC	-	-

Table A3. *Cont.*

Study	Wireless Transmission	Wired Transmission	Processing Station	Battery Capacity	Battery Life (Type Battery)
Min 2014 [126]	-	-	PC	-	-
Petrovic 2014 [127]	-	Interrogator	PC	-	-
Sanchez 2014 [128]	-	Spectrometer	PC	-	-
Wo 2014 [129]	-	DAQ	PC	-	-
Yang 2014 [130]	Bluetooth (low energy)	-	Smartphone	-	24 h
Yoon 2014 [131]	Bluetooth	-	PC	-	(Li-polymer battery)
Chan 2013 [132]	Bluetooth (low energy)	-	Smartphone	-	(Coin battery)
Huang 2013 [133]	-	USB	PC	-	-
Kundu 2013 [161]	-	-	-	-	-
Padasdao 2013 [135]	-	-	-	-	-
Cao 2012 [2]	Bluetooth	-	Smartphone	1000 mAh	>10 h
Chiu 2012 [136]	-	-	PC	-	-
Favero 2012 [137]	-	Interrogator	-	-	-
Mathew 2012 [138]	-	Interrogator	PC	-	-
Scully 2012 [139]	-	Data storage	PC	-	-
Trobec 2012 [140]	-	-	PC	-	-
Witt 2012 [141]	-	USB	PC	-	-
Zieba 2012 [142]	-	-	PC	-	-
Carlos 2011 [143]	Bluetooth	-	PC, cloud storage	-	-
Ciobotariu 2011 [144]	Wi-Fi, GSM	-	Tablet device	-	5 weeks
Guo 2011 [146]	Bluetooth	-	PC	-	-
Hoffmann 2011 [17]	Bluetooth	-	PC	590 mAh	12 h
Liu 2011 [147]	-	Data Storage (SD card)	PC	370 mAh	54 h
Liu 2011 [148]	Radio-frequency (transceiver)	-	Base station	-	-
Mann 2011 [149]	-	-	PC	-	-
Ono 2011 [150]	-	Data storage	PC	-	-
Silva 2011 [151]	-	Interrogator	-	-	-
Yang 2011 [152]	Bluetooth	-	PC	-	-
Yoo 2010–2011 [153–155]	-	DAQ	PC	-	-
Ansari 2010 [157]	-	-	-	-	-
De Jonckheere 2010 [158]	-	USB	PC	-	-
Mitchell 2010 [159]	Zigbee	-	PC	-	-
Zhang 2010 [160]	Bluetooth	-	PC	-	-

Table A4. Analysis of the processing algorithm, performance evaluation, and software for the studies of the wearable category published before 2018.

Study	Algorithm	Performance Evaluation	Performance Value	Analysis Software
Agcayazi 2017 [123]	-	Graphical monitoring	-	-
Aileni 2017 [134]	-	-	-	-
Basra 2017 [145]	Frequency analysis	Graphical monitoring	-	MATLAB

Table A4. *Cont.*

Study	Algorithm	Performance Evaluation	Performance Value	Analysis Software
Bhattacharya 2017 [156]	Threshold detection	Graphical comparison	-	Blynk
Das 2017 [162]	-	Graphical monitoring	-	Audacity
Fajkus 2017 [83]	Frequency analysis	Relative error	3.9%	MATLAB
Gorgutsa 2017 [84]	Received signal strength indicator	Graphical monitoring	-	Custom application
Guay 2017 [85]	-	Graphical monitoring	-	Labview
Kam 2017 [86–88]	-	Relative error	<4.08%	Labview MATLAB
Kano 2017 [89]	-	Graphical monitoring	-	-
Koch 2017 [90]	Custom algorithm	Graphical monitoring	-	-
Milici 2017 [91]	Peak detection	Graphical comparison	-	-
Nakazumi 2017 [92]	-	Graphical monitoring	-	-
Park 2017 [93]	-	Graphical monitoring	-	MATLAB
Presti 2017 [94]	Max-min detection	Bland-Altman analysis	0.006–0.008 bpm (BA MOD)	MATLAB
Valipour 2017 [95]	-	Root mean square error Bland-Altman analysis	1.26 bpm (RMSE) 0.1 bpm (BA, MOD)	-
White 2017 [96]	Frequency analysis	-	-	MATLAB
Yan 2017 [97]	-	Graphical monitoring	-	-
Mahbub 2016–2017 [98,99]	-	Graphical monitoring	-	-
Chethana 2016 [100]	Frequency analysis	-	-	-
Güder 2016 [101]	-	Graphical monitoring	-	-
Lepine 2016 [102]	Kalman filter	Absolute error	2.11–5.98 bpm	MATLAB
Massaroni 2016 [103]	Max-min detection	Bland-Altman analysis Percentage error	<0.14 s (BA, MOD) 1.14% (PE)	-
Massaroni 2016 [49]	Max-min detection Custom algorithm	Relative error	−1.59% (RE for RR) 14% (RE for TV)	MATLAB
Moradian 2016 [104]	-	Graphical monitoring	-	-
Nag 2016 [105]	-	Graphical monitoring	-	-
Nam 2016 [106]	Frequency analysis	Mean relative error	<1%	MATLAB
Raji 2016 [107]	Threshold detection	Root mean square error	1.7–2 bpm	-
Ramos-García 2016 [108]	Peak detection Frequency analysis	Correlation factor	0.41	-
Rotariu 2016 [109]	Peak detection	-	-	LabWindows/CVI
Atalay 2015 [110]	Frequency analysis	-		-
Ciocchetti 2015 [111]	Peak detection Custom algorithm Manual verification	Correlation factor Percentage error Bland-Altman analysis	0.87 (correlation) 8.3% (PE) <0.002 s (BA, mean difference, time between peaks)	MATLAB
Estrada 2015 [112]	Peak detection Custom Algorithm	Correlation factor Bland-Altman analysis	0.8–0.97 (correlation) −0.01 bpm (BA, MOD)	MATLAB
Gargiulo 2015 [113]	-	Relative error	<10%	MATLAB
Grlica 2015 [114]	-	Graphical monitoring	-	C#

Table A4. *Cont.*

Study	Algorithm	Performance Evaluation	Performance Value	Analysis Software
Hernandez 2015 [115]	Max-min detection Frequency analysis	Bland-Altman analysis Mean absolute error Root mean square error	0.15 bpm (BA, MOD) 0.38 bpm (MAE) 1.25 bpm (RMSE)	-
Jiang 2015 [116]	Custom algorithm	Respiration simulation	-	-
Karlen 2015 [117]	Custom algorithm	Bland-Altman analysis Root mean square error	6.01 bpm (RMSE)	MATLAB
Kazmi 2015 [118]	-	Graphical comparison	-	Easy pulse analyzer Cool term software Kuvios HRV
Metshein 2015 [21]	-	Graphical comparison	-	-
Teichmann 2015 [119]	Frequency analysis (Frequency modulation) Custom algorithm	Graphical comparison	-	Microcontroller
Wei 2015 [120]	-	-	-	-
Yang 2015 [3]	Manual verification	Graphical comparison	-	Labview
Bifulco 2014 [121]	-	-	-	-
Fekr 2014 [122]	Numeric integration algorithm	Correlation factor Relative error	0.85 (correlation) 0.2% (RE)	-
Hesse 2014 [124]	Peak detection	Mean absolute error	0.32 bpm	Microcontroller
Krehel 2014 [125]	-	Correlation factor Bland-Altman analysis	±3 bpm (BA)	MATLAB
Min 2014 [126]	Peak detection Custom Algorithm	Correlation factor Bland-Altman analysis	0.98 (correlation) 0.0015 bpm (BA, MOD)	MATLAB
Petrovic 2014 [127]	-	Mean relative error Bland-Altman analysis	8.7% (RE-MV-) 10.5% (RE-TV-) −1 (BA, MOD)	MATLAB Labview
Sanchez 2014 [128]	-	-	-	-
Wo 2014 [129]	Frequency analysis	-	-	Labview
Yang 2014 [130]	-	Graphical monitoring	-	-
Yoon 2014 [131]	Kalman filter	Relative error	7.3%	MATLAB Labview
Chan 2013 [132]	-	Absolute error	<2 bpm	-
Huang 2013 [133]	-	Accuracy	98.8%	-
Kundu 2013 [161]	-	Accuracy Coefficient of determination	100% (acc) 0.906 (r^2)	-
Padasdao 2013 [135]	Frequency analysis (Fast Fourier Transform)	Bland-Altman analysis Mean absolute error	0.23–0.48 bpm (BA, MOD) 0.00027 bpm (MAE)	-
Cao 2012 [2]	Peak detection	Graphical comparison	-	Labview
Chiu 2012 [136]	Frequency analysis	Paired t-test	No statistical difference with reference	MATLAB
Favero 2012 [137]	-	-	-	-
Mathew 2012 [138]	Zero-crossing detection	Graphical monitoring	-	Labview

Table A4. *Cont.*

Study	Algorithm	Performance Evaluation	Performance Value	Analysis Software
Scully 2012 [139]	Frequency analysis (Frequency modulation)	Graphical comparison	-	MATLAB
Trobec 2012 [140]	ECG-derived algorithm	-	-	MATLAB
Witt 2012 [141]	-	Graphical comparison	-	-
Zieba 2012 [142]	Manual verification	-	-	Labview
Carlos 2011 [143]	-	Graphical monitoring	-	Custom application
Ciobotariu 2011 [144]	Max-min detection Custom algorithm	Graphical comparison	-	C#
Guo 2011 [146]	Peak detection	Simulation Graphical comparison	-	Labview
Hoffmann 2011 [17]	Custom algorithm	Correlation factor Relative error	0.92 (correlation)	-
Liu 2011 [147]	Empirical Mode Decomposition	Mean percentage error Root mean square error	6.1%, 14.6% (MPE) 4.1 bpm, 9.8 bpm (RMSE)	-
Liu 2011 [148]	Principal Component Analysis Frequency analysis	Relative error	10%	-
Mann 2011 [149]	Threshold detection	Correlation factor	0.97	-
Ono 2011 [150]	Custom algorithm	Displacement comparison	-	Objective-C
Silva 2011 [151]	Frequency analysis	Graphical comparison	-	-
Yang 2011 [152]	-	-	-	-
Yoo 2010–2011 [153–155]	-	Graphical monitoring	-	Labview
Ansari 2010 [157]	Frequency analysis	-	-	-
De Jonckheere 2010 [158]	-	Graphical comparison Bland-Altman analysis	-	-
Mitchell 2010 [159]	Manual verification	Graphical comparison	-	Physput
Zhang 2010 [160]	-	Biofeedback (audiovisual feedback signal)	-	MATLAB

Table A5. Analysis of the processing algorithm, performance evaluation, and software for the studies of the environmental category published before 2018.

Study	Algorithm	Performance Evaluation	Performance Value	Analysis Software
Azimi 2017 [183]	Peak detection Custom algorithm	Linear regression	0.968 and 1.0223 (slope)	-
Cho 2017 [184]	Custom algorithm	-	-	-
Leicht 2017 [185]	-	Graphical comparison	-	MATLAB
Li 2017 [186]	Frequency analysis	Graphical monitoring	-	MATLAB
Li 2017 [187]	Custom algorithm	Root mean square error	1.12 bpm	OpenCV
Prathosh 2017 [10]	Custom algorithm	Correlation factor Bland-Altman analysis	0.94 (correlation) 0.88 bpm (BA, MOD)	-
Prochazka 2017 [188]	Neural Network	-	-	-
Tataraidze 2017 [7]	Peak detection Custom algorithm	Accuracy	97%	MATLAB

Table A5. *Cont.*

Study	Algorithm	Performance Evaluation	Performance Value	Analysis Software
Wang 2017 [189]	Frequency analysis (Short-Time Fourier Transform)	Absolute error	0.11–0.33 bpm	-
Heldt 2016 [5]	Threshold detection	Mean absolute error	1.2 bpm	Acknowledge
Kukkapalli 2016 [190]	Peak detection	Accuracy	>95%	
Prochazka 2016 [191]	Custom algorithm	Relative error	0.06–0.26%	-
Tveit 2016 [192]	Phase-based respiration detection Pixel-intensity detection	Manual verification Relative error	7.21–11.57%	-
Ushijima 2016 [6]	-	Graphical comparison	-	-
Erden 2015 [193]	Wavelet transform Empirical mode decomposition	Accuracy	93%	-
Huang 2015 [54]	Peak detection Threshold detection	-	-	-
Liu 2015 [194]	Peak detection Threshold detection	Relative error	1.8–5.7%	-
Pereira 2015 [195]	Custom algorithm	Correlation factor Mean Absolute Error Bland-Altman analysis	0.92 (correlation) 0.53 bpm (MAE) 0.025 bpm (BA, MOD)	MATLAB
Ravichandran 2015 [196]	Zero-crossing detection Frequency analysis Linear predictive coding Least-squares harmonic analysis	Absolute error	2.16 bpm	-
Sasaki 2015 [197]	-	Relative error	3%	-
Zakrzewski 2015 [198]	Linear/ non-Linear demodulation	Mean squared error	-	MATLAB
Arlotto 2014 [199]	-	Graphical comparison	-	-
Bernacchia 2014 [200]	Custom algorithm	Correlation factor Bland-Altman analysis	0.96 (correlation) 0 bpm (BA, MOD)	MATLAB
Bernal 2014 [51]	Peak detection Zero-crossing detection Custom algorithm	Graphical comparison	-	-
Chen 2014 [201]	Peak detection	Absolute error Relative error	1.65 bpm (AE) 9.9% (RE)	Labview
Lee 2014 [52]	Frequency analysis	Correlation factor Root mean square error	0.90–0.976 (correlation) 0.0038–0.076 bpm (RMSE)	MATLAB
Luis 2014 [202]	Custom algorithm	-	-	MATLAB
Mukai 2014 [203]	Frequency analysis	-	-	-
Nukaya 2014 [204]	-	Scatterplot	-	-
Patwari 2014 [205]	Frequency analysis	Relative error	1 bpm	-
Patwari 2014 [206]	Custom algorithm	Relative error	0.1 to 0.4 bpm	-

Table A5. *Cont.*

Study	Algorithm	Performance Evaluation	Performance Value	Analysis Software
Shao 2014 [48]	Custom algorithm	Correlation factor Bland-Altman analysis Root mean square error	0.93 (correlation) 0.02 bpm (BA, MOD) 1.2 bpm (RMSE)	MATLAB
Taheri 2014 [207]	Custom algorithm	Mean absolute error Accuracy	0.93–1.77 bpm (MAE) 79–89% (Acc)	-
Wang 2014 [53]	Threshold detection	Others (confusion matrix)	94%	-
Bartula 2013 [208]	Custom algorithm	Correlation factor	0.98	-
Chen 2013 [209]	Frequency analysis	Linear regression Bland-Altman analysis	0.999 (r^2)	-
Dziuda 2013 [210]	Max detection	Relative error Bland-Altman analysis	<8% (RE) 0 bpm (BA, MOD)	Custom application
Klap 2013 [211]	Proprietary algorithms	Relative error	4–8% (RE)	-
Lau 2013 [19]	Peak detection	Correlation factor Mean absolute error	0.971 (correlation) 2 bpm (MAE)	Labview
Nijsure 2013 [50]	Custom algorithm	Correlation factor	0.814	-
Sprager 2013 [212]	Wavelet transform	Relative error	7.37 ± 7.20%	MATLAB
Vinci 2013 [213]	Frequency analysis	Graphical comparison	-	MATLAB
Yavari 2013 [214]	-	Graphical comparison	-	-
Aoki 2012 [215]	Custom algorithm	Correlation factor Bland-Altman plot	0.98 (correlation)	Kinect SDK
Boccanfuso 2012 [216]	Sinusoidal curve-fitting function	Accuracy	-	OpenCV
Bruser 2012 [217]	-	-	-	-
Chen 2012 [218]	Frequency analysis	Mean absolute error	2 bpm	Labview
Dziuda 2012 [9,236]	Max-min detection	Relative error	12%	C#
Gu 2012 [219]	-	Graphical comparison	-	Labview
Lokavee 2012 [220]	-	Graphical comparison	-	Labview
Shimomura 2012 [221]	Frequency analysis	Relative error	1.61%	-
Xia 2012 [222]	-	Correlation factor	0.958–0.978	-
Lai 2011 [223]	Multipeak detection	Correlation factor	0.5–0.83	MATLAB Labview
Otsu 2011 [224]	Custom algorithm	Absolute error	0.19 bpm	-
Postolache 2011 [225]	Peak detection	-	-	Labview Android app
Zito 2011 [226]	-	Graphical comparison	-	-
Heise 2010 [227]	Zero-crossing detection	-	-	-
Min 2010 [228]	Envelop detection Zero-crossing detection	Correlation factor Bland-Altman analysis	0.93–0.98 (correlation) −0.002–0.006 bpm (BA, MOD)	MATLAB
Mostov 2010 [229]	Custom algorithm	-	-	-
Nishiyama 2010 [230,231]	-	Graphical monitoring	-	-
Scalise 2010 [232]	Wavelet transform	Correlation factor Bland-Altman analysis	0.98 (correlation) 13 ms (BAP, MOD)	-
Silvious 2010 [233]	-	Graphical comparison	-	-
Tan 2010 [234]	Custom algorithm	Graphical comparison	-	Custom application

References

1. Milenković, A.; Otto, C.; Jovanov, E. Wireless sensor networks for personal health monitoring: Issues and an implementation. *Comput. Commun.* **2006**, *29*, 2521–2533. [CrossRef]
2. Cao, Z.; Zhu, R.; Que, R.-Y. A wireless portable system with microsensors for monitoring respiratory diseases. *IEEE Trans. Biomed. Eng.* **2012**, *59*, 3110–3116.
3. Yang, X.; Chen, Z.; Elvin, C.S.M.; Janice, L.H.Y.; Ng, S.H.; Teo, J.T.; Wu, R. Textile Fiber Optic Microbend Sensor Used for Heartbeat and Respiration Monitoring. *IEEE Sens. J.* **2015**, *15*, 757–761. [CrossRef]
4. Subbe, C.P.; Kinsella, S. Continuous monitoring of respiratory rate in emergency admissions: Evaluation of the RespiraSense^{TM} sensor in acute care compared to the industry standard and gold standard. *Sensors* **2018**, *18*, 2700. [CrossRef]
5. Heldt, G.P.; Ward, R.J., III. Evaluation of Ultrasound-Based Sensor to Monitor Respiratory and Nonrespiratory Movement and Timing in Infants. *IEEE Trans. Biomed. Eng.* **2016**, *63*, 619–629. [CrossRef] [PubMed]
6. Ushijima, T.; Satake, J. Development of a Breathing Detection Robot for a Monitoring System. In Proceedings of the Joint 8th International Conference on Soft Computing and Intelligent Systems (SCIS) and 17th International Symposium on Advanced Intelligent Systems (ISIS), Sapporo, Japan, 25–28 August 2016; pp. 790–795.
7. Tataraidze, A.; Anishchenko, L.; Korostovtseva, L.; Bochkarev, M.; Sviryaev, Y.; Alborova, I. Detection of movement activity and breathing cycles on bioradiolocation signals. In Proceedings of the IEEE nternational Conference on Microwaves, Antennas, Communications and Electronic Systems (COMCAS), Tel Aviv, Israel, 13–15 November 2017; pp. 1–4.
8. Gatti, U.C.; Schneider, S.; Migliaccio, G.C. Physiological condition monitoring of construction workers. *Autom. Constr.* **2014**, *44*, 227–233. [CrossRef]
9. Dziuda, L.; Skibniewski, F.W.; Krej, M.; Lewandowski, J. Monitoring Respiration and Cardiac Activity Using Fiber Bragg Grating-Based Sensor. *IEEE Trans. Biomed. Eng.* **2012**, *59*, 1934–1942. [CrossRef] [PubMed]
10. Prathosh, A.P.; Praveena, P.; Mestha, L.K.; Bharadwaj, S. Estimation of Respiratory Pattern From Video Using Selective Ensemble Aggregation. *IEEE Trans. Signal Process.* **2017**, *65*, 2902–2916. [CrossRef]
11. Liu, X.; Wang, Q.; Liu, D.; Wang, Y.; Zhang, Y.; Bai, O.; Sun, J. Human emotion classification based on multiple physiological signals by wearable system. *Technol. Health Care* **2018**, *26*, 459–469. [CrossRef]
12. Homma, I.; Masaoka, Y. Breathing rhythms and emotions. *Exp. Physiol.* **2008**, *93*, 1011–1021. [CrossRef]
13. Ćosić, D. Neuromarketing in market research. *Interdiscip. Descr. Complex Syst. INDECS* **2016**, *14*, 139–147. [CrossRef]
14. Kowalczuk, Z.; Czubenko Michałand Merta, T. Emotion monitoring system for drivers. *IFAC-PapersOnLine* **2019**, *52*, 200–205. [CrossRef]
15. Granato, M. Emotions Recognition in Video Game Players Using Physiological Information. Ph.D. Thesis, Università degli studi di Milano, Milano, Italy, 2019.
16. Kołakowska, A.; Landowska, A.; Szwoch, M.; Szwoch, W.; Wrobel, M.R. Emotion recognition and its applications. In *Human-Computer Systems Interaction: Backgrounds and Applications 3*; Springer: Berlin/Heidelberg, Germany, 2014; pp. 51–62.
17. Hoffmann, T.; Eilebrecht, B.; Leonhardt, S. Respiratory Monitoring System on the Basis of Capacitive Textile Force Sensors. *IEEE Sens. J.* **2011**, *11*, 1112–1119. [CrossRef]
18. Sperlich, B.; Aminian, K.; Düking, P.; Holmberg, H.-C. Wearable Sensor Technology for Monitoring Training Load and Health in the Athletic Population. *Front. Physiol.* **2019**, *10*. [CrossRef]
19. Lau, D.; Chen, Z.; Teo, J.T.; Ng, S.H.; Rumpel, H.; Lian, Y.; Yang, H.; Kei, P.L. Intensity-Modulated Microbend Fiber Optic Sensor for Respiratory Monitoring and Gating During MRI. *IEEE Trans. Biomed. Eng.* **2013**, *60*, 2655–2662. [CrossRef]
20. Krebber, K.; Lenke, P.; Liehr, S.; Schukar, M.; Wendt, M.; Witt, J.; Wosniok, A. Technology and applications of smart technical textiles based on fiber optic sensors. *Adv. Photonics Renew. Energy* **2008**. [CrossRef]
21. Metshein, M. A device for measuring the electrical bioimpedance with variety of electrode placements for monitoring the breathing and heart rate. In Proceedings of the 26th Irish Signals and Systems Conference (ISSC), Carlow, UK, 24–25 June 2015; pp. 1–4.
22. Friedl, K.E. Military applications of soldier physiological monitoring. *J. Sci. Med. Sport* **2018**, *21*, 1147–1153. [CrossRef]

23. Scalise, L.; Mariani Primiani, V.; Russo, P.; De Leo, A.; Shahu, D.; Cerri, G. Wireless sensing for the respiratory activity of human beings: Measurements and wide-band numerical analysis. *Int. J. Antennas Propag.* **2013**, *2013*, 396459. [CrossRef]
24. Massaroni, C.; Nicolò, A.; Lo Presti, D.; Sacchetti, M.; Silvestri, S.; Schena, E. Contact-based methods for measuring respiratory rate. *Sensors* **2019**, *19*, 908. [CrossRef]
25. Mukhopadhyay, S.C. Wearable Sensors for Human Activity Monitoring: A Review. *IEEE Sens. J.* **2015**, *15*, 1321–1330. [CrossRef]
26. Nag, A.; Mukhopadhyay, S.C.; Kosel, J. Wearable Flexible Sensors: A Review. *IEEE Sens. J.* **2017**, *17*, 3949–3960. [CrossRef]
27. Chung, M.; Fortunato, G.; Radacsi, N. Wearable flexible sweat sensors for healthcare monitoring: A review. *J. R. Soc. Interface* **2019**, *16*, 20190217. [CrossRef]
28. Bandodkar, A.J.; Jeang, W.J.; Ghaffari, R.; Rogers, J.A. Wearable sensors for biochemical sweat analysis. *Annu. Rev. Anal. Chem.* **2019**, *12*, 1–22. [CrossRef] [PubMed]
29. López-Nava, I.H.; Muñoz-Meléndez, A. Wearable Inertial Sensors for Human Motion Analysis: A Review. *IEEE Sens. J.* **2016**, *16*, 7821–7834. [CrossRef]
30. Seshadri, D.R.; Li, R.T.; Voos, J.E.; Rowbottom, J.R.; Alfes, C.M.; Zorman, C.A.; Drummond, C.K. Wearable sensors for monitoring the internal and external workload of the athlete. *NPJ Digit. Med.* **2019**, *2*, 71. [CrossRef] [PubMed]
31. Aroganam, G.; Manivannan, N.; Harrison, D. Review on Wearable Technology Sensors Used in Consumer Sport Applications. *Sensors* **2019**, *19*, 1983. [CrossRef] [PubMed]
32. Al-Eidan, R.M.; Al-Khalifa, H.; Al-Salman, A.M. A Review of Wrist-Worn Wearable: Sensors, Models, and Challenges. *J. Sens.* **2018**, *2018*, 5853917. [CrossRef]
33. Baig, M.M.; Afifi, S.; GholamHosseini, H.; Mirza, F. A Systematic Review of Wearable Sensors and IoT-Based Monitoring Applications for Older Adults—A Focus on Ageing Population and Independent Living. *J. Med. Syst.* **2019**, *43*, 233. [CrossRef] [PubMed]
34. Heikenfeld, J.; Jajack, A.; Rogers, J.; Gutruf, P.; Tian, L.; Pan, T.; Li, R.; Khine, M.; Kim, J.; Wang, J.; et al. Wearable sensors: Modalities, challenges, and prospects. *Lab Chip* **2018**, *18*, 217–248. [CrossRef] [PubMed]
35. Witte, A.-K.; Zarnekow, R. Transforming Personal Healthcare through Technology—A Systematic Literature Review of Wearable Sensors for Medical Application. In Proceedings of the 52nd Hawaii International Conference on System Sciences, Grand Wailea, Maui, 8–11 January 2019; pp. 3848–3857.
36. Pantelopoulos, A.; Bourbakis, N.G. A Survey on Wearable Sensor-Based Systems for Health Monitoring and Prognosis. *Healthc. Inform. Res.* **2010**, *40*, 1–12. [CrossRef]
37. Liang, T.; Yuan, Y.J. Wearable Medical Monitoring Systems Based on Wireless Networks: A Review. *IEEE Sens. J.* **2016**, *16*, 8186–8199. [CrossRef]
38. Charlton, P.H.; Birrenkott, D.A.; Bonnici, T.; Pimentel, M.A.F.; Johnson, A.E.W.; Alastruey, J.; Tarassenko, L.; Watkinson, P.J.; Beale, R.; Clifton, D.A. Breathing Rate Estimation From the Electrocardiogram and Photoplethysmogram: A Review. *IEEE Sens. J.* **2018**, *11*, 2–20. [CrossRef] [PubMed]
39. AL-Khalidi, F.Q.; Saatchi, R.; Burke, D.; Elphick, H.; Tan, S. Respiration rate monitoring methods: A review. *Pediatr. Pulmonol.* **2011**, *46*, 523–529. [CrossRef] [PubMed]
40. Van Loon, K.; Zaane, B.; Bosch, E.J.; Kalkman, C.; Peelen, L.M. Non-Invasive Continuous Respiratory Monitoring on General Hospital Wards: A Systematic Review. *PLoS ONE* **2015**, *10*, e0144626. [CrossRef] [PubMed]
41. Rajala, S.; Lekkala, J. Film-Type Sensor Materials PVDF and EMFi in Measurement of Cardiorespiratory Signals—A Review. *IEEE Sens. J.* **2012**, *12*, 439–446. [CrossRef]
42. Massaroni, C.; Zaltieri, M.; Lo Presti, D.; Nicolò, A.; Tosi, D.; Schena, E. Fiber Bragg Grating Sensors for Cardiorespiratory Monitoring: A Review. *IEEE Sens. J.* **2020**, 1. [CrossRef]
43. IEEE Xplore Search Results Page. Available online: https://ieeexplore.ieee.org/Xplorehelp/searching-ieee-xplore/search-results-page (accessed on 8 September 2020).
44. Google Sholar About. Available online: https://scholar.google.com/intl/es/scholar/about.html (accessed on 8 September 2020).
45. PRISMA. Transparent Reporting of Systematic Reviews and Meta-Analyses. Available online: http://prisma-statement.org/ (accessed on 14 September 2020).

46. Igual, R.; Medrano, C.; Plaza, I. Challenges, issues and trends in fall detection systems. *Biomed. Eng. Online* **2013**, *12*. [CrossRef]
47. Warner, M.A.; Patel, B. Mechanical ventilation. In *Benumof and Hagberg's Airway Management*; Elsevier: Amsterdam, The Netherlands, 2013; pp. 981–997.
48. Shao, D.; Yang, Y.; Liu, C.; Tsow, F.; Yu, H.; Tao, N. Noncontact Monitoring Breathing Pattern, Exhalation Flow Rate and Pulse Transit Time. *IEEE Trans. Biomed. Eng.* **2014**, *61*, 2760–2767. [CrossRef]
49. Massaroni, C.; Saccomandi, P.; Formica, D.; Lo Presti, D.; Caponero, M.A.; Di Tomaso, G.; Giurazza, F.; Muto, M.; Schena, E. Design and Feasibility Assessment of a Magnetic Resonance-Compatible Smart Textile Based on Fiber Bragg Grating Sensors for Respiratory Monitoring. *IEEE Sens. J.* **2016**, *16*, 8103–8110. [CrossRef]
50. Nijsure, Y.; Tay, W.P.; Gunawan, E.; Wen, F.; Yang, Z.; Guan, Y.L.; Chua, A.P. An Impulse Radio Ultrawideband System for Contactless Noninvasive Respiratory Monitoring. *IEEE Trans. Biomed. Eng.* **2013**, *60*, 1509–1517. [CrossRef]
51. Bernal, E.A.; Mestha, L.K.; Shilla, E. Non contact monitoring of respiratory function via depth sensing. In Proceedings of the IEEE-EMBS International Conference on Biomedical and Health Informatics (BHI), Valencia, Spain, 1–4 June 2014; pp. 101–104.
52. Lee, Y.S.; Pathirana, P.N.; Steinfort, C.L.; Caelli, T. Monitoring and Analysis of Respiratory Patterns Using Microwave Doppler Radar. *IEEE J. Transl. Eng. Health Med.* **2014**, *2*, 1–12. [CrossRef] [PubMed]
53. Wang, C.; Hunter, A.; Gravill, N.; Matusiewicz, S. Unconstrained Video Monitoring of Breathing Behavior and Application to Diagnosis of Sleep Apnea. *IEEE Trans. Biomed. Eng.* **2014**, *61*, 396–404. [CrossRef] [PubMed]
54. Huang, X.; Sun, L.; Tian, T.; Huang, Z.; Clancy, E. Real-time non-contact infant respiratory monitoring using UWB radar. In Proceedings of the 16th IEEE International Conference on Communication Technology, Hangzhou, China, 18–21 October 2015; pp. 493–496.
55. Igual, R.; Plaza, I.; Medrano, C.; Rubio, M.A. Personalizable smartphone-based system adapted to assist dependent people. *J. Ambient Intell. Smart Environ.* **2014**, *6*, 569–593. [CrossRef]
56. Igual, R.; Plaza, I.; Martín, L.; Corbalan, M.; Medrano, C. Guidelines to Design Smartphone Applications for People with Intellectual Disability: A Practical Experience. In *Ambient Intelligence—Software and Applications*; Advances in Intelligent Systems and Computing; Springer: Heidelberg, Germany, 2013; Volume 219, ISBN 9783319005652.
57. Aitkulov, A.; Tosi, D. Optical fiber sensor based on plastic optical fiber and smartphone for measurement of the breathing rate. *IEEE Sens. J.* **2019**, *19*, 3282–3287. [CrossRef]
58. Aitkulov, A.; Tosi, D. Design of an all-POF-fiber smartphone multichannel breathing sensor with camera-division multiplexing. *IEEE Sens. Lett.* **2019**, *3*, 1–4. [CrossRef]
59. Balasubramaniyam, H.; Vignesh, M.S.; Abhirami, A.; Abanah, A. Design and Development of a IoT based Flexible and Wearable T-Shirt for Monitoring Breathing Rate. In Proceedings of the 3rd International Conference on Computing Methodologies and Communication (ICCMC), Erode, India, 27–29 March 2019; pp. 376–379.
60. Bricout, A.; Fontecave-Jallon, J.; Colas, D.; Gerard, G.; Pépin, J.-L.; Guméry, P.-Y. Adaptive Accelerometry Derived Respiration: Comparison with Respiratory Inductance Plethysmography during Sleep. In Proceedings of the 41st Annual International Conference of the IEEE Engineering in Medicine and Biology Society (EMBC), Berlin, Germany, 23–27 July 2019; pp. 6714–6717.
61. Chu, M.; Nguyen, T.; Pandey, V.; Zhou, Y.; Pham, H.N.; Bar-Yoseph, R.; Radom-Aizik, S.; Jain, R.; Cooper, D.M.; Khine, M. Respiration rate and volume measurements using wearable strain sensors. *NPJ Digit. Med.* **2019**, *2*, 1–9. [CrossRef]
62. Elfaramawy, T.; Fall, C.L.; Arab, S.; Morissette, M.; Lellouche, F.; Gosselin, B. A Wireless Respiratory Monitoring System Using a Wearable Patch Sensor Network. *IEEE Sens. J.* **2019**, *19*, 650–657. [CrossRef]
63. Fajkus, M.; Nedoma, J.; Martinek, R.; Brablik, J.; Vanus, J.; Novak, M.; Zabka, S.; Vasinek, V.; Hanzlikova, P.; Vojtisek, L. MR fully compatible and safe FBG breathing sensor: A practical solution for respiratory triggering. *IEEE Access* **2019**, *7*, 123013–123025. [CrossRef]
64. Hurtado, D.E.; Abusleme, A.; Chávez, J.A.P. Non-invasive continuous respiratory monitoring using temperature-based sensors. *J. Clin. Monit. Comput.* **2019**, 1–9. [CrossRef]

65. Jayarathna, T.; Gargiulo, G.D.; Breen, P.P. Polymer sensor embedded, IOT enabled t-shirt for long-term monitoring of sleep disordered breathing. In Proceedings of the IEEE 5th World Forum on Internet of Things (WF-IoT), Limerick, UK, 15–18 April 2019; pp. 139–143.
66. Kano, S.; Yamamoto, A.; Ishikawa, A.; Fujii, M. Respiratory rate on exercise measured by nanoparticle-based humidity sensor. In Proceedings of the 41st Annual International Conference of the IEEE Engineering in Medicine and Biology Society (EMBC), Berlin, Germany, 23–27 July 2019; pp. 3567–3570.
67. Karacocuk, G.; Höflinger, F.; Zhang, R.; Reindl, L.M.; Laufer, B.; Möller, K.; Röell, M.; Zdzieblik, D. Inertial sensor-based respiration analysis. *IEEE Trans. Instrum. Meas.* **2019**, *68*, 4268–4275. [CrossRef]
68. Massaroni, C.; Nicolò, A.; Girardi, M.; La Camera, A.; Schena, E.; Sacchetti, M.; Silvestri, S.; Taffoni, F. Validation of a wearable device and an algorithm for respiratory monitoring during exercise. *IEEE Sens. J.* **2019**, *19*, 4652–4659. [CrossRef]
69. Massaroni, C.; Di Tocco, J.; Presti, D.L.; Longo, U.G.; Miccinilli, S.; Sterzi, S.; Formica, D.; Saccomandi, P.; Schena, E. Smart textile based on piezoresistive sensing elements for respiratory monitoring. *IEEE Sens. J.* **2019**, *19*, 7718–7725. [CrossRef]
70. Nguyen, T.-V.; Ichiki, M. MEMS-Based Sensor for Simultaneous Measurement of Pulse Wave and Respiration Rate. *Sensors* **2019**, *19*, 4942. [CrossRef] [PubMed]
71. Presti, D.L.; Massaroni, C.; Di Tocco, J.; Schena, E.; Carnevale, A.; Longo, U.G.; D'Abbraccio, J.; Massari, L.; Oddo, C.M.; Caponero, M.A. Single-plane neck movements and respiratory frequency monitoring: A smart system for computer workers. In Proceedings of the 2019 II Workshop on Metrology for Industry 4.0 and IoT (MetroInd4. 0&IoT), Naples, Italy, 4–6 June 2019; pp. 167–170.
72. Presti, D.L.; Massaroni, C.; D'Abbraccio, J.; Massari, L.; Caponero, M.; Longo, U.G.; Formica, D.; Oddo, C.M.; Schena, E. Wearable system based on flexible FBG for respiratory and cardiac monitoring. *IEEE Sens. J.* **2019**, *19*, 7391–7398. [CrossRef]
73. Puranik, K.A.; Kanthi, M. Wearable Device for Yogic Breathing. In Proceedings of the 2019 Amity International Conference on Artificial Intelligence (AICAI), Dubai, UAE, 4–6 February 2019; pp. 605–610.
74. Soomro, A.M.; Jabbar, F.; Ali, M.; Lee, J.-W.; Mun, S.W.; Choi, K.H. All-range flexible and biocompatible humidity sensor based on poly lactic glycolic acid (PLGA) and its application in human breathing for wearable health monitoring. *J. Mater. Sci. Mater. Electron.* **2019**, *30*, 9455–9465. [CrossRef]
75. Xiao, S.; Nie, J.; Tan, R.; Duan, X.; Ma, J.; Li, Q.; Wang, T. Fast-response ionogel humidity sensor for real-time monitoring of breathing rate. *Mater. Chem. Front.* **2019**, *3*, 484–491. [CrossRef]
76. Yuasa, Y.; Suzuki, K. Wearable device for monitoring respiratory phases based on breathing sound and chest movement. *Adv. Biomed. Eng.* **2019**, *8*, 85–91. [CrossRef]
77. Zhang, H.; Zhang, J.; Hu, Z.; Quan, L.; Shi, L.; Chen, J.; Xuan, W.; Zhang, Z.; Dong, S.; Luo, J. Waist-wearable wireless respiration sensor based on triboelectric effect. *Nano Energy* **2019**, *59*, 75–83. [CrossRef]
78. Dan, G.; Zhao, J.; Chen, Z.; Yang, H.; Zhu, Z. A Novel Signal Acquisition System for Wearable Respiratory Monitoring. *IEEE Access* **2018**, *6*, 34365–34371. [CrossRef]
79. Koyama, Y.; Nishiyama, M.; Watanabe, K. Smart Textile Using Hetero-Core Optical Fiber for Heartbeat and Respiration Monitoring. *IEEE Sens. J.* **2018**, *18*, 6175–6180. [CrossRef]
80. Malik, S.; Ahmad, M.; Punjiya, M.; Sadeqi, A.; Baghini, M.S.; Sonkusale, S. Respiration Monitoring Using a Flexible Paper-Based Capacitive Sensor. In Proceedings of the 2018 IEEE Sensors, New Delhi, India, 28–31 October 2018; pp. 1–4.
81. Martin, A.; Voix, J. In-Ear Audio Wearable: Measurement of Heart and Breathing Rates for Health and Safety Monitoring. *IEEE Trans. Biomed. Eng.* **2018**, *65*, 1256–1263. [CrossRef] [PubMed]
82. Pang, Y.; Jian, J.; Tu, T.; Yang, Z.; Ling, J.; Li, Y.; Wang, X.; Qiao, Y.; Tian, H.; Yang, Y.; et al. Wearable humidity sensor based on porous graphene network for respiration monitoring. *Biosens. Bioelectron.* **2018**, *116*, 123–129. [CrossRef] [PubMed]
83. Fajkus, M.; Nedoma, J.; Martinek, R.; Vasinek, V.; Nazeran, H.; Siska, P. A non-invasive multichannel hybrid fiber-optic sensor system for vital sign monitoring. *Sensors* **2017**, *17*, 111. [CrossRef] [PubMed]
84. Gorgutsa, S.; Bellemare-Rousseau, S.; Guay, P.; Miled, A.; Messaddeq, Y. Smart T-shirt with wireless respiration sensor. In Proceedings of the 2017 IEEE Sensors, Glasgow, UK, 29 October–1 November 2017; pp. 1–3.
85. Guay, P.; Gorgutsa, S.; LaRochelle, S.; Messaddeq, Y. Wearable contactless respiration sensor based on multi-material fibers integrated into textile. *Sensors* **2017**, *17*, 1050. [CrossRef] [PubMed]

86. Kam, W.; Mohammed, W.S.; Leen, G.; O'Sullivan, K.; O'Keeffe, M.; O'Keeffe, S.; Lewis, E. All plastic optical fiber-based respiration monitoring sensor. In Proceedings of the 2017 IEEE Sensors, Glasgow, UK, 29 October–1 November 2017; pp. 1–3.
87. Kam, W.; Mohammed, W.S.; Leen, G.; O'Keeffe, M.; O'Sullivan, K.; O'Keeffe, S.; Lewis, E. Compact and Low-Cost Optical Fiber Respiratory Monitoring Sensor Based on Intensity Interrogation. *J. Light. Technol.* **2017**, *35*, 4567–4573. [CrossRef]
88. Kam, W.; Mohammed, W.S.; O'Keeffe, S.; Lewis, E. Portable 3-D Printed Plastic Optical Fibre Motion Sensor for Monitoring of Breathing Pattern and Respiratory Rate. In Proceedings of the IEEE 5th World Forum on Internet of Things (WF-IoT), Limerick, UK, 15–18 April 2019; pp. 144–148.
89. Kano, S.; Fujii, M. Battery-powered wearable respiration sensor chip with nanocrystal thin film. In Proceedings of the 2017 IEEE Sensors, Glasgow, UK, 29 October–1 November 2017; pp. 1–3.
90. Koch, E.; Dietzel, A. Stretchable sensor array for respiratory monitoring. In Proceedings of the 19th International Conference on Solid-State Sensors, Actuators and Microsystems (TRANSDUCERS), Kaohsiung, Taiwan, 18–22 June 2017; pp. 2227–2230.
91. Milici, S.; Lorenzo, J.; Lázaro, A.; Villarino, R.; Girbau, D. Wireless Breathing Sensor Based on Wearable Modulated Frequency Selective Surface. *IEEE Sens. J.* **2017**, *17*, 1285–1292. [CrossRef]
92. Nakazumi, R.; Inoue, M.; Yoshimi, T.; Fuchiyama, S.; Tsuchiya, H. Development of a respiration monitoring sensor for diving worker. In Proceedings of the 56th Annual Conference of the Society of Instrument and Control Engineers of Japan (SICE), Kanazawa, Japan, 19–22 September 2017; pp. 206–208.
93. Park, S.W.; Das, P.S.; Chhetry, A.; Park, J.Y. A Flexible Capacitive Pressure Sensor for Wearable Respiration Monitoring System. *IEEE Sens. J.* **2017**, *17*, 6558–6564. [CrossRef]
94. Presti, D.L.; Massaroni, C.; Formica, D.; Saccomandi, P.; Giurazza, F.; Caponero, M.A.; Schena, E. Smart Textile Based on 12 Fiber Bragg Gratings Array for Vital Signs Monitoring. *IEEE Sens. J.* **2017**, *17*, 6037–6043. [CrossRef]
95. Valipour, A.; Abbasi-Kesbi, R. A heartbeat and respiration rate sensor based on phonocardiogram for healthcare applications. In Proceedings of the Iranian Conference on Electrical Engineering (ICEE), Tehran, Iran, 2–4 May 2017; pp. 45–48.
96. White, N.M.; Ash, J.; Wei, Y.; Akerman, H. A Planar Respiration Sensor Based on a Capaciflector Structure. *IEEE Sens. Lett.* **2017**, *1*, 1–4. [CrossRef]
97. Yan, H.; Zhang, L.; Yu, P.; Mao, L. Sensitive and fast humidity sensor based on a redox conducting supramolecular ionic material for respiration monitoring. *Anal. Chem.* **2017**, *89*, 996–1001. [CrossRef]
98. Mahbub, I.; Wang, H.; Islam, S.K.; Pullano, S.A.; Fiorillo, A.S. A low power wireless breathing monitoring system using piezoelectric transducer. In Proceedings of the IEEE International Symposium on Medical Measurements and Applications (MeMeA), Benevento, Italy, 15–18 May 2016; pp. 1–5.
99. Mahbub, I.; Pullano, S.A.; Wang, H.; Islam, S.K.; Fiorillo, A.S.; To, G.; Mahfouz, M.R. A low-power wireless piezoelectric sensor-based respiration monitoring system realized in CMOS process. *IEEE Sens. J.* **2017**, *17*, 1858–1864. [CrossRef]
100. Chethana, K.; Guru Prasad, A.S.; Omkar, S.N.; Asokan, S. Fiber bragg grating sensor based device for simultaneous measurement of respiratory and cardiac activities. *J. Biophotonics* **2017**, *10*, 278–285. [CrossRef] [PubMed]
101. Güder, F.; Ainla, A.; Redston, J.; Mosadegh, B.; Glavan, A.; Martin, T.J.; Whitesides, G.M. Paper-based electrical respiration sensor. *Angew. Chem. Int. Ed.* **2016**, *55*, 5727–5732. [CrossRef] [PubMed]
102. Lepine, N.N.; Tajima, T.; Ogasawara, T.; Kasahara, R.; Koizumi, H. Robust respiration rate estimation using adaptive Kalman filtering with textile ECG sensor and accelerometer. In Proceedings of the 38th Annual International Conference of the IEEE Engineering in Medicine and Biology Society (EMBC), Orlando, FL, USA, 16–20 August 2016; pp. 3797–3800.
103. Massaroni, C.; Ciocchetti, M.; Di Tomaso, G.; Saccomandi, P.; Caponero, M.A.; Polimadei, A.; Formica, D.; Schena, E. Design and preliminary assessment of a smart textile for respiratory monitoring based on an array of Fiber Bragg Gratings. In Proceedings of the of the 38th Annual International Conference of the IEEE Engineering in Medicine and Biology Society (EMBC), Orlando, FL, USA, 16–20 August 2016; pp. 6054–6057.
104. Moradian, S.; Abdolvand, R. MEMS-based passive wireless respiration profile sensor. In Proceedings of the 2016 IEEE Sensors, Orlando, FL, USA, 30 October–3 November 2016; pp. 1–3.

105. Nag, A.; Mukhopadhyay, S.C.; Kosel, J. Flexible carbon nanotube nanocomposite sensor for multiple physiological parameter monitoring. *Sens. Actuators A Phys.* **2016**, *251*, 148–155. [CrossRef]
106. Nam, Y.; Reyes, B.A.; Chon, K.H. Estimation of Respiratory Rates Using the Built-in Microphone of a Smartphone or Headset. *IEEE J. Biomed. Health Inform.* **2016**, *20*, 1493–1501. [CrossRef] [PubMed]
107. Raji, A.; Kanchana Devi, P.; Golda Jeyaseeli, P.; Balaganesh, N. Respiratory monitoring system for asthma patients based on IoT. In Proceedings of the Online International Conference on Green Engineering and Technologies (IC-GET), Coimbatore, India, 19 November 2016; pp. 1–6.
108. Ramos-Garcia, R.I.; Da Silva, F.; Kondi, Y.; Sazonov, E.; Dunne, L.E. Analysis of a coverstitched stretch sensor for monitoring of breathing. In Proceedings of the 10th International Conference on Sensing Technology (ICST), Nanjing, China, 11–13 November 2016; pp. 1–6.
109. Rotariu, C.; Cristea, C.; Arotaritei, D.; Bozomitu, R.G.; Pasarica, A. Continuous respiratory monitoring device for detection of sleep apnea episodes. In Proceedings of the IEEE 22nd International Symposium for Design and Technology in Electronic Packaging (SIITME), Oradea, Romania, 20–23 October 2016; pp. 106–109.
110. Atalay, O.; Kennon, W.R.; Demirok, E. Weft-Knitted Strain Sensor for Monitoring Respiratory Rate and Its Electro-Mechanical Modeling. *IEEE Sens. J.* **2015**, *15*, 110–122. [CrossRef]
111. Ciocchetti, M.; Massaroni, C.; Saccomandi, P.; Caponero, M.A.; Polimadei, A.; Formica, D.; Schena, E. Smart textile based on fiber bragg grating sensors for respiratory monitoring: Design and preliminary trials. *Biosensors* **2015**, *5*, 602–615. [CrossRef]
112. Estrada, L.; Torres, A.; Sarlabous, L.; Jané, R. Respiratory signal derived from the smartphone built-in accelerometer during a Respiratory Load Protocol. In Proceedings of the 37th Annual International Conference of the IEEE Engineering in Medicine and Biology Society (EMBC), Milan, Italy, 25–29 August 2015; pp. 6768–6771.
113. Gargiulo, G.D.; Gunawardana, U.; O'Loughlin, A.; Sadozai, M.; Varaki, E.S.; Breen, P.P. A wearable contactless sensor suitable for continuous simultaneous monitoring of respiration and cardiac activity. *J. Sens.* **2015**, *2015*, 151859. [CrossRef]
114. Grlica, J.; Martinović, T.; Džapo, H. Capacitive sensor for respiration monitoring. In Proceedings of the IEEE Sensors Applications Symposium (SAS), Zadar, Croatia, 13–15 April 2015; pp. 1–6.
115. Hernandez, J.; McDuff, D.; Picard, R.W. Biowatch: Estimation of heart and breathing rates from wrist motions. In Proceedings of the 9th International Conference on Pervasive Computing Technologies for Healthcare (PervasiveHealth), Istanbul, Turkey, 20–23 May 2015; pp. 169–176.
116. Jiang, P.; Zhao, S.; Zhu, R. Smart Sensing Strip Using Monolithically Integrated Flexible Flow Sensor for Noninvasively Monitoring Respiratory Flow. *Sensors* **2015**, *15*, 31738–31750. [CrossRef]
117. Karlen, W.; Garde, A.; Myers, D.; Scheffer, C.; Ansermino, J.M.; Dumont, G.A. Estimation of Respiratory Rate From Photoplethysmographic Imaging Videos Compared to Pulse Oximetry. *IEEE J. Biomed. Health Inform.* **2015**, *19*, 1331–1338. [CrossRef]
118. Kazmi, S.A.; Shah, M.H.; Khan, S.; Khalifa, O.O. Respiratory rate (RR) based analysis of PPG signal for different physiological conditions. In Proceedings of the International Conference on Smart Sensors and Application (ICSSA), Kuala Lumpur, Malaysia, 26–28 May 2015; pp. 166–171.
119. Teichmann, D.; De Matteis, D.; Bartelt, T.; Walter, M.; Leonhardt, S. A Bendable and Wearable Cardiorespiratory Monitoring Device Fusing Two Noncontact Sensor Principles. *IEEE J. Biomed. Health Inform.* **2015**, *19*, 784–793. [CrossRef] [PubMed]
120. Wei, C.; Lin, Y.; Chen, T.; Lin, R.; Liu, T. Respiration Detection Chip with Integrated Temperature-Insensitive MEMS Sensors and CMOS Signal Processing Circuits. *IEEE Trans. Biomed. Circuits Syst.* **2015**, *9*, 105–112. [CrossRef] [PubMed]
121. Bifulco, P.; Gargiulo, G.D.; d'Angelo, G.; Liccardo, A.; Romano, M.; Clemente, F.; Cesarelli, M.; Angelo, G.; Liccardo, A.; Romano, M.; et al. Monitoring of respiration, seismocardiogram and heart sounds by a PVDF piezo film sensor. *Measurement* **2014**, *11*, 786–789.
122. Fekr, A.R.; Radecka, K.; Zilic, Z. Tidal volume variability and respiration rate estimation using a wearable accelerometer sensor. In Proceedings of the 4th International Conference on Wireless Mobile Communication and Healthcare—Transforming Healthcare Through Innovations in Mobile and Wireless Technologies (MOBIHEALTH), Athens, Greece, 3–5 November 2014; pp. 1–6.
123. Agcayazi, T.; Yokus, M.A.; Gordon, M.; Ghosh, T.; Bozkurt, A. A stitched textile-based capacitive respiration sensor. In Proceedings of the 2017 IEEE Sensors, Glasgow, UK, 29 October–1 November 2017; pp. 1–3.

124. Hesse, M.; Christ, P.; Hörmann, T.; Rückert, U. A respiration sensor for a chest-strap based wireless body sensor. In Proceedings of the 2014 IEEE Sensors, Valencia, Spain, 2–5 November 2014; pp. 490–493.
125. Krehel, M.; Schmid, M.; Rossi, R.; Boesel, L.; Bona, G.-L.; Scherer, L. An Optical Fibre-Based Sensor for Respiratory Monitoring. *Sensors* **2014**, *14*, 13088–13101. [CrossRef]
126. Min, S.D.; Yun, Y.; Shin, H. Simplified Structural Textile Respiration Sensor Based on Capacitive Pressure Sensing Method. *IEEE Sens. J.* **2014**, *14*, 3245–3251. [CrossRef]
127. Petrović, M.D.; Petrovic, J.; Daničić, A.; Vukčević, M.; Bojović, B.; Hadžievski, L.; Allsop, T.; Lloyd, G.; Webb, D.J. Non-invasive respiratory monitoring using long-period fiber grating sensors. *Biomed. Opt. Express* **2014**, *5*, 1136–1144. [CrossRef]
128. Sanchez, P.; Zamarreno, C.R.; Zamarreo, C.R.; Hernaez, M.; Matias, I.R.; Arregui, F.J. Exhaled breath optical fiber sensor based on LMRs for respiration monitoring. In Proceedings of the 2014 IEEE Sensors, Valencia, Spain, 2–5 November 2014; pp. 1142–1145.
129. Wo, J.; Wang, H.; Sun, Q.; Shum, P.P.; Liu, D. Noninvasive respiration movement sensor based on distributed Bragg reflector fiber laser with beat frequency interrogation. *J. Biomed. Opt.* **2014**, *19*, 17003. [CrossRef]
130. Yang, C.M.; Yang, T.L.; Wu, C.C.; Hung, S.H.; Liao, M.H.; Su, M.J.; Hsieh, H.C. Textile-based capacitive sensor for a wireless wearable breath monitoring system. In Proceedings of the IEEE International Conference on Consumer Electronics (ICCE), Las Vegas, NV, USA, 11–14 January 2014; pp. 232–233.
131. Yoon, J.-W.; Noh, Y.-S.; Kwon, Y.-S.; Kim, W.-K.; Yoon, H.-R. Improvement of dynamic respiration monitoring through sensor fusion of accelerometer and gyro-sensor. *J. Electr. Eng. Technol.* **2014**, *9*, 334–343. [CrossRef]
132. Chan, A.M.; Selvaraj, N.; Ferdosi, N.; Narasimhan, R. Wireless patch sensor for remote monitoring of heart rate, respiration, activity, and falls. In Proceedings of the 35th Annual international conference of the IEEE engineering in medicine and biology society (EMBC), Osaka, Japan, 3–7 July 2013; pp. 6115–6118.
133. Huang, Y.; Huang, K. Monitoring of breathing rate by a piezofilm sensor using pyroelectric effect. In Proceedings of the 1st International Conference on Orange Technologies (ICOT), Tainan, Taiwan, 12–16 March 2013; pp. 99–102.
134. Aileni, R.M.; Pasca, S.; Strungaru, R.; Valderrama, C. Biomedical signal acquisition for respiration monitoring by flexible analog wearable sensors. In Proceedings of the 2017 E-Health and Bioengineering Conference (EHB), Sinaia, Romania, 22–24 June 2017; pp. 81–84.
135. Padasdao, B.; Shahhaidar, E.; Stickley, C.; Boric-Lubecke, O. Electromagnetic Biosensing of Respiratory Rate. *IEEE Sens. J.* **2013**, *13*, 4204–4211. [CrossRef]
136. Chiu, Y.-Y.; Lin, W.-Y.; Wang, H.-Y.; Huang, S.-B.; Wu, M.-H. Development of a piezoelectric polyvinylidene fluoride (PVDF) polymer-based sensor patch for simultaneous heartbeat and respiration monitoring. *Sens. Actuators A Phys.* **2013**, *189*, 328–334. [CrossRef]
137. Favero, F.C.; Pruneri, V.; Villatoro, J. Microstructured optical fiber interferometric breathing sensor. *J. Biomed. Opt.* **2012**, *17*, 37006. [CrossRef] [PubMed]
138. Mathew, J.; Semenova, Y.; Farrell, G. A miniature optical breathing sensor. *Biomed. Opt. Express* **2012**, *3*, 3325–3331. [CrossRef] [PubMed]
139. Scully, C.G.; Lee, J.; Meyer, J.; Gorbach, A.M.; Granquist-Fraser, D.; Mendelson, Y.; Chon, K.H. Physiological Parameter Monitoring from Optical Recordings With a Mobile Phone. *IEEE Trans. Biomed. Eng.* **2012**, *59*, 303–306. [CrossRef] [PubMed]
140. Trobec, R.; Rashkovska, A.; Avbelj, V. Two proximal skin electrodes—A body sensor for respiration rate. *Sensors* **2012**, *12*, 13813–13828. [CrossRef] [PubMed]
141. Witt, J.; Narbonneau, F.; Schukar, M.; Krebber, K.; De Jonckheere, J.; Jeanne, M.; Kinet, D.; Paquet, B.; Depre, A.; D'Angelo, L.T.; et al. Medical Textiles with Embedded Fiber Optic Sensors for Monitoring of Respiratory Movement. *IEEE Sens. J.* **2012**, *12*, 246–254. [CrossRef]
142. Zięba, J.; Frydrysiak, M.; Błaszczyk, J. Textronic clothing with resistance textile sensor to monitoring frequency of human breathing. In Proceedings of the IEEE International Symposium on Medical Measurements and Applications Proceedings, Budapest, Hungary, 18–19 May 2012; pp. 1–6.
143. Carlos, R.; Coyle, S.; Corcoran, B.; Diamond, D.; Tomas, W.; Aaron, M.; Stroiescu, F.; Daly, K. Web-based sensor streaming wearable for respiratory monitoring applications. In Proceedings of the 2011 IEEE Sensors, Limerick, UK, 28–31 October 2011; pp. 901–903.

144. Ciobotariu, R.; Rotariu, C.; Adochiei, F.; Costin, H. Wireless breathing system for long term telemonitoring of respiratory activity. In Proceedings of the 7th International Symposium on Advanced Topics in Electrical (ATEE), Bucharest, Romania, 12–14 May 2011; pp. 1–4.
145. Basra, A.; Mukhopadhayay, B.; Kar, S. Temperature sensor based ultra low cost respiration monitoring system. In Proceedings of the 9th International Conference on Communication Systems and Networks (COMSNETS), Bengaluru, India, 4–8 January 2017; pp. 530–535.
146. Guo, L.; Berglin, L.; Li, Y.J.; Mattila, H.; Mehrjerdi, A.K.; Skrifvars, M. 'Disappearing Sensor'-Textile Based Sensor for Monitoring Breathing. In Proceedings of the International Conference on Control, Automation and Systems Engineering (CASE), Singapore, 30–31 July 2011; pp. 1–4.
147. Liu, S.; Gao, R.X.; Freedson, P.S. Non-invasive respiration and ventilation prediction using a single abdominal sensor belt. In Proceedings of the 2011 IEEE Signal Processing in Medicine and Biology Symposium (SPMB), New York, NY, USA, 10 December 2011; pp. 1–5.
148. Liu, G.-Z.; Guo, Y.-W.; Zhu, Q.-S.; Huang, B.-Y.; Wang, L. Estimation of respiration rate from three-dimensional acceleration data based on body sensor network. *Telemed. E-Health* **2011**, *17*, 705–711. [CrossRef]
149. Mann, J.; Rabinovich, R.; Bates, A.; Giavedoni, S.; MacNee, W.; Arvind, D.K. Simultaneous Activity and Respiratory Monitoring Using an Accelerometer. In Proceedings of the 2011 International Conference on Body Sensor Networks, Dallas, TX, USA, 23–25 May 2011; pp. 139–143.
150. Ono, T.; Takegawa, H.; Ageishi, T.; Takashina, M.; Numasaki, H.; Matsumoto, M.; Teshima, T. Respiratory monitoring with an acceleration sensor. *Phys. Med. Biol.* **2011**, *56*, 6279–6289. [CrossRef]
151. Silva, A.F.; Carmo, J.; Mendes, P.M.; Correia, J.H. Simultaneous cardiac and respiratory frequency measurement based on a single fiber Bragg grating sensor. *Meas. Sci. Technol. Meas. Sci. Technol.* **2011**, *22*, 75801. [CrossRef]
152. Yang, C.M.; Yang, T.; Wu, C.C.; Chu, N.N.Y. A breathing game with capacitive textile sensors. In Proceedings of the IEEE International Games Innovation Conference (IGIC), Orange, CA, USA, 2–3 November 2011; pp. 134–136.
153. Yoo, W.J.; Jang, K.W.; Seo, J.K.; Heo, J.Y.; Moon, J.S.; Jun, J.H.; Park, J.-Y.; Lee, B. Development of optical fiber-based respiration sensor for noninvasive respiratory monitoring. *Opt. Rev.* **2011**, *18*, 132–138. [CrossRef]
154. Yoo, W.-J.; Jang, K.-W.; Seo, J.-K.; Heo, J.-Y.; Moon, J.-S.; Park, J.-Y.; Lee, B.-S. Development of respiration sensors using plastic optical fiber for respiratory monitoring inside MRI system. *J. Opt. Soc. Korea* **2010**, *14*, 235–239. [CrossRef]
155. Yoo, W.; Jang, K.; Seo, J.; Heo, J.Y.; Moon, J.S.; Lee, B.; Park, J.-Y. Development of Nasal-cavity-and Abdomen-attached Fiber-optic Respiration Sensors. *J. Korean Phys. Soc.* **2010**, *57*, 1550–1554.
156. Bhattacharya, R.; Bandyopadhyay, N.; Kalaivani, S. Real time Android app based respiration rate monitor. In Proceedings of the International Conference of Electronics, Communication and Aerospace Technology (ICECA), Coimbatore, India, 20–22 April 2017; Volume 1, pp. 709–712.
157. Ansari, S.; Belle, A.; Najarian, K.; Ward, K. Impedance plethysmography on the arms: Respiration monitoring. In Proceedings of the IEEE International Conference on Bioinformatics and Biomedicine Workshops (BIBMW), Hong Kong, China, 18 December 2010; pp. 471–472.
158. De Jonckheere, J.; Jeanne, M.; Narbonneau, F.; Witt, J.; Paquet, B.; Kinet, D.; Kreber, K.; Logier, R. OFSETH: A breathing motions monitoring system for patients under MRI. In Proceedings of the Annual International Conference of the IEEE Engineering in Medicine and Biology, Buenos Aires, Argentina, 31 August–4 September 2010; pp. 1016–1019.
159. Mitchell, E.; Coyle, S.; O'Connor, N.E.; Diamond, D.; Ward, T. Breathing Feedback System with Wearable Textile Sensors. In Proceedings of the International Conference on Body Sensor Networks, Singapore, 7–9 June 2010; pp. 56–61.
160. Zhang, Z.; Wu, H.; Wang, W.; Wang, B. A smartphone based respiratory biofeedback system. In Proceedings of the 3rd International Conference on Biomedical Engineering and Informatics, Yantai, China, 16–18 October 2010; Volume 2, pp. 717–720.
161. Kundu, S.K.; Kumagai, S.; Sasaki, M. A wearable capacitive sensor for monitoring human respiratory rate. *Jpn. J. Appl. Phys.* **2013**, *52*, 04CL05. [CrossRef]
162. Das, T.; Guha, S.; Banerjee, N.; Basak, P. Development of thermistor based low cost high sensitive respiration rate measurement system using audio software with audio input. In Proceedings of the Third International Conference on Biosignals, Images and Instrumentation (ICBSII), Chennai, India, 16–18 March 2017; pp. 1–3.

163. Al-Wahedi, A.; Al-Shams, M.; Albettar, M.A.; Alawsh, S.; Muqaibel, A. Wireless Monitoring of Respiration and Heart Rates Using Software-Defined-Radio. In Proceedings of the 2019 16th International Multi-Conference on Systems, Signals & Devices (SSD), Istanbul, Turkey, 21–24 March 2019; pp. 529–532.
164. Chen, Y.; Kaneko, M.; Hirose, S.; Chen, W. Real-time Respiration Measurement during Sleep Using a Microwave Sensor. In Proceedings of the 41st Annual International Conference of the IEEE Engineering in Medicine and Biology Society (EMBC), Berlin, Germany, 23–27 July 2019; pp. 3791–3794.
165. Gunaratne, P.; Tamura, H.; Yoshida, C.; Sakurai, K.; Tanno, K.; Takahashi, N.; Nagata, J. A Study on Breathing and Heartbeat Monitoring System during Sleeping Using Multi-Piezoelectric Elements. In Proceedings of the 2019 Moratuwa Engineering Research Conference (MERCon), Moratuwa, Sri Lanka, 3–5 June 2019; pp. 382–387.
166. Guo, S.; Zhao, X.; Matsuo, K.; Liu, J.; Mukai, T. Unconstrained Detection of the Respiratory Motions of Chest and Abdomen in Different Lying Positions Using a Flexible Tactile Sensor Array. *IEEE Sens. J.* **2019**, *19*, 10067–10076. [CrossRef]
167. Isono, S.; Nozaki-Taguchi, N.; Hasegawa, M.; Kato, S.; Todoroki, S.; Masuda, S.; Iida, N.; Nishimura, T.; Noto, M.; Sato, Y. Contact-free unconstraint respiratory measurements with load cells under the bed in awake healthy volunteers: Breath-by-breath comparison with pneumotachography. *J. Appl. Physiol.* **2019**, *126*, 1432–1441. [CrossRef]
168. Ivanovs, A.; Nikitenko, A.; Di Castro, M.; Torims, T.; Masi, A.; Ferre, M. Multisensor low-cost system for real time human detection and remote respiration monitoring. In Proceedings of the Third IEEE 7International Conference on Robotic Computing (IRC), Naples, Italy, 25–27 February 2019; pp. 254–257.
169. Joshi, R.; Bierling, B.; Feijs, L.; van Pul, C.; Andriessen, P. Monitoring the respiratory rate of preterm infants using an ultrathin film sensor embedded in the bedding: A comparative feasibility study. *Physiol. Meas.* **2019**, *40*, 45003. [CrossRef]
170. Krej, M.; Baran, P.; Dziuda, Ł. Detection of respiratory rate using a classifier of waves in the signal from a FBG-based vital signs sensor. *Comput. Methods Programs Biomed.* **2019**, *177*, 31–38. [CrossRef]
171. Lorato, I.; Bakkes, T.; Stuijk, S.; Meftah, M.; De Haan, G. Unobtrusive respiratory flow monitoring using a thermopile array: A feasibility study. *Appl. Sci.* **2019**, *9*, 2449. [CrossRef]
172. Massaroni, C.; Lo Presti, D.; Formica, D.; Silvestri, S.; Schena, E. Non-contact monitoring of breathing pattern and respiratory rate via RGB signal measurement. *Sensors* **2019**, *19*, 2758. [CrossRef]
173. Park, S.; Choi, H.; Yang, H.C.; Yoon, J.; Shin, H. Force-Sensing-Based Unobtrusive System for Awakening and Respiration Rate Analysis during Sleep. *IEEE Sens. J.* **2019**, *19*, 1917–1924. [CrossRef]
174. Walterscheid, I.; Biallawons, O.; Berens, P. Contactless Respiration and Heartbeat Monitoring of Multiple People Using a 2-D Imaging Radar. In Proceedings of the 2019 41st Annual International Conference of the IEEE Engineering in Medicine and Biology Society (EMBC), Berlin, Germany, 23–27 July 2019; pp. 3720–3725.
175. Wang, T.; Zhang, D.; Wang, L.; Zheng, Y.; Gu, T.; Dorizzi, B.; Zhou, X. Contactless respiration monitoring using ultrasound signal with off-the-shelf audio devices. *IEEE Internet Things J.* **2018**, *6*, 2959–2973. [CrossRef]
176. Xu, X.; Yu, J.; Chen, Y.; Zhu, Y.; Kong, L.; Li, M. BreathListener: Fine-grained Breathing Monitoring in Driving Environments Utilizing Acoustic Signals. In Proceedings of the 17th Annual International Conference on Mobile Systems, Applications, and Services, Breckenridge, CO, USA, 17–20 June 2019; pp. 54–66.
177. Yang, Y.; Cao, J.; Liu, X.; Liu, X. Multi-Breath: Separate Respiration Monitoring for Multiple Persons with UWB Radar. In Proceedings of the IEEE 43rd Annual Computer Software and Applications Conference (COMPSAC), Milwaukee, WI, USA, 15–19 July 2019; Volume 1, pp. 840–849.
178. Chen, C.; Han, Y.; Chen, Y.; Lai, H.; Zhang, F.; Wang, B.; Liu, K.J.R. TR-BREATH: Time-Reversal Breathing Rate Estimation and Detection. *IEEE Trans. Biomed. Eng.* **2018**, *65*, 489–501. [CrossRef] [PubMed]
179. Chen, S.; Wu, N.; Ma, L.; Lin, S.; Yuan, F.; Xu, Z.; Li, W.; Wang, B.; Zhou, J. Noncontact heartbeat and respiration monitoring based on a hollow microstructured self-powered pressure sensor. *ACS Appl. Mater. Interfaces* **2018**, *10*, 3660–3667. [CrossRef] [PubMed]
180. Massaroni, C.; Schena, E.; Silvestri, S.; Taffoni, F.; Merone, M. Measurement system based on RBG camera signal for contactless breathing pattern and respiratory rate monitoring. In Proceedings of the IEEE International Symposium on Medical Measurements and Applications (MeMeA), Rome, Italy, 11–13 June 2018; pp. 1–6.

181. Massaroni, C.; Lo Presti, D.; Saccomandi, P.; Caponero, M.A.; D'Amato, R.; Schena, E. Fiber Bragg Grating Probe for Relative Humidity and Respiratory Frequency Estimation: Assessment During Mechanical Ventilation. *IEEE Sens. J.* **2018**, *18*, 2125–2130. [CrossRef]
182. Sadek, I.; Seet, E.; Biswas, J.; Abdulrazak, B.; Mokhtari, M. Nonintrusive Vital Signs Monitoring for Sleep Apnea Patients: A Preliminary Study. *IEEE Access* **2018**, *6*, 2506–2514. [CrossRef]
183. Azimi, H.; Soleimani Gilakjani, S.; Bouchard, M.; Bennett, S.; Goubran, R.A.; Knoefel, F. Breathing signal combining for respiration rate estimation in smart beds. In Proceedings of the IEEE International Symposium on Medical Measurements and Applications (MeMeA), Rochester, MN, USA, 7–10 May 2017; pp. 303–307.
184. Cho, Y.; Bianchi-Berthouze, N.; Julier, S.J.; Marquardt, N. ThermSense: Smartphone-based breathing sensing platform using noncontact low-cost thermal camera. In Proceedings of the 2017 7th International Conference on Affective Computing and Intelligent Interaction Workshops and Demos (ACIIW), San Antonio, TX, USA, 23–26 October 2017; pp. 83–84.
185. Leicht, L.; Vetter, P.; Leonhardt, S.; Teichmann, D. The PhysioBelt: A safety belt integrated sensor system for heart activity and respiration. In Proceedings of the 2017 IEEE International Conference on Vehicular Electronics and Safety (ICVES), Vienna, Austria, 27–28 June 2017; pp. 191–195.
186. Li, K.; Xu, W.; Zhan, N.; Wan, K.; Yu, C.; Yu, C. Non-wearable respiration monitoring based on Mach-Zehnder interferometer. In Proceedings of the Conference on Lasers and Electro-Optics Pacific Rim (CLEO-PR), Singapore, 31 July–4 August 2017; pp. 1–2.
187. Li, M.H.; Yadollahi, A.; Taati, B. Noncontact Vision-Based Cardiopulmonary Monitoring in Different Sleeping Positions. *IEEE J. Biomed. Health Inform.* **2017**, *21*, 1367–1375. [CrossRef]
188. Procházka, A.; Charvátová, H.; Vyšata, O.; Kopal, J.; Chambers, J. Breathing Analysis Using Thermal and Depth Imaging Camera Video Records. *Sensors* **2017**, *17*, 1408. [CrossRef] [PubMed]
189. Wang, X.; Huang, R.; Mao, S. SonarBeat: Sonar Phase for Breathing Beat Monitoring with Smartphones. In Proceedings of the 26th International Conference on Computer Communication and Networks (ICCCN), Vancouver, BC, Canada, 31 July–3 August 2017; pp. 1–8.
190. Kukkapalli, R.; Banerjee, N.; Robucci, R.; Kostov, Y. Micro-radar wearable respiration monitor. In Proceedings of the 2016 IEEE Sensors, Orlando, FL, USA, 30 October–3 November 2016; pp. 1–3.
191. Procházka, A.; Schätz, M.; Vyšata, O.; Vališ, M. Microsoft Kinect Visual and Depth Sensors for Breathing and Heart Rate Analysis. *Sensors* **2016**, *16*, 996. [CrossRef]
192. Tveit, D.M.; Engan, K.; Austvoll, I.; Meinich-Bache, Ø. Motion based detection of respiration rate in infants using video. In Proceedings of the IEEE International Conference on Image Processing (ICIP), Phoenix, AZ, USA, 25–28 September 2016; pp. 1225–1229.
193. Erden, F.; Alkar, A.Z.; Cetin, A.E. Contact-free measurement of respiratory rate using infrared and vibration sensors. *Infrared Phys. Technol.* **2015**, *73*, 88–94. [CrossRef]
194. Liu, J.J.; Huang, M.; Xu, W.; Zhang, X.; Stevens, L.; Alshurafa, N.; Sarrafzadeh, M. BreathSens: A Continuous On-Bed Respiratory Monitoring System With Torso Localization Using an Unobtrusive Pressure Sensing Array. *IEEE J. Biomed. Health Inform.* **2015**, *19*, 1682–1688. [CrossRef]
195. Pereira, C.B.; Yu, X.; Blazek, V.; Leonhardt, S. Robust remote monitoring of breathing function by using infrared thermography. In Proceedings of the 37th Annual International Conference of the IEEE Engineering in Medicine and Biology Society (EMBC), Milan, Italy, 25–29 August 2015; pp. 4250–4253.
196. Ravichandran, R.; Saba, E.; Chen, K.-Y.; Goel, M.; Gupta, S.; Patel, S.N. WiBreathe: Estimating respiration rate using wireless signals in natural settings in the home. In Proceedings of the IEEE International Conference on Pervasive Computing and Communications (PerCom), St. Louis, MO, USA, 23–27 March 2015; pp. 131–139.
197. Sasaki, E.; Kajiwara, A. Multiple Respiration Monitoring by Stepped-FM UWB Sensor. In Proceedings of the 2015 IEEE International Conference on Computational Intelligence Communication Technology, Ghaziabad, India, 13–14 February 2015; pp. 406–409.
198. Zakrzewski, M.; Vehkaoja, A.; Joutsen, A.S.; Palovuori, K.T.; Vanhala, J.J. Noncontact Respiration Monitoring During Sleep with Microwave Doppler Radar. *IEEE Sens. J.* **2015**, *15*, 5683–5693. [CrossRef]
199. Arlotto, P.; Grimaldi, M.; Naeck, R.; Ginoux, J.-M. An ultrasonic contactless sensor for breathing monitoring. *Sensors* **2014**, *14*, 15371–15386. [CrossRef] [PubMed]
200. Bernacchia, N.; Scalise, L.; Casacanditella, L.; Ercoli, I.; Marchionni, P.; Tomasini, E.P. Non contact measurement of heart and respiration rates based on Kinect™. In Proceedings of the 2014 IEEE International Symposium on Medical Measurements and Applications (MeMeA), Lisboa, Portugal, 11–12 June 2014; pp. 1–5.

201. Chen, Z.; Lau, D.; Teo, J.T.; Ng, S.H.; Yang, X.; Kei, P.L. Simultaneous measurement of breathing rate and heart rate using a microbend multimode fiber optic sensor. *J. Biomed. Opt.* **2014**, *19*, 1–11. [CrossRef] [PubMed]
202. Luis, J.; Roa Romero, L.M.; Galan, J.A.; Naranjo, D.; Estudillo-Valderrama, M.; Barbarov-Rostán, G.; Rubia-Marcos, C. Design and Implementation of a Smart Sensor for Respiratory Rate Monitoring. *Sensors* **2014**, *14*, 3019–3032. [CrossRef] [PubMed]
203. Mukai, T.; Matsuo, K.; Kato, Y.; Shimizu, A.; Guo, S. Determination of locations on a tactile sensor suitable for respiration and heartbeat measurement of a person on a bed. In Proceedings of the 36th Annual International Conference of the IEEE Engineering in Medicine and Biology Society, Chicago, IL, USA, 26–30 August 2014; pp. 66–69.
204. Nukaya, S.; Sugie, M.; Kurihara, Y.; Hiroyasu, T.; Watanabe, K.; Tanaka, H. A noninvasive heartbeat, respiration, and body movement monitoring system for neonates. *Artif. Life Robot.* **2014**, *19*, 414–419. [CrossRef]
205. Patwari, N.; Brewer, L.; Tate, Q.; Kaltiokallio, O.; Bocca, M. Breathfinding: A Wireless Network That Monitors and Locates Breathing in a Home. *IEEE J. Sel. Top. Signal Process.* **2014**, *8*, 30–42. [CrossRef]
206. Patwari, N.; Wilson, J.; Ananthanarayanan, S.; Kasera, S.K.; Westenskow, D.R. Monitoring Breathing via Signal Strength in Wireless Networks. *IEEE Trans. Mob. Comput.* **2014**, *13*, 1774–1786. [CrossRef]
207. Taheri, T.; Sant'Anna, A. Non-invasive breathing rate detection using a very low power ultra-wide-band radar. In Proceedings of the IEEE International Conference on Bioinformatics and Biomedicine (BIBM), Belfast, UK, 2–5 November 2014; pp. 78–83.
208. Bartula, M.; Tigges, T.; Muehlsteff, J. Camera-based system for contactless monitoring of respiration. In Proceedings of the 35th Annual International Conference of the IEEE Engineering in Medicine and Biology Society (EMBC), Osaka, Japan, 3–7 July 2013; pp. 2672–2675.
209. Chen, R.; Formenti, F.; Obeid, A.; Hahn, C.E.W.; Farmery, A. A fibre-optic oxygen sensor for monitoring human breathing. *Physiol. Meas.* **2013**, *34*, N71–N81. [CrossRef]
210. Dziuda, Ł.; Krej, M.; Skibniewski, F.W. Fiber Bragg Grating Strain Sensor Incorporated to Monitor Patient Vital Signs during MRI. *IEEE Sens. J.* **2013**, *13*, 4986–4991. [CrossRef]
211. Klap, T.; Shinar, Z. Using piezoelectric sensor for continuous-contact-free monitoring of heart and respiration rates in real-life hospital settings. In Proceedings of the Computing in Cardiology, Zaragoza, Spain, 22–25 September 2013; pp. 671–674.
212. Šprager, S.; Zazula, D. Detection of heartbeat and respiration from optical interferometric signal by using wavelet transform. *Comput. Methods Programs Biomed.* **2013**, *111*, 41–51. [CrossRef]
213. Vinci, G.; Lindner, S.; Barbon, F.; Mann, S.; Hofmann, M.; Duda, A.; Weigel, R.; Koelpin, A. Six-port radar sensor for remote respiration rate and heartbeat vital-sign monitoring. *IEEE Trans. Microw. Theory Tech.* **2013**, *61*, 2093–2100. [CrossRef]
214. Yavari, E.; Jou, H.; Lubecke, V.; Boric-Lubecke, O. Doppler radar sensor for occupancy monitoring. In Proceedings of the IEEE Topical Conference on Power Amplifiers for Wireless and Radio Applications, Santa Clara, CA, USA, 20 January 2013; pp. 145–147.
215. Aoki, H.; Miyazaki, M.; Nakamura, H.; Furukawa, R.; Sagawa, R.; Kawasaki, H. Non-contact respiration measurement using structured light 3-D sensor. In Proceedings of the SICE Annual Conference (SICE), Akita, Japan, 20–23 August 2012; pp. 614–618.
216. Boccanfuso, L.; O'Kane, J.M. Remote measurement of breathing rate in real time using a high precision, single-point infrared temperature sensor. In Proceedings of the 4th IEEE RAS EMBS International Conference on Biomedical Robotics and Biomechatronics (BioRob), Rome, Italy, 24–27 June 2012; pp. 1704–1709.
217. Brüser, C.; Kerekes, A.; Winter, S.; Leonhardt, S. Multi-channel optical sensor-array for measuring ballistocardiograms and respiratory activity in bed. In Proceedings of the Annual International Conference of the IEEE Engineering in Medicine and Biology Society, San Diego, CA, USA, 28 August–1 September 2012; pp. 5042–5045.
218. Chen, Z.; Teo, J.T.; Ng, S.H.; Yang, X. Plastic optical fiber microbend sensor used as breathing sensor. In Proceedings of the 2012 IEEE Sensors, Taipei, Taiwan, 28–31 October 2012; pp. 1–4.
219. Gu, C.; Li, R.; Zhang, H.; Fung, A.Y.C.; Torres, C.; Jiang, S.B.; Li, C. Accurate respiration measurement using DC-coupled continuous-wave radar sensor for motion-adaptive cancer radiotherapy. *IEEE Trans. Biomed. Eng.* **2012**, *59*, 3117–3123. [PubMed]

220. Lokavee, S.; Puntheeranurak, T.; Kerdcharoen, T.; Watthanwisuth, N.; Tuantranont, A. Sensor pillow and bed sheet system: Unconstrained monitoring of respiration rate and posture movements during sleep. In Proceedings of the IEEE International Conference on Systems, Man, and Cybernetics (SMC), Seoul, Korea, 14–17 October 2012; pp. 1564–1568.
221. Shimomura, N.; Otsu, M.; Kajiwara, A. Empirical study of remote respiration monitoring sensor using wideband system. In Proceedings of the 6th International Conference on Signal Processing and Communication Systems, Gold Coast, Australia, 12–14 December 2012; pp. 1–5.
222. Xia, J.; Siochi, R.A. A real-time respiratory motion monitoring system using KINECT: Proof of concept. *Med. Phys.* **2013**, *39*, 2682–2685. [CrossRef] [PubMed]
223. Lai, J.C.Y.; Xu, Y.; Gunawan, E.; Chua, E.C.; Maskooki, A.; Guan, Y.L.; Low, K.; Soh, C.B.; Poh, C. Wireless Sensing of Human Respiratory Parameters by Low-Power Ultrawideband Impulse Radio Radar. *IEEE Trans. Instrum. Meas.* **2011**, *60*, 928–938. [CrossRef]
224. Otsu, M.; Nakamura, R.; Kajiwara, A. Remote respiration monitoring sensor using stepped-FM. In Proceedings of the IEEE Sensors Applications Symposium, San Antonio, TX, USA, 22–24 February 2011; pp. 155–158.
225. Postolache, O.; Girão, P.S.; Postolache, G.; Gabriel, J. Cardio-respiratory and daily activity monitor based on FMCW Doppler radar embedded in a wheelchair. In Proceedings of the Annual International Conference of the IEEE Engineering in Medicine and Biology Society, Boston, MA, USA, 30 August–3 September 2011; pp. 1917–1920.
226. Zito, D.; Pepe, D.; Mincica, M.; Zito, F.; Tognetti, A.; Lanata, A.; De Rossi, D. SoC CMOS UWB pulse radar sensor for contactless respiratory rate monitoring. *IEEE Trans. Biomed. Circuits Syst.* **2011**, *5*, 503–510. [CrossRef]
227. Heise, D.; Skubic, M. Monitoring pulse and respiration with a non-invasive hydraulic bed sensor. In Proceedings of the Annual International Conference of the IEEE Engineering in Medicine and Biology, Buenos Aires, Argentina, 31 August–4 September 2010; pp. 2119–2123.
228. Min, S.D.; Kim, J.K.; Shin, H.S.; Yun, Y.H.; Lee, C.K.; Lee, M. Noncontact Respiration Rate Measurement System Using an Ultrasonic Proximity Sensor. *IEEE Sens. J.* **2010**, *10*, 1732–1739. [CrossRef]
229. Mostov, K.; Liptsen, E.; Boutchko, R. Medical applications of shortwave FM radar: Remote monitoring of cardiac and respiratory motion. *Med. Phys.* **2010**, *37*, 1332–1338. [CrossRef]
230. Nishiyama, M.; Miyamoto, M.; Watanabe, K. Respiration rhythm monitoring in sleep based on weight movement using hetero-core fiber optic sensors. In Proceedings of the ICCAS 2010, Gyeonggi-do, Korea, 27–30 October 2010; pp. 205–208.
231. Nishyama, M.; Miyamoto, M.; Watanabe, K. Respiration and body movement analysis during sleep in bed using hetero-core fiber optic pressure sensors without constraint to human activity. *J. Biomed. Opt.* **2011**, *16*, 17002. [CrossRef]
232. Scalise, L.; Marchionni, P.; Ercoli, I. Optical method for measurement of respiration rate. In Proceedings of the IEEE International Workshop on Medical Measurements and Applications, Ottawa, ON, Canada, 30 April–1 May 2010; pp. 19–22.
233. Silvious, J.; Tahmoush, D. UHF measurement of breathing and heartbeat at a distance. In Proceedings of the IEEE Radio and Wireless Symposium (RWS), New Orleans, LA, USA, 10–14 January 2010; pp. 567–570.
234. Tan, K.S.; Saatchi, R.; Elphick, H.; Burke, D. Real-time vision based respiration monitoring system. In Proceedings of the 7th International Symposium on Communication Systems, Networks Digital Signal Processing (CSNDSP 2010), Newcastle upon Tyne, UK, 21–23 July 2010; pp. 770–774.
235. Brady, S.; Dunne, L.E.; Tynan, R.; Diamond, D.; Smyth, B.; O'Hare, G.M.P. Garment-based monitoring of respiration rate using a foam pressure sensor. In Proceedings of the Ninth IEEE International Symposium on Wearable Computers (ISWC'05), Osaka, Japan, 18–21 October 2005; pp. 214–215.
236. Dziuda, L.; Skibniewski, F.; Rozanowski, K.; Krej, M.; Lewandowski, J. Fiber-optic sensor for monitoring respiration and cardiac activity. In Proceedings of the 2011 IEEE Sensors, Limerick, UK, 28–31 October 2011; pp. 413–416.
237. Gutierrez Pascual, M.D. Indoor Location Systems Based on Zigbee Networks. Bachelor's Thesis, Faculty of Computing, Karlskrona, Sweden, 2012.
238. Wei, Y.-H.; Leng, Q.; Han, S.; Mok, A.K.; Zhang, W.; Tomizuka, M. RT-WiFi: Real-time high-speed communication protocol for wireless cyber-physical control applications. In Proceedings of the IEEE 34th Real-Time Systems Symposium, Vancouver, BC, Canada, 3–6 December 2013; pp. 140–149.

239. Bettstetter, C.; Vogel, H.-J.; Eberspacher, J. GSM phase 2+ general packet radio service GPRS: Architecture, protocols, and air interface. *IEEE Commun. Surv.* **1999**, *2*, 2–14. [CrossRef]
240. Delnavaz, A.; Voix, J. Electromagnetic micro-power generator for energy harvesting from breathing. In Proceedings of the IECON 38th Annual Conference on IEEE Industrial Electronics Society, Montreal, QC, Canada, 25–28 October 2012; pp. 984–988.
241. Goreke, U.; Habibiabad, S.; Azgin, K.; Beyaz, M.I. A MEMS turbine prototype for respiration harvesting. *Proc. J. Phys. Conf. Ser.* **2015**, *660*, 12059. [CrossRef]
242. Shahhaidar, E.; Padasdao, B.; Romine, R.; Stickley, C.; Boric-Lubecke, O. Piezoelectric and electromagnetic respiratory effort energy harvesters. In Proceedings of the 35th Annual International Conference of the IEEE Engineering in Medicine and Biology Society (EMBC), Osaka, Japan, 3–7 July 2013; pp. 3439–3442.
243. Li, K.; He, Q.; Wang, J.; Zhou, Z.; Li, X. Wearable energy harvesters generating electricity from low-frequency human limb movement. *Microsyst. Nanoeng.* **2018**, *4*, 1–13. [CrossRef]
244. Wang, J.-J.; Su, H.-J.; Hsu, C.-I.; Su, Y.-C. Composite piezoelectric rubber band for energy harvesting from breathing and limb motion. *Proc. J. Phys. Conf. Ser.* **2014**, *557*, 12022. [CrossRef]
245. Sun, C.; Shi, J.; Bayerl, D.J.; Wang, X. PVDF microbelts for harvesting energy from respiration. *Energy Environ. Sci.* **2011**, *4*, 4508–4512. [CrossRef]
246. Zhang, Z.; Zhang, J.; Zhang, H.; Wang, H.; Hu, Z.; Xuan, W.; Dong, S.; Luo, J. A Portable Triboelectric Nanogenerator for Real-Time Respiration Monitoring. *Nanoscale Res. Lett.* **2019**, *14*, 354. [CrossRef] [PubMed]
247. Vasandani, P.; Gattu, B.; Wu, J.; Mao, Z.-H.; Jia, W.; Sun, M. Triboelectric nanogenerator using microdome-patterned PDMS as a wearable respiratory energy harvester. *Adv. Mater. Technol.* **2017**, *2*, 1700014. [CrossRef]
248. Seo, M.-H.; Choi, D.-H.; Han, C.-H.; Yoo, J.-Y.; Yoon, J.-B. An electrostatic energy harvester exploiting variable-area water electrode by respiration. In Proceedings of the 28th IEEE International Conference on Micro Electro Mechanical Systems (MEMS), Estoril, Portugal, 18–22 January 2015; pp. 126–129.
249. Xue, H.; Yang, Q.; Wang, D.; Luo, W.; Wang, W.; Lin, M.; Liang, D.; Luo, Q. A wearable pyroelectric nanogenerator and self-powered breathing sensor. *Nano Energy* **2017**, *38*, 147–154. [CrossRef]
250. Fan, F.-R.; Tian, Z.-Q.; Wang, Z.L. Flexible triboelectric generator. *Nano Energy* **2012**, *1*, 328–334. [CrossRef]
251. Aljadiri, R.T.; Taha, L.Y.; Ivey, P. Electrostatic energy harvesting systems: A better understanding of their sustainability. *J. Clean Energy Technol.* **2017**, *5*, 409–416. [CrossRef]
252. Nozariasbmarz, A.; Collins, H.; Dsouza, K.; Polash, M.H.; Hosseini, M.; Hyland, M.; Liu, J.; Malhotra, A.; Ortiz, F.M.; Mohaddes, F.; et al. Review of wearable thermoelectric energy harvesting: From body temperature to electronic systems. *Appl. Energy* **2020**, *258*, 114069. [CrossRef]
253. Enescu, D. Thermoelectric Energy Harvesting: Basic Principles and Applications. In *Green Energy Advances*; IntechOpen: London, UK, 2019.
254. Vanegas, E.; Igual, R.; Plaza, I. Piezoresistive Breathing Sensing System with 3D Printed Wearable Casing. *J. Sens.* **2019**, *2019*. [CrossRef]
255. Doerffel, D.; Sharkh, S.A. A critical review of using the Peukert equation for determining the remaining capacity of lead-acid and lithium-ion batteries. *J. Power Sources* **2006**, *155*, 395–400. [CrossRef]
256. Kirchev, A. Battery management and battery diagnostics. In *Electrochemical Energy Storage for Renewable Sources and Grid Balancing*; Elsevier: Amsterdam, The Netherlands, 2015; pp. 411–435.
257. Lee, S.; Kim, J.; Lee, J.; Cho, B.H. State-of-charge and capacity estimation of lithium-ion battery using a new open-circuit voltage versus state-of-charge. *J. Power Sources* **2008**, *185*, 1367–1373. [CrossRef]
258. Association, W.M. World Medical Association Declaration of Helsinki. Ethical principles for medical research involving human subjects. *Bull. World Health Organ.* **2001**, *79*, 373–374.
259. Zhu, W.; Zeng, N.; Wang, N. Sensitivity, Specificity, Accuracy, Associated Confidence Interval and ROC Analysis with Practical SAS ®Implementations. *Health Care Life Sci.* **2010**, *19*, 67.
260. The R Foundation. The R Project for Statistical Computing. Available online: https://www.r-project.org/ (accessed on 20 March 2020).
261. Microsoft C#. Available online: https://docs.microsoft.com/es-es/dotnet/csharp/ (accessed on 3 August 2020).
262. Team, O. OpenCV. Available online: https://opencv.org/about/ (accessed on 20 March 2020).
263. Microsoft Kinect for Windows. Available online: https://www.microsoft.com/en-us/download/details.aspx?id=40278 (accessed on 20 March 2020).

264. ADINSTRUMENTS. LabChart Lightning. Available online: https://www.adinstruments.com/products/labchart (accessed on 20 March 2020).
265. Biopac Systems Inc. Acqknowledge Software. Available online: https://www.biopac.com/product/acqknowledge-software/ (accessed on 20 March 2020).
266. National Instruments LabWindows/CVI. 2020. Available online: http://sine.ni.com/nips/cds/view/p/lang/es/nid/11104 (accessed on 18 September 2020).
267. MathWorks Peak Analysis. Available online: https://es.mathworks.com/help/signal/examples/peak-analysis.html (accessed on 1 July 2020).
268. Mallat, S. *A Wavelet Tour of Signal Processing*; Academic Press: Boston, MA, USA, 2009; ISBN 978-0-12-374370-1.
269. Jawerth, B.; Sweldens, W. An overview of wavelet based multiresolution analyses. *SIAM Rev.* **1994**, *36*, 377–412. [CrossRef]
270. Welch, G.; Bishop, G. *An Introduction to the Kalman Filter*; Citeseer: University Park, PA, USA, 1995.
271. Chen, A.T.-Y.; Biglari-Abhari, M.; Wang, K.I.-K. Trusting the Computer in Computer Vision: A Privacy-Affirming Framework. In Proceedings of the IEEE Conference on Computer Vision and Pattern Recognition (CVPR) Workshops, Honolulu, HI, USA, 21–26 July 2017.
272. Venkatesh, V.; Morris, M.G.; Davis, G.B.; Davis, F.D. User Acceptance of Information Technology: Toward a Unified View. *MIS Q.* **2003**, *27*, 425–478. [CrossRef]
273. Sundaravej, T. Empirical Validation of Unified Theory of Acceptance and Use of Technology Model. *J. Glob. Inf. Technol. Manag.* **2010**, *13*, 5–27.
274. Moon, Y.-J.; Hwang, Y.-H.; Cho, S. An Empirical Study of Impacts of User Intention for Smart Wearable Devices and Use Behavior. *Adv. Multimed. Ubiquitous Eng.* **2016**, *354*, 357–365. [CrossRef]
275. Wolbring, G.; Leopatra, V. Sensors: Views of Staff of a Disability Service Organization. *J. Pers. Med.* **2013**, *3*, 23–39. [CrossRef]
276. Gao, Y.; Li, H.; Luo, Y. An empirical study of wearable technology acceptance in healthcare. *Ind. Manag. Data Syst.* **2015**, *115*, 1704–1723. [CrossRef]
277. Alam, M.Z.; Hu, W.; Barua, Z. Using the UTAT model to determine factors affecting acceptance and use of mobile health (mHealth) services in Bangladesh. *J. Stud. Soc. Sci.* **2018**, *3*, 137–172.
278. Lo Presti, D.; Romano, C.; Massaroni, C.; Abbraccio, J.D.; Massari, L.; Caponero, M.A.; Oddo, C.M.; Formica, D.; Schena, E. Cardio-Respiratory Monitoring in Archery Using a Smart Textile Based on Flexible Fiber Bragg Grating Sensors. *Sensors* **2019**, *19*, 3581. [CrossRef] [PubMed]
279. Igual, R.; Medrano, C.; Plaza, I.; Orrite, C. Adaptive tracking algorithms to improve the use of computing resources. *IET Comput. Vis.* **2013**, *7*, 415–424. [CrossRef]
280. Kim, J.D.; Lee, W.H.; Lee, Y.; Lee, H.J.; Cha, T.; Kim, S.H.; Song, K.-M.; Lim, Y.-H.; Cho, S.H.; Cho, S.H.; et al. Non-contact respiration monitoring using impulse radio ultrawideband radar in neonates. *R. Soc. Open Sci.* **2019**, *6*, 190149. [CrossRef] [PubMed]
281. Giavarina, D. Understanding Bland Altman analysis. *Biochem. Med.* **2015**, 141–151. [CrossRef]
282. Barré, A.; Deguilhem, B.; Grolleau, S.; Gérard, M.; Suard, F.; Riu, D. A review on lithium-ion battery ageing mechanisms and estimations for automotive applications. *J. Power Sources* **2013**, *241*, 680–689. [CrossRef]

Anexo J

Force-Sensitive Mat for Vertical Jump Measurement to Assess Lower Limb Strength: Validity and Reliability Study

Original Paper

Force-Sensitive Mat for Vertical Jump Measurement to Assess Lower Limb Strength: Validity and Reliability Study

Erik Vanegas[1*], MSc; Yolocuauhtli Salazar[2*], PhD; Raúl Igual[1*], PhD; Inmaculada Plaza[1*], PhD

[1]Electrical/Electronics Engineering and Communications Department, EUP Teruel, Universidad de Zaragoza, Teruel, Spain

[2]Tecnológico Nacional de México, IT Durango, Durango, Mexico

[*]all authors contributed equally

Corresponding Author:
Erik Vanegas, MSc
Electrical/Electronics Engineering and Communications Department, EUP Teruel
Universidad de Zaragoza
Atarazana 2
Teruel, 44003
Spain
Phone: 34 978618102
Email: erikvanegas599@gmail.com

Abstract

Background: Vertical jump height is widely used in health care and sports fields to assess muscle strength and power from lower limb muscle groups. Different approaches have been proposed for vertical jump height measurement. Some commonly used approaches need no sensor at all; however, these methods tend to overestimate the height reached by the subjects. There are also novel systems using different kind of sensors like force-sensitive resistors, capacitive sensors, and inertial measurement units, among others, to achieve more accurate measurements.

Objective: The objective of this study is twofold. The first objective is to validate the functioning of a developed low-cost system able to measure vertical jump height. The second objective is to assess the effects on obtained measurements when the sampling frequency of the system is modified.

Methods: The system developed in this study consists of a matrix of force-sensitive resistor sensors embedded in a mat with electronics that allow a full scan of the mat. This mat detects pressure exerted on it. The system calculates the jump height by using the flight-time formula, and the result is sent through Bluetooth to any mobile device or PC. Two different experiments were performed. In the first experiment, a total of 38 volunteers participated with the objective of validating the performance of the system against a high-speed camera used as reference (120 fps). In the second experiment, a total of 15 volunteers participated. Raw data were obtained in order to assess the effects of different sampling frequencies on the performance of the system with the same reference device. Different sampling frequencies were obtained by performing offline downsampling of the raw data. In both experiments, countermovement jump and countermovement jump with arm swing techniques were performed.

Results: In the first experiment an overall mean relative error (MRE) of 1.98% and a mean absolute error of 0.38 cm were obtained. Bland-Altman and correlation analyses were performed, obtaining a coefficient of determination equal to R^2=.996. In the second experiment, sampling frequencies of 200 Hz, 100 Hz, and 66.6 Hz show similar performance with MRE below 3%. Slower sampling frequencies show an exponential increase in MRE. On both experiments, when dividing jump trials in different heights reached, a decrease in MRE with higher height trials suggests that the precision of the proposed system increases as height reached increases.

Conclusions: In the first experiment, we concluded that results between the proposed system and the reference are systematically the same. In the second experiment, the relevance of a sufficiently high sampling frequency is emphasized, especially for jump trials whose height is below 10 cm. For trials with heights above 30 cm, MRE decreases in general for all sampling frequencies, suggesting that at higher heights reached, the impact of high sampling frequencies is lesser.

(JMIR Mhealth Uhealth 2021;9(4):e27336) doi: 10.2196/27336

KEYWORDS

vertical jump; mHealth; mobile health; force-sensitive resistor; lower limb strength; leg strength

Introduction

Vertical jump height is one of the physical skills commonly used to assess overall performance in human beings, and more specifically, it is used to assess performance and muscle power of the quadriceps, hamstrings, and gastrocnemius muscle groups in the lower limbs [1,2]. Measurement of the performance of this skill is commonly performed on athletes in sports like basketball [3,4], football [5], netball [6], swimming [7], and others. This skill performance can also provide important data from people with no relevant sports past.

In the literature, there are many protocols to prove or validate the proposed systems. Among the different kind of jumps performed in those protocols, there are jumps with and without countermovement [1,4,5,8-15], jumps with and without arm swing [12,16], drop jumps [1,8,17], single and double leg jump [6], continuous jumps [4,17], squat jumps [1,2,4,12], and loaded squat jumps [7]. With any of these types of jumps, height reached by the user can be analyzed, but the jumps most commonly used in all related work are the countermovement and squat jumps.

Kibele [15] and Moir [18] reported that irregularities detected in measurements of any kind of jump execution may be linked to changes in the posture of a subject during flight due to change in the center of mass of the subject during the jump. Bui et al [13] found that some common errors obtained during measurement were caused by body movements like knee, hip, and ankle bending during flight time and landing. Also, Aragon-Vargas [19] states that ascending and descending phases of flight time must be of the same length of time, but in his work descending time was significantly longer, suggesting that participants descended with their bodies partially crouched.

There are several techniques to measure jump height, each of which uses a different kind of sensor or no sensors at all. Methods like the Sargent jump [13] and Vertec device [6,9,10] require no sensors and often are used as reference measurements. However, these methods often show overestimation on jump height, and this could be due to arm stretching performed unconsciously by the user. Among systems developed in the literature, different kind of sensors are used like force-sensitive resistors (FSRs) [3,16], capacitive sensors [5], inertial measurement units [2,4,8,10,17], electromyography sensors [1,6], kinematic sensors [6], ultrasonic sensors [20], microswitches [9], video cameras, [11] and optical sensors [4,12].

The studies of Drazan et al [3] and Boukhenous and Attari [16] are most closely related to our work, as both of their systems also use resistive sensors. However, only one sensor is used for the whole sensing area. Drazan et al [3] proposed a system based on a single FSR sensor whose total sensing area is around 3 cm^2, with an Arduino board as microcontroller. This system calculated jump height through the flight-time formula, by measuring the time the FSR sensor is not detecting any pressure. In the work presented by Boukhenous and Attari [16], two metallic strain gauges were placed in the center of a rigid platform to measure the force applied by the ground. In this case, vertical ground reaction forces were used to calculate jump height. Rico et al [2] used pressure sensors located at the forefoot of the user to calculate flight time during vertical jump and compare it with data obtained from an inertial measurement unit system. However, few or no specific number of subjects are used in these studies, and no specific protocols or jump trials are performed. Also, no reference systems are used to compare the performance of the developed systems.

Camera-based systems are used as reference systems or as proposed methods to validate. In some studies, the famous motion capture system commonly used in videogames is used as a reference device [5,17,21]. Other studies use a similar method by tracking body markers placed strategically on the body [4,14,21]. Balsalobre-Fernandez et al [11,22] have analyzed the effectiveness and reliability of high-speed cameras as methods to estimate vertical jump height. In these studies, flight time of the subject is calculated by selecting the takeoff and landing frames of the recorded videos of jump trials, and, by applying the flight-time formula, jump height is obtained [3,8,9,11,14,16,22].

Only a few studies perform a validation with a relatively high number of subjects. Some studies that fulfill this criterion are the ones presented by Nuzzo et al [10], Casartelli et al [4], Glatthorn et al [12], Moir [18], and Aragon-Vargas [19]. However, these studies compare different commercially available devices (contact mat, force plate, cameras, etc), and no novel system is developed by the researchers. Bui et al [13] fulfills the criterion and proposes a novel optical system whose performance is compared against commercial devices. This system calculates jump height through the flight-time formula.

This study presents a newly developed low-cost system for measuring height reached by users during vertical jump comprising a matrix of FSR sensors embedded on a mat. The height of the vertical jump is calculated through the flight-time formula [3,8,9,14,16]. One advantage this system offers against other pressure-sensitive systems [2,3,16] is a higher real sensing area, higher resolution, and higher precision, as this system works with 256 FSR sensors distributed around the mat in 16 rows and 16 columns, in comparison with the other systems that use a single sensor. The total sensing area, dimensions of FSR sensors matrix, and each individual FSR sensor area can be modified on different versions of the proposed mat. Also, as this system is environmental, it needs no adjustment regardless of the physical characteristics of the user like body type, weight, height, or foot size [2]. Another advantage of this system is that the calculated vertical jump height is directly sent to a PC or mobile device of the health care professional's choice, unlike other methods that require postprocessing analysis, as in the high-speed camera method. The main objective of this study is to validate the reliability of the proposed system for future clinical studies.

Methods

System Construction

The proposed system consists of 2 parts: a resistive pressure-sensitive mat constructed with an FSR sensor array and the electronic system. The mat is composed of 3 layers.

One layer contains thin and flat copper wires distributed in a column arrangement along a flexible 3D printed grid; another layer is composed of the same copper wires but distributed in a row arrangement on another flexible 3D printed grid. A third layer is placed between the layers consisting of Velostat material, a pressure-sensitive material that behaves as a resistor whose value drops whenever pressure is exerted upon it. In this way, variations on the resistance values on every intersection of rows and columns when pressure is exerted over the mat can be measured. Some typical characteristic problems with Velostat material are repeatability, nonlinearity, and hysteresis [23,24]. For this application, however, these features are not relevant because high precision is not needed; the mat only needs to be able to detect a heavy body placed on it (average human body weight). More information about the development of this mat is documented on the work of Medrano et al [25].

Figure 1 shows the different layers of an FSR matrix with smaller dimensions (4 rows and 4 columns). Figure 2 shows an example of the placement of the overlapped layers. The total sensing area of the mat used for this study is 30×30 cm, with 16 rows and 16 columns, 1 cm width each. This way, the area of each of the individual FSR sensors is equal to 1 cm^2. In Figure 3, a developed mat is shown.

Figure 1. Different layers comprising a force-sensitive resistor matrix with smaller dimensions.

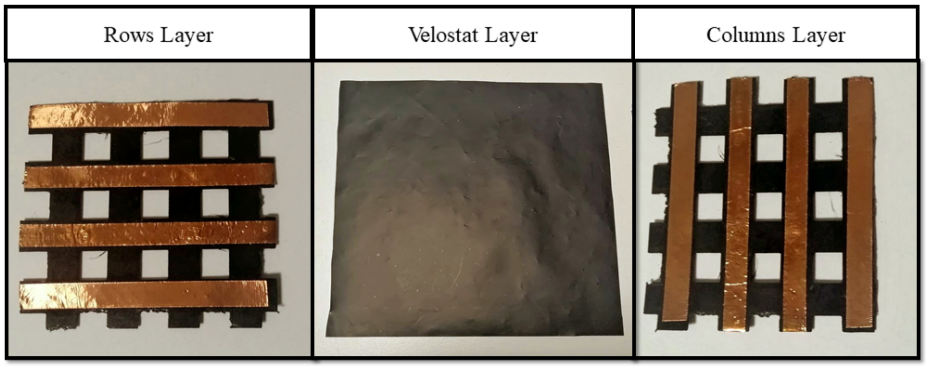

Figure 2. Example of a smaller size matrix and how layers are placed.

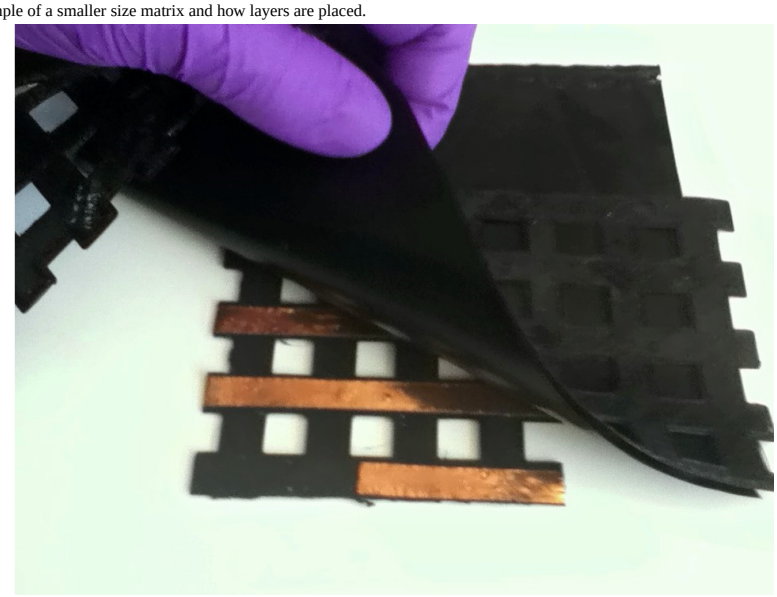

Figure 3. Developed force-sensitive resistor sensor mat.

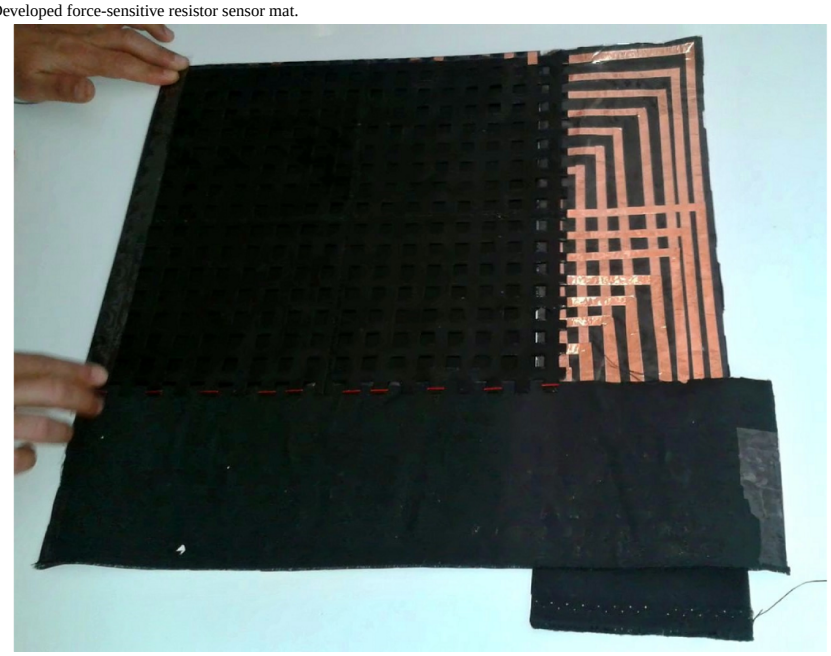

Due to the number of operations needed for a full scan of the mat, a high frequency microprocessor must be used for data processing, as the time complexity of these operations grows in exponential order. The STM32F103C8T6 microprocessor (STMicroelectronics) was selected due to its 72 MHz CPU frequency, with which a sampling frequency of 200 Hz is achieved. Other microprocessors with lower CPU frequencies (like the ATmega328P, Microchip Technology Inc) would not achieve the desired sampling frequency. Also two 16-1 multiplexers 74HC4067 are needed for an efficient scan process of the whole mat. For data transmission, a Bluetooth HC-05 module is used. Bluetooth technology was selected due to its ease of connection with different devices, especially with smartphones and tablets, which offers health care professionals the choice of an easy-to-transport monitoring device. Other electronic elements included in the system are a TP4056 battery-charging module and a Lipo battery of 3.7 V and 150 mAh capacity, allowing continuous functioning of the system for up to 2 hrs. A block diagram of the proposed system is shown in Figure 4.

The algorithm used for this system consists of calculating the summation of every FSR sensor of the mat. For each FSR sensor, the voltage value obtained by the analog-to-digital converter of the microcontroller is given in bits (from 0 to 4095), and this resulting value is used for the calculations. A threshold is used for the system to decide whether a person is standing on the mat or not. To calculate an appropriate value for this threshold, data were collected from 16 volunteers (5 female and 11 male), with an average weight of 74.81 (SD 15.25) kg and foot size of 26.93 (SD 1.94) cm. The volunteers were asked to stand on the mat barefoot in 4 different positions: with both feet standing still and on their forefoot and with one foot standing still and on their forefoot. Maximum values of pressure exerted on FSR sensors were used as reference for normalization, and the minimum value for activation of FSR sensors was considered as no volunteer standing on the mat.

Using such criteria, on average when standing still over the mat with both feet subjects activated 71.66% of the FSR sensors, and when standing on their forefoot with both feet, 28.9% of the FSR sensors were activated. When standing still and on their forefoot with only one foot an activation of 40.37% and 18.40% of the FSR sensors was registered, respectively. The minimum value of FSR sensors activation is registered when standing on one foot on their forefoot, with a value of 12.09%. All results are summarized in Table 1. By taking these results into account, and if it is assumed that volunteers may land first with one foot on their forefoot after a jump, a proper threshold should be proposed below the minimum value of FSR sensors activation. For this study, a threshold of 9% of FSR sensors activation is used. This threshold was chosen to be at three-quarters between the zero FSR sensor activation and the minimum FSR sensor activation recorded, to avoid any misreading from mechanical oscillation. It is worth noting that the minimum recorded value from sensor activation is an outlier. In future studies, the possibility of adding a personalized threshold for every subject could be assessed.

Figure 4. Block diagram of the proposed system.

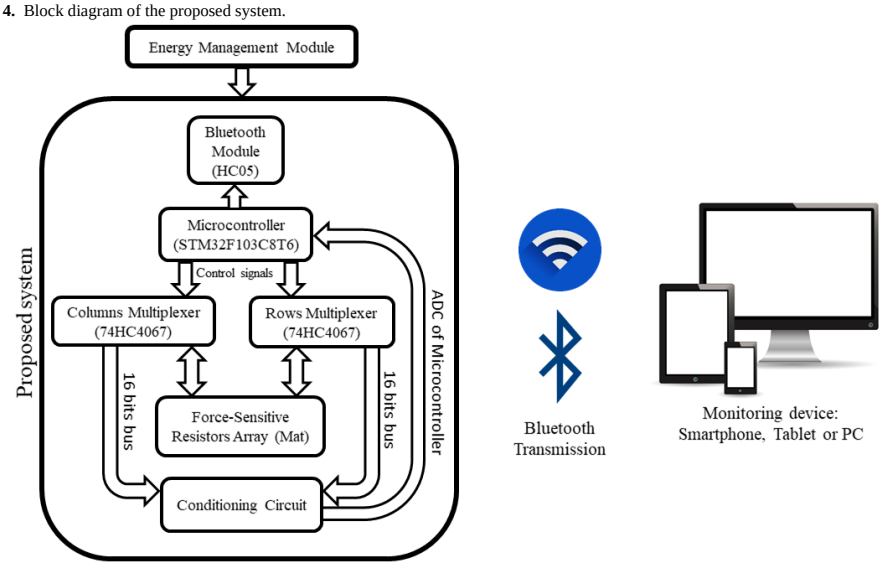

Table 1. Normalized force-sensitive resistor sensors activation registered from volunteers standing at different positions on the mat; standing still and on their toes with both feet and standing still and on their toes with one foot.

Sensor activation	Both feet %		One foot %	
	Standing	Toes	Standing	Toes
Average	71.66	28.90	40.37	18.40
Maximum	100.00	43.31	61.45	27.00
Minimum	44.00	23.70	22.64	12.09

For every position sensor activation percentage, a correlation analysis with the weight and foot size of the volunteers was performed. Analysis suggests that sensor activation is only moderately impacted by the weight of volunteers, and foot size of volunteers has a low impact on sensor activation. In Table 2, correlation values for different positions analyzed on the mat are shown.

To calculate the height reached by the user during the vertical jump, when the subject jumps and there is no contact on the mat, the system counts the elapsed time until the subject lands on the mat again (flight time), and with the calculated time the flight-time formula is used [3,8,9,14,16] to predict the height reached. This formula is defined as: $Height = g\Delta t^2/8$, where g is the constant value of gravity force g=9.81 m/s^2 and Δt is the flight time obtained by the system. Once the height of the vertical jump is obtained, this value is wirelessly sent via Bluetooth to the monitoring device selected by the health care professional.

Table 2. Pearson correlation coefficient values (R values) for different positions analyzed, calculated for weight and foot size of volunteers.

Position	Weight	Foot size
Both feet		
Standing	–.684	–.522
Forefoot	–.411	–.241
One foot		
Standing	–.447	–.397
Forefoot	–.394	–.463

Experimental Setup

Two different experiments were performed. The purpose of the first experiment, in which 38 volunteers participated, was to validate the reliability of the proposed system. For the second experiment, the objective was to compare the effects of different sampling frequencies when calculating the height reached on the jumps, and 15 volunteers participated. The protocol used for each experiment is the same. For the first experiment, data are directly processed by the microcontroller and the predicted value is sent to the selected monitoring station. In the second experiment, raw data are obtained to perform an offline downsampling to analyze the effects of different sampling frequencies on the predicted result.

Researchers asked for assistance from a sports and fitness center to recruit volunteers who attended the center regularly for physical training. Researchers visited this center with all the necessary equipment for the implementation of the protocols, and installed it in an area specified by the managers of the center. No specific physical attributes were required from the volunteers, as these characteristics should not affect the performance of the system. Researchers approached people at the center, explained the purpose of the study, and politely asked for their collaboration on the protocols if they were available at any given moment. Before starting any trial, volunteers were asked if they had any kind of injury that could affect their physical integrity when performing the protocol, and if so, the trials would not proceed. Every volunteer gave their written consent for the performance of the proposed protocol. The countermovement jump (CMJ) and countermovement jump with arm swing (CMJAS) techniques were selected for this protocol. These jumping techniques are commonly used as a measure to assess the overall force and explosive power of the lower body muscles on a person [26], and it is considered as the most reliable jumping test for this purpose [27]. By adding an arm swing to the CMJ, with the proper technique, the height reached by the person is increased around one-third and up to two-thirds [28-30], which increases the dynamic range of data obtained.

In the proposed protocol, volunteers were asked to stand on a marker placed on the center of the mat and perform 3 medium-to-maximal effort CMJs, with their hands fixed at the waist, with 5 to 10 seconds rest between trials. This technique is depicted in Figure 5. After these jumps, the volunteers were asked to perform CMJAS this time, and following the same scheme. This technique is depicted in Figure 6. As a reference system, all trials were recorded on video with a high-speed camera (120 fps). The camera was placed 1.3 m away from the mat, perpendicular to the sagittal plane of the volunteer and 20 cm above the ground, held by a tripod. The setup for this protocol is depicted in Figure 7.

To measure height reached by the subject with the video reference, the takeoff and landing frames were selected manually like in the studies of Balsalobre-Fernandez et al [11,22], and height was calculated by using the elapsed time between the frames using the flight-time formula.

Figure 5. Countermovement jump technique, step by step.

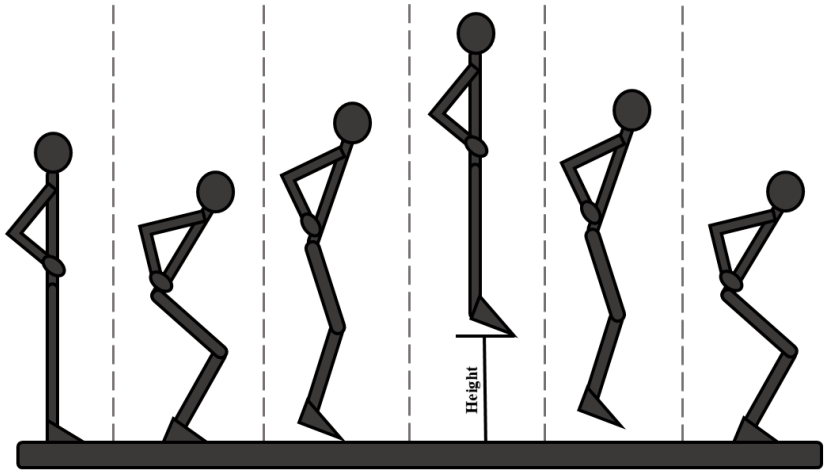

Figure 6. Countermovement jump with arm swing technique, step by step.

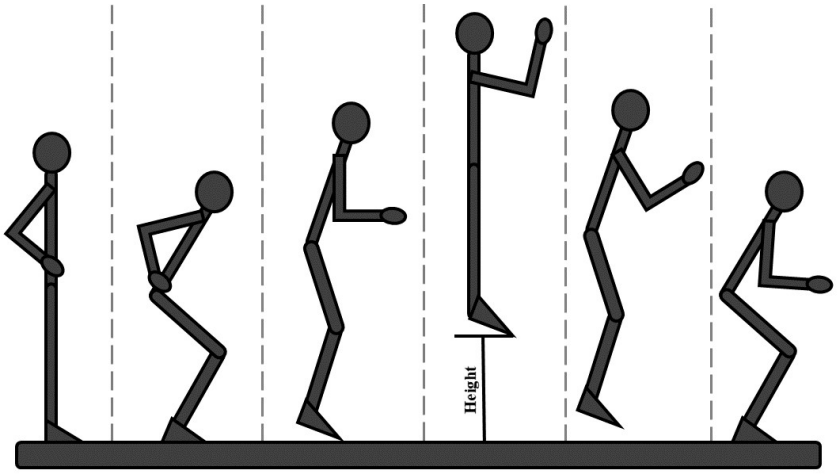

Figure 7. Experimental setup used for proposed experiments.

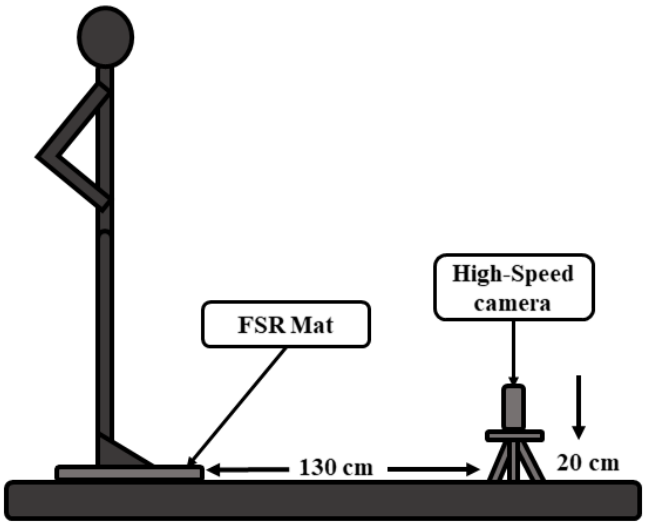

Results

First Experiment: System Validation

For the first experiment, a total of 228 jumps (114 CMJs and 114 CMJASs) were performed for each, the proposed system and the video reference. An example of the recorded jumps is shown in Figure 8.

To analyze the proposed system performance, mean relative error (MRE) and mean absolute error (MAE) were calculated for the overall jump trials and for each technique, CMJ and CMJAS. The MRE obtained from all 228 trials was 1.98%. For CMJ and CMJAS, relative errors were 2.17% and 1.78%, respectively. MAE obtained from all jump trials was 0.38 cm, and for CMJ and CMJAS, the errors obtained were 0.34 cm and 0.42 cm, respectively. These results are summarized in Table 3.

Figure 8. Two volunteers performing the proposed protocol showing the different phases of the jumps: takeoff frame, maximum-height frame, and landing frame.

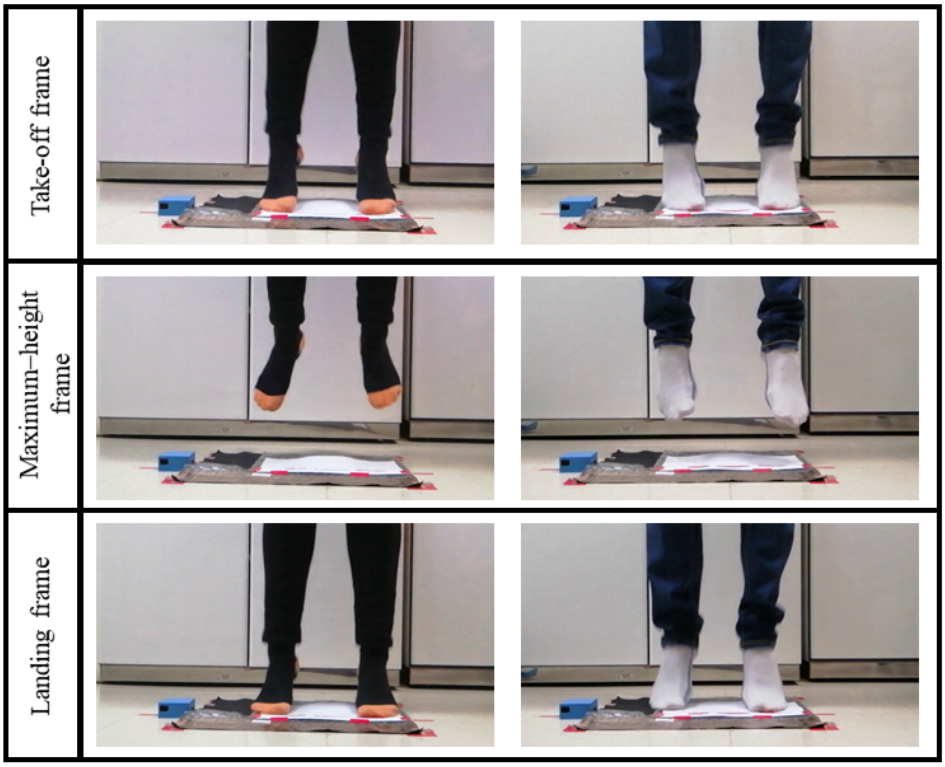

Table 3. Mean absolute error and mean relative error values for overall jump trials, only countermovement jump, and only countermovement jump with arm swing trials.

Trials	MAE[a] (cm)	MRE[b] (%)
Overall	0.38	1.98
CMJ[c]	0.34	2.17
CMJAS[d]	0.42	1.78

[a]MAE: mean absolute error.

[b]MRE: mean relative error.

[c]CMJ: countermovement jump.

[d]CMJAS: countermovement jump with arm swing.

Correlation and Bland-Altman analyses were performed from data obtained and are shown in Figure 9 and Figure 10, respectively. Correlation analysis shows a coefficient of determination of R^2=.996. These analyses demonstrate that the proposed system not only has a high correlation, but it shows that the difference of the two paired measurements is really low, which means that both methods produce systematically the same results.

Figure 9. Correlation graph comparing both measuring methods for the first experiment, showing a coefficient of determination of R^2=.996.

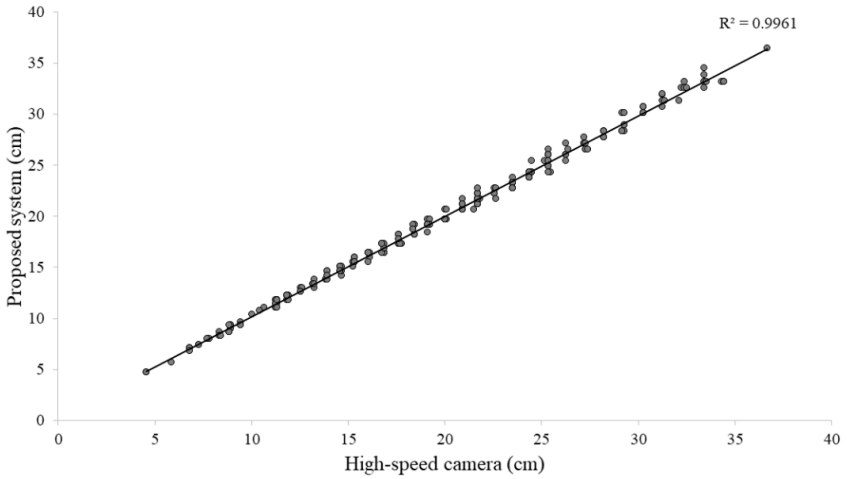

Figure 10. Bland-Altman plot of both measuring methods: countermovement jump depicted by dark gray points and countermovement jump with arm swing depicted by light gray points.

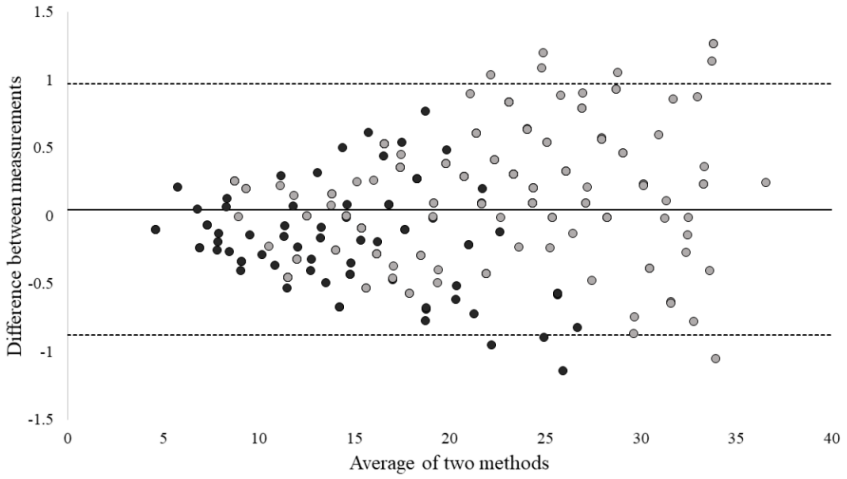

In Figure 11, the normalized MAE and MRE are shown for different ranges of jump heights reached. By analyzing the different ranges of height reached by the volunteers, which are <10 cm, 10 to 20 cm, 20 to 30 cm, and >30 cm, MREs obtained were 2.38%, 2.07%, 1.90%, and 1.54%, respectively. MAE obtained were 0.18 cm, 0.31 cm, 0.46 cm, and 0.50 cm, respectively. From this data, no significant difference can be found. However, it can be noticed that MAE increases as jump height increases, while MRE decreases.

Figure 12 shows the charts with distribution of the heights reached by the volunteers when performing the jump trials. For CMJ, no volunteer was able to surpass the 30 cm height. However, by adding the arm swing, 22% of the volunteers surpassed the 30 cm height. Also, for CMJAS trials, 47% of the subjects reached a height ranging from 20 to 30 cm, compared with CMJ, in which only 31% of the subjects reached this height.

Figure 11. Normalized mean absolute error and mean relative error, divided in different ranges of height reached during vertical jump.

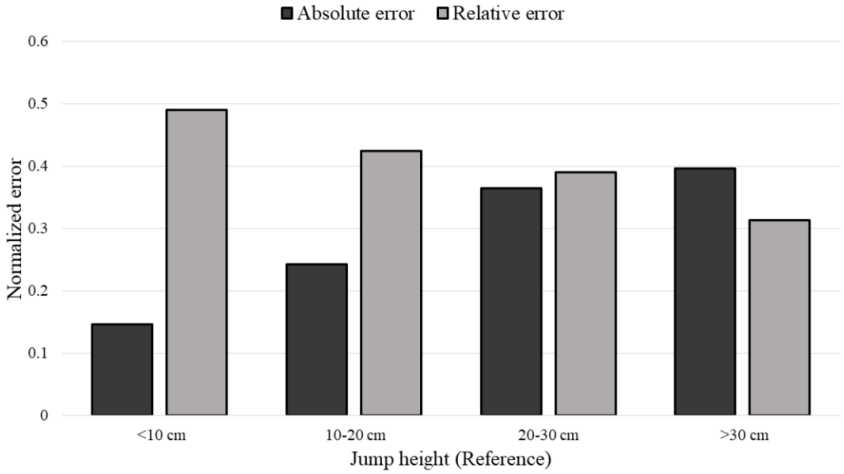

Figure 12. Distribution of different height ranges reached by the users. Overall trials, only countermovement jump trials, and only countermovement jump with arm swing trials are shown.

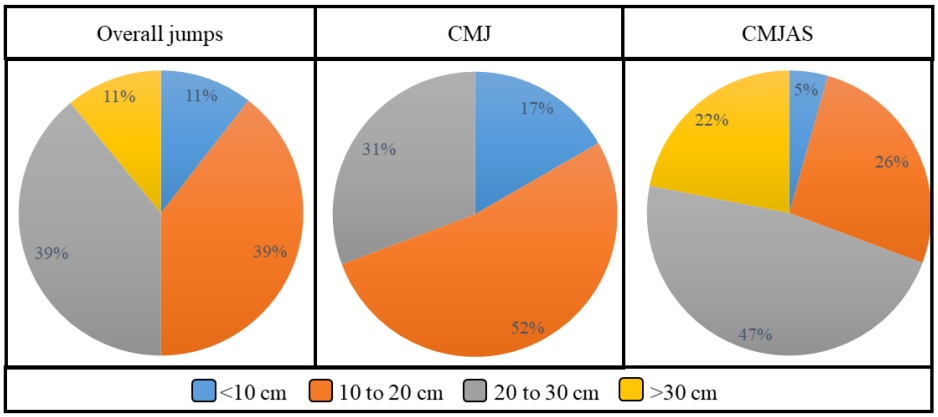

Second Experiment: Sampling Frequencies Comparison

In this experiment, the effects of different sampling frequencies were analyzed. Raw data from the system was obtained for a total of 90 jumps (45 CMJs and 45 CMJASs). An offline emulation of different sampling frequencies was performed through downsampling of this raw data. This means samples are removed to emulate a slower sampling frequency. With this method, and with the base sampling period of 5 ms from the system, 200 Hz, 100 Hz, 66.6 Hz, 50 Hz, 40 Hz, 33.3 Hz, 28.5 Hz, 25 Hz, 22.2 Hz, and 20 Hz frequencies were emulated.

Similar to the first experiment, the error was calculated using the high-speed camera as reference. For this analysis, only MRE was obtained for each sampling frequency to assess which frequencies are able to maintain a relative error below 5%. Results show that sampling frequencies of 200 Hz, 100 Hz, and 66.6 Hz have similar performance, with relative errors of 1.88%, 2.22%, and 2.88%, respectively. However, the maximum error among the 90 trials increases considerably between these frequencies, with maximum errors of 5.27%, 7.02%, and 8.25% for each respective frequency. Sampling frequencies of 50 Hz, 40 Hz, and 33.3 Hz also show good performance regarding the relative error, which is maintained below 5% for the 3 cases, but the maximum relative error found in these 3 frequencies is considerably higher than the found in the previous set.

In Table 4, MRE and maximum and minimum relative errors found among trials for the different sampling frequencies are shown. With slower sampling frequencies, MRE increases exponentially as shown in Figure 13, which suggests that sampling frequencies equal to or below 28.5 Hz are not reliable enough to maintain MRE below 5%. Also, sampling frequencies

slower than 50 Hz and 33.3 Hz show maximum relative error among trials higher than 10% and 20%, respectively.

Table 5 shows how MRE is distributed in different ranges. Only 200 Hz and 100 Hz sampling frequencies are able to maintain 95% of their results within 5% of relative error. Also, sampling frequencies slower than 50 Hz considerably increase the percentage of relative errors found above 5%. These results suggest that sampling frequencies of 200 Hz and 100 Hz are the most reliable, frequencies of 66.6 Hz and 50 Hz have an acceptable performance, and the remaining sampling frequencies are unreliable for this specific application.

Figure 13. Mean relative error obtained for each proposed sampling frequency. As sampling frequency decreases, relative error increases exponentially.

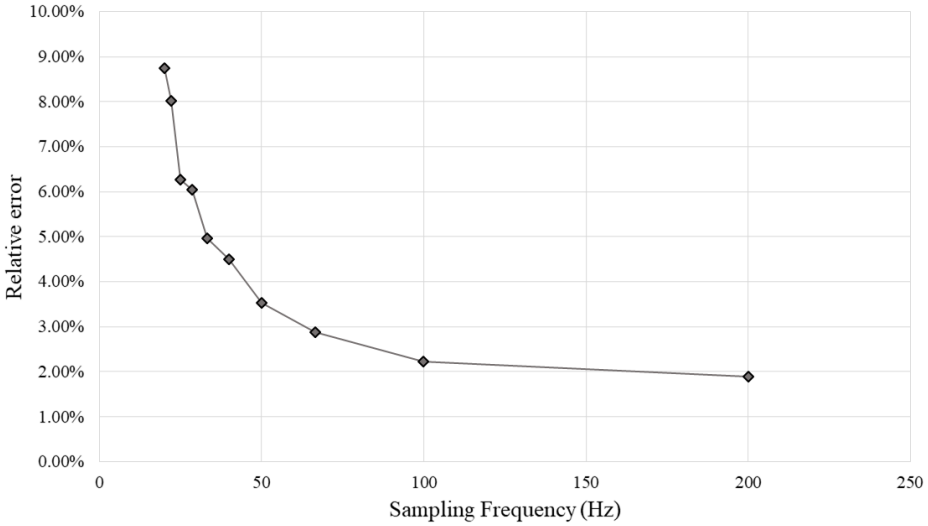

Table 4. Mean relative error and maximum and minimum relative errors obtained from all 90 trials for each sampling frequency analyzed.

Relative error	Sampling periods/frequencies									
	5 ms, 200 Hz	10 ms, 100 Hz	15 ms, 66.6 Hz	20 ms, 50 Hz	25 ms, 40 Hz	30 ms, 33.3 Hz	35 ms, 28.5 Hz	40 ms, 25 Hz	45 ms, 22.2 Hz	50 ms, 20 Hz
MRE[a]	1.88	2.22	2.88	3.52	4.50	4.97	6.04	6.27	8.02	8.75
MAX[b]	5.27	7.02	8.25	9.73	14.25	14.25	21.30	19.73	28.39	32.11
MIN[c]	0	0	0	0	0.70	0	0	0	0	0.73

[a]MRE: mean relative error.

[b]MAX: maximum relative error.

[c]MIN: minimum relative error.

Table 5. Percentage of trials whose relative error is within the ranges of 5% or less, higher than 5% and lower than 15%, and higher than 15%.

Relative error	Sampling periods/frequencies									
	5 ms, 200 Hz	10 ms, 100 Hz	15 ms, 66.6 Hz	20 ms, 50 Hz	25 ms, 40 Hz	30 ms, 33.3 Hz	35 ms, 28.5 Hz	40 ms, 25 Hz	45 ms, 22.2 Hz	50 ms, 20 Hz
RE[a] ≤5%	98.89	94.44	87.78	76.67	58.89	57.78	48.89	52.22	35.56	27.78
RE 5% to 15%	1.11	5.56	12.22	23.33	41.11	42.22	47.78	43.33	54.44	57.78
RE >15%	0	0	0	0	0	0	3.33	4.44	10	14.44

[a]RE: relative error.

When MRE is obtained from different jump heights (≤10 cm, 10 to 20 cm, 20 to 30 cm, and >30 cm) at each sampling frequency, the relevance of a proper sampling frequency when calculating height reached for small jumps (<20 cm) is observed. When using sampling frequencies slower than 50 Hz, MRE obtained from these small jumps is always higher than 5%, and for the slowest sampling frequency, MRE reaches a value of 21.50% for jump heights smaller than 10 cm. For higher jump heights, an increase in MRE (>5%) is noticeable for sampling frequencies slower than 40 Hz, reaching a value of up to 9.15% for the slowest sampling frequency. A summary of these results is shown in Table 6.

Table 6. Mean relative error obtained from each of the analyzed sampling frequencies for different ranges of height reached during the vertical jump.

Jump height	Sampling periods/frequencies									
	5 ms, 200 Hz	10 ms, 100 Hz	15 ms, 66.6 Hz	20 ms, 50 Hz	25 ms, 40 Hz	30 ms, 33.3 Hz	35 ms, 28.5 Hz	40 ms, 25 Hz	45 ms, 22.2 Hz	50 ms, 20 Hz
<10 cm	1.31	2.29	4.33	2.62	5.28	5.09	5.40	6.29	10.77	21.50
10-20 cm	2.23	2.40	2.89	4.29	5.21	5.45	7.55	8.60	9.65	8.42
20-30 cm	1.91	2.31	3.02	3.55	4.62	5.29	5.06	6.12	6.96	9.15
>30 cm	1.60	1.95	2.50	2.92	3.63	4.17	5.83	4.34	7.32	6.85

Discussion

Principal Findings

The vertical jump is a test commonly used by health care professionals to assess strength in the lower limb muscles of a subject. Although this test is widely used for strength assessment among athletes, relevant information can be obtained from people with no relevant sports background.

An important point to highlight about the system developed in this study is its low price. The total for components used in construction is approximately US $40. In comparison with commercially available devices, this developed system is significantly more affordable. Among the devices commonly used on medical and sports fields to measure vertical jump height are the vertical jump test mat (Gill Athletics) [31], Just Jump system (Perform Better) [10,32], Vertec device (Gill Athletics) [10,33], electronic vertical jump tester (Gill Athletics) [34], Optojump testing (Perform Better) [12,35], and bilateral force plate (Hawkin Dynamics) [18,36]. Our proposed system will have to pass through different standards and certifications (like ISO standards [37]) before it can be considered as a standard medical device. Table 7 shows a comparison of prices between commercially available devices and the system proposed here. Prices of the commercially available devices are listed as found at the moment of writing this article.

Table 7. Comparison of prices between commercially available devices and the system developed in this study.

Device for vertical jump measurement	Price $
Proposal from this study (estimated price of components)	40
Vertical jump test mat (Gill Athletics) [31]	360
Just Jump System (Perform Better) [32]	629
Vertec device (Gill Athletics) [33]	760
Electronic vertical jump tester (Gill Athletics) [34]	2925
Optojump testing (Perform Better) [35]	3804
Bilateral force plate (Hawkin Dynamics) [36]	5000

Throughout data capturing in both experiments, some important points can be highlighted. Despite the advantages that the proposed system and reference device offer, both have an inherent error due to their sampling frequency (more specifically due to their sampling period). The proposed system has a sampling frequency of 200 Hz, and thus the sampling period is 5 ms. Likewise, the reference device has a sampling frequency of 120 Hz and a sampling period of 8.3 ms. This means that every sampling period each device updates its readings, which implies an uncertainty of the sampling period between data updates. In other words, there is an inherent uncertainty in the system during the takeoff and landing phases of the jump, time span that is used to calculate height reached. From both phases, the proposed system has a total uncertainty of 10 ms, while the reference device has a total uncertainty of 16.6 ms. This inherent error is characteristic of electronic devices and directly related to their sampling frequency. Nonelectronic methods for jump height measuring lack of this inherent error, but as stated before, these methods tend to overestimate obtained measurements and are less precise.

Regarding the high-speed camera used as a reference device, when the recorded videos were analyzed, the ease of selecting the correct frames depended on the correct technique execution of the volunteer: taking off from both forefeet at the same time during the takeoff phase and landing with both forefeet at the same time during the landing phase. This was the ideal technique execution. On the other hand, some volunteers either took off or landed with only one forefoot and not with the same foot in

some occasions. In such cases, it was harder to select the takeoff and landing frames. This is difficult for volunteers to control without long-term training in the proper technique.

On the proposed protocol, the inclusion of two different jump techniques proved to be useful in order to increase the dynamic range of the data. The difference between the CMJ and CMJAS was significant. The addition of an arm swing increased jump height an average of 44.84% in the first experiment and 34.86% in the second experiment.

Limitations

One of the main limitations of the developed system was its sampling frequency. Although the microcontroller used had a high CPU frequency, the sampling frequency was limited because of the number of operations needed for a full scan of the mat (16 rows and 16 columns, a scan of 256 individual cells) and number of operations this implies. Another limitation was the total sensing area of the system of 30×30 cm. Although no volunteer reported discomfort, the total area limits the stance of volunteers; in addition, the landing phase of every jump trial must be performed in a controlled manner, so the volunteer lands inside this area.

These limitations can be solved in future versions of the mat. The design of the mat can be modified to increase its total sensing area and the size of each row and column, so in this way with fewer number of rows and columns the same sensing area could be achieved, thus increasing the sampling frequency of the system. However, this would diminish the resolution of the system.

Conclusions

In this study, a novel low-cost system for measurement of the jump height is proposed. Two experiments were performed—one to validate the system and the other to assess the effects of different sampling frequencies.

When evaluating the performance of the proposed system in the first experiment, results show that with the proposed sampling frequency of 200 Hz relative error for all of the 228 jump trials is maintained below 5%. In the second experiment, with sampling frequencies of 200 Hz and 100 Hz, relative error is maintained below 5% for 98.89% and 94.44% of the jump trials, respectively.

The flight-time formula is a widely used, validated method to calculate height reached during vertical jumps. A high-speed camera as reference device has been used in related studies along with the flight-time formula, proving to be a reliable tool. Our first experiment showed through correlation and Bland-Altman analyses that the proposed system and a high-speed camera reference device produced systematically similar results when calculating jump height.

Our second experiment concluded that 200 Hz and 100 Hz sampling frequencies have similar performance, and both frequencies are reliable when calculating jump height using the flight-time formula. This implies that if access to hardware capable of processing data at 200 Hz were limited, hardware capable of processing data to at least 100 Hz could offer similar results. However, if higher sampling frequencies are available, they should be used.

These results demonstrate that the proposed system is as reliable as a commercially available device, and the selected sampling frequency of 200 Hz is reliable for obtaining relative errors below 5% for at least 95% of the jump trials. The proposed system offers an alternative for health care professionals to use a mobile monitoring station of their choice, and its price is more affordable than commercially available devices.

Acknowledgments

This research was funded by grant Programa Operativo FEDER Construyendo Europa desde Aragon T49_20R from the European Union and Gobierno de Aragón, grant UZCUD2019-TEC-02 from the Universidad de Zaragoza and Centro Universitario de la Defensa de Zaragoza, and grant 709365 from the Consejo Nacional de Ciencia y Tecnología.

Conflicts of Interest

None declared.

References

1. Rodrigues C, Correia M, Abrantes J, Nadal J, Benedetti Rodrigues MA. Consistency of surface electromyography assessment at lower limb selected muscles during vertical countermovement. Annu Int Conf IEEE Eng Med Biol Soc 2017 Jul;2017:402-405. [doi: 10.1109/EMBC.2017.8036847] [Medline: 29059895]
2. Garcia M, Guzmán L, Valencia J, Henao V. Portable measurement system of vertical jump using an inertial measurement unit and pressure sensors. 2016 Presented at: 2016 XXI Symposium on Signal Processing, Images and Artificial Vision (STSIVA); 2016; Bucaramanga p. 1-5. [doi: 10.1109/stsiva.2016.7743299]
3. Drazan J, Danielsen H, Vercelletto M, Loya A, Davis J, Eglash R. A case study for integrated STEM outreach in an urban setting using a do-it-yourself vertical jump measurement platform. Annu Int Conf IEEE Eng Med Biol Soc 2016 Aug;2016:3027-3030. [doi: 10.1109/EMBC.2016.7591367] [Medline: 28268950]
4. Casartelli N, Müller R, Maffiuletti N. Validity and reliability of the Myotest accelerometric system for the assessment of vertical jump height. J Strength Cond Res 2010 Nov;24(11):3186-3193. [doi: 10.1519/JSC.0b013e3181d8595c] [Medline: 20940642]

5. Mijailovic N, Radakovic R, Peulic A, Milankovic I, Filipovic N. Using force plate, computer simulation and image alignment in jumping analysis. 2015 Presented at: 2015 IEEE 15th International Conference on Bioinformatics and Bioengineering (BIBE); 2015; Belgrade p. 1-4. [doi: 10.1109/bibe.2015.7367672]
6. Yahya U, Senanayake S, Naim A. Intelligent integrated wearable sensing mechanism for vertical jump height prediction in female netball players. 2017 Presented at: 2017 Eleventh International Conference on Sensing Technology (ICST); 2017; Sydney p. 1-7. [doi: 10.1109/icsenst.2017.8304483]
7. García-Ramos A, Štirn I, Padial P, Argüelles-Cienfuegos J, De la Fuente B, Strojnik V, et al. Predicting vertical jump height from bar velocity. J Sports Sci Med 2015 Jun;14(2):256-262 [FREE Full text] [Medline: 25983572]
8. Howard R, Conway R, Harrison A. Estimation of force during vertical jumps using body fixed accelerometers. 2014 Presented at: 25th IET Irish Signals & Systems Conference 2014 and 2014 China-Ireland International Conference on Information and Communications Technologies (ISSC 2014/CIICT 2014); 2014; Limerick p. 102-107. [doi: 10.1049/cp.2014.0667]
9. Whitmer T, Fry A, Forsythe C, Andre M, Lane M, Hudy A, et al. Accuracy of a vertical jump contact mat for determining jump height and flight time. J Strength Cond Res 2015 Apr;29(4):877-881. [doi: 10.1519/JSC.0000000000000542] [Medline: 24852256]
10. Nuzzo J, Anning J, Scharfenberg J. The reliability of three devices used for measuring vertical jump height. J Strength Cond Res 2011 Sep;25(9):2580-2590. [doi: 10.1519/JSC.0b013e3181fee650] [Medline: 21804426]
11. Balsalobre-Fernández C, Glaister M, Lockey RA. The validity and reliability of an iPhone app for measuring vertical jump performance. J Sports Sci 2015;33(15):1574-1579. [doi: 10.1080/02640414.2014.996184] [Medline: 25555023]
12. Glatthorn J, Gouge S, Nussbaumer S, Stauffacher S, Impellizzeri F, Maffiuletti N. Validity and reliability of Optojump photoelectric cells for estimating vertical jump height. J Strength Cond Res 2011 Feb;25(2):556-560. [doi: 10.1519/JSC.0b013e3181ccb18d] [Medline: 20647944]
13. Bui HT, Farinas M, Fortin A, Comtois A, Leone M. Comparison and analysis of three different methods to evaluate vertical jump height. Clin Physiol Funct Imaging 2015 May;35(3):203-209. [doi: 10.1111/cpf.12148] [Medline: 24690449]
14. Dias J, Dal Pupo J, Reis D, Borges L, Santos S, Moro A, et al. Validity of two methods for estimation of vertical jump height. J Strength Cond Res 2011 Jul;25(7):2034-2039. [doi: 10.1519/JSC.0b013e3181e73f6e] [Medline: 21701288]
15. Kibele A. Possibilities and limitations in the biomechanical analysis of countermovement jumps: a methodological study. J Appl Biomech 1998;14(1):105-117. [doi: 10.1123/jab.14.1.105]
16. Boukhenous S, Attari M. A vertical jumping performance with and without arms swing by using a dynamometric platform. Int Workshop Syst Signal Processing Appl 2011:17-20. [doi: 10.1109/wosspa.2011.5931450]
17. Zihajehzadeh S, Lee TJ, Lee JK, Hoskinson R, Park EJ. Integration of MEMS inertial and pressure sensors for vertical trajectory determination. IEEE Trans Instrum Meas 2015 Mar;64(3):804-814. [doi: 10.1109/tim.2014.2359813]
18. Moir GL. Three different methods of calculating vertical jump height from force platform data in men and women. Meas Phys Educ Exer Sci 2008 Oct 15;12(4):207-218. [doi: 10.1080/10913670802349766]
19. Aragón LF. Evaluation of four vertical jump tests: methodology, reliability, validity, and accuracy. Meas Phys Educ Exer Sci 2000 Dec;4(4):215-228. [doi: 10.1207/s15327841mpee0404_2]
20. Kassim A, Miskon M, Rahim N, Yasuno T. Effectiveness of reference height control system for tripod hopping robot. 2011 Presented at: 2011 4th International Conference on Mechatronics (ICOM); 2011; Kuala Lumpur p. 1-4. [doi: 10.1109/icom.2011.5937123]
21. Leard J, Cirillo M, Katsnelson E, Kimiatek D, Miller T, Trebincevic K, et al. Validity of two alternative systems for measuring vertical jump height. J Strength Cond Res 2007 Nov;21(4):1296-1269. [doi: 10.1519/R-21536.1] [Medline: 18076265]
22. Balsalobre-Fernández C, Tejero-González CM, del Campo-Vecino J, Bavaresco N. The concurrent validity and reliability of a low-cost, high-speed camera-based method for measuring the flight time of vertical jumps. J Strength Cond Res 2014 Feb;28(2):528-533. [doi: 10.1519/JSC.0b013e318299a52e] [Medline: 23689339]
23. Valle-Lopera DA, Castraño-Franco AF, Gallego-Londoño J, Hernández-Valdivieso AM. Test and fabrication of piezoresistive sensors for contact pressure measurement. Rev Fac Ing Univ Antioquia 2017 Mar(82):47-52. [doi: 10.17533/udea.redin.n82a06]
24. Giovanelli D, Farella E. Force sensing resistor and evaluation of technology for wearable body pressure sensing. J Sensors 2016;2016:1-13. [doi: 10.1155/2016/9391850]
25. Medrano-Sanchez C, Igual-Catalan R, Rodriguez-Ontiveros VH, Plaza-Garcia I. Circuit analysis of matrix-like resistor networks for eliminating crosstalk in pressure sensitive mats. IEEE Sensors J 2019 Sep 15;19(18):8027-8036. [doi: 10.1109/jsen.2019.2918592]
26. Young W. Laboratory strength assessment of athletes. 1995. URL: https://www.worldathletics.org/download/downloadnsa?filename=9daf7a4d-c52b-4956-8453-caa4b378606c.pdf&urlslug=laboratory-strength-assessment-of-athletes [accessed 2021-03-05]
27. Markovic G, Dizdar D, Jukic I, Cardinale M. Reliability and factorial validity of squat and countermovement jump tests. J Strength Cond Res 2004 Aug;18(3):551-555. [doi: 10.1519/1533-4287(2004)18<551:RAFVOS>2.0.CO;2] [Medline: 15320660]

28. Cheng KB, Wang C, Chen H, Wu C, Chiu H. The mechanisms that enable arm motion to enhance vertical jump performance-a simulation study. J Biomech 2008;41(9):1847-1854. [doi: 10.1016/j.jbiomech.2008.04.004] [Medline: 18514208]
29. Feltner ME, Fraschetti DJ, Crisp RJ. Upper extremity augmentation of lower extremity kinetics during countermovement vertical jumps. J Sports Sci 1999 Jun;17(6):449-466. [doi: 10.1080/026404199365768] [Medline: 10404494]
30. Harman EA, Rosenstein MT, Frykman PN, Rosenstein RM. The effects of arms and countermovement on vertical jumping. Med Sci Sports Exerc 1990 Dec;22(6):825-833. [doi: 10.1249/00005768-199012000-00015] [Medline: 2287261]
31. Vertical jump test mat. Gill Athletics. URL: https://www.gillporter.com/gill_store/catalog/product/view/id/12661/ [accessed 2021-03-05]
32. Just jump system. Perform Better. URL: https://www.performbetter.com/Just-Jump-System_2 [accessed 2021-03-05]
33. Vertec jump measuring device. Gill Athletics. URL: https://www.gillporter.com/gill_store/vertec-jump-measuring-device.html [accessed 2021-03-05]
34. Electronic vertical jump tester. Gill Athletics. URL: https://www.gillporter.com/gill_store/catalog/product/view/id/12673/ [accessed 2021-03-05]
35. Optojump jump testing. Perform Better. URL: https://performbetter.co.uk/product/optojump/ [accessed 2021-03-05]
36. Hawkin dynamics G3 bilateral force plate set. Hawkin Dynamics. URL: https://hawkindynamics.shop/products/hawkin-dynamics-g3-bilateral-force-plate-set [accessed 2021-03-05]
37. ISO 13485 – medical devices. International Organization for Standardisation. URL: https://www.iso.org/iso-13485-medical-devices.html [accessed 2021-03-03]

Abbreviations

CMJ: countermovement jump
CMJAS: countermovement jump with arm swing
FSR: force-sensitive resistor
MAE: mean absolute error
MRE: mean relative error

Edited by L Buis; submitted 21.01.21; peer-reviewed by O Aragón Banderas, J Seitz; comments to author 02.03.21; revised version received 10.03.21; accepted 19.03.21; published 09.04.21

Please cite as:
Vanegas E, Salazar Y, Igual R, Plaza I
Force-Sensitive Mat for Vertical Jump Measurement to Assess Lower Limb Strength: Validity and Reliability Study
JMIR Mhealth Uhealth 2021;9(4):e27336
URL: https://mhealth.jmir.org/2021/4/e27336
doi: 10.2196/27336
PMID:

Anexo K

The effect of measurement trends in belt breathing sensors

I3S 2021

sciforum

Proceedings

The Effect of Measurement Trends in Belt Breathing Sensors †

Erik Vanegas, Raúl Igual * and Inmaculada Plaza

EduQTech, Electrical/Electronics Engineering and Communications Department, EUP Teruel, Universidad de Zaragoza, 44003 Teruel, Spain; 790974@unizar.es (E.V.); inmap@unizar.es (I.P.)

* Correspondence: rigual@unizar.es

† Presented at the 8th International Symposium on Sensor Science, 17–26 May 2021; Available online: https://i3s2021dresden.sciforum.net/.

Published: date

Abstract: Sensors for respiratory monitoring can be classified into wearable and non-wearable systems. Wearable sensors can be worn in several positions, the chest being one of the most effective. In this paper, we have studied the performance of a new piezoresistive breathing sensing system to be worn on the chest with a belt. One of the main problems of belt-attached sensing systems is that they present trends in measurements due to subject movements or differences in subject constitution. These trends affect sensor performance. To mitigate them, it is possible to post-process the data to remove trends in measurements, but relevant data from the respiration signal may be lost. In this study, two different detrending methods are applied to respiration signals. After conducting an ex-perimental study with 21 subjects who breathed in different positions with a chest piezoresistive sensor attached to a belt, detrending method 2 proved to be better at improving quality of respiration signals.

Keywords: wearable sensors; breathing sensors; piezoresistive; measurements; trends; belt; respiration rate

1. Introduction

Continuous monitoring of physiological signals is frequently used by healthcare professionals, mostly with hospital patients. For instance, monitoring of respiration rate is commonly used to diagnose overall health of the patients [1], and several diseases can be detected through respiration rate, like asthma or sleep apnea [2]. Other common applications for respiration rate monitoring are in sports to analyze the performance of athletes [3], monitoring of health state of drivers and commercial builders [4], and emotion recognition [5].

When designing a system for respiration rate monitoring, two different approaches are used by researchers, wearable and environmental systems, each of which has different techniques to achieve its purpose. For wearable systems, the most common technique is to measure chest diameter variations due to inhalation and exhalation of the user. This is commonly achieved by placing a flexible strap around the chest of the user. Through this strap, chest movements are transferred to the sensor of the system. Such sensor could be a piezoresistive sensor [6], capacitive sensor [3], piezoelectric sensor [7], optical fiber sensors [8], or inertial measurement units [9], among others [10].

When measuring physiological signals through wearable devices for a relatively prolonged time, signals show some trend, which is a systematic increase or decrease on the obtained signal due movements of the system or subject. However, linear fit can be applied offline to the registered respiration signals to mitigate this effect, as these trends may hinder data analysis [11]. A disadvantage of doing so, is that relevant information from the original signal may be lost.

In this study, we show that the effectiveness of eliminating trends in signals depends on the length of the segmentation window of the measurements. To do so, different segmentation windows (period of time analyzed by the algorithms) are proposed, and two different algorithms are used to analyze the respiration signals from 21 volunteers. Respiration signals were obtained through a chest-strap sensing system from a previous work [12].

2. Results

To analyze the respiration signals from all 21 volunteers, two different algorithms are used, whose basic principle consists in detecting all zero-crossings from the obtained signals by determining the zero-axis of such signals. Algorithm 1 measures the time difference between consecutive zero-crossings (breath cycles), whilst Algorithm 2 counts the number of crosses by zero. In this way, both algorithms are capable of calculating the respiration rate from the signal in breaths per minute (bpm). Both algorithms perform a segmentation of the signal (from 6 to 30 seconds); from each segmented window the respiration rate is calculated, and then the mean from all the segments is taken as the average respiration rate. From each volunteer, a total of 30 respiration signals are analyzed (six different respiration rates set by a metronome, and five different activities) for a total of 630 respiration signals analyzed. In a previous work [12], a complete description of this database is included.

When detrending the respiration signals, two different method were used. In the first method the whole signal was detrended before calculating the respiration rate from each segment, whilst with the second method each segmentation window was detrended individually. A depiction of both methods is shown in Figure 1. Relative error from each signal and each segmentation window was obtained from the original signals and each detrending method; then, a comparison in the increase or reduction of relative error was performed.

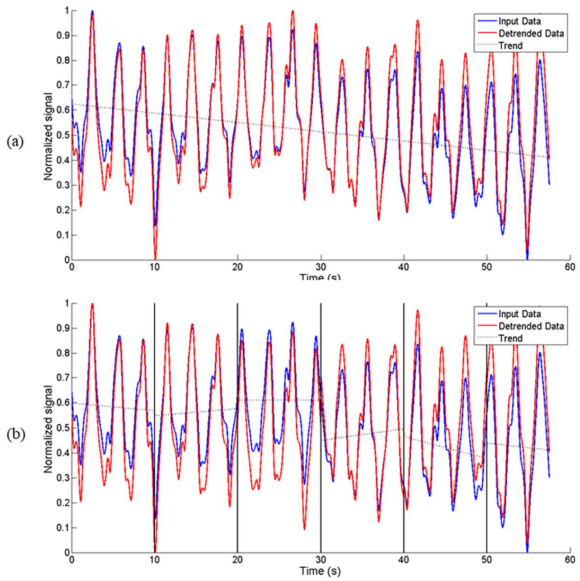

Figure 1. Signal detrend techniques used: (**a**) Method 1, detrend is applied in the whole signal; (**b**) Method 2, detrend is applied in each segmentation window.

For detrending method 1 and algorithm 1, the 6-second segmentation window shows an increase in relative error by 5.46%, whilst for the rest of the windows the relative error decreases. By detrending the signals and calculating respiration rate with algorithm 1, there is an average improvement (decrease in relative error) of 1.08%, with a maximum improvement of 2.52% (11s window) and maximum deterioration (increase in relative error) of 5.46% (6s window). For algorithm 2, only windows from 12 to 15 seconds show a deterioration of predicted respiration rate. There is an average improvement of 0.48%, with maximum improvement of 1.78% (30s window) and maximum deterioration of 0.55% (13s window).

When detrending original signal with method 2 for algorithm 1, an average improvement of 1.54% is achieved, with a maximum improvement of 3.19% (11s window) and maximum deterioration of 3.58% (6s window). For algorithm 2, only windows of 6-8 seconds show a deterioration in the predicted respiration rate. There is an average improvement of 1.28%, maximum improvement of 2.88% (30s window), and maximum deterioration of 2.35% (6s window). A summary of these results are shown in Table 1. The improvement and deterioration obtained from each segmentation window are show in Figure 2 and Figure 3 for detrending method 1 and detrending method 2, respectively.

Table 1. Improvement on respiration signal after detrending the original signal with both methods, for each algorithm.

	Algorithm 1			**Algorithm 2**		
	Average	**MI[1]**	**MD[2]**	**Average**	**MI[1]**	**MD[2]**
Method 1	1.08	2.52	5.46	0.48	1.78	0.55
Method 2	1.54	3.19	3.58	1.28	2.88	2.35

[1] Maximum improvement. [2] Maximum deterioration.

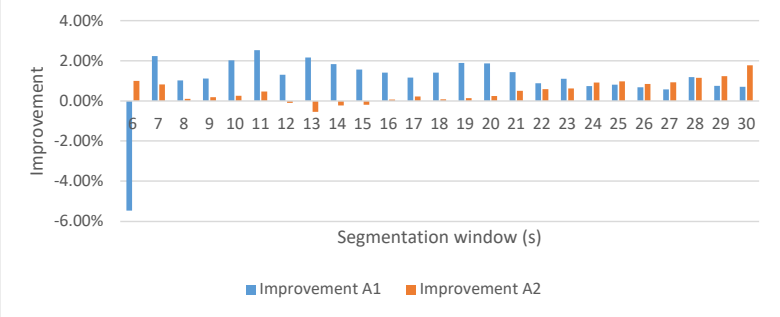

Figure 2. Improvement and deterioration obtained when calculating respiration rate after detrending the original signal with method 1.

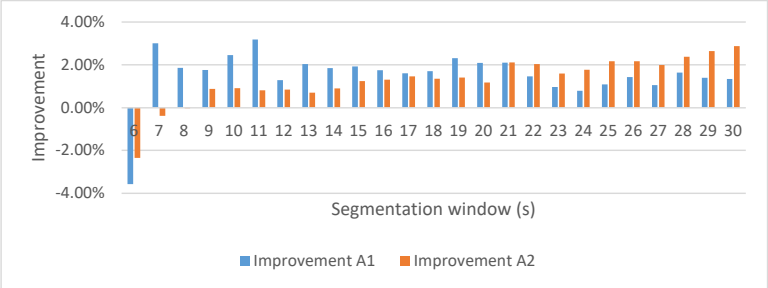

Figure 3. Improvement and deterioration obtained when calculating respiration rate after detrending the original signal with method 2.

3. Conclusions

Both detrending methods show an improvement when calculating respiration rate; however, detrending method 2 shows a better performance, as the average improvement is higher for both algorithms. From detrending method 2 and algorithm 1, only the 6s window shows deterioration, and all other windows show improvement when calculating respiration rate. However, this improvement is not consistent when moving along the different windows. On the other hand, for algorithm 2 it is noticed that, as the segmentation window increases, the improvement increases accordingly. Therefore, even though improvement in respiration rate prediction is moderate when detrending the signals, both detrending methods shows improvement when compared with the original signals with trends. For this specific application, detrending method 2 proves to be better.

References

1. Milenkovic, Aleksandar; Otto, Chris; Jovanov, Emil. Wireless sensor networks for personal health monitoring: Issues and an implementation. *Comput. Commun.* **2006**, *29*, 13–14.
2. Cao, Zhe; Zhu, Rong; Que, Rui-Yi. A wireless portable system with microsensors for monitoring respiratory diseases. *IEEE Trans. Biomed. Eng.* **2012**, *59*, 3110–3116.
3. Hoffmann, T.; Eilebrecht, B.; Leonhardt, S. Respiratory monitoring system on the basis of capacitive textile force sensors. *IEEE Sens. J.* **2010**, *11*, 1112–1119.
4. Gatti, Umberto, C.; Schneider, Suzanne; MIGLIACCIO, Giovanni, C. Physiological condition monitoring of construction workers. *Autom. Constr.* **2014**, *44*, 227–233.
5. Ćosic, Dijana. Neuromarketing in market research. *Interdiscip. Descr. Complex Syst.* **2016**, *14*, 139–147.
6. Hesse, Marc; Christ, Peter; Hörmann, Timm; Rückert, Ulrich. A respiration sensor for a chest-strap based wireless body sensor. In Proceedings of SENSORS, 2014 IEEE, Valencia, Spain, 2–5 November 2014, 490–493.
7. Mahbub, Ifana; Wang, Hanfeng; Islam, Syed K.; Pullano, Salvatore A.; Fiorillo, Antonino S. A low power wireless breathing monitoring system using piezoelectric transducer. In Proceedings of the 2016 IEEE International Symposium on Medical Measurements and Applications (MeMeA), Benevento, Italy, 15–18 May 2016, 1–5
8. Witt, Jens; Narbonneau, François; Schukar, Marcus; Krebber, Katerina; De Jonckheere, Julien; Jeanne, Mathieu; Kinet, Damien; Paquet, Bernard; Depre, Annick. Medical textiles with embedded fiber optic sensors for monitoring of respiratory movement. *IEEE Sens. J.* **2011**, *12*, 246–254.
9. Dan, Guo; Zhao, Junhao; Chen, Zihao; Yang, Huanyu; Zhu, Zhemin. A novel signal acquisition system for wearable respiratory monitoring. *IEEE Access* **2018**, *6*,34365–34371.
10. Vanegas, Erik; Igual, Raul; Plaza, Inmaculada. Sensing systems for respiration monitoring: A technical systematic review. *Sensors* **2020**, *20*, 34365–34371.

11. MathWorks. Remove Trends from Data. Available online: https://www.mathworks.com/help/signal/ug/remove-trends-from-data.html#:~:text=To%20eliminate%20the%20linear%20trend,the%20signal%20and%20subtract%20it. (Accessed on 7 April 2021).
12. Vanegas, Erik; Igual, Raul; Plaza, Inmaculada. Piezoresistive Breathing Sensing System with 3D Printed Wearable Casing. *J. Sens.* **2019**, *2019*, doi:10.1155/2019/2431731

Anexo L

Repositorio

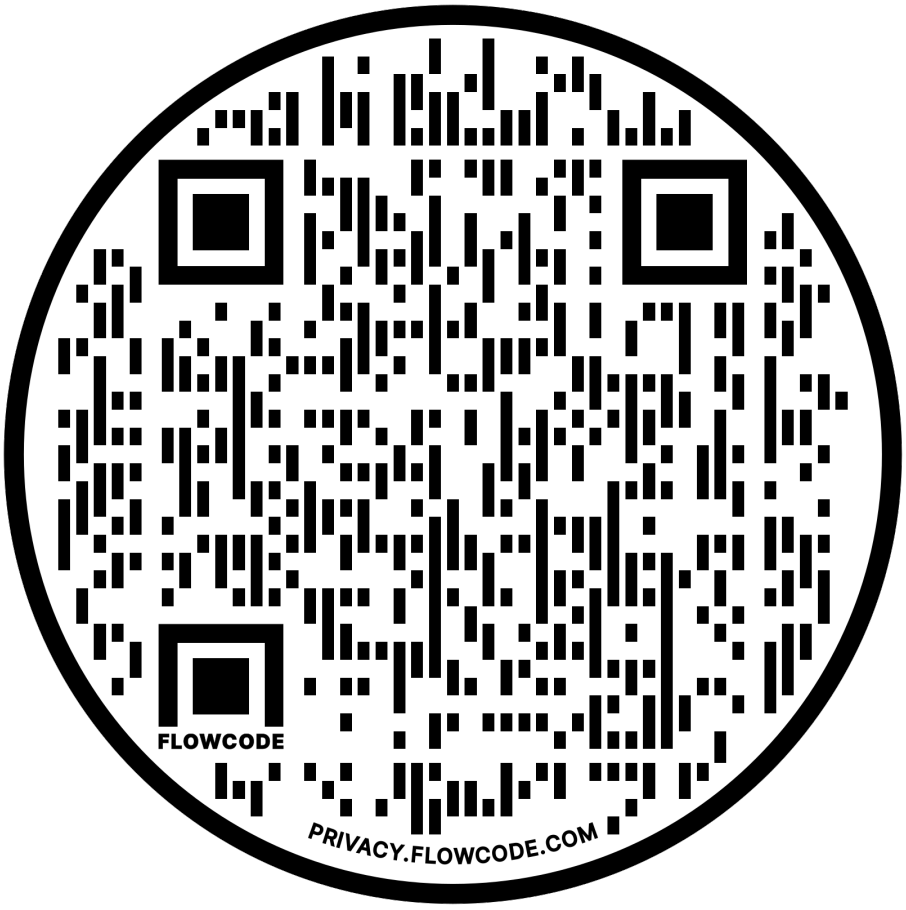

Figura L.1: Al escanear este código QR se puede acceder al repositorio con todos los archivos obtenidos como resultado del trabajo de la presente tesis. Entre los archivos del repositorio se encuentran: Archivos "Gerber" para construcción de PCBs, diseños 3D para impresión de armazones de los sitemas desarrollados, códigos utilizados por los mincrocontroladores de los sistemas y datos en crudo obtenidos por los sistemas.